KU LEUVEN

ARENBERG DOCTORAL SCHOOL
Faculty of Engineering Science

A probabilistic design methodology for building performance optimisation

An application to low-energy dwellings

Liesje VAN GELDER

Supervisors
Prof. dr. ir. arch. S. Roels
Prof. dr. ir. H. Janssen

Dissertation presented in partial fulfillment of the requirements for the degree of Doctor in Engineering Science

December 2014

A probabilistic design methodology for building performance optimisation

An application to low-energy dwellings

Liesje VAN GELDER

Examination committee:
Prof. dr. ir. J. Vandewalle, chair
Prof. dr. ir. arch. S. Roels, supervisor
Prof. dr. ir. H. Janssen, co-supervisor
Prof. dr. ir. G. Lombaert
Prof. dr. ir. J. Van Dyck
Prof. dr. ir. arch. F. De Troyer
Prof. dr. ir. A. Mahdavi
(Vienna University of Technology)
Prof. dr. ir. arch. G. Verbeeck
(Universiteit Hasselt)

Dissertation presented in partial fulfillment of the requirements for the degree of Doctor in Engineering Science

December 2014

© 2014 KU Leuven – Faculty of Engineering Science
Uitgegeven in eigen beheer, Liesje VAN GELDER, Kasteelpark Arenberg 40 box 2447, B-3001 Heverlee (Belgium)

Alle rechten voorbehouden. Niets uit deze uitgave mag worden vermenigvuldigd en/of openbaar gemaakt worden door middel van druk, fotokopie, microfilm, elektronisch of op welke andere wijze ook zonder voorafgaande schriftelijke toestemming van de uitgever.

All rights reserved. No part of the publication may be reproduced in any form by print, photoprint, microfilm, electronic or any other means without written permission from the publisher.

ISBN 978-94-6018-932-6

D/2014/7515/155

Voorwoord

It always seems impossible until it's done - Nelson Mandela

Vier jaar geleden begon ik er aan: mijn doctoraat. In het begin waren er veel vraagtekens en gaandeweg kwamen er daar alleen maar bij. Na veel, erg veel, vallen en opstaan, kan ik eindelijk trots zijn op *mijn boekje*. Het heeft me letterlijk bloed, zweet en tranen gekost, maar ik ben er des te fier op. Daarom zou ik graag iedereen bedanken die mij hierin heeft geholpen. Zonder hun steun was u deze tekst niet aan het lezen.

Allereerst wil ik mijn promoter Staf bedanken. Bedankt om mij steeds weer de goede weg te wijzen als ik weer eens verdwaald was. Bedankt om er voor te zorgen dat ik door projecten voldoende financiering had om mijn doctoraat te kunnen voltooien. Bedankt om verder ook te helpen in de nodige bijsturing van zowel projecten als doctoraat zodat deze beter op elkaar afgestemd konden worden en beiden binnen de voorziene tijd konden worden uitgevoerd. Bedankt om me ook steeds weer te motiveren en vooral om in mij te blijven geloven.

Mijn co-promotor Hans verdient ook een prominente plaats in dit dankwoord. Bedankt voor de steeds kritische blik op mijn werk. Bedankt om me steeds te *dwingen* het onderste uit de kan te halen, zelfs als ikzelf dacht dat reeds bereikt te hebben. En uiteraard ook bedankt dat je deur steeds open stond en dat je elke vraag die ik ook maar had steeds met veel plezier beantwoordde.

Verder zou ik ook graag alle andere leden van mijn doctoraatscommissie uitdrukkelijk bedanken voor het nalezen van mijn manuscript en hun kritische opmerkingen. Bedankt ook aan Daniel, Evy, Inneke, Jeroen, Philippe en Steven voor het nalezen van (enkele stukken van) mijn tekst en aan Tony voor het helpen bij enkele LaTeX-problemen.

Ik bedank ook graag alle collega's. Met pijn in het hart zal ik de afdeling verlaten. Ik zal de gezellige koffiepauzes en de overvloedige hoeveelheid taart missen, en natuurlijk ook jullie aanwezigheid. Bedank aan al mijn (ex-)rekencollega's om mij soms voorrang te geven en geduld te hebben met mijn miljoenen simulaties en vervelende opspringende venstertjes. In het bijzonder wil ik nog Evy bedanken voor

alle goede tips en om mijn probabilistische binnenisolatiestudie af te ronden zodat die toch nog (hopelijk) gepubliceerd is geraakt. Verder dank ik ook graag Patricia, Greet, Laura en Esther voor alle logistieke en administratieve ondersteuning van mijn doctoraat. En Wim en An-Heleen voor de lekkere culinaire momenten.

Ook buiten de afdeling kon ik samenwerken met toffe en gemotiveerde collega's. Bedankt Griet en Liesbeth voor de boeiende gesprekken omtrent *IWT TETRA BEP2020*. Ook bedankt aan alle collega's van het WTCB, NAV, Passiefhuisplatform en KU Leuven campus Geel voor de samenwerking rond *IWT VIS Renofase*. Uiteraard wordt ook de financiële steun voor deze projecten sterk gewaardeerd. I also want to thank my colleagues of *IEA EBC Annex 55 RAP-RETRO* for the fruitful discussions and especially Payel and Valentina for the pleasant stays abroad. I definitely will miss you girls.

Verder ben ik ook al mijn vrienden dankbaar voor de leuke momenten naast mijn doctoraat. Bedankt aan Annelore, Annemie, Dennis, Griet, Hans, Jochen, Jonas, Judith, Liesbeth, Lien, Line, Nathalie, Nathalie, Nicolas, Philippe, Simon, Sofie en alle partners voor de vele leuke avonden en ook de immense steun die ik van jullie kreeg in de 501 voordat ik de liefde nareisde naar het verre Antwerpen. Bedankt aan Daniel en Tony om me tijdens de laatste maanden te vergezellen bij het klimmen zodat ik toch nog een beetje kon ontspannen. Bedankt aan Steven voor de wekelijkse gezonde lunch en om steeds naar mij te luisteren. Verder ook bedankt aan wie nog niet is vermeld voor de leuke concerten, festivals, vrijgezellen, trouwfeesten, babyborrels en avonden op café. Sorry dat ik er niet altijd (lang) bij kon zijn. Ik maak het zeker goed in 2015!

Als laatste zou ik graag nog mijn familie bedanken met in het bijzonder mijn ouders. Ondanks alle moeilijkheden hebben jullie mij steeds gesteund en mij alle mogelijke kansen aangereikt. Zonder jullie geloof in mij was ik niet geworden wie ik nu ben. Ook al zeg ik het niet vaak, ik kan jullie daar niet genoeg voor bedanken.

Dan rest er mij alleen nog een woordje gericht aan mijn Jeroen. Schat, je hebt me ongelooflijk hard gesteund het laatste jaar. Bedankt voor alle lekkere maaltijden, de taxiritjes, de huistaakjes, de knuffels, de momenten waarop je me gewoon alleen liet, ... Het klinkt misschien cliché, maar ik zou écht niet weten hoe ik zonder jou dit boek voltooid zou hebben. Maar het is me gelukt, het is *ons* gelukt, en dat, lieve schat, dat vergeet ik nooit.

Abstract

Building performance calculations often use deterministic simulations. Since many influencing parameters are generally inherently uncertain, this may lead to unreliable predictions of design impact and hence excessive deviations between design and reality. Such excessive deviations of building performances are usually undesirable: clients want guarantees that their investments have the desired impact. Hence, the overall aims of this research are (1) the development of a probabilistic robust design methodology to incorporate these uncertainties for building performance analysis and optimisation and (2) its illustrative application on the thermal design of comfortable and affordable robust low-energy dwellings.

In the developed methodology, several design options can be compared based on the probability distributions of the studied performances. In order to do so, a multi-layered Monte Carlo uncertainty analysis is performed to subject all options to the same input uncertainties and hence calculate the corresponding performance distributions. An additional sensitivity analysis is applied to investigate which input uncertainties are most dominant for these distributions. Because this approach might be very time-consuming, the computational model is in this thesis optionally replaced by a much faster meta-model, without compromising the reliability. The methodology also enables an explicit evaluation of the design options for potential scenarios, such as the user type or economic evolutions, when desired. In order to numerically compare the probability distributions in view of the robust design principles, effectiveness and robustness indicators are introduced. Here, effectiveness is defined as the ability of the design option to optimise the performance, while robustness is defined as the ability to stabilise this performance for the entire range of input uncertainties.

At the end of the thesis, the methodology is illustrated on the thermal design of comfortable and affordable robust low-energy dwellings. Although this application is simplified, general observations can be made. Most attention needs to be paid on the ventilation system and air tightness, since ventilation losses are more important than conductive heat losses when U-values around 0.2 W/m^2K are applied for walls, roofs and floors. In order to avoid overheating in summer, sunscreens seem to be essential. Furthermore, raising awareness for the impact of user behaviour, night ventilation and the size of the dwelling seem to be as important as the application of energy efficient measures.

Beknopte samenvatting

Bij het berekenen van gebouwprestaties worden doorgaans deterministische simulaties gebruikt. Aangezien vele invloedsparameters van nature onzeker zijn, kan dit leiden tot onbetrouwbare voorspellingen van de ontwerpimpact en vandaar tot extreme verschillen tussen ontwerp en werkelijkheid. Zulke verschillen zijn gewoonlijk ongewenst: opdrachtgevers willen immers garanties dat hun investeringen de gewenste impact hebben. Daarom zijn de algemene doelstellingen van dit onderzoek (1) de ontwikkeling van een probabilistische robuuste ontwerpmethodologie om deze onzekerheden mee te nemen in de analyse en optimalisatie van gebouwprestaties en (2) haar illustratieve toepassing op het thermische ontwerp van comfortabele en betaalbare robuuste lage-energiewoningen.

In de ontwikkelde methodologie worden verschillende ontwerpopties met elkaar vergeleken op basis van de kansverdeling van de bestudeerde prestaties. Daarvoor wordt een meerlagige Monte Carlo onzekerheidsanalyse uitgevoerd die alle opties onderwerpt aan dezelfde onzekerheden en zo de overeenkomstige kansverdelingen van de prestaties berekent. Een bijkomende gevoeligheidsanalyse onderzoekt welke onzekerheden het meest dominant zijn voor deze distributies. Omdat deze benadering erg tijdrovend kan zijn, kan het rekenmodel in deze thesis optioneel worden vervangen door een veel sneller metamodel, zonder de betrouwbaarheid aan te tasten. De methodologie maakt ook een expliciete studie van de ontwerpopties voor verschillende scenario's, zoals het gebruikerstype of economische evoluties, mogelijk, als dit gewenst is. Om de kansverdelingen numeriek te vergelijken met oog op de principes van robuust ontwerp, worden de indicatoren effectiviteit en robuustheid geïntroduceerd. Effectiviteit is gedefinieerd als de mogelijkheid van de ontwerpoptie om de prestatie te optimaliseren, terwijl robuustheid als de mogelijkheid om de prestatie te stabiliseren over het hele bereik van de onzekere invloedsparameters.

Op het einde van de thesis wordt de methodologie geïllustreerd met het thermische ontwerp van comfortabele en betaalbare robuuste lage-energiewoningen. Hoewel deze toepassing vereenvoudigd is, kunnen enkele algemene opmerkingen worden gemaakt. Het ventilatiesysteem en de luchtdichtheid verdienen de meeste aandacht aangezien ventilatieverliezen belangrijker zijn dan geleidingsverliezen als U-waarden van ongeveer 0.2 W/m^2K worden gekozen voor wanden, daken en vloeren. Om oververhitting in de zomer tegen te gaan, lijkt zonwering essentieel. Bovendien blijkt de bewustmaking over de impact van gebruikersgedrag, nachtventilatie en woninggrootte net zo belangrijk als de toepassing van energie-efficiënte maatregelen.

Abbreviations

std	standard deviation
AIC	Akaike Information Criterion
BES	Building Energy Simulation
BIC	Bayesian Information Criterion
CDF	Cumulative Distribution Function
EED	Energy Efficiency Directive
EPBD	Energy Performance of Buildings Directive
EPC	Energy Performance Contracting
ESCO	Energy Service Company
GCV	Generalised Cross-Validation
IDEAS	Integrated District Energy Assessment Simulation
KR	Kriging
LHS	Latin Hypercube Sampling
MAE	Maximal Absolute Error
MARS	Multivariate Adaptive Regression Splines
NN	Neural Network
PR	Polynomial Regression
RBF	Radial Basis Function
RMSE	Root Mean Squared Error
SNR	Signal-to-Noise Ratio
SRC	Standardised Regression Coefficient
SSM	State Space Model
TE25	Temperature Exceeding hours of 25 °C
QMC	Quasi Monte Carlo
WTE25	Weighted Temperature Exceeding hours of 25 °C

List of Symbols

μ	Mean value
ρ	Density (kg/m^3)
ρ	Spearman's rank correlation coefficient
σ	Standard deviation
ε	Effectiveness
c	Specific thermal capacitance (J/kgK)
$CDF(x)$	Cumulative distribution function
$CDF^{-1}(x)$	Inverse cumulative distribution function
e	Error
$f(x)$	Function
n_{50}	Air change rate at pressure difference of 50 Pa (h^{-1})
P	Percentile
Q	Heat transfer (W)
r	Pearson product-moment correlation coefficient
R_P	Robustness for percentage P included sample points
T	Temperature (K)
t	Time (s)
U_t	Input vector at state t
V	Volume (m^3)
v_{50}	Air change rate per m^2 heat loss area at pressure difference of 50 Pa (m^3/hm^2)
X	Input (parameter, vector or matrix)
X_t	State vector at state t
Y	Output (parameter, vector or matrix)

Contents

List of Figures

List of Tables

1

Introduction

1.1 Problem statement and objectives

In engineering and economics, uncertainty analysis by means of reliability and risk assessment is already well established for calculations regarding structural engineering (Melchers, 1987), earthquake risks (Mcguire, 2001), nuclear safety (Marquès et al., 2005), flood risks (Apel et al., 2006), wind turbine reliability (Tavner et al., 2007; Wu et al., 2009), spacecraft design reliability (Bozzano et al., 2014), the insurance business (Gatzert and Wesker, 2014), etc. The aim of such assessments is to quantify the system reliability or the failure risk in order to guarantee the system performance. For that purpose, several methods have been developed, which are related to the probability theory for gambling applications.

When focussing on the area of building performance, some studies on hygrothermal reliability and risk assessments can be found as well, such as the air exchange reliability (Pietrzyk and Hagentoft, 2008*a*,*b*) and mould growth risk (Sadovsky et al., 2014). However, such studies are rather limited because building performance analyses and designs are rarely determined by strict failure criteria. Nevertheless, many aspects in such building physical problems would benefit from a probabilistic approach. Most problems, such as following examples, however, make use of deterministic[1] simulations, hence neglecting the inherent variability and uncertainty of the problem. Building performance **analyses** typically examine the performances of specific configurations for comparison with performance criteria. Some examples are the analysis of Hens et al. (2001) in which the reduction of CO_2 emissions of a building stock is studied and the analysis of Abuku et al. (2009) that examined the impact of wind-driven rain on mould growth risk, indoor climate and energy use in historic brick buildings. Decision-making or **design**, moreover, optimises these analysed performances in order to choose the most optimal solution between several

[1] In fact, the word *deterministic* refers to a situation in which no uncertainty is involved, and hence, everything is known about the system. However, in literature and also in this thesis, it is used as a synonym for a *fixed value* approach.

alternatives. This is, for example, illustrated for the decision on retrofit measures based on CO_2 emission and financial costs by Verbeeck and Hens (2005), and based on CO_2 emission and energy savings by Cellura et al. (2013), and by the design of extremely low-energy dwellings based on energy use, environmental impact and financial costs by Verbeeck and Hens (2007).

The neglection of the inherent variability and uncertainty of geometries and configurations, of workmanship and realisation failures, of material and component properties, of internal loads and boundary conditions, of economical and environmental parameters, etc. in such problems may lead to inconclusive analyses and non-optimal designs. Hence, a **probabilistic methodology** as proposed in this thesis is therefore to be preferred. This methodology will allow the propagation of the input uncertainties to the uncertainty of the performance in order to include not only the mean performance but also its corresponding spread in the assessment. Furthermore, the methodology will facilitate the consideration of robustness. In **robust design**, mean performance is optimised while spread is minimised, resulting in a design that can resist the influence of uncontrollable factors as good as possible without eliminating the uncertain influences (Sanchez et al., 1996; Zang et al., 2005). Robust design thus implies quality improvement and assurance, as clearly illustrated in Fig. 1.1. Such robust designs enhance the reliability of the results and would hence be beneficial in building performance design.

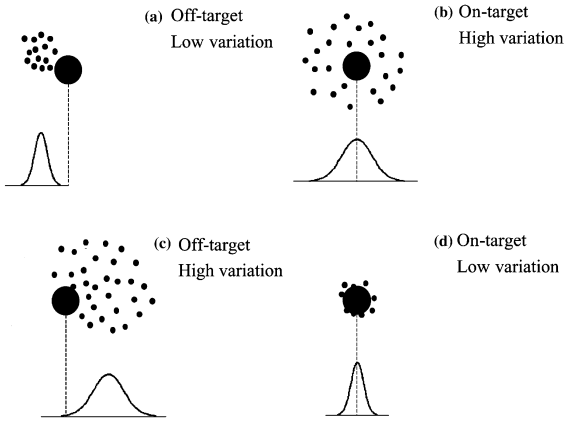

Figure 1.1: Robust design illustration. Figure taken from (Zang et al., 2005). (d) is a robust design since its performance is close to the target value with a low variation.

In this thesis, the probabilistic methodology will be illustrated on the robust design of low-energy dwellings. Due to climate change and fossil fuel depletion challenges, energy efficiency is a rising concern of policy makers. Therefore, several countries agreed on limiting their greenhouse gas emissions in the frame of the Kyoto Protocol (UNFCCC, 2008). The European Union furthermore approved the binding targets - known as 20-20-20 - for 2020 to (1) reduce greenhouse gas emissions by 20 % compared to 1990, (2) raise the share of energy use produced by renewable sources to 20 %, and (3) improve the energy efficiency by 20 % (European Commission, 2007). Since the building stock is responsible for about 40 % of the total energy use in industrialised countries (IEA, 2008), major efforts are made on energy efficiency of

these buildings, both for renovations and new constructions. Consequently, all new buildings should be low-energy (EPBD, 2002), while passive and nearly zero-energy buildings will become the standard in the near future (EPBD, 2010). Despite this movement towards energy-efficient dwellings, it is not clear how to design a dwelling that will perform as targeted. Large performance gaps are undesirable, both from the point of view of the building owner and/or occupant in particular as well as society in general. Building owners and/or occupants need confidence in the return on their investments in, for example, energy efficiency and indoor climate, while governments want to ensure that their subsidy programs have the desired impact to meet the described targets. In order to study this, three very different geometries of real Flemish dwellings will be selected for which the performances - concerning thermal comfort, energy and costs - will be optimised by selecting the most appropriate design options. Building physical decisions such as the choice of insulation thickness and ventilation system will be made without changing the architectural design in order to provide overall applicable design guidelines. Probabilistic parameters such as user preferences and energy price evolutions will be taken into consideration in order to introduce this uncertainty in the dwelling performance.

The overall aim of this thesis is thus:

- to develop an overall applicable probabilistic design methodology in order to include inherent uncertainties in the design process and to be able to incorporate the robust design principles, and
- to illustrate the methodology on the thermal design of comfortable and affordable robust low-energy dwellings.

1.2 Outline

In order to achieve the overall aim, this thesis is divided into several chapters. **Chapter 2** provides a literature overview of uncertainty quantification, mainly in building performance analysis and design. Based on this, the objectives will be established.

Chapter 3 then describes the case study of the low-energy dwelling that will be used to illustrate the methodology throughout the thesis. The semi-detached dwelling of Fig. 1.2 is chosen as case study geometry. In this example, the dwelling geometry is fixed and the building physical elements, such as insulation thicknesses, have to be selected.

Chapter 4 explains the fundamentals of the proposed probabilistic design methodology, of which a brief overview is given at the start of the chapter. Uncertainty quantification is used to study the propagation of the uncertainties of the input to the uncertainties of the output. Sensitivity analysis moreover identifies those input parameters that are most dominant in this propagation. Furthermore, meta-modelling is introduced as time-efficient method by replacing a time-inefficient model by a fast mathematical model and multi-layered sampling is proposed to reliably compare several design options, optionally for certain future scenarios.

Figure 1.2: Case study dwelling.

Based on references in literature and simple illustrations, the utility of these four fundamentals of the global methodology (uncertainty quantification, sensitivity analysis, meta-modelling and multi-layered sampling) will be demonstrated.

The actual probabilistic design methodology is described in further detail in **Chapter 5**. In order to provide a clear understanding of the different steps, each step is illustrated based on the low-energy dwelling case study. Furthermore, several alternatives of the methodology steps are discussed.

After the probabilistic design methodology is developed, it is illustrated on the design of affordable and comfortable low-energy dwellings in **Chapter 6**. Several objective functions will be used in order to select a robust low-energy dwelling design for the fixed geometry of the dwelling in Fig. 1.2. These results will be compared with the results of two additional dwellings with a different geometry in order to generalise the conclusions.

Finally, **Chapter 7** will provide a global discussion of the proposed methodology and corresponding research results. Future perspectives of follow-up research will be discussed as well.

1.3 Content source

Each of the chapters is based on the work presented in the following publications:

- **Journal papers:**

  - **Van Gelder, L.**, Das, P., Janssen, H., Roels, S. Comparative study of metamodelling techniques in building energy simulation: guidelines for practitioners. *Simulation Modelling Practice and Theory, 49,* 245-257. **Contribution**: main author, responsible for content and research.

  - **Van Gelder, L.**, Janssen, H., Roels, S. (2014). Probabilistic design and analysis of building performances: methodology and application example. *Energy and*

Buildings, 79, 202-211. **Contribution**: main author, responsible for content and research.

- **Conference papers:**

  - **Van Gelder, L.**, Janssen, H., Roels, S. (2014). Economically effective and robust low-energy dwellings. In Malki-Epsthein, L. (Ed.), Spataru, C. (Ed.), Marjanovic-Halburd, L. (Ed.), Mumovic, D. (Ed.), *Proceedings of the 2014 Building Simulation and Optimization Conference.* Londen, UK, June 23-24. **Contribution**: main author, responsible for content and research.

  - **Van Gelder, L.**, Janssen, H., Roels, S. (2014). Reliability of meta-modelling in robust low-energy dwelling design. *Proceedings of 10th Nordic Symposium on Building Physics.* Lund, Sweden, June 15-19. **Contribution**: main author, responsible for content and research.

  - **Van Gelder, L.**, Janssen, H., Roels, S., Verbeeck, G., Staepels, L. (2013). Effective and robust measures for energy efficient dwellings: probabilistic determination. *Building Simulation 2013.* Chambéry, France, August 26-28. **Contribution**: main author, responsible for content and research.

- **Research reports:**

  - Janssen, H., Roels, S., **Van Gelder, L.** and Das, P. (2014). *IEA EBC Annex 55, Subtask 2, Probabilistic tools.* **Contribution**: main author and researcher of meta-modelling chapter, co-responsible for research of other chapters.

  - Staepels, L., Verbeeck, G., Bauwens, G., Deconinck, A., Roels, S., **Van Gelder, L.** (2013). *BEP2020: betrouwbare energieprestaties van woningen. Naar een robuuste en gebruikersonafhankelijke performantie.* (in Dutch) **Contribution**: main author and responsible for dynamic simulations and related research.

2

Objectives

Chapter 1 described the need for a probabilistic design methodology in order to include inherent uncertainties in the design process and to be able to incorporate the robust design principles as illustrated in Fig. 1.1. This robust design approach will be one of the major innovative aspects of the developed methodology. This chapter will provide an overview of the state-of-the-art in probabilistic problem solving and robust design in order to translate the objectives of Chapter 1 in concrete research questions. Since the methodology will be illustrated on the design of affordable and comfortable low-energy dwellings and in order to keep this overview concise and focused on the problem statement, this overview is mainly given based on building performance literature, in which probabilistic assessments were introduced in the eighties. More technical literature will be provided in Chapter 4, where the several probabilistic techniques used in the probabilistic design methodology of Chapter 5 are explained.

2.1 State-of-the-art

Building performance problems deal with several uncertainties. These uncertainties can be due to 'the lack of knowledge or data' needed for the studied problem or due to 'the intrinsic randomness of the phenomenon' examined in the problem (Beyer and Sendhoff, 2007; Kiureghian and Ditlevsen, 2009). Amongst other uncertainties, uncertainty of thermal conductivity of insulation materials (Domínguez-Muñoz, Anderson, Cejudo-López and Carrillo-Andrés, 2010), thermophysical properties of envelope materials (Prada et al., 2014), weather data (Taylor et al., 2014) and construction quality (Guerra-Santin et al., 2013) are studied in literature. Besides these sporadic studies, a huge interest in the variability of user behaviour is noticed (Sonderegger, 1977; Van Raaij and Verhallen, 1983; Haas et al., 1998; Mahdavi, 2009; Guerra-Santin and Itard, 2010; de Meester et al., 2013).

Section 2.1.1 first describes a measurement campaign in which such uncertainties were studied in order to provide insight into what extent they may vary. Then,

section 2.1.2, 2.1.3, 2.1.4 and 2.1.5 provide an overview of how these uncertainties were handled in literature and what the remaining issues are.

2.1.1 IWT TETRA BEP2020 measurement campaign

The variability in input parameters such as user behaviour and dwelling characteristics has been studied in literature. However, in order to be used in building performance problems such as the one that will be described in Chapter 3, they need to be studied for the considered situation, since they may depend on location, climate and building tradition. Hence, such variabilities have been sporadically studied in measurement campaigns. A recent example of such a measurement campaign, that will be used in this thesis, is the one performed within the Flemish research project *IWT TETRA BEP2020* (Staepels et al., 2013*a*), which investigated reliable solutions for energy efficiency of new dwellings. The project was performed by the Department of Arts & Architecture at PHL University College (UHasselt) and the Building Physics Section at KU Leuven, with the author as main researcher for the latter. Major parts of this thesis were developed within the framework of this study.

A substantial part of the research project consisted of a measurement campaign of 74 new dwellings in Flanders. A data set was collected containing detached, semi-detached and terraced dwellings with both massive and lightweight constructions, and equipped with natural, exhaust and balanced ventilation systems. In order to study the energy-efficiency, the global energy use was measured. Furthermore, detailed monitoring of indoor temperature, CO_2 concentration and relative humidity provided information on variability in user behaviour. A study of as-built specifications and air infiltration measurements additionally provided information on variability in building design. Since all these variations are thought to significantly impact the energy performance, this dataset is presented below in more detail. These results will provide the basis for input distributions further on in this thesis as will be explained in Chapter 3.

Fig. 2.1 and 2.2 show the measured mean **indoor temperatures** of the considered living rooms and master bedrooms, respectively, and this for both winter and summer period (Staepels et al., 2013*c*). Standard deviations of these temperatures are indicated as well. For each dwelling, the **heat loss coefficient** (K level) is given. This is a theoretical indication concerning the overall heat transfer coefficient and the compactness of the building according to the Energy Performance of Buildings Directive (EPBD) in Flanders (EPBD, 2002): the lower the heat loss coefficient, the better the dwelling is insulated. Here, compactness is defined as the heated volume of the dwelling divided by the overall heat loss area. One can see a considerable variation in both mean and standard deviation of indoor temperatures of the considered dwellings. A trend between heat loss coefficient and indoor temperature, however, is not observed. Although external climatic conditions are influencing these temperatures as well, major variability is assigned to differences in user preferences. The constant indoor temperature of 18 °C, which is considered in EPBD, is thus a significant simplification. And since it is believed that the indoor temperature has great influence on the energy use, taking into account the spread of these indoor temperatures will thus be important.

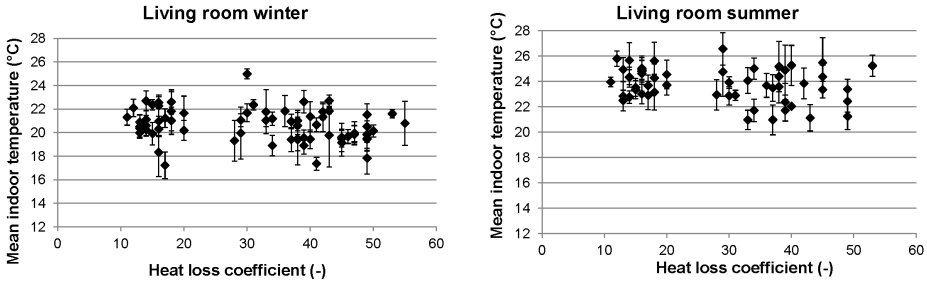

(a) *(b)*

Figure 2.1: Measured mean indoor temperatures of the living rooms plotted as a function of the overall heat loss coefficient of the dwelling with indication of standard deviations.

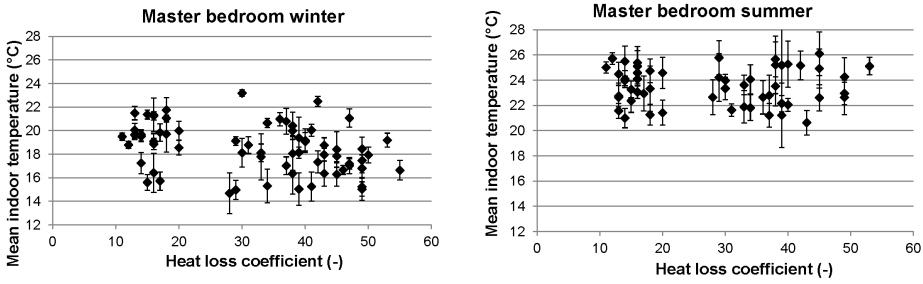

(a) *(b)*

Figure 2.2: Measured mean indoor temperature of the master bedrooms plotted as a function of the overall heat loss coefficient of the dwelling with indication of standard deviations.

Fig. 2.3 shows **CO_2 measurements** in living rooms and master bedrooms as an indication for the indoor air quality (Staepels et al., 2013*b*). For the bedrooms, only measurements between 01:00 and 05:00 AM are taken into account, because CO_2 concentrations are only essential when people are present. As **indoor air humidity** can provide an indicator for this indoor air quality as well, Fig. 2.4a shows dwelling-averaged vapour pressure differences in function of outdoor temperature (Staepels et al., 2013*b*). Each point is a weekly average and thus multiple points per dwelling are provided. For all **ventilation systems**, a significant variation in indoor air quality is noticed. Although indoor CO_2 and moisture production affect these CO_2 and indoor humidity as well, major variability probably can be assigned to differences in air change rates. These in turn are caused by variations in user behaviour or set points of the ventilation system, and to a lesser extent in climatic conditions. Air change rates do not only affect indoor air quality, but of course also have an inversely proportional relationship to the energy performance.

Finally, Fig. 2.4b shows **air tightness** (v_{50}) in function of dwelling **compactness** for all detached, semi-detached and terraced dwellings in the data set. The v_{50}-value indicates the usually undesirable air change rate through building components, connections and gaps per m^2 heat loss area at a pressure difference of 50 Pa. One

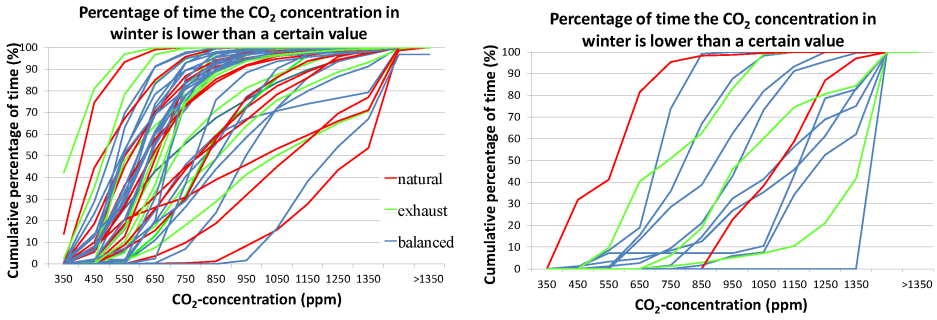

(a) living room *(b) master bedroom*

Figure 2.3: CO_2 concentration of dwellings in winter.

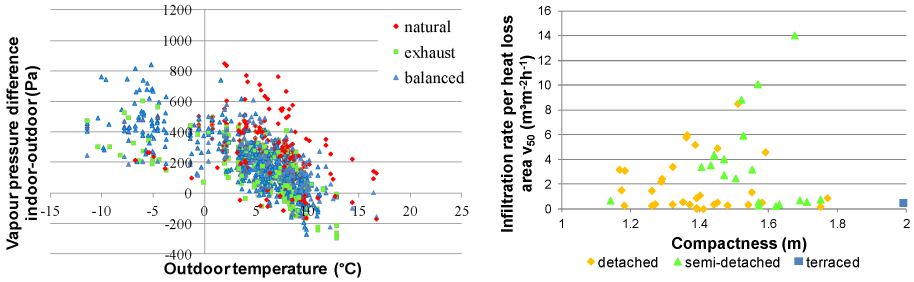

(a) *(b)*

Figure 2.4: Week-averaged vapour pressure difference (a), and infiltration rate per heat loss area (b) of dwellings.

can observe a large variety in v_{50}-value for all dwelling types, independent of the compactness. When attention is being paid to limit this air infiltration, v_{50}-values are usually lower.

2.1.2 Uncertainty and sensitivity analysis

In order to deal with the variability and uncertainty of input parameters in building performance problems, probabilistic procedures are necessary to propagate the uncertainties of the input to the uncertainties of the output and to identify these input parameters that are most dominant in this uncertainty quantification. In areas where reliability is crucial, such as nuclear safety (Marquès et al., 2005) and structural engineering (Vanmarcke, 1983; Melchers, 1987; Ghanem and Spanos, 1991; Sudret, 2007; Lemaire, 2009), it is already common to deal with such variability by means of reliability and risk assessments. The aim of such assessments is to quantify the system reliability or the failure risk in order to guarantee its performance.

Problems in which such reliability assessment is not mandatory, deterministic simulations are commonly used. However, in order to incorporate the inherent uncertainties, methods to calculate the probability distribution of the performance

are preferred and have been developed as well, such as spectral methods using polynomial chaos expansion (Ghanem and Spanos, 1991; Debusschere et al., 2004; Sudret, 2007). Since many problems, such as the building performance case study described in Chapter 3, often are characterised by transient and non-linear behaviour and numerous contributing input parameters, the developed methods cannot be translated in a straightforward way (Janssen et al., 2014). Therefore, a variety of methods have been explored in literature, for which a concise overview for building performance problems is given below. However, until today, an overall applicable methodology has not been provided.

Uncertainty quantification

Hokoi and Matsumoto (1988) and Jiang and Hong (1993), for example, experimented with **stochastic differential equations**, which is a probabilistic problem formulation, to calculate the heat demand and indoor temperature distribution of a building based on simplified thermal models. More recently, also Brohus et al. (2012) applied this stochastic differential equation method on two more complicated, although still simplified, case studies in order to determine the variability in dynamic thermal response based on a general heat balance. Although showing the possibilities of the methodology, their approach is very time-consuming.

Some studies on simplified hygrothermal reliability and risk assessments are found as well. Pietrzyk (2000) and Pietrzyk and Hagentoft (2008*a*,*b*), for example, investigated on using the **first order reliability method** (FORM) in order to calculate the air change rate and heat loss reliability. A **safety factor approach** is also frequently used in structural reliability. Such an approach allows the use of deterministic simulations without considering the probabilistic input, however, the safety factors have to be determined in a probabilistic way. Brohus et al. (2009) illustrated this safety factor approach as a simple check whether the energy requirements might be exceeded or not. It is, however, very difficult to determine correct values for the safety factors.

The **Monte Carlo method** is a solution method for probabilistic problems. It is easy in use and has no limitations on the number and type of input parameters and model. One of the first applications on a building performance problem was by Pettersen (1994). A real break-trough of this method in building performance is however attributed to the work of Macdonald and Strachan (2001), Macdonald (2002) and de Wit and Augenbroe (2002). They described how the Monte Carlo technique can be practically used in the building design stage when a detailed simulation program is used. Since then, this technique has numerous applications in building performance problems, such as the studies performed by Haarhoff and Mathews (2006), Verbeeck (2007), Breesch and Janssens (2010), Tian and de Wilde (2011) and Sadovsky et al. (2014). This method will be described in more detail in section 4.2.

Sensitivity analysis

Besides the explorations in uncertainty quantification, building performance researchers also started to study sensitivity analysis. One of the first sensitivity analyses in building physics was performed by Lomas and Eppel (1992). Among several techniques, they concluded that the **Monte Carlo analysis** was the most

flexible to calculate sensitivity indices. Although such Monte Carlo based techniques appeared in literature very frequently (Breesch and Janssens, 2010; Domínguez-Muñoz, Cejudo-López and Carrillo-Andrés, 2010; Tian and de Wilde, 2011), also the one-at-a-time **Morris method** has been very popular for sensitivity analyses. de Wit (1997) found that the Morris method is economical for models with a large number of parameters and it does not depend on any assumptions such as a linear relation between input and output. Examples can be found in the work of de Wit and Augenbroe (2002), Brohus et al. (2009), Corrado and Mechri (2009), Booth et al. (2012), Heo et al. (2012) and Garcia Sanchez et al. (2014). Both the Monte Carlo based techniques and the Morris method will be described in more detail in section 4.3.

Calculation efficiency

During the circulation of the Monte Carlo based techniques, systematically more attention was given to calculation efficiency by means of improved sampling schemes since such techniques are usually time-intensive, especially for complex deterministic models. Besides the basic random sampling, also Latin Hypercube, optimised Latin Hypercube and quasi-random sampling were applied in building performance analyses, since these sampling techniques decrease the number of samples needed as will also be discussed in section 4.2.1. Some examples can be found in the work of Corrado and Mechri (2009) who used Latin Hypercube sampling for the uncertainty analysis of building energy ratings and the work of Eisenhower, O'Neill, Fonoberov and Mezić (2012) who used quasi-random sampling to investigate the energy use distribution of an office building. Janssen (2013) illustrated the improved sampling efficiency of optimised Latin Hypercube sampling on several simple hygrothermal case studies. Burhenne (2013) did the same for quasi-random sampling for a simple mathematical model and a building performance simulation model.

Limitations

Although uncertainty and sensitivity analyses are already widespread for building performance problems and a lot of research has been done with respect to reliability, efficiency and applicability of these techniques, much of the applications have focused on specific and delimited issues without providing an overall applicable methodology. The current state-of-the-art thus remains highly fragmented. This thesis therefore aims at merging that fragmented knowledge into a structured and comprehensive methodology including all described achievements, while tackling the remaining shortcomings and limitations as will be described in section 2.2.

2.1.3 Probabilistic output evaluation and design

As a result of the above-mentioned probabilistic analysis, the building performance indicators are no longer single-valued, but are to be evaluated based on their probability distribution, such as illustrated in Fig. 2.5. This example shows one of the evaluated design options of Chapter 6. In here, the probability distribution of the output performance WTE25, which is an overheating indication, is presented. In

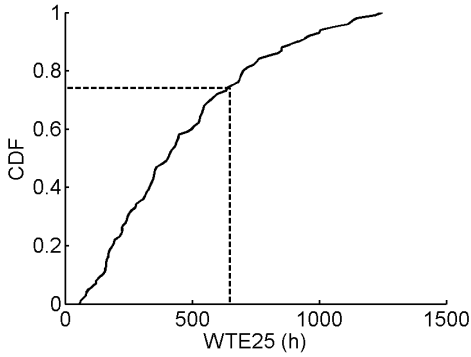

Figure 2.5: Cumulative distribution function of WTE25, which is an overheating indication. Probability that performance is lower than a certain value is indicated.

order to evaluate this design option, the probability that WTE25 is lower than 650 h, which is the preferred upper limit as described in Chapter 3, is indicated.

Based on such probability distributions, the performance can be compared with the performance criteria and probabilistic designs can be performed. Probabilistic design is a more recent extension to this uncertainty quantification in building performance problems and aims at comparing several design options in order to select the most optimal one. Several examples of how was dealt with the probability distributions in building performance design are given below.

Examples in building performance designs

de Wit and Augenbroe (2002) and Kim et al. (2014) proposed to compare design alternatives based on a utility function that describes how preferred a certain (deterministic) performance is by the decision maker. In order to include the variability of the performance, they calculated the expected utility for each alternative based on the average performance. Determining this utility function, however, is not straightforward. Kim et al. (2014) also took the preferences of multiple stakeholders into account. Booth and Choudhary (2013) visually compared output distributions for some refurbishment measures in order to decide how to cost-effectively retrofit the UK housing stock. Although they describe the overall methodology extensively, the question how probabilistic output distributions should be numerically evaluated and optimised in probabilistic design is not answered. Hopfe et al. (2013) described the comparison of two heating/cooling systems in view of ten performances such as the overheating hours and energy use based on the individual preferences of three stakeholders. The performances are compared based on minimal and maximal values. Sulaiman and Olsina (2014) moreover proposed several indicators to account for the time that certain indoor comfort limits for temperature and relative humidity are exceeded in order to allow for a comparison of several designs.

Limitations

Previous literature review shows that probabilistic design based on uncertainty analysis was only recently introduced in building performance assessments. Since

until today there is no straightforward approach how to numerically evaluate output distributions, no coherent approach for probabilistic design is yet available. This thesis therefore aims at extending the uncertainty analysis approach to a probabilistic design approach. A structured and comprehensive methodology including all described achievements, while tackling the remaining shortcomings and limitations is therefore the objective as will be described in section 2.2.

2.1.4 Robust design

As already described in Chapter 1, robust design is a very interesting approach in many engineering problems when dealing with uncertainties. In robust design, mean performance is optimised, while spread is minimised, resulting in a design that can resist the influence of uncontrollable factors as good as possible without eliminating the uncertain influences (Phadke, 1989; Sanchez et al., 1996; Tsui, 1996; Jin and Sendhoff, 2003; Zang et al., 2005).

Robust design in literature

Since this robust design will be crucial in the probabilistic methodology proposed in this thesis and only very limited applications in building performance problems are found, first the development is briefly presented. This robust design was introduced by Taguchi for physical experiments in manufacturing and product design since the 1950s. He proposed maximising the signal-to-noise ratio (SNR), equal to $-10\log_{10}(MSD)$ with MSD the mean squared deviation of the performance. Maximising this SNR means minimising the variation and thus improving the robustness. In order to do so, a carefully selected set of design options was combined with a set of noise factors in the so-called crossed array approach and a statistical model of this SNR was then created (Phadke, 1989; Zang et al., 2005; Beyer and Sendhoff, 2007). The panel discussion of Nair et al. (1992) pointed out that the ideas of Taguchi have been very useful and resulted in a breakthrough of the robust design method, however, also provoked a lot of discussion. A critical review is also provided by Tsui (1996). Shoemaker et al. (1991), for example, proposed to first make a meta-model to capture all design options and noise factors based on a combined array and perform the robust design based on this meta-model, since the crossed array of design and noise parameters can be time-consuming. They modelled the performance instead of the SNR, also because this is much simpler. Their approach was illustrated by Sanchez et al. (1996) and Hijar-Rivera and Garcia-Castellanos (2009) as well on computer and physical experiments respectively.

Furthermore, a direct trade-off between mean performance and variation instead of only the SNR, for example, is often preferred since optimisation of the mean might conflict with minimisation of the variation (Jin and Sendhoff, 2003; Du et al., 2004; Zang et al., 2005). Du and Chen (2000) provided an overview of methods for this purpose. The probabilistic feasibility formulation using Monte Carlo simulations is believed to be the most appropriate method. Amongst others, Jin et al. (2003) suggested the use of meta-modelling for that purpose.

In more recent research, the combination of reliability-based and robust design was also explored. This is, for example, done by Rathod et al. (2013) and Shahraki and Noorossana (2014).

Robust design in building performance problems

Based on this widespread robust design research, the ideas of robustness were also introduced in the building performance field (Nguyen et al., 2014). Bordass and Leaman (1997) and Leyten and Kurvers (2006), for example, described the need to focus more on robust instead of optimal performance when designing building systems. More complex systems usually have a better theoretical performance. However, more errors can occur with these systems, hence resulting in worse performance. Moreover, de Wilde (2014) reviewed the gap between predicted and measured energy performance of whole buildings due to inherent uncertainties in the design stage. He stressed the benefit of testing buildings for their robustness, so that they can accommodate change of use and occupancy.

To respond to this increasing interest in robust design, some robustness assessments already appeared in literature. Hoes et al. (2009), for example, studied the thermal performance of a simplified office room. However, as the study only focused on robustness against user behaviour, the optimal design resulted in a building with low thermal mass and large glassed facades, that is indeed least influenced by user behaviour but most by external influences. Moreover, the indoor comfort of this optimal design is far from optimal: the internal temperatures rise up to 48 °C. Hoes et al. (2011) improved this approach in a study of the energy use and thermal performance of a simple apartment. In a first approach, they deterministically calculated the set of optimal designs and then selected one based on their robustness. In a second approach, they calculated the set of optimal designs based on the mean performances. Since the robustness was, however, only examined after the set of optimal design solutions was selected, the benefit of robust design - the trade-off between mean performance and variation - was partially missed and some robust designs might be overlooked.

Also in later studies, this trade-off did not appear. Hopfe et al. (2012, 2013), for instance, investigated robustness by means of best and worst performances for respectively the energy performance and thermal comfort of an office building. Rysanek and Choudhary (2013) studied the cost optimisation of building energy retrofits for an office building. Therefore, they considered technical and economic uncertainties. For these uncertainties, however, only optimistic and pessimistic values are selected and combined with each other. To assess the robustness, they also considered only best and worst case, or they looked only at the robustness and not at the overall performance. When no trade-off is applied, only obvious solutions can be found as was the case in the study of Fabi et al. (2013). They studied a robust office building design in view of occupant behaviour. Therefore, the standard deviations of energy performance and air change rate are examined under variation of user behaviour, and this for three different climates. O'Brien (2013) already had a look at the whole probability distribution when comparing the robustness of two sunscreen

systems for several occupant types in view of energy use for lighting. However, these distributions were only visually compared.

Limitations

In contrast to the widespread robust design theory, the building performance applications only deal with a limited approach to robustness. Furthermore, when only focussing on robustness, there is a potential pitfall that the obtained designs are far from architectural desires, i.e. concrete bunkers. Therefore, the developed probabilistic methodology will incorporate and enhance these robust design principles in order to provide a full method for robustness assessments for building performance applications in practice.

2.1.5 Meta-modelling

Another movement is ascribed to the development of meta-modelling, which will be further discussed in section 4.4. Meta-models mimic the original, potentially time-intensive model with a simpler and faster surrogate model. Applications are, however, rather rare in building performance uncertainty and sensitivity analysis. Eisenhower, O'Neill, Fonoberov and Mezić (2012) and Burhenne (2013), for example, suggested meta-model based sensitivity analysis to overcome the potential time barrier linked to the Monte Carlo techniques. According to Hopfe (2009), meta-models are also very useful in probabilistic optimisation, which makes use of probabilistic analysis. Hopfe et al. (2012) therefore applied this on a building performance problem.

Besides this sporadic use in probabilistic analysis and design, some more applications of meta-models can be found in building performance literature for deterministic optimisation (Mahdavi and Gurtekin, 2004; Chlela et al., 2009; Eisenhower, O'Neill, Narayanan, Fonoberov and Mezić, 2012; Ferreira et al., 2012; Gossard et al., 2013) or prediction (Hygh et al., 2012; Catalina et al., 2013) purposes.

Meta-models can be used to improve the calculation efficiency by replacing a time-consuming deterministic model by a much faster model. Although the meta-models themselves are computationally inexpensive to run, they are not always constructed in the most time-efficient way. Mahdavi and Gurtekin (2004), for example, used about 1 000 samples to fit their meta-models, Eisenhower, O'Neill, Narayanan, Fonoberov and Mezić (2012) and Ferreira et al. (2012) both about 5 000, Catalina et al. (2013) about 9 000 and Hygh et al. (2012) even used 20 000 samples.

Because of the benefits of meta-modelling in view of calculation efficiency, it will be included and further developed in the methodology as will be described in section 2.2.

2.1.6 Conclusions

Based on the state-of-the-art review, this thesis aims at proposing a methodology to quantify performance spread, and to design materials, components, buildings,

neighbourhoods, ... taking uncertainties into account in an efficient and reliable way. This methodology will combine the already existing achievements in the literature of section 2.1.2, 2.1.3, 2.1.4 and 2.1.5. Meanwhile, the remaining shortcomings and limitations, such as calculation efficiency, reliability, output evaluation and applicability of robust design, will be tackled. Compared to probabilistic analysis, much less effort has been put in probabilistic design. Therefore, the developed probabilistic methodology will mainly focus on probabilistic design, in which probabilistic analysis will be seen as a special (simplified) application.

2.2 Objectives

As described in Chapter 1, the overall aims of this thesis are:

- **Objective 1** to develop an overall applicable probabilistic design methodology in order to include inherent uncertainties in the design process and to be able to incorporate the robust design principles, and
- **Objective 2** to illustrate the methodology on the thermal design of affordable and comfortable low-energy dwellings based on this methodology.

These objectives are divided into the following concrete research questions based on the literature review.

Question 1.1: How can we take uncertainties into account in evaluating building performances?

As introduced in section 2.1, building performance problems deal with several input uncertainties. These uncertainties obviously have an impact on the calculated performance. Since a deterministic approach neglects the expected performance spread, while the quantification of this spread might be very meaningful for the addressed problem, a probabilistic approach is often highly desirable. Several techniques are available to propagate the input uncertainties to the performance uncertainties as described in section 2.1.2, however, the knowledge how to efficiently and reliably use them is highly fragmented.

Since design problems are based on such analyses, a probabilistic approach is also needed to reliably select most optimal design options, as described in section 2.1.3. To illustrate this, Fig. 2.6 presents a dwelling design problem. In here, a ventilation system has to be selected based on the net present cost of the studied dwelling. One can see that both the natural and balanced system have a significant variability. Hence, making this design decision based on the deterministic net present cost (i.e. about the median value), would ignore this useful information and would not always be reliable. Furthermore, the variability seems to be much higher for the natural system, whereas the deterministic values (i.e. about the median value) are almost identical.

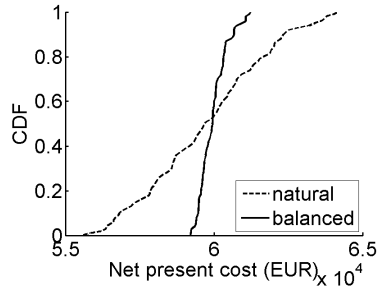

Figure 2.6: Comparison of two ventilation systems based on the net present cost. The probabilistic solution can be compared with the deterministic because the deterministic values are about the median values.

Question 1.2: How can we select well-performing design options with a reduced spread through robust design?

As discussed before, a potential spread on the performance might be undesirable in design problems. Building owners and/or occupants need confidence in the return on their investments in, for example, energy efficiency and indoor climate, while governments want to ensure that their subsidy programs have the desired impact to meet public targets. The development and promotion of effective and robust building envelopes and service solutions is thus an important step to avoid large deviations between design and actual performances, and thus to reduce the influence of uncertain conditions. Therefore, section 2.1.4 already described the robust design principles from literature.

In the design problem of Fig. 2.6, the balanced system seems to be much more robust against the net present cost compared to the natural system. Their average performance is however very similar. Hence, the balanced system would be preferred because of its more guaranteed net present cost.

Question 1.3: How can we select optimal designs that are scenario-independent?

In such probabilistic or robust design problems, one might also be interested in an explicit evaluation for several scenarios. Such scenarios are, for example for a dwelling, the future climate, energy price evolutions or the user behaviour of the occupants. Since it is not possible to predict these parameters and they might be important in the assessment, an explicit evaluation might be wanted. That way, design options that are (almost) optimal in all future situations can be selected to overcome potentially bad future performances. Such design options then are called scenario-independent.

Again, this can be illustrated with the design problem of Fig.2.6. Since the net present cost is a trade-off between the investment costs and the energy cost, this future energy cost may influence the decision-making. Therefore, in order to guarantee the optimal net present cost of the balanced ventilation system, the robust design can be performed for a range of energy price evolutions.

Question 2: How can we design affordable and comfortable low-energy dwellings?

The probabilistic methodology (objective 1) will be illustrated on the robust design of low-energy dwellings to show that the methodology works. As described in Chapter 1, a shift towards energy-efficient dwellings in noticed, however, it is not clear how to design a dwelling that will perform as targeted. In order to study this, different geometries of real Flemish dwellings will be selected for which the performances - concerning thermal comfort, energy and costs - will be optimised by selecting the most appropriate design options. Building physical decisions such as the choice of insulation thickness and ventilation system will be made without changing the architecture of the dwelling in order to provide illustrative design guidelines.

2.3 Applicability of developed methodology

In order to ensure the applicability of the proposed probabilistic design methodology, each step will be accurately illustrated and, based on the second objective, a complete illustrative design problem will be provided at the end of the thesis. Although this application is simplified, general observations can be made that might help architects in the decision-making of a dwelling design and governments in the formulation of their policy concerning energy-efficiency in dwellings. Additional studies might examine the most interesting retrofit measures to subsidise. The methodology allows to investigate which measures are less sensitive to user behaviour and potential future scenarios such as climate change.

Based on the methodology, several other and more complex applications can be performed as well. Due to the extent of the methodology, it is not suitable for single projects of architects. Nevertheless, beside being a very interesting decision tool for governments, the methodology is of huge potential for building companies, project developers and energy service companies (ESCO). One might think of the development of a new social housing neighbourhood, or a large retrofitting project. As stated by Lee et al. (2013), the further development of such ESCOs is indeed hindered by the lack of a proper methodology to calculate the risks of an energy performance contracting (EPC) project. Such an EPC project implies that energy efficiency improvement measures are invested and monitored during the whole term of the contract by the ESCO and the building owners pay for these investments in relation to a contractually agreed level of energy efficiency improvement (EED, 2012). This means that ESCOs want to be able to accurately predict the energy savings and the potential financial risk, but also want to minimise the spread on those savings and thus on the risk by means of robust design.

3

Case study

In order to guide the development of affordable and comfortable low-energy dwellings, this case study handles the performance optimisation of a typical Flemish dwelling. In the frame of the Kyoto Protocol (UNFCCC, 2008) and the 20-20-20 targets (European Commission, 2007), as described in Chapter 1, several governments agreed on limiting their greenhouse gas emissions and increasing the energy efficiency. As a consequence, governments aim at reducing the net energy demand of new buildings as much as possible. From the user perspective, this reduction is only wanted if their investments return. Therefore, their focus is on, for example, the net present cost and the initial investment cost. In order to ensure a comfortable dwelling without the need for cooling, this case study also focuses on the thermal comfort. Since not only a high performance is required, but also a high robustness, this case study will be employed by the robust design method developed in this thesis.

Building physical decisions such as the choice of insulation thickness and ventilation system are being made without changing the architecture of the dwelling. In the robust design method, this is done by selecting the most effective and robust design options. Probabilistic parameters such as user preferences and energy price evolutions are taken into consideration in order to introduce this uncertainty in the dwelling performances. The focus of this case study is mainly on the thermal characteristics and user behaviour. Although this application is simplified, general observations can be made.

The geometry of this typical dwelling is described in section 3.1. Thereafter, the thermal simulation with a building energy model and the cost calculation tool can be found in section 3.2 with all input and output parameters. The optimisation of the thermal comfort, energy use and costs will be presented in Chapter 6 after the robust design method is described in section 5.

3.1 Dwelling geometry

The *IWT TETRA BEP2020* research project (Staepels et al., 2013*a*) investigated reliable solutions for energy efficiency of dwellings. Besides the measurement campaign, of which some results are already described in section 2.1.1, this project included a performance optimisation of five Flemish dwellings, that are representative for the studied building stock. One of these is the semi-detached dwelling (see Fig. 3.1) chosen in this case study. This dwelling has an adjacent dwelling on its west side, in addition to an uninsulated, ventilated basement and overhangs for sun shading on the south and east facade. The facades are presented in Fig. 3.2 and the architectural plans in Fig. 3.3. In the latter figure the day zone (living room, kitchen, ...) is marked in yellow and the night zone (bedrooms, bathroom, ...) in blue. The day zone has a double-height zone which is marked in grey. More characteristics are found in Table 3.1.

In the following chapters, the geometry of this dwelling will be kept fixed to leave the architectural design unchanged, while building physical decisions are being made. This means that the dimensions, orientation and adjacent dwelling are maintained. The construction type of walls and floors can however be replaced by massive components, and the insulation thicknesses and the type of ventilation system for example have to be chosen. Moreover, since this dwelling can house several user types, user behaviour is considered probabilistic, as well as deviations from design values and future economic scenarios.

*Table 3.1: Case study dwelling characteristics. All areas and volumes are calculated based on outer dimensions similar to EPBD, except for the areas marked with *.*

Volume day zone	427 m^3
Volume night zone	163 m^3
Volume basement	265 m^3
Area roof	88 m^2
Area wall	169 m^2
Area floor	88 m^2
Area windows	36 m^2
Area party wall	61 m^2
Width	9.60 m
Depth	9.20 m
Height	6.68 m
Double-height zone*	14 m^2
Liveable floor area*	126 m^2
Compactness	1.54 m
Percentage glazing/floor	22 %

Figure 3.1: Case study dwelling. Replica of Fig. 1.2

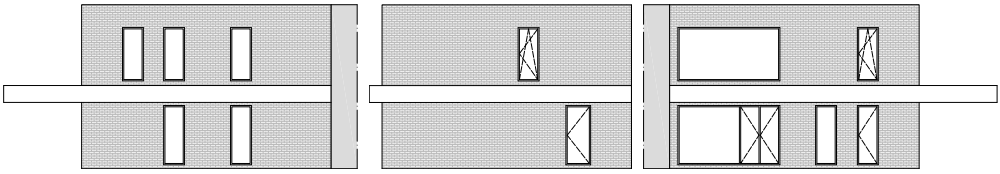

(a) north *(b) east* *(c) south*

Figure 3.2: Facades of case study dwelling.

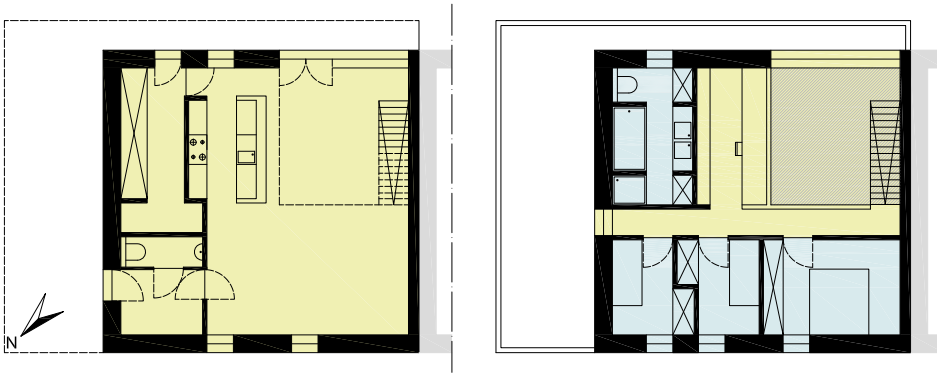

(a) ground floor *(b) storey*

Figure 3.3: Architectural plans of case study dwelling with day zone indicated in yellow and night zone in blue. South orientation is on the top of the figure.

3.2 Simulation model

The dwelling presented in section 3.1 is modelled in a building energy simulation (BES) tool explained in section 3.2.1 in order to perform a robust optimisation of the dwelling performances concerning thermal comfort, energy and costs. The cost-calculation tool needed is described in section 3.2.2. The input and output parameters required in this robust design are discussed in sections 3.2.3 and 3.2.4. Coupling *MATLAB* to the BES and cost calculation tool facilitates changing these input parameter values in order to use them in the probabilistic design.

The same simulation model is used throughout the thesis to illustrate the several steps in the probabilistic design methodology, but some modifications of inputs and outputs are made to vary in case study complexity. These modifications are mentioned in the following chapters when the case study is applied.

3.2.1 Building model

The transient *Integrated District Energy Assessment Simulation* (IDEAS) tool developed in computer language *Modelica* by Baetens et al. (2012), is used to model the case study dwelling and to simulate the outputs needed to evaluate the building performances (see section 3.2.4).

The thermal building model of IDEAS, which is based on the finite volume method, consists of coupled zone and envelope components (Baetens et al., 2012). For these components, the heat flows and temperatures are calculated every time step based on four differential algebraic equations.

The heat balance of a zone component is given by

$$\rho Vc \frac{\partial T(t)}{\partial t} = \sum_s Q_{cs,s}(t) + Q_{c,oa}(t) + Q_v(t) + Q_{inf}(t) + Q_h(t) \tag{3.1}$$

with ρVc the thermal capacity of the air volume, $T(t)$ the zone air temperature, $Q_{cs,s}(t)$ the convective heat transfer of adjacent surfaces s (see Eq. 3.3), $Q_{c,oa}(t)$ the convective internal heat gains by accommodated occupants and allocated appliances, $Q_v(t)$ the heat load by ventilation, $Q_{inf}(t)$ the heat load by infiltration and $Q_h(t)$ the heat load by the heating system.

The exterior surface heat balance of a building envelope component is given by

$$Q_{net,e}(t) = Q_{c,e}(t) + Q_{SW,e}(t) + Q_{LW,e}(t) \tag{3.2}$$

with $Q_{net}(t)$ the heat flow into the component, $Q_{c,e}(t)$ the convective heat transfer, $Q_{SW,e}(t)$ the shortwave absorption and $Q_{LW,e}(t)$ the longwave heat exchange with the surroundings. For slab-on-ground components, this equation is modified based on EN ISO 13370 (2004).

The interior surface heat balance of a building envelope component is given by

$$Q_{net,i}(t) = Q_{c,i}(t) + \sum_s Q_{SW,i,s}(t) + \sum_s Q_{LW,i,s}(t) \tag{3.3}$$

with $Q_{net,i}(t)$ the heat flow into the component, $Q_{c,i}(t)$ the convective heat transfer linked to Eq. 3.1, $Q_{SW,i,s}(t)$ the shortwave absorption of solar light entering the interior zone and $Q_{LW,i,s}(t)$ the longwave radiation exchange with surrounding interior surfaces and accommodated occupants and allocated appliances. Here, shortwave radiation is distributed based on the area and absorptivity of surfaces. Longwave radiation exchange is simplified with a zone radiant temperature for which longwave radiative internal gains are distributed based on the area and emissivity of surfaces (Seem, 1987). For house separating components, radiation is not considered in the adjacent dwelling.

Finally, the one-dimensional heat transfer between the interior and exterior surfaces of building envelope components is solved by subdividing the component in finite volumes. In IDEAS, the number of volumes is related to the reference of three volumes for 20 cm of concrete by the thickness and thermal diffusivity, thus capacity, of the material (personal communication with Baetens R.). For each finite volume, the heat balance is given by

$$\rho V c \frac{\partial T_{FV}(t)}{\partial t} = \sum_c Q_{FV,c}(t) \tag{3.4}$$

with $\rho V c$ the thermal capacity of the control volume, $T_{FV}(t)$ the temperature of the control volume and $Q_{FV,c}(t)$ the energy flux between different control volumes. For windows, Eq. 3.4 is extended for solar absorption by the multiple glass panes, and the presence of gas cavities. Both transmission (in Eq. 3.3) and absorption are made dependent on the angle of incidence of solar irradiation.

The following paragraphs first explain how the dwelling geometry of section 3.1 is implemented in this IDEAS tool. Then, the most essential parameters of Eq. 3.1 to 3.4 are described for this case study. To structure them, they are categorised in boundary conditions, building fabric, building systems and user behaviour. Values for these parameters are chosen in section 3.2.3, inspired by the measurement campaign of section 2.1.1.

Dwelling implementation

The dwelling is modelled in two main zones to differentiate between day and night zones (see Fig. 3.3) and an extra zone for the uninsulated, ventilated basement. External walls, floor, roof and windows are all implemented with determination of the orientation and material layers. The overhangs for sun shading are implemented for the involved windows. Internal walls and floors are modelled as well in order to connect the zones and to add their capacity.

Instead of using outside dimensions for these components and zones as in Table 3.1 used for EPBD calculations, the centerlines of the components are chosen to calculate envelope areas and volumes in the building model in order to balance between

correct inside and outside dimensions for heat loss calculations. This means that the heat loss areas and volumes of Table 3.1 are slightly smaller in the building model.

Boundary conditions

Ground and adjacent dwelling temperatures determine the heat transfer through the basement floor and walls, and the party walls, according to Eq. 3.2 and 3.3 and can be chosen either fixed or variable in time. The external climate is determined by the dwelling location, the meteorological year weather data and the cloud factor. The first term in Eq. 3.2 is defined by the outdoor temperature of the weather data, the second by the solar irradiance and the third by the sky temperature, which is calculated based on the outdoor temperature and cloud factor.

Building fabric

The building fabric consists of several components such as walls, floors, roof and windows, which are implemented in the building model. These components contain several layers with a certain thickness and material. Thermal conductivity, thermal capacity and density of these layers are defined by the choice of material and these material characteristics are included by Eq. 3.4. Note that the heat transfer through the components is one-dimensional and thermal bridges are thus not taken into account.

Solar absorption and longwave heat exchange in Eq. 3.2 and 3.3 are determined by the shortwave absorptivity and longwave emissivity of the outer layers respectively, which are also given by the choice of material. The solar absorption of interior surfaces in Eq. 3.3 is moreover defined by the solar transmissivity of the window glass panes. In Eq. 3.4, the solar absorption of window components is formulated based on this transmissivity as well and on the absorptivity of the glass panes. Both transmissivity and absorptivity are dependent on the incidence angle and determined by the window type.

Furthermore, the air tightness of the building fabric determines the heat load by infiltration in Eq. 3.1. The overall air tightness for the dwelling is given by the n_{50}-value as described in section 2.1.1. This n_{50}-value is assumed to be the same for both considered zones. The air flows are thus considered to be distributed based on the volumes, however when considering them to be distributed based on the loss areas, only slightly different n_{50}-values would be obtained. As the n_{50}-value is given for a pressure difference of 50 Pa, which is not reached in normal conditions, this value is simply scaled by dividing it by the rule of thumb value 20 (Parys, 2013).

Building systems

Both day and night zones are heated in winter with an ideal heating system determined by a nominal heating power and a time-dependent set point for the operative temperature. The actual heating power is directly inserted in Eq. 3.1. The ventilation in Eq. 3.1 is defined by a time-dependent air change rate and optionally a constant heat recovery efficiency. In summer, this heat recovery is switched off.

Sunscreens are implemented by adding a reduced shortwave transmissivity to the exterior layer of windows in Eq. 3.3 and 3.4. These sunscreens can be controlled based on solar irradiance, indoor temperature and/or occupancy patterns.

User behaviour

The above-mentioned building systems are controlled by user behaviour (by means of occupancy profiles, preferred indoor temperatures and applied air change rates). These are used to determine the time-dependent set point temperature and air change rate. The occupancy profiles are also used in sunscreen control.

The indoor temperature measurements of the measurement campaign in section 2.1.1 indicate a terrible summer comfort for part of the dwellings. Hence, to improve the summer comfort in the simulated dwellings, additional summer ventilation is taken into account: when occupants are present and the day zone temperature exceeds the user dependent comfort temperature, the air change rate is doubled for the next six hours or until the occupants leave the dwelling. This algorithm simulates the user behaviour to assist in achieving a comfortable indoor climate.

Furthermore, internal heat gains by accommodated occupants and allocated appliances are considered 50 % convective and 50 % radiative in Eq. 3.1 and 3.3 (EN ISO 13790, 2007). Several time-dependent profiles can be provided.

Finally, the zone air capacity in Eq. 3.1 may be influenced by placing furniture in this zone, which can be considered as user behaviour as well. To include this phenomenon, a multiplicator factor for the zone air capacity is applied.

3.2.2 Cost calculation tool

In order to study building and energy costs in addition to energy use and thermal comfort, a cost calculation tool was made in *Microsoft Excel* in the research project IWT TETRA BEP2020. This tool corresponds to European standard EN ISO 15459 (2007), which only takes the costs of energy-related components into account. It calculates net present costs based on yearly heat demands and auxiliary energy for ventilation with

$$C_G(\tau) = C_I + \sum_{i=1}^{\tau} C_R(i)R_d(i) + \sum_{i=1}^{\tau} C_M(i)R_d(i) + \sum_{i=1}^{\tau} C_E(i)R_d(i) - V_R R_d(\tau) \quad (3.5)$$

with C_G the global cost or net present cost, τ the lifespan of the dwelling, C_I the initial investment costs, C_R the replacement costs, R_d the discount rate, C_M the annual maintenance costs, C_E the annual energy costs and V_R the residual value. The net present cost thus sums the costs in the lifespan of the dwelling, whereby all future costs are discounted to represent its current value.

Investment, maintenance and replacement costs of building components are considered in this tool, as well as the lifespan of these components and of the whole dwelling. Furthermore, a certain heat generation and distribution efficiency for the heating system, the market interest rate and the inflation rate are considered.

The current energy cost for electricity and gas is assumed to increase or decrease every year by the same percentage.

3.2.3 Model input

All input parameters described in sections 3.2.1 and 3.2.2 are divided into deterministic and probabilistic parameters. Fixed values or probability distributions are then ascribed in Table 3.2 and 3.3. This ascription is discussed in the following five categories: boundary conditions, building fabric, building systems, user behaviour, and building and energy costs. Some parameters have strictly discrete values, while others are described by continuous uniform, normal or Weibull distributions. These distributions are inspired by the measurement campaign of 70 new Flemish dwellings described in section 2.1.1. It needs to be emphasised that the results of the robust design presented in Chapter 6 are dependent of the chosen input distributions, that are only as good as known.

Boundary conditions

All boundary conditions are considered deterministic in this case study. Therefore, the values of adjacent dwelling temperature, dwelling location, meteorological year weather data and cloud factor are default values in the BES tool. The typical moderate climate year of Uccle (Belgium) is assumed to be representative for new dwellings in Flanders.

Although these assumptions might have significant influence on energy use and thermal comfort, the focus of this case study is on the thermal characteristics and user behaviour.

Building fabric

Massive constructions are traditionally more common in Belgium, even though timberframe constructions have increased in popularity. Because of this, the construction type of party walls, outer walls, flat roofs, internal walls and internal floors are changeable in the model by providing a massive and timberframe version for each component in order to vary in construction capacity. These components are traditionally composed and have a plaster finishing. The facades are made of masonry. Basement walls and floors are all considered massive as this is also common for timberframe constructions.

The insulation thickness of these components is considered probabilistic and calculated based on the selected U-values. The range of U-values is determined by the observed values for low-energy dwellings in the measurement campaign of section 2.1.1. The U-value of party walls is taken deterministic as heat losses through these walls are negligible when a certain level of insulation is applied. Based on commercially available glazing types, five window types are considered with different U- and g-values to vary heat losses and solar gains through windows.

Overall n_{50}-values are observed in the measurement campaign of section 2.1.1 as well (see Fig. 2.4b) and thus chosen as probabilistic input.

Table 3.2: Deterministic input parameters.

PARAMETER	VALUE
Boundary conditions	
adjacent dwelling temperature	19 °C
dwelling location	Uccle (Belgium)
meteorological year weather data	Uccle (Belgium)
cloud factor	0.2
Building fabric	
basement floor and walls	uninsulated concrete slab
floor between basement and day zone	insulated concrete slab
infiltration rate at 50 Pa in basement	0 h^{-1}
U-value party wall	0.5 W/m^2K
Building systems	
nominal heating power	10 kW
air change rate in basement	2 h^{-1}
User behaviour	
multiplicator factor zone air capacity	5
Building and energy costs	
auxiliary energy for ventilation	according to EPBD
investment, maintenance and replacement costs	see (Staepels et al., 2013*a*)
lifespan building components	see (Staepels et al., 2013*a*)
dwelling lifespan	30 years
heat distribution efficiency heating system	89 %
heat generation efficiency heating system	97 %
market interest rate	4.5 %
inflation rate	2.3 %
current average energy cost for electricity	0.21 EUR/kWh
current average energy cost for gas	0.07 EUR/kWh

Because the building fabric is sensitive to deviations from design values, except for manufactured windows, it is assumed that measured U- and n_{50}-values will be different from the target values. To account for this, a deviation from the design value is introduced by:

$$X_{\text{res}} = X_{\text{des}} \cdot e_{\text{dev}} \tag{3.6}$$

with X_{res} the resulting parameter value, X_{des} the target or design value and e_{dev} the deviation, of which resulting values are used in the BES model. The deviations are assumed normally distributed with a standard deviation of 10 %.

Building systems

The ideal heating system in both day and night zone is determined by a nominal heating power, which is considered deterministic and high enough to heat all studied input combinations. The set point temperature needed for this heating system will be discussed as user behaviour parameter.

Table 3.3: Probabilistic input parameters.

PARAMETER	DISTRIBUTION*
Building fabric	
construction type	massive / timberframe
U-value roof (W/m^2K)	Uni(0.1,0.3)
U-value floor (W/m^2K)	Uni(0.1,0.3)
U-value wall (W/m^2K)	Uni(0.1,0.3)
window type	2.07 W/m^2K & g = 0.613 / 2.07 W/m^2K & g = 0.512 / 1.29 W/m^2K & g = 0.631 / 1.31 W/m^2K & g = 0.551 / 0.7 W/m^2K & g = 0.407
infiltration rate at 50 Pa (1/h)	Uni(0.44,12.3)
deviation from design U-values	Nor(1,0.1)
deviation from design infiltration rate	Nor(1,0.1)
Building systems	
ventilation system	A / A+ / C / C+ / D / D+
heat recovery efficiency (D and D+)	Uni(0.7,0.95)
deviation from design heat recovery efficiency	Nor(1,0.1)
sunscreen type	none / 10 % / 10 % south / 30 % / 30 % south
sunscreen control	manual / automatic 1 / automatic 2 / automatic 3
User behaviour	
occupancy profile day zone	see Table 3.4
occupancy profile night zone	see Table 3.4
set temperature occupancy day zone (°C)	Nor(21,1.35)
set temperature absence day zone (°C)	15 / no reduction
set temperature occupancy night zone (°C)	Nor(19,2)
air change rate (1/h)**	
day zone	Wei(0.4976,4.670)
night zone	Wei(0.8545,4.670)
internal gains persons (W)	Uni(35,175)
basis internal gains appliances day zone (W)	Uni(20,180)
summer internal gains appliances day zone (W)	Uni(130,1000)
winter internal gains appliances day zone (W)	Uni(180,1300)
spring and autumn internal gains appliances (W)	Uni(140,1150)
Building and energy costs	
nominal energy price evolution	-1.5 % / 2.3 % / 10 %

* Explanation of the symbols used:
Nor(μ,σ): normal distribution with mean value μ and standard deviation σ
Uni(a,b): uniform distribution between a and b
Wei(λ,k): Weibull distribution with scale factor λ and shape factor k
Discrete uniform distributions are indicated by the sample values
** In Chapter 4 and 5, as well as in the corresponding papers, an accidentally wrong value for these air change rates is used.

Six types of ventilation systems are implemented: A, A+, C, C+, D and D+. The labelling corresponds to Belgian standard NBN D 50-001 (1991), where natural ventilation is indicated with A, mechanical exhaust ventilation with C and mechanical balanced ventilation with D. The '+' indicates the control by occupant detection. Constant air change rates of day and night zone are coupled to these ventilation systems and are discussed as user behaviour parameter. When occupant detection is applied, the air change rate is lowered 1.67 times for natural ventilation and 100 times for mechanical ventilation when occupants are absent (see Table 3.4 of user behaviour), according to the reduction factors in the Flanders EPBD regulation (EPBD, 2002). These reduction factors are applied to the auxiliary energy in the cost calculation tool as well. Furthermore, type D and D+ are equipped with heat recovery for which several efficiencies are commercially available. Because heat recovery is sensitive to deviations, it is assumed that the actual values will be different from the target values as described by Eq. 3.6. The deviation from the design value is assumed normally distributed with a standard deviation of 10 %. Additionally to day and night zone ventilation, a constant air change rate of 2 h^{-1} is deterministically defined in the basement.

Sunscreens are implemented with five possibilities: no sunscreens, sunscreens on the south facade with a solar transmission of 10 % or 30 % or sunscreens on all facades with a transmission of 10 % or 30 %. The sunscreens are controlled manually or automatically. Four options are studied:

- manually controlled in summer based on indoor temperature (down above 23 °C and up below 20 °C) and occupancy profile day zone (see Table 3.4 of user behaviour),
- automatic 1: control on solar irradiance (down above 250 W/m^2 and up below 145 W/m^2),
- automatic 2: control on solar irradiance (down above 250 W/m^2 and up below 145 W/m^2) when indoor temperature is above 23 °C, and
- automatic 3: control on indoor temperature in summer (down above 23 °C and up below 20 °C).

User behaviour

Based on different work and life-style schedules in the measurement campaign of section 2.1.1, four different day zone and three night zone occupancy profiles are (arbitrarily) considered as presented in Table 3.4. All profiles are considered equally probable. These profiles are used to determine the heating, ventilation and sunscreen control as mentioned above. During weekends, profile 4 is taken for the day zone.

The distributions for the user preferred operative temperatures are based on the measurement campaign of section 2.1.1 (see Fig. 2.1 and 2.2). Set point temperatures for occupancy in day and night zone are presented in Fig. 3.4a. Furthermore, based on the measurement campaign of section 2.1.1 it is assumed that half of the households lower the set temperature of the day zone to 15 °C and all households switch off the heating of the night zone when absent.

Table 3.4: Occupancy profiles.

	Day zone				Night zone		
	1	**2**	**3**	**4**	**5**	**6**	**7**
00:00-06:00					X	X	X
06:00-09:00	X	X	X	X			X
09:00-12:30		X		X			
12:30-17:00			X	X			
17:00-22:30	X	X	X	X		X	
22:30-00:00					X	X	X

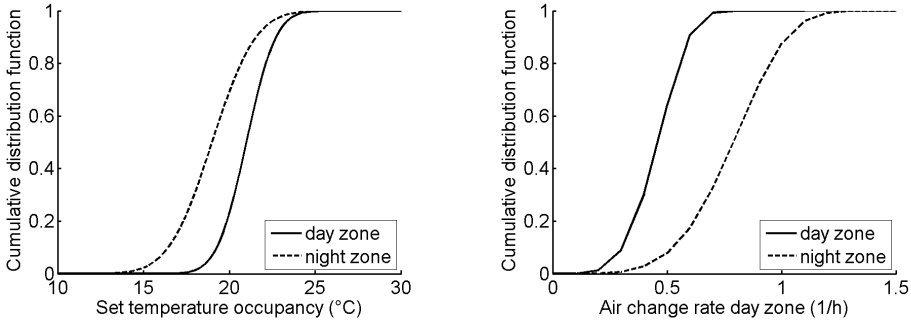

Figure 3.4: Cumulative distribution functions of set temperatures and air change rates.

CO_2 and vapour pressure measurements of section 2.1.1 (see Fig. 2.3 and 2.4a) indicate that air change rates are very variable. Inspired by these findings, Weibull distributions are assumed for the actual air change rates. In these assumed distributions, there is a 50 % probability to have a lower air change rate than the design rate and 99 % for an air change rate lower than 1.5 times this design rate. To illustrate this, Fig. 3.4b shows the implemented distributions of the air change rate for both zones. Unless otherwise stated, the air change rates for day and night zone are fully correlated. For each input combination, one value of these distributions is selected and this air change rate is then kept constant over the year, with exception of temporary changes due to occupant detection or additional summer ventilation as explained before. The comfort temperature at which these air change rates are temporary increased is defined 2 °C above the occupancy set temperature of the day zone given above.

The internal heat gains contain gains by present persons, standby appliances and lighting, and appliances and lighting in use. For each input combination, one value of all presented distributions is selected and these values are then considered constant over the seasons and over the time that someone is present in the zone, and are thus averaged values coupled to the occupancy profiles in Table 3.4. The averaged heat production by individuals is assumed to vary uniformly between 35 and 175 W. This assumes an averaged presence of 0.5 to 2.5 adult persons (when someone is present according to the occupancy profile). In the day zone, the standby

heat production is assumed uniformly distributed and allocated during the whole year. When someone is present in the day zone, a season dependent heat gain by appliances and lighting is added. The three values for those seasonal heat gains are fully correlated to each other.

Finally, the multiplicator factor for the zone air capacity to incorporate furniture is given the default value of the BES tool.

Building and energy costs

Most input parameters for the cost calculation tool are considered deterministic as the focus of the case study is on heat losses, thermal comfort and corresponding energy costs. Moreover, accurate information for these variabilities is lacking. The thermal installation is simplified as a gas boiler with a given heat generation and distribution efficiency according to EPBD (EPBD, 2002) for Flanders, Belgium. The auxiliary energy for ventilation is assumed direct current and estimated according to EPBD as well, potentially influenced by occupant detection as explained before. All inputs are chosen equal to the values in IWT TETRA BEP2020 (Staepels et al., 2013*a*). Inflation is estimated based on Belgian data from the past ten years.

Although energy price evolutions are difficult to predict, three potential scenarios are assumed. A small drop (-1.5 %), a price evolution equal to inflation (+2.3 %) and a sharp increase (+10 %) are considered equally probable.

3.2.4 Evaluated building performances

As dynamic BES model outputs, the heat demand and indoor temperature of both zones are evaluated at intervals of 20 minutes. Building performances concerning indoor thermal comfort, energy use and financial cost are post-processed and studied to compare several dwelling design options in this thesis.

1. Indoor thermal comfort

Indoor thermal comfort can be assessed through different parameters, which are all determined by an acceptable upper limit. It is essential that these limits are not exceeded frequently in order to avoid the need for cooling.

One of the output parameters to assess indoor thermal comfort is the **maximal temperature**. Based on the study of Peeters et al. (2009), a maximal acceptable value for this output is derived. Peeters et al. (2009) provide an upper limit for the indoor temperature as a function of the outdoor temperature at which 90 % of persons are comfortable. This roughly corresponds to a maximal acceptable indoor temperature in summer of 28 °C.

Overheating can be assessed as well based on **temperature exceeding hours**. Therefore, the number of hours with temperatures exceeding 25 °C is calculated for each zone. This output will be referred to as TE25.

These temperature exceeding hours can be further examined by means of **weighted temperature exceeding hours** (WTE). In order to not only account for whether a

certain temperature is exceeded, the weight of this exceeding is also considered according to European standard EN ISO 15251 (2007) and (van der Linden et al., 2002). This weight corresponds to the percentage of dissatisfied persons for that specific temperature. The recommended value of WTE25 for office buildings is 150 occupied weighted excess hours per year. This is translated into 650 weighted excess hours per year for dwellings.

2. Energy use

To assess the energy use, the **heat demand** is computed. For this purpose, the heating power inserted in the zones by the ideal heating system is cumulated over the whole simulated year. Alternatively, this heat demand can be augmented with the auxiliary energy for ventilation in order to obtain the **net energy demand** for heating. Since low-energy dwellings are studied, the purpose is to minimise this heat demand or net energy demand.

3. Financial cost

The heat demand is post-processed to compute the **net present cost** with the cost calculation tool of section 3.2.2. European standard EN ISO 15459 (2007), on which this tool is based, only takes the costs of energy-related components into account. In the further analysis, all costs which are assumed identical for all considered dwelling designs, such as foundation, and household electricity, are thus neglected. The heating system cost is also not included as this is, for reasons of simplicity, assumed independent of the heat demand. Compared to the heat demand, the net present cost will be minimised in the case study. Besides this, also the **initial investment cost** will be studied and minimised.

3.3 Conclusions

This chapter described the case study used throughout the thesis to illustrate the developed probabilistic design methodology. The dwelling geometry of section 3.1 is fixed and the aim is to determine the building physical decisions in order to obtain an effective and robust dwelling concerning thermal comfort, energy use and energy related costs in Chapter 6. For that purpose, building fabric and system parameters of Table 3.3 will be selected as design parameters, except for the deviations from these design values. User behaviour, building and energy costs and deviation parameters will be chosen as uncertainty or scenario parameters. This categorisation will become clear in the next chapter.

To vary in case study complexity, some modifications of inputs and outputs will be made. These modifications are mentioned in the following chapters where the case study is applied.

4

Fundamentals

The probabilistic design methodology which is described in Chapter 5, relies on four probabilistic procedures: uncertainty quantification (section 4.2), sensitivity analysis (section 4.3), meta-modelling (section 4.4) and multi-layered sampling (section 4.5). Uncertainty quantification propagates the input distributions to the output distributions. Multi-layered sampling is used to subject all design options to the same uncertainties and to enable a direct comparison for several scenarios. Meta-modelling allows to replace the original model by a much faster surrogate model. Sensitivity analysis is moreover used to rank contributing input parameters in order to select and determine input parameter distributions.

This chapter aims at providing a good understanding of these procedures that were introduced into building physics over the last decades, inspired by other engineering disciplines as described in Chapter 2. Therefore, a concise overview of available techniques in literature is given. In order to illustrate and compare these techniques, they are applied on the global case study introduced in Chapter 3. The different techniques are discussed and benefits for the probabilistic design methodology are demonstrated. In order to understand why these procedures are fundamentals for the methodology described in section 5, section 4.1 provides a brief overview in which the role of each procedure is handled.

4.1 Overview probabilistic design methodology

The probabilistic design methodology consists of four main steps (see Fig. 4.1), of which only the main aspects are discussed in this section, as they are explained and illustrated in the referred sections of Chapter 5. These steps consist of selecting the input parameters and distributions (step 1), determining the most dominant input parameters and developing a meta-model to improve calculation efficiency (step 2), updating the input distributions (step 3), and finally performing the actual probabilistic design (step 4). In this methodology, both convergence and sampling efficiency are crucial to overcome time issues while obtaining reliable results.

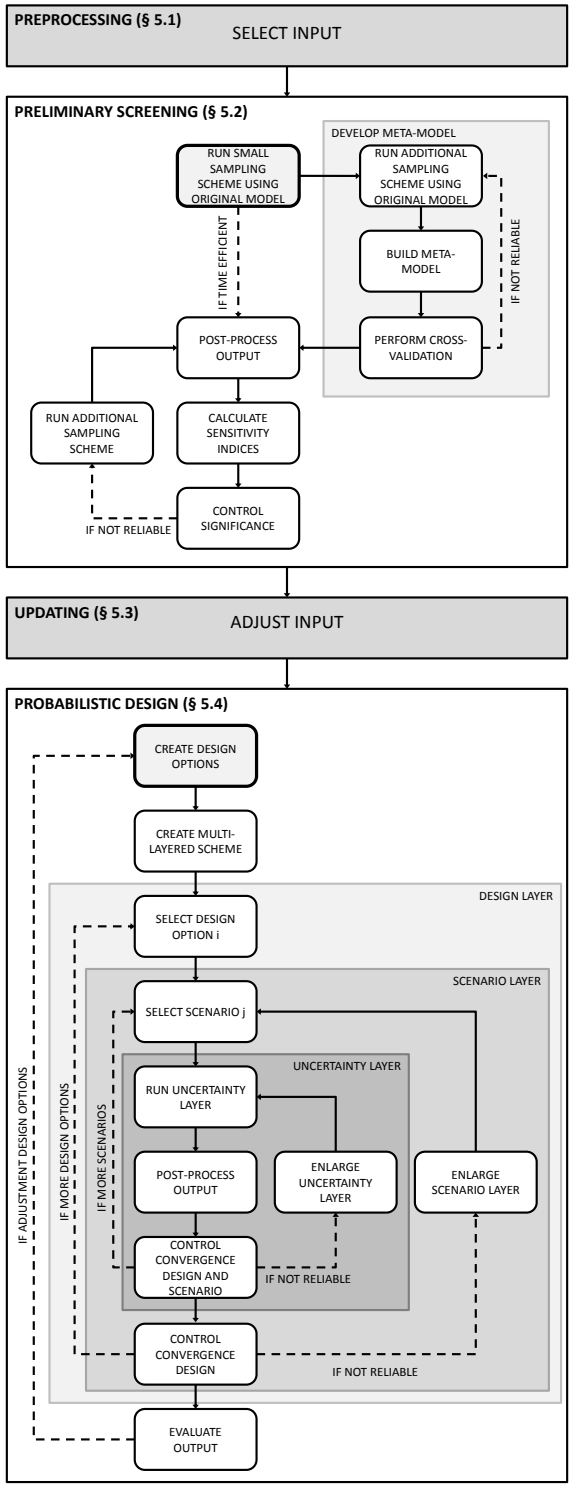

Figure 4.1: Flowchart of probabilistic design methodology.

4.1.1 Probabilistic design

Contributing input parameters of a probabilistic design problem, such as the case study of Chapter 3, can be divided into three categories (Sanchez et al., 1996; Dehlendorff et al., 2011; Hopfe and Hensen, 2011). **Design parameters**, such as the preferred air tightness or thermal resistance, are fully controllable. They are the unknown parameters in the design process, but once a **design option** is selected, the parameter values are known. Inherently **uncertain parameters**, such as user behaviour, are completely uncontrollable by the designer as their values are neither known in the design process nor after, but they can significantly influence the design performance. Finally, **scenario parameters** are inherently uncertain parameters dealing with potential future scenarios, such as economic or climatic evolutions, for which an explicit evaluation is wanted.

Because of these parameter categories, the probabilistic design (step 4) is performed through a Monte Carlo loop with a multi-layered sampling scheme - explained in section 4.2 and 4.5 respectively. The Monte Carlo loop propagates the uncertainties of the input parameters to the uncertainties of the considered performances. By combining this with a multi-layered sampling scheme, all design options are subjected to the same uncertainties and a direct comparison for several future scenarios is enabled. Hence, the performance distributions of all design options due to the inherent uncertainties can be compared for all considered scenarios. As a result, this probabilistic design can be used as an effective decision tool.

4.1.2 Preliminary steps

Prior to performing the probabilistic design of section 4.1.1, the problem is first preprocessed (step 1) to select the output parameters needed for decision making and a suitable simulation model. Contributing input parameters are determined and fixed values or (provisional) input distributions are ascribed for respectively deterministic and stochastic parameters.

Since the proposed multi-layered sampling scheme significantly increases the needed number of runs, time-inefficient models are preferably replaced by a meta-model in the preliminary screening (step 2). Meta-models mimic the original, potentially time-intensive model with a simpler and faster surrogate model as explained in section 4.4 and are therefore already sporadically used in literature to improve optimisation efficiency (see section section 2.1.5). For that purpose, small training and validation sets are run in the original model to construct and validate the meta-model. These sample sets are also used to calculate sensitivity indices - explained in section 4.3 - to rank the input parameters from most to least influencing the output distributions. Such sensitivity analyses have been already widely used in literature as described in section 2.1.2. The time-efficiency and reliability aspects in literature are incorporated in this preliminary screening as well.

Based on the sensitivity ranking, the provisional distributions of most influencing parameters are updated (step 3), while the less influencing parameters can be omitted. Limiting the number of parameters eases collecting the required input distributions

as this can be time-consuming. Moreover, this limits the number of considered design options in the multi-layered scheme. This stresses the importance of the preliminary screening in addition to the actual probabilistic design.

4.2 Uncertainty quantification

The aim of uncertainty quantification is to propagate the variabilities of the input to the uncertainties of the output. Due to the complex, non-linear and transient character of most building performance problems, such as the global case study of Chapter 3, Monte Carlo simulations are often preferred. An overview of Monte Carlo and related sampling techniques is therefore provided in section 4.2.1. Section 4.2.2 describes how the sampling schemes can be efficiently used while controlling the output convergence. Section 4.2.3 deals with taking input correlations into account. These concepts are illustrated in section 4.2.4.

4.2.1 Monte Carlo simulation

The Monte Carlo method, which has its origin in nuclear physics (Metropolis and Ulam, 1949), refers to the repeated execution of a deterministic simulation model $f(x)$ for different values of the input parameters in order to estimate the probability distribution of the output parameters, as illustrated in Fig. 4.2. The Monte Carlo simulation can thus be presented by

$$Y = f(X) \tag{4.1}$$

with $X \in \mathbb{R}^{n \times p}$ the input matrix and $Y \in \mathbb{R}^{n \times q}$ the output matrix, where n is the number of samples, p the number of input parameters and q the number of output parameters.

Traditionally the n input parameter values are randomly selected according to their probability distributions, which can be discrete, uniform, normal, ... Therefore, a random value between 0 and 1 is selected and ascribed to the cumulative

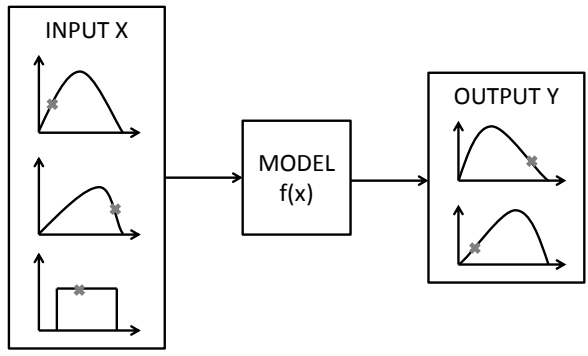

Figure 4.2: Monte Carlo simulation.

distribution function $CDF(X_i)$ of the input parameter i, as illustrated in Fig. 4.3. The corresponding input parameter value can then be calculated using the inverse cumulative distribution function $CDF_{X_i}^{-1}$. In this way, also probabilities based on experimental data which can not be described by theoretical distributions are facilitated.

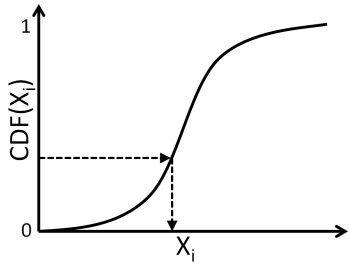

Figure 4.3: Sampling input parameter X_i by sampling value between 0 and 1 of its cumulative distribution function $CDF(X_i)$.

During the past decades, researchers have been developing alternatives for this random sampling with the purpose of decreasing the number of samples needed to assure a reliable output distribution. The evolution of sampling schemes in terms of sampling efficiency has already been widely described in literature (Koehler and Owen, 1996; Burhenne et al., 2011; Prozanto and Müller, 2012; Janssen, 2013) and is summarised here focussing on the most important sampling principles. In this concise review, random sampling, Latin Hypercube sampling, optimised Latin hypercube sampling and number-theoretic methods are described. More sampling strategies can be found in literature, however they are not included in this review because they have no clear advantage for the considered case study of Chapter 3. Importance sampling (Bucher, 1988) is for example more useful for reliability assessments where rare events are more important than for robust design, because this technique aims at sampling more values in one or both 'tails' of the input distributions.

Random sampling

Simple random sampling is the first and most used sampling technique to create the input matrix X as described before (Metropolis and Ulam, 1949). By randomly selecting numerous values of the CDF of the input parameters with a pseudorandom number generator, the input and thus also the output distributions are approached. When, however, only a limited set of samples is used as in Fig. 4.4a, there is no guarantee that all input probabilities are equally sampled. This will of course result in an unreliable output distribution.

Latin Hypercube Sampling

In order to ensure a better coverage of the parameter distributions for few samples, Latin Hypercube Sampling (LHS) was proposed by McKay et al. (1979). LHS divides the cumulative probabilities in n equally probable intervals. Each interval is then randomly sampled once, as can be seen in Fig. 4.4b. When discrete distributions

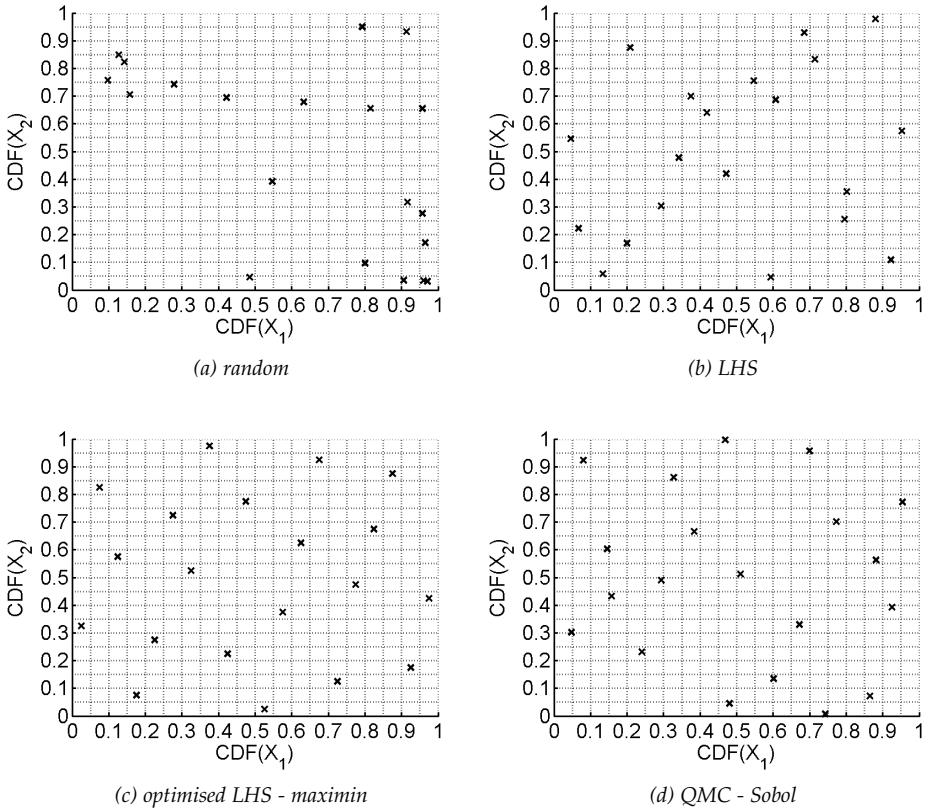

(a) random *(b) LHS*

(c) optimised LHS - maximin *(d) QMC - Sobol*

Figure 4.4: Sampling techniques applied to sample uniform distributed cumulative distribution functions CDF of input parameters X_1 and X_2 twenty times.

are used, n is preferably a multiple of the number of discrete values to equally sample these values. It is proved that less samples are needed for a reliable output distribution when LHS is used instead of random sampling (Stein, 1987; Helton and Davis, 2003; Helton et al., 2005). Although each parameter is sufficiently covered, it is shown in Fig. 4.4b that LHS does not guarantee the whole p-dimensional probability space to be explored. The latter will be solved by using *space-filling* sampling schemes as explained below.

Optimised Latin Hypercube Sampling

The previously described LHS can be further improved by not only covering the input parameter distributions but also filling the p-dimensional probability space. For that purpose, several optimal criteria can be considered to select well-performing LHS schemes in which usually the midpoints of the intervals are sampled.

Two widely used and intuitive criteria are the *maximin* and *minimax* distance (Johnson et al., 1990), respectively maximising the minimal (mostly Euclidean) distance of sampling points and vice-versa. Morris and Mitchell (1995) proposed using a very similar variant of this maximin distance criterion. In order to use such a criterion in

optimising LHS schemes, Morris and Mitchell (1995) presented an iterative algorithm which was further improved by Jin et al. (2005) and implemented by Husslage et al. (2008). The latter algorithm is applied in this thesis (see Fig. 4.4c).

According to Jin et al. (2005), *uniform LHS schemes* are also widely used. These schemes minimise the centered L_2 discrepancy, which is a measure of non-uniformity of a sampling scheme (Fang et al., 2002). The uniformity of the design is thus maximised. Furthermore the authors refer to optimising LHS schemes by maximising the *entropy criterion*, which quantifies the 'amount of information' related to the correlation matrix of matrix X: the higher the entropy, the less knowledge we have on the sample points, thus also the more uniformly sampled they are (Park, 1994).

Number-theoretic methods

Instead of using optimised LHS schemes based on pseudorandom numbers to obtain space-filling sampling schemes, number-theoretic methods that deterministically select sampling points can be used. These methods are also known as Quasi Monte Carlo (QMC) methods and produce point sets or sequences with low discrepancy, thus with a sample distribution close to uniformity as described earlier (Niederreiter, 1987, 1992).

Several low-discrepancy sequences can be found in literature of which the *Sobol sequence* is the most known (see Fig. 4.4d). In this fixed sequence, each sample is calculated based on the previous sample (Sobol', 1967; Bratley and Fox, 1988). A random digital scrambling is used to determine the first point to introduce random behaviour of the sample set in order to create differing sample sets needed for error estimation as will be seen in section 4.2.2 (Hong and Hickernell, 2003).

Other sequences found in literature are for example the *Hammersley sequence* (Hammersley, 1960; Kalagnanam and Diwekar, 1997), the *Halton sequence* (Halton and Smith, 1964), the *Niederreiter sequence* (Niederreiter, 1988) and more recently the *rank-1 lattice rules* of Cools et al. (2006).

4.2.2 Convergence

Sampling efficiency and convergence are two key aspects in Monte Carlo simulation. Efficiency of random and improved sampling was addressed in section 4.2.1, while sampling convergence will be discussed here. Janssen (2013) highlights the value of sequentially adding sample runs and monitoring sampling convergence for being able to stop adding more samples when sufficient accuracy has been reached. Because (optimised) LHS is characterised by the selected number of runs and both (optimised) LHS and QMC lost the random behaviour of random sampling needed for error estimation (Stein, 1987; Hong and Hickernell, 2003), additional samples need to be added in sets in order to control convergence.

Therefore, Janssen (2013) proposed creating s sets of small sampling schemes with size n/s so that the s sets have n samples in total, instead of directly creating a sampling scheme of size n. An indicator for the order of magnitude for the accuracy of the n-run percentiles (or average or standard deviation) can then be calculated

for $s \geq 2$ as follows. First the considered percentile is computed for each available sample set separately. The expected internal standard deviation *std* of the considered Monte Carlo result is then given by

$$std(P) = std_s(P_{1...s})/\sqrt{s} \tag{4.2}$$

where s is the number of sample sets of size n/s, P the considered percentile of a n-run solution, $P_{1...s}$ the s percentiles of the s sample sets and std_s the standard deviation of these s percentiles. Note that the calculation for average and standard deviation is analogous. This expected internal standard deviation can be normalised by division with μ_n, the average value of the n runs, to get a relative deviation. The relative deviations of several outputs can therefore be compared and convergence criteria can be handled when sequentially adding sample sets. For example, one can consider the Monte Carlo result based on s sampling sets as sufficiently converged when a relative deviation lower than 5 % is found. This percentage is of course dependent on the studied problem.

Creating additional sample sets needed for this approach is trivial as randomness is used to generate the samples as explained in section 4.2.1. Additional schemes can also be created by random column permutations of the initial matrix $X \in \mathbb{R}^{\frac{n}{s} \times p}$. As the algorithms for optimised LHS can be quite time-consuming due to the used iterations, the latter approach is preferred by Janssen (2013).

4.2.3 Input correlations

Input matrix X can be easily constructed with one of the sampling techniques described in section 4.2.1. When some input parameters are however correlated, some modifications are needed. For that purpose, the matrix equation approach of Scheuer and Stoller (1962) can be used as described here.

First, the desired correlation matrix Σ of X is defined and decomposed into matrix L:

$$\Sigma = LL^T \tag{4.3}$$

with L any matrix for which Eq. 4.3 is true. Usually the lower-triangular Cholesky matrix as proposed by Scheuer and Stoller (1962) or $L = V\Lambda^{1/2}$ is used with V the Eigenvector matrix and Λ the Eigenvalue matrix. The former is known as the Cholesky decomposition while the latter the Eigendecomposition or principal component analysis. In order to contain the matrix characteristics of X when LHS or QMC are applied, the Eigendecomposition is preferred (Giles, 2013).

The cumulative distributions of p uncorrelated parameters are then uniformly sampled between 0 and 1 (see section 4.2.1) and normalised into matrix Z with zero mean and unit variance, for which

$$U = ZL^T \tag{4.4}$$

is valid. This equation produces a normalised correlated random matrix U based on matrix L and the normalised uncorrelated random matrix Z.

Finally, these normalised samples U need to be translated into the correct distributions of matrix X by:

$$X = CDF_X^{-1}(CDF(U)) \tag{4.5}$$

with CDF_X^{-1} the inverse cumulative distribution functions of X and $CDF(U)$ the cumulative distribution functions of normalised U.

Note that due to the normalisation needed here, the correlation matrix Σ is ascribed to U and is not exactly the same as for the desired X, but is not greatly varying. However, one should be careful and check the resulting correlations and eventually adapt the correlation matrix Σ in order to obtain the desired correlations for X.

For some parameter correlations, it is also possible to combine the correlated parameters into one sampled parameter. This can be the case for for example ventilation system and heat recovery efficiency or fully correlated parameters such as seasonal internal heat gains. Another possibility is to sample one of the correlated parameters and to construct the other based on a correlation function and the sampled deviation from this perfect correlation.

4.2.4 Application

The sampling schemes described in section 4.2.1 are applied to the global case study of Chapter 3, which is adapted to accelerate the dynamic simulation. These schemes are compared based on their cumulative distribution functions and their convergence as introduced in section 4.2.2 in order to illustrate the differences and to select the best performing scheme for further use in this thesis. The convergence control for the different performances will show that the required number of samples cannot be decided in advance, but has to be monitored during the Monte Carlo process. Monte Carlo simulations with and without taking the correlations into account, as explained in section 4.2.3, are also compared to illustrate the impact of such correlations.

Case study

The parameters 'occupancy profile day zone' (1), 'occupancy profile night zone' (5), 'ventilation system' (C), 'construction type' (massive) and 'sunscreen control' (automatic 1) are considered deterministic and their values are mentioned between brackets. For the parameter 'sunscreen type' only the values 'none' and '30 %' are taken into account. The internal heat gains are simplified by a uniform distribution between 100 and 500 W assigned to 'basis internal heat gains appliances day zone'. Only the core BES model is run to obtain the heat demand, maximal temperature and TE25. The cost calculation tool and corresponding input parameters are consequently not needed. These simplifications result in 14 input parameters with the aforementioned distributions. Furthermore, following (fictive) input correlations r are defined:

- set temperature occupancy day zone - set temperature absence day zone: 0.7,

- set temperature occupancy day zone - set temperature occupancy night zone: 0.6,
- set temperature absence day zone - set temperature occupancy night zone: 0.5,
- air change rate day zone - air change rate night zone: 0.8, and
- deviation from design infiltration rate - deviation from design U-values: 0.75.

Sampling schemes

For each sampling technique, ten sets of twenty samples are created while taking the correlations into account with the Eigendecomposition. Fig. 4.5 shows the calculated CDFs of the output parameters. One can see that in this case using all 200 samples results in very similar CDFs. When looking at the extreme values, they are not always sampled with the maximin technique as a result of the midpoint sampling. In the case studies in this thesis, we are however not interested in these rare extremes.

Fig. 4.6 shows the relative deviations according to the normalised version of Eq. 4.2 for the three output parameters and different sampling schemes for two times until ten times 20 samples. To illustrate this equation, the convergence of mean values and 50 % and 75 % percentiles are shown. One can see that for all sampling techniques the accuracy of the Monte Carlo results generally increases with increasing number of samples. Janssen (2013) therefore correctly stresses that the suggestion of Lomas and Eppel (1992) and Macdonald (2009) that the accuracy does not improve much above 100 runs, needs to be falsified.

As Fig. 4.4 already suggested, random sampling performs worst and improved sampling best for most results. The differences between the improved sampling schemes are however limited. Although, one might conclude that the space-filling maximin and Sobol schemes perform generally best, especially for smaller sample sizes. Note that it is not impossible that random and LHS sampling can provide reliable results even for few samples, however, this is less likely and space-filling schemes are thought to be more reliable for that purpose (Koehler and Owen, 1996; Burhenne et al., 2011; Prozanto and Müller, 2012; Janssen, 2013).

Moreover, the accuracy is dependent on the output distribution. The accuracy of the maximal temperature is much higher than of TE25. To obtain a relative deviation less than 5 %, one needs more samples for random sampling than for maximin sampling and much more for TE25 than for maximal temperatures. More samples are also needed to obtain accurate percentiles compared to accurate mean values.

Input correlations

Since the maximin sampling scheme appeared to have one of the best performances, this technique will be used in this thesis. Hence, correlations are only studied for such schemes. Taking input correlations into account has an influence on the output distributions, as shown in Fig. 4.7 for the maximin sampling scheme. Coupling input parameters by their correlations can be seen as an increase of output variability. For the heat demand for example, the standard deviation is increased by about 20 % when correlations are taken into account. Small differences can be observed

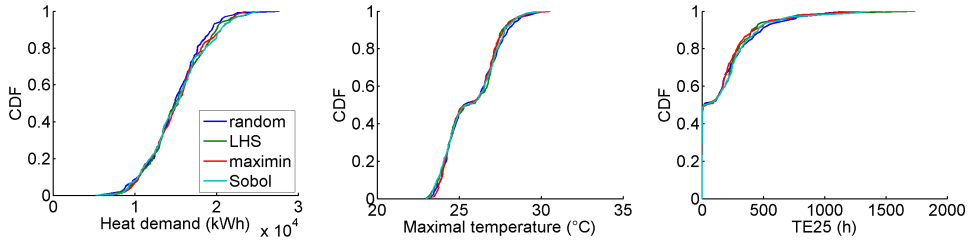

(a) (b) (c)

Figure 4.5: Cumulative distribution functions for different sampling schemes.

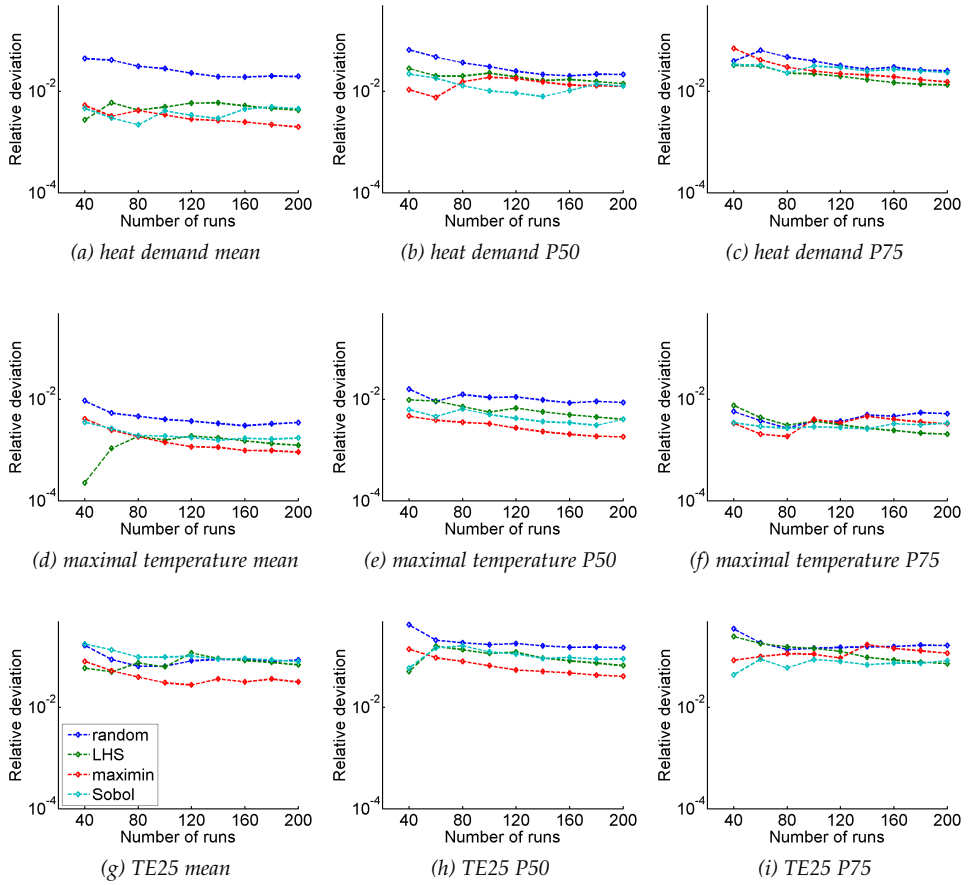

(a) heat demand mean (b) heat demand P50 (c) heat demand P75

(d) maximal temperature mean (e) maximal temperature P50 (f) maximal temperature P75

(g) TE25 mean (h) TE25 P50 (i) TE25 P75

Figure 4.6: Convergence of mean values (left column) and 50 % (middle column) and 75 % percentiles (right column) for different sampling schemes.

between the application of Cholesky decomposition and Eigendecomposition as well. When looking at output convergence in Fig. 4.8 for TE25, one notices the slightly better performance of the Eigendecomposition over the Cholesky decomposition. The Eigendecomposition is thus preferred when applying a space-filling scheme such as the maximin LHS, as also stated by Giles (2013).

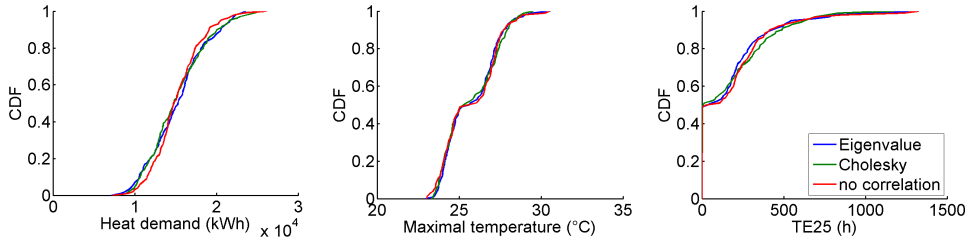

(a) *(b)* *(c)*

Figure 4.7: Cumulative distribution functions with and without correlations.

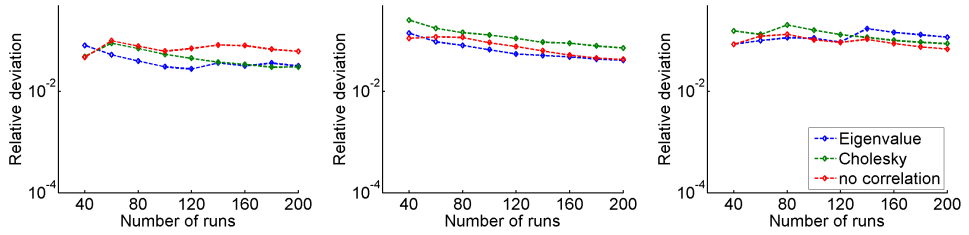

(a) mean *(b) P50* *(c) P75*

Figure 4.8: Convergence of mean values and 50 % and 75 % percentiles of TE25 with and without input correlations.

4.2.5 Conclusions on uncertainty quantification

This section described how uncertainties in input parameters can be propagated to uncertainties in the output parameters through several Monte Carlo sampling techniques. The better performance of optimised LHS (such as maximin) and number-theoretic methods (such as Sobol) over random sampling and LHS was illustrated.

It was also shown that the number of samples needed for reliable outputs is dependent on the output distribution itself. Therefore, it cannot be decided in advance how many samples are required. For that purpose, sampling convergence monitoring was handled. The most efficient way of sampling is to simultaneously add small sample sets until the outputs are sufficiently converged.

Furthermore, including input correlations in the sampling schemes was discussed. The Eigendecomposition is slightly preferred over the Cholesky decomposition when applying a space-filling scheme.

4.3 Sensitivity analysis

Sensitivity analysis is linked to uncertainty analysis, described in section 4.2, as its aim is to identify these input parameters that are most dominant in the uncertainty analysis. Several sensitivity techniques are described in section 4.3.1. Section 4.3.2

explains how the reliability of sensitivity results can be studied. These concepts are illustrated in section 4.3.3 in order to demonstrate the importance of sensitivity analysis in the probabilistic design methodology.

4.3.1 Sensitivity analysis techniques

Sensitivity analysis is the determination of the impact that input parameter distributions have on the output distributions based on a set of input/output combinations. Analogously to section 4.2.1, a set of input values (input matrix X) is therefore run in simulation model $f(x)$ to obtain a set of output values (output matrix Y). How input matrix X is created depends on the used sensitivity technique; some techniques need a Monte Carlo set similar to uncertainty analysis, while for other techniques a specific input matrix is required. Sensitivity indices are then calculated, and these allow to rank the input parameters from most to least influencing the output distributions (Saltelli et al., 2008).

Dozens of sensitivity techniques are available in literature (Hamby, 1994, 1995; Helton and Davis, 2002; Saltelli et al., 2008; Das et al., 2014), however not all of them are reliable, as observed in IEA EBC Annex 55 Subtask 2 (Janssen et al., 2014). A limited selection of techniques that are most flexible, reliable and widely used is discussed here. First, the Morris method, which is a one-at-a-time screening method, is discussed. This is followed by scatter plot, standardised regression coefficient, Pearson product-moment correlation coefficient and Spearman's rank correlation coefficient. These are all related correlation based methods for which Monte Carlo is used to create input matrix X.

Morris method

The Morris method or elementary effects method is a widely used one-step-at-a-time method, meaning that in each sample of matrix X only one parameter value is changed (Saltelli et al., 2008). An elementary effect is defined as:

$$EE_i = \frac{f(CDF_X^{-1}(q_1, q_2, \ldots, q_i + \Delta, ..., q_p)) - f(CDF_X^{-1}(q_1, q_2, \ldots, q_p))}{\Delta} \tag{4.6}$$

with p the number of independent input parameters, q_i the quantile of input value x_i, CDF_X^{-1} the inverse CDF to calculate value x_i from q_i, $f(x)$ the model to create output Y and Δ a fixed increment. The input parameters are thus sampled according to their cumulative distributions in the p-dimensional unit space, which is divided in k equal probable levels, including 0 and 1. Δ is then a value in $\{1/(k-1), \ldots, 1-1/(k-1)\}$, preferably equal to $k/(2(k-1))$ with k an even number.

The distribution of elementary effects for the i^{th} input parameter F_i is obtained by randomly sampling different quantiles in the discretised unit probability space and is finite. The total number of elementary effects is $k^{p-1}[k - \Delta(k-1)]$ for Δ equal to $k/(2(k-1))$. Instead of calculating all elementary effects, r elementary effects are sampled from each F_i, resulting in $r(p+1)$ simulation runs. The first sample of each trajectory r is sampled randomly in the discretised unit probability space.

Then in each following run the quantiles are one by one successively augmented with Δ. Each trajectory r thus contains $p+1$ samples and the j^{th} sample is only differing from the $(j-1)^{\text{th}}$ for one of the input parameters. These r trajectories can be generated randomly, but more optimal is to generate multiple trajectories and select the subset with the highest Euclidean spread. In order to generate input matrix X, values for k and r have to be chosen. The higher these values, the more reliable the method, however also the more time-consuming. The higher k is chosen, the higher r should be.

Once input matrix X is generated and run, r elementary effects are available for each of the i input parameters. In order to rank the input parameters, the sensitivity indices are calculated as follows:

$$\mu_i = \frac{1}{r}\sum_{l=1}^{r} EE_i^l \tag{4.7}$$

$$\mu_i^* = \frac{1}{r}\sum_{l=1}^{r} |EE_i^l| \tag{4.8}$$

$$\sigma_i^2 = \frac{1}{r-1}\sum_{l=1}^{r} (EE_i^l - \mu)^2 \tag{4.9}$$

with i the input parameter, μ_i the mean of F_i, μ_i^* the mean of the distribution of absolute elementary effects, σ_i the standard deviation of F_i and EE_i^l the l^{th} elementary effect of input parameter i. μ indicates the overall influence of the input parameter on the output and σ the variation of this influence. It is recommended to evaluate both statistics at the same time, because when the sign of the elementary effects is changing, μ would be low but σ high. Based on these statistics the input parameters can be classified as negligible (low μ and low σ), linear (high μ and low σ), or non-linear or interacting with other input parameters (high σ) (Garcia Sanchez et al., 2014). An alternative is to study μ^* as the only statistic. High values of μ^* then indicate the most influencing input parameters.

Scatter plot

The most intuitive technique of determining parameter sensitivity is plotting the output parameter values Y against the input parameter values X, which are created with a Monte Carlo technique as described in section 4.2.1 (Hamby, 1994; Helton and Davis, 2002; Saltelli et al., 2008). These plots allow to qualitatively identify the most influencing input parameters. Because of their simplicity, scatter plots are often used.

Standardised regression coefficient

Standardised regression coefficients (SRCs) are sensitivity indices based on a simple linear regression (Helton and Davis, 2002; Saltelli et al., 2008). The input parameters are for that purpose sampled in matrix X and run according to section 4.2.1. Model

$f(x)$ is for each output parameter approximated with:

$$\hat{Y} = b_0 + \sum_{i=1}^{p} b_i X_i \tag{4.10}$$

with $\hat{Y}$ the estimation of $f(X)$, p the total number of input parameters, b_i the regression coefficients and X_i the input values. The coefficients b_i are computed by least-square minimisation of the errors between $\hat{Y}$ and output vector Y_j. In order to exclude influence by parameter magnitudes, the coefficients are standardised by:

$$\beta_i = b_i \sigma_{X_i} / \sigma_{Y_j} \tag{4.11}$$

with β_i the standardised regression coefficients, σ_{X_i} the standard deviation of input parameter i and σ_{Y_j} the standard deviation of output parameter j. This standardisation allows to compare the coefficients and rank the input parameters.

Because SRCs are based on Monte Carlo simulations, this technique provides an exploration of the entire input parameter space. Although the coefficients are calculated for a linear model, they give an indication of sensitivity for slightly non-linear models as well (Saltelli et al., 2008). As long as the relation has an overall trend, non-monotonous relations can be captured by such linear regression as well.

Pearson product-moment correlation coefficient

The Pearson product-moment correlation coefficient, or Pearson's r, is a sensitivity index that indicates the linear correlation between an output and input parameter based on Monte Carlo results and is thus related to the regression coefficient (Hamby, 1994; Helton and Davis, 2002). The values r can vary between -1 and +1, with -1 a total negative linear correlation, 0 no linear correlation and +1 a total positive linear correlation. Pearson's r for input parameter X_i and output parameter Y_j is calculated as:

$$r_{X_i,Y_j} = \frac{\sum_{k=1}^{n}(x_{i,k} - \bar{X}_i)(y_{j,k} - \bar{Y}_j)}{\sqrt{\sum_{k=1}^{n}(x_{i,k} - \bar{X}_i)^2}\sqrt{\sum_{k=1}^{n}(y_{j,k} - \bar{Y}_j)^2}} \tag{4.12}$$

with n the number of samples, $x_{i,k}$ the k^{th} value of input parameter vector X_i, $\bar{X}_i$ the mean value of input parameter i, $y_{j,k}$ the k^{th} value of output parameter vector Y_j and $\bar{Y}_j$ the mean value of output parameter j.

Spearman's rank correlation coefficient

The Spearman's rank correlation coefficient, or Spearman's ρ, is related to the Pearson's r (Hamby, 1994). Both the input values of X_i and output values of Y_j are ranked according to their magnitude and renumbered according to this ranking, with 1 the lowest value and n, which is the sample size, the largest. The Pearson's r of these ranked inputs is then calculated with Eq. 4.12, resulting in the Spearman's ρ. This sensitivity index thus indicates the degree of monotonicity between input and output and varies between -1 and +1 as well. Non-monotonous relations will therefore been overlooked as well.

4.3.2 Reliability of the sensitivity analysis

Since as few samples as needed are preferred due to computational costs and as it is believed that reliability of sensitivity indices increases with increasing number of samples, it is essential to check the significance of influencing parameters by the p-value or the convergence of the indices.

P-value

P-values can be calculated for SRCs, Pearson's r's and Spearman's ρ's by testing the hypothesis of zero coefficients. These p-values are the probability of randomly getting a coefficient as large as calculated, when the true coefficient is zero. This means that low p-values, usually smaller than 5 %, indicate significant coefficients (Das et al., 2014). Typically, these p-values are larger for less influencing parameters and when less samples are used. If some parameters show significant impact on the output, one can conclude the preliminary screening; otherwise, more samples are needed.

Convergence

For all sensitivity techniques, the convergence of the indices can be controlled similar to the convergence of Monte Carlo results in section 4.2.2. Therefore, matrix X is sampled in s sets, the sensitivity indices are calculated for each of these s sets and according to Eq. 4.2 the expected internal standard deviation is calculated. The indices are sufficiently converged when their relative deviations are below a user defined percentage, eg. 5 %. More samples can be added if the indices of dominant parameters are not yet converged.

4.3.3 Application

The sensitivity techniques described in section 4.3.1 are applied to the global case study of Chapter 3, which is simplified as described in section 4.2.4. First the Morris method is discussed, followed by the Monte Carlo based techniques, in order to compare them and to decide on the most appropriate technique for the current case study. Finally, the advantages of sensitivity analysis for the probabilistic design methodology are explored.

Morris method

As described in section 4.3.1, the Morris method requires a set of new samples with specific characteristics and neglecting input correlations. The number of input parameters p is 14 and the number of levels k and trajectories r has to be chosen. Increasing r will increase reliability and therefore r will be selected based on the results as shown later. k is chosen even and equal to 10 to deal with the discrete values of both 'window type' and 'sunscreen type' with respectively five and two options. Increment Δ is then determined by $k/(2(k-1))$ and the total number of elementary effects is $5{\times}10^{13}$.

Tables 4.1 and 4.2 show the statistics for respectively two and ten trajectories. Each trajectory contains 15 samples, thus respectively 30 and 150 samples are processed. Dominant parameters can be determined by comparing mean values and standard deviations of r elementary effects, as illustrated in Fig. 4.9 for ten trajectories. Negligible parameters are indicated in grey in the tables. The dominant parameters have both high mean values and high standard deviations. This means that the overall influence of these parameters is high and that the values of the elementary effects are also influenced by the values of the other input parameters. Comparing both tables learns that the same dominant parameters are determined by both sample sizes, although the values change significantly. Both statistics can be replaced by μ^*, which determines indeed the same dominant parameters as presented in Tables 4.1 and 4.2. Comparing μ with μ^* learns that the signs of the effects are for this case always the same because their magnitudes are almost equal.

In order to decide on the number of trajectories r, the convergence of two input/output combinations is checked in Fig. 4.10. One can see that the relative deviation of μ^* of ten trajectories is still above 5 %, which is not sufficiently reliable. Because of the ten input levels, more trajectories are thus needed to have more reliable sensitivity results.

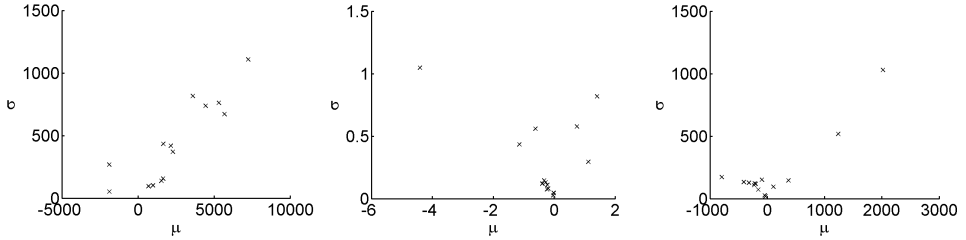

(a) heat demand *(b) maximal temperature* *(c) TE25*

Figure 4.9: Standard deviations of elementary effects in function of mean values for Morris method with ten trajectories.

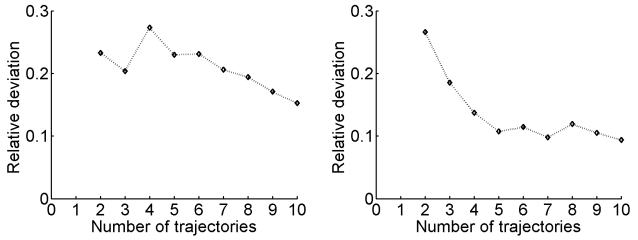

(a) Heat demand - set temperature occupancy day zone *(b) Heat demand - U-value wall*

Figure 4.10: Convergence of μ^* of dominant and non-dominant input parameters in Morris method.

Table 4.1: Morris method with two trajectories. Non-dominant input parameters are indicated in grey.

		μ^*	μ	σ
HEAT DEMAND	set temp. occ. day zone	11950.474	11950.474	2787.549
	set temp. abs. day zone	2670.637	2670.637	224.445
	set temp. occ. night zone	7231.837	7231.837	1222.930
	air change rate day zone	3251.830	3251.830	1636.318
	air change rate night zone	3204.936	3204.936	2175.784
	infiltration rate at 50 Pa	7003.871	7003.871	1485.429
	U-value roof	908.769	908.769	43.583
	U-value floor	792.830	792.830	506.491
	U-value wall	1502.388	1502.388	400.342
	window type	2499.849	-2499.849	51.539
	sunscreen type	1437.535	1437.535	620.230
	internal heat gains	2036.570	-2036.570	24.383
	deviation infiltration	2038.094	2038.094	1537.774
	deviation U-values	1734.769	1734.769	58.628
MAXIMAL TEMPERATURE	set temp. occ. day zone	2.946	2.946	2.943
	set temp. abs. day zone	0.003	-0.003	0.003
	set temp. occ. night zone	0.546	0.546	0.520
	air change rate day zone	0.418	-0.418	0.415
	air change rate night zone	0.622	-0.622	0.540
	infiltration rate at 50 Pa	0.166	0.155	0.166
	U-value roof	0.172	-0.172	0.170
	U-value floor	0.238	-0.238	0.234
	U-value wall	0.030	-0.030	0.023
	window type	0.217	-0.217	0.171
	sunscreen type	4.326	-4.326	0.704
	internal heat gains	0.371	0.371	0.370
	deviation infiltration	0.005	-0.005	0.005
	deviation U-values	0.019	0.014	0.019
TE25	set temp. occ. day zone	4689.300	4689.300	4418.700
	set temp. abs. day zone	29.10	29.10	29.10
	set temp. occ. night zone	1303.800	1303.800	1303.800
	air change rate day zone	108.00	-108.00	102.00
	air change rate night zone	118.80	-118.80	118.20
	infiltration rate at 50 Pa	129.60	-129.60	121.20
	U-value roof	15.90	-15.90	14.70
	U-value floor	55.50	-55.50	54.30
	U-value wall	80.40	-80.40	80.40
	window type	21.60	-19.80	21.60
	sunscreen type	1039.80	-1039.80	389.40
	internal heat gains	68.40	68.40	62.40
	deviation infiltration	25.50	-25.50	23.70
	deviation U-values	42.90	-42.90	40.50

Table 4.2: Morris method with ten trajectories. Non-dominant input parameters are indicated in grey.

		μ^*	μ	σ
HEAT DEMAND	set temp. occ. day zone	7245.024	7245.024	1108.111
	set temp. abs. day zone	2290.735	2290.735	371.057
	set temp. occ. night zone	4443.539	4443.539	737.490
	air change rate day zone	5311.286	5311.286	760.102
	air change rate night zone	3604.510	3604.510	815.766
	infiltration rate at 50 Pa	5680.752	5680.752	669.843
	U-value roof	988.215	988.215	101.640
	U-value floor	696.455	696.455	94.423
	U-value wall	1651.631	1651.631	154.760
	window type	1886.482	-1886.482	267.461
	sunscreen type	1540.955	1540.955	137.018
	internal heat gains	1876.009	-1876.009	51.273
	deviation infiltration	1663.073	1663.073	434.544
	deviation U-values	2164.306	2164.306	419.423
MAXIMAL TEMPERATURE	set temp. occ. day zone	0.748	0.748	0.577
	set temp. abs. day zone	0.034	-0.030	0.026
	set temp. occ. night zone	1.416	1.409	0.819
	air change rate day zone	1.193	-1.141	0.433
	air change rate night zone	0.389	-0.389	0.120
	infiltration rate at 50 Pa	0.291	-0.226	0.109
	U-value roof	0.095	-0.016	0.046
	U-value floor	0.249	-0.234	0.073
	U-value wall	0.193	-0.193	0.080
	window type	1.189	-0.614	0.560
	sunscreen type	4.404	-4.404	1.047
	internal heat gains	1.124	1.124	0.294
	deviation infiltration	0.285	-0.280	0.131
	deviation U-values	0.335	-0.328	0.146
TE25	set temp. occ. day zone	2019.480	2019.480	1029.319
	set temp. abs. day zone	107.76	106.20	94.86
	set temp. occ. night zone	1239.960	1239.240	517.975
	air change rate day zone	411.96	-411.96	132.29
	air change rate night zone	319.32	-319.32	126.58
	infiltration rate at 50 Pa	157.56	-157.56	71.50
	U-value roof	49.32	-44.28	26.36
	U-value floor	32.52	-31.20	17.38
	U-value wall	229.68	-229.68	107.42
	window type	330.42	-94.38	150.12
	sunscreen type	793.74	-793.74	172.44
	internal heat gains	368.82	368.82	144.70
	deviation infiltration	205.26	-204.42	117.86
	deviation U-values	220.80	-220.80	120.36

Monte Carlo based techniques

The 200 maximin Monte Carlo runs with Eigendecomposition of section 4.2.4 are reused in this section to determine the dominant input parameters. As previously mentioned, scatter plots are the most intuitive tool to examine input sensitivity. However, no quantitative information is provided in order to rank the input parameters and the interpretation of these scatter plots is subjective and sometimes even ambiguous. Because of their simplicity however, scatter plots are useful to verify sensitivity indices (Das et al., 2014). To illustrate this, Fig. 4.11 shows output parameter 'heat demand' in function of two input parameters. 'Set temperature occupancy day zone' appears to influence the 'heat demand' more than 'U-value wall'.

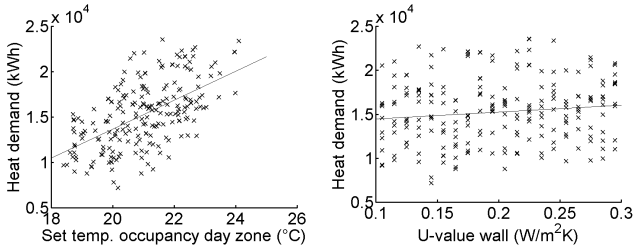

Figure 4.11: Scatter plots of dominant and non-dominant input parameters with regression line.

SRCs, Pearson's r's and Spearman's ρ's are calculated based on 20 and 200 samples and presented in Tables 4.3 and 4.4 with their p-value for all input and output parameters. Because of the differences in the methods, the indices cannot be compared directly, however, the rankings can. The same dominant parameters are identified by the three methods and by both sample sizes, although the rankings are not exactly the same. By comparing both tables, one can see that the exact values still change by adding more samples and that the p-values decrease, thus reliability increases. Furthermore, high sensitivity indices are combined with high reliability, also for a small sample size. This means that the most important parameters can be reliably detected with few Monte Carlo samples for this case study. The most important parameters can be verified based on scatter plots such as those in Fig. 4.11.

As an alternative to calculating p-values, Fig. 4.12 shows the convergence of the sensitivity indices for the two input/output combinations of Fig. 4.11. The corresponding indices are converged when the relative deviation is smaller than 5 %. One can see that adding samples indeed increases the reliability and that more dominant parameters are already reliable with a smaller sample size. As already concluded from the p-values, the most significant indices can be determined with few samples for this case study.

Taking input correlations (see section 4.2.4) into account when calculating sensitivity indices needs some more attention as this obviously influences the results. In linear regression, all sensitivities - and thus also these of the correlated inputs - are

Table 4.3: Sensitivity indices calculated from 20 Monte Carlo simulations. Non-dominant input parameters are indicated in grey.

		SRC	p-value	r	p-value	ρ	p-value
HEAT DEMAND	set temp. occ. day zone	0.38	0.00	0.69	0.00	0.67	0.00
	set temp. abs. day zone	0.13	0.07	0.53	0.02	0.57	0.01
	set temp. occ. night zone	0.18	0.03	0.55	0.01	0.52	0.02
	air change rate day zone	0.24	0.02	0.48	0.03	0.48	0.03
	air change rate night zone	0.27	0.01	0.44	0.05	0.40	0.08
	infiltration rate at 50 Pa	0.45	0.00	0.50	0.02	0.51	0.02
	U-value roof	0.04	0.45	0.05	0.83	0.04	0.88
	U-value floor	-0.01	0.75	0.12	0.62	0.16	0.50
	U-value wall	0.08	0.12	0.08	0.73	0.16	0.51
	window type	-0.24	0.00	-0.08	0.73	-0.08	0.74
	sunscreen type	0.12	0.07	0.10	0.66	0.10	0.66
	internal heat gains	-0.11	0.05	-0.28	0.22	-0.33	0.16
	deviation infiltration	0.00	0.95	0.25	0.30	0.19	0.43
	deviation U-values	0.15	0.08	0.21	0.37	0.17	0.48
MAXIMAL TEMPERATURE	set temp. occ. day zone	-0.15	0.38	-0.27	0.25	-0.23	0.34
	set temp. abs. day zone	0.06	0.67	-0.15	0.52	-0.18	0.45
	set temp. occ. night zone	0.12	0.40	-0.02	0.94	-0.04	0.88
	air change rate day zone	-0.02	0.91	-0.28	0.23	-0.29	0.21
	air change rate night zone	-0.21	0.23	-0.17	0.48	-0.14	0.54
	infiltration rate at 50 Pa	0.05	0.67	0.18	0.45	0.15	0.51
	U-value roof	-0.07	0.52	-0.20	0.39	-0.28	0.24
	U-value floor	-0.02	0.82	-0.22	0.35	-0.18	0.44
	U-value wall	-0.02	0.81	0.10	0.67	0.19	0.43
	window type	-0.03	0.79	-0.12	0.60	-0.05	0.84
	sunscreen type	-0.92	0.00	-0.92	0.00	-0.87	0.00
	internal heat gains	0.19	0.10	0.18	0.45	0.27	0.26
	deviation infiltration	0.17	0.31	-0.07	0.76	-0.08	0.74
	deviation U-values	-0.26	0.16	-0.02	0.94	0.00	1.00
TE25	set temp. occ. day zone	-0.29	0.46	-0.30	0.19	-0.27	0.25
	set temp. abs. day zone	0.02	0.95	-0.20	0.40	-0.21	0.37
	set temp. occ. night zone	0.23	0.47	-0.06	0.81	-0.06	0.82
	air change rate day zone	-0.08	0.82	-0.36	0.11	-0.24	0.31
	air change rate night zone	-0.33	0.38	-0.30	0.20	-0.10	0.68
	infiltration rate at 50 Pa	0.07	0.76	0.09	0.71	0.21	0.37
	U-value roof	-0.11	0.67	-0.15	0.54	-0.22	0.36
	U-value floor	-0.06	0.78	-0.22	0.36	-0.26	0.27
	U-value wall	-0.17	0.45	-0.04	0.85	0.11	0.65
	window type	-0.10	0.65	-0.19	0.43	-0.14	0.55
	sunscreen type	-0.69	0.04	-0.74	0.00	-0.91	0.00
	internal heat gains	0.16	0.50	0.23	0.32	0.12	0.62
	deviation infiltration	0.19	0.59	-0.18	0.46	-0.11	0.65
	deviation U-values	-0.36	0.35	-0.13	0.59	-0.03	0.88

Table 4.4: Sensitivity indices calculated from 200 Monte Carlo simulations. Non-dominant input parameters are indicated in grey.

		SRC	p-value	r	p-value	ρ	p-value
HEAT DEMAND	set temp. occ. day zone	0.33	0.00	0.57	0.00	0.57	0.00
	set temp. abs. day zone	0.20	0.00	0.54	0.00	0.54	0.00
	set temp. occ. night zone	0.23	0.00	0.53	0.00	0.53	0.00
	air change rate day zone	0.29	0.00	0.46	0.00	0.45	0.00
	air change rate night zone	0.22	0.00	0.43	0.00	0.43	0.00
	infiltration rate at 50 Pa	0.45	0.00	0.46	0.00	0.45	0.00
	U-value roof	0.06	0.00	0.04	0.59	0.03	0.69
	U-value floor	0.06	0.00	0.06	0.40	0.04	0.54
	U-value wall	0.13	0.00	0.13	0.07	0.13	0.07
	window type	-0.22	0.00	-0.21	0.00	-0.21	0.00
	sunscreen type	0.12	0.00	0.09	0.20	0.08	0.26
	internal heat gains	-0.15	0.00	-0.14	0.06	-0.12	0.10
	deviation infiltration	0.07	0.00	0.12	0.10	0.09	0.19
	deviation U-values	0.09	0.00	0.15	0.04	0.15	0.04
MAXIMAL TEMPERATURE	set temp. occ. day zone	0.06	0.09	0.03	0.67	0.04	0.53
	set temp. abs. day zone	0.00	0.95	-0.02	0.75	-0.01	0.88
	set temp. occ. night zone	-0.01	0.68	-0.02	0.81	-0.01	0.88
	air change rate day zone	-0.07	0.07	-0.10	0.17	-0.08	0.29
	air change rate night zone	-0.03	0.48	-0.08	0.29	-0.06	0.43
	infiltration rate at 50 Pa	-0.05	0.03	0.02	0.73	0.05	0.46
	U-value roof	0.01	0.52	-0.02	0.78	-0.01	0.89
	U-value floor	-0.07	0.00	-0.11	0.11	-0.11	0.11
	U-value wall	-0.05	0.02	-0.06	0.38	-0.05	0.45
	window type	-0.08	0.00	-0.12	0.10	-0.13	0.07
	sunscreen type	-0.92	0.00	-0.90	0.00	-0.87	0.00
	internal heat gains	0.25	0.00	0.20	0.00	0.28	0.00
	deviation infiltration	-0.05	0.11	-0.01	0.92	0.00	0.96
	deviation U-values	0.02	0.57	0.02	0.74	0.01	0.90
TE25	set temp. occ. day zone	0.07	0.27	0.07	0.33	0.06	0.38
	set temp. abs. day zone	0.02	0.75	0.02	0.75	0.01	0.92
	set temp. occ. night zone	0.00	0.94	0.01	0.91	0.01	0.85
	air change rate day zone	-0.22	0.00	-0.22	0.00	-0.11	0.12
	air change rate night zone	0.00	0.95	-0.17	0.02	-0.08	0.28
	infiltration rate at 50 Pa	-0.15	0.00	-0.09	0.19	0.03	0.71
	U-value roof	-0.01	0.86	-0.04	0.59	-0.04	0.60
	U-value floor	-0.08	0.06	-0.10	0.16	-0.09	0.19
	U-value wall	-0.12	0.00	-0.14	0.06	-0.05	0.50
	window type	-0.09	0.04	-0.13	0.07	-0.12	0.10
	sunscreen type	-0.73	0.00	-0.70	0.00	-0.91	0.00
	internal heat gains	0.25	0.00	0.21	0.00	0.12	0.10
	deviation infiltration	-0.09	0.18	-0.06	0.41	0.00	0.96
	deviation U-values	0.01	0.93	-0.03	0.72	0.01	0.91

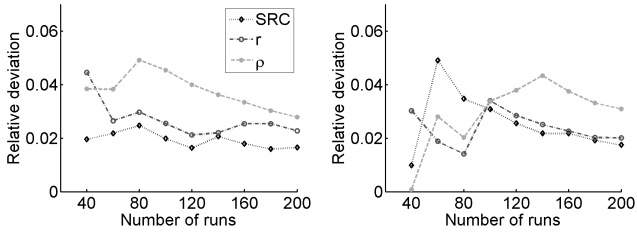

(a) Heat demand - set temperature occupancy day zone

(b) Heat demand - U-value wall

Figure 4.12: Convergence of dominant and non-dominant input parameters.

considered at the same time, while for the correlation coefficients each sensitivity is considered separately. The SRCs of correlated input parameters are thus incorrectly lower, while the r's and ρ's are correctly higher. When input correlations are considered, the correlation coefficients r and ρ are thus preferred.

Comparison

Compared to the Monte Carlo based sensitivity indices, the results of the Morris method are not exactly the same. Especially for TE25, the indicated dominant parameters are completely different. This is caused by the fact that the statistics are not yet converged to reliable values and that correlations cannot be taken into account. The Monte Carlo based indices were already reliable for few samples, while for the Morris method in this case more than 150 samples are needed. However, for some output parameters the most dominant parameters are already indicated.

Although the Morris method is widely used (see section 2.1.2), far more runs are needed for reliable sensitivity indices compared to simple Monte Carlo based methods. Except for more flexibility concerning non-linear behaviour, no advantages of the Morris method are found. The fact that correlations cannot be taken into account is though a huge disadvantage. Monte Carlo based methods are thus preferred. Spearman's ρ in combination with scatter plots seems to be most useful.

Advantages of sensitivity analysis

In the further developed methodology, it will be essential that only the precise input distributions of the dominant input parameters, as identified by the sensitivity analysis, need to be collected. This is a major advantage as collecting the required input distributions can be time-consuming. This is illustrated for the current example. According to Tables 4.1, 4.2, 4.3 and 4.4, 'U-value roof', 'U-value floor', 'U-value wall', and 'deviation from design U-values' are the overall least influencing parameters. Instead of sampling these input parameters, their average value is selected. When sampling the other input parameters and calculating the corresponding outputs, the CDFs in Fig. 4.13 are obtained. When comparing the results of the full uncertainty with the reduced uncertainty, no significant differences are noticed. This observation stresses the importance of sensitivity analysis.

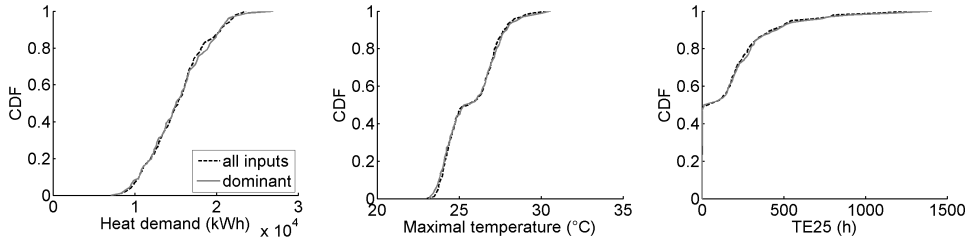

Figure 4.13: Cumulative distribution functions with all input parameter distributions and only most dominant distributions based on 200 maximin samples.

4.3.4 Conclusions on sensitivity analysis

This section described several techniques for identifying most dominant input parameters. It was shown that when only the input distributions of most dominant parameters are taken into account, the output distributions are approached very well. Therefore, only the input distributions of these dominant parameters need to be collected. This is a major benefit since collecting the required input distributions can be time-consuming.

Monte Carlo based techniques and the one-at-a-time Morris method were compared. Regression coefficients (SRC) and correlation coefficients (Pearson's r and Spearman's ρ) appeared to be all able to indicate most influencing input parameters. Spearman's ρ is however the most flexible since only assumptions on monotonic relations between input and output are made and not on linearity. When input correlations are considered, the correlation coefficients r and ρ are preferred. Because of their simplicity, scatter plots are useful to verify these sensitivity indices. Although the Morris method is widely used, far more runs are needed for reliable sensitivity indices compared to simple Monte Carlo based methods. Except for more flexibility concerning non-linear behaviour, no advantages of the Morris method are found. The fact that correlations cannot be taken into account is though a major disadvantage. Monte Carlo based methods are thus preferred over the Morris method. Spearman's ρ in combination with scatter plots seems to be most useful for the considered case study.

Furthermore, it is essential to check the reliability of sensitivity indices, similar to uncertainty analysis. Therefore, one can check the significance of influencing parameters by the p-value or the convergence of the indices.

4.4 Meta-modelling

Optimisation problems, such as the probabilistic design methodology of section 4.1, usually require series of simulations. Depending on the model complexity, these simulations can take from only a second to several days or weeks. Despite the huge potential of these simulations, excessive calculation time might be a limiting factor.

To counter this computational barrier, meta-models - also known as surrogate models - have been introduced to replace potentially time-consuming models (Simpson et al., 2001; Wang and Shan, 2007). Meta-models aim at mimicking the original complex simulation model via a simplified mathematical model, statistically determined based on original model realisations. The simulation then only takes a fraction of the original simulation time, allowing significant computational savings without compromising the reliability. Meta-modelling was only very recently introduced in the building physics field as described in section 2.1.5. Although the meta-models themselves are computationally inexpensive to run, they are not always constructed in the most time-efficient way. As this is usually not feasible for very computationally expensive simulation models, this section proposes a practical meta-modelling strategy dealing with both time-efficiency and reliability: a well-performing meta-model trained on as few samples as possible will be preferred.

Therefore, first a review of the meta-modelling theory concerning fitting and validating is given in section 4.4.1. An overview of available techniques is provided in section 4.4.2. The meta-modelling strategy is then proposed in section 4.4.3. To compare the techniques and illustrate the proposed strategy, meta-models to replace the BES model of the global case study of Chapter 3 are created in section 4.4.4. Furthermore, section 4.4.5 describes and illustrates a time-variant meta-modelling approach.

4.4.1 Meta-modelling theory

Kleijnen and Sargent (2000) and Wang and Shan (2007) emphasise the importance of both fitting and validating meta-models in view of model reliability. This is indeed one of the major concerns as meta-modelling aims to replace a model without becoming unreliable. Therefore, this section describes the fitting of a meta-model followed by the validation.

Fitting

A meta-model is a mathematical function for which the coefficients are determined based on a limited number of input/output combinations. Analogously to section 4.2, a set of input values, input matrix X, is therefore run in simulation model $f(x)$ to obtain a set of output values, output matrix Y. Matrix X can be sampled in several ways, such as the sampling techniques described in section 4.2.1. These input/output data will be referred to as *training data*. In general, these training data are standardised (zero mean, unit variance) to overcome influences from parameter units. Each output is then modelled separately or together with a meta-modelling technique, such as those described in section 4.4.2 and 4.4.5. With these techniques, the training process results in an independent model to estimate new input/output combinations within the range of the sampled combinations. The more training data are used, the better the meta-model can perform in general. It is however possible that the training data are perfectly fitted, while unseen data are not approximated well at all. This phenomenon is called *overfitting* and can be avoided by employing generalisation methods that reduce the complexity of the model by

- *regularisation*: limiting the Euclidean norm of the coefficients vector, in order to avoid unnecessarily large coefficients, or
- *pruning*: reducing the number of coefficients before or after fitting them, in order to avoid too many coefficients.

Amongst the variety of readily available algorithms for each of the meta-modelling groups described in section 4.4.2, algorithms employing these generalisation methods will be selected. All algorithms are provided by MATLAB toolboxes and are referred to when the techniques are described.

Each of the selected algorithms contain several settings that have to be defined by the user. Different settings might result in differing meta-models, of which only the best is retained, selected via a model selection criterion. Such a criterion indicates the trade off between the goodness of fit and model complexity in order to avoid more coefficients than needed. The Akaike information criterion (AIC) (Ljung, 1999) is commonly used for that purpose and is given by

$$AIC = n \log(SSE) + 2n_p \tag{4.13}$$

with n the number of training samples, SSE the sum of squared errors, and n_p the effective number of parameters. The model with the lowest AIC score has the best trade off between the smallest error and the least number of coefficients, the latter of which enhances the generalisation ability of the model.

Validation

The meta-modelling techniques that will be described in section 4.4.2 are thus all optimised to prevent overfitting of the training data, enhancing the goodness of fit on unseen data. To validate this performance however, goodness of fit needs to be assessed on unseen data, the *validation data*, instead of on training data. Extra input/output combinations are thus created via sampling methods and used to compare the predictions of the meta-model with the original model output.

This goodness of fit can be determined by several indicators. Amongst others, Root Mean Squared Error ($RMSE$), coefficient of determination (r^2), and Maximal Absolute Error (MAE) are commonly used indicators. They are illustrated in Fig. 4.14 and given by

$$RMSE = \sqrt{\frac{1}{n} \sum_{i=1}^{n} (\hat{y}_i - y_i)^2} \tag{4.14}$$

$$r^2 = 1 - \frac{\sum_{i=1}^{n} (\hat{y}_i - y_i)^2}{\sum_{i=1}^{n} (\bar{y} - y_i)^2} \tag{4.15}$$

$$MAE = max(|\hat{y}_1 - y_1|, \ldots, |\hat{y}_n - y_n|) \tag{4.16}$$

with y_i the original model outputs, $\hat{y}_i$ the meta-model outputs, $\bar{y}$ the mean simulation output value, and n the number of samples.

$RMSE$ measures the standard deviation of the error between the meta-model and original output. It thus indicates the overall approximation ability of the meta-model;

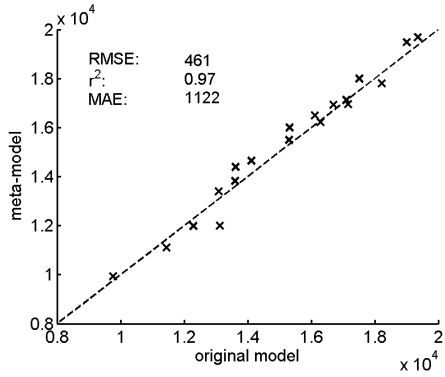

Figure 4.14: Illustration of goodness-of-fit indicators to compare the meta-model output with the original model output.

the lower the value, the better the approximation. The coefficient of determination r^2 is a relative indicator for the overall approximation. In fact, it indicates the correlation between the original model output and the meta-model output. A perfect correlation is given by an r^2-value of 1. Complementary to the above-mentioned indicators, MAE indicates the maximal absolute error that can be expected, and is thus an indicator for the local approximation ability of the meta-model. $RMSE$ and MAE can be made relative to the standard deviation of the simulation output in order to allow a comparison between several outputs of varying magnitudes. In this thesis, this is however not done since r^2 already provides such a relative indicator.

Depending on the meta-model's goal, one or more validation indicators are selected. One of the most important steps in meta-modelling is then to select validation criteria for these indicators. These criteria depend on the problem as well, and might be hard to determine. As the accuracy required for a predictive meta-model is usually very high, a low $RMSE$ and MAE, and a high r^2 are sought (Wang and Shan, 2007; Kleijnen and Sargent, 2000).

4.4.2 Meta-modelling techniques

Several meta-modelling techniques were developed, and different applications appeared in the literature during the last few decades. Based on both mathematical and engineering test problems with a varying number of inputs, number of samples, degree of non-linearity, noisy behaviour, and applied fitting algorithm, several meta-modelling techniques were compared (Simpson et al., 2001; Jin et al., 2001; Hussain et al., 2002; Jin et al., 2003; Fang et al., 2005; Mullur and Messac, 2006; Chen et al., 2006). Amongst others, mainly polynomial regression (PR), multivariate adaptive splines (MARS), kriging (KR), radial basis function networks (RBF), and neural networks (NN) were explored and will be described below. In the above-mentioned literature, PR is considered as the worst performing technique, while NN is advised for problems with many inputs, and KR is recommended for highly non-linear problems. When the considered problem is noisy however, KR typically performs the worst. Depending on the number of samples, the degree of non-linearity and noisy behaviour of the particular problem and also the employed algorithm, yet

other techniques may provide better models. Therefore, these five techniques will be tested on the global case study of Chapter 3 in section 4.4.4 as these are thought to be most useful based on literature.

As mentioned in section 4.4.1, each of the five selected meta-modelling techniques uses at least one generalisation method to avoid overfitting, and in each algorithm, several settings have to be defined by the user. Several options are therefore selected and the best model is then selected based on their AIC scores, as summarised in Table 4.5. The content of this table will be explained in following sections.

Table 4.5: Overview of algorithms, comparison criteria and user-defined settings for the meta-modelling techniques.

	generalisation method	**internal settings**	**comp. crit.**	**external settings**	**comp. crit.**
PR	regularisation (ridge regression)			- model order (1, 2, 3) - regularisation factor (50 values between 10^{-6} and 10^{6})	AIC
MARS	pruning (GCV)			maximal number of basis functions (values between 20 and 140)	AIC
KR	pruning (order 0)			correlation function (Gaussian, exponential, Matérn32 and Matérn52)	AIC
RBF	- pruning (forward sel. BIC) - regularisation (ridge regression)	- scale factor (10 values between 10 % and 100 %) - reg. factor (50 values between 10^{-6} and 10^{6})	BIC	- basis function type (Gaussian, Cauchy, multiquadric, inverse) - technique (forward selection, ridge regression)	AIC
NN	regularisation (Bayesian)			- architecture (feed forward, cascade forward) - number of layers (1, 2) - number of neurons (between 1 and 20)	AIC

Polynomial regression

PR is one of the most widely used meta-modelling techniques and fits an m^{th} order polynomial between the sampled input and output data using the method of least squares. In general, the model is a function of the form

$$\hat{y} = b_0 + \sum_{n=1}^{m}\sum_{i=1}^{p} b_{ni} x_i^n + \sum_{n=1}^{m}\sum_{k=1}^{m}\sum_{i=1}^{p}\sum_{j=1}^{p} b_{nkij} x_i^n x_j^k \tag{4.17}$$

with $\hat{y}$ the estimated output, x the input vectors, p the number of inputs, m the order of the polynomial, and b the regression coefficients (Jin et al., 2001). Simple first order regression without interaction terms can also be used for sensitivity analysis (see section 4.3.1).

In the selected algorithm (MathWorks, 2014*f*), not only are the summed squares of the errors minimised, but also the magnitude of the coefficients to avoid overfitting as described before. Therefore, the least square cost function is modified by an additional term, which aims at keeping the Euclidean norm of the coefficients vector small, often referred to as ridge regression. The cost function is then

$$\sum(\hat{y} - y)^2 + \gamma \sum b^2 \tag{4.18}$$

with γ the regularisation factor (Marquardt and Snee, 1975).

Several model orders, m, and regularisation factors, γ, can be used to determine the coefficients, b (MathWorks, 2014*f*). In this thesis, model orders one, two, and three, and 50 values for γ logarithmically distributed between 10^{-6} and 10^{6} are chosen to build the polynomial meta-models.

Multivariate adaptive regression splines

MARS models are of the form

$$\hat{y} = \sum_{i=1}^{k} c_i B_i(x) \tag{4.19}$$

with $\hat{y}$ the estimated output, x the input vectors, k the number of basis functions B_i, and c_i the weight factors (Friedman, 1991; Jin et al., 2001). Non-linearities between outputs and inputs can be taken into account because of the use of hinge functions as basis functions. A hinge function has the form $\max(0, x - constant)$ or $max(0, constant - x)$ and thus produces a kink. The basis functions in Eq. 4.19 are a constant, a hinge function, or a product of hinge functions to take interactions into account. Both the hinge functions and weight factors have to be determined, which is done through a forward selection and a backward deletion iterative approach. In the forward phase, basis functions giving the largest reduction in the training error are added until (1) the (change in) training error becomes small, (2) more weight factors than training samples are expected, or (3) the user-defined maximum number of basis functions is reached. Typically an overfit model is the result. In the backward phase, the model is pruned by trading off goodness of fit against model complexity using the Generalised Cross-validation (GCV) criterion, similar to AIC, given by

$$GCV = MSE / \left(1 - \frac{n_p}{n}\right)^2 \tag{4.20}$$

with MSE the mean-squared error. This pruning means that the least effective terms are deleted one by one to improve the generalisation ability (Jekabsons, 2011). Any value can be selected for the maximum number of basis functions, but the calculation time significantly increases when adding more functions. Several values between 20 and 140 are selected in this thesis.

Kriging

KR is an interpolation method originating in the field of geostatistics (Matheron, 1963) and was proposed by Sacks et al. (1989) for computer experiments without random errors, as a better alternative to statistical techniques designed for physical experiments with random errors, such as PR. KR models provide a global regression model analogous to simple polynomial regression that is augmented with a Gaussian process to interpolate the residuals. A well-specified regression model is thus not needed to obtain a well-performing model, in contrast to the other techniques explained in this thesis. KR models are of the form

$$\hat{y} = \sum_{i=1}^{k} b_i h_i(x) + Z(x) \tag{4.21}$$

with $\hat{y}$ the estimated output, x the input vectors, k the number of polynomial basis functions h_i, b_i the regression coefficients determined with the least squares method, and Z a Gaussian process. This process has mean zero, variance σ^2, and correlation functions $\psi(x, x')$, between any two samples of the input vector. A typical correlation function is the Gaussian:

$$\psi\left(x, x'\right) = \exp\left(-\sum_{i=1}^{p} \theta_i |x_i - x_i'|^2\right) \tag{4.22}$$

Several correlation function types are available, which are all determined by a correlation parameter θ, with the same dimension as the input vector, i.e. p. These correlation functions inform nearby sample points about the residuals in these points. The smaller the distance between the sample points, the more the prediction of one of the points is influenced by the other. Selecting satisfying correlation functions and correlation parameter values is thus crucial for this method. The former have to be selected by the user, while the latter are automatically determined by maximum likelihood estimation (Simpson et al., 2001; Couckuyt et al., 2012; Staum, 2009). Note that when the training data are noisy, stochastic kriging can be used, which combines interpolation and smoothing to avoid overfitting (Staum, 2009). The considered data is noisy when two simulations with the same input do not result in the same output, for example when stochastic inputs are used in the model.

Four correlation functions (Gaussian, exponential, Matérn32 and Matérn52) (Couckuyt et al., 2012) are selected in this thesis. Note that in kriging, more coefficients than available samples cannot be estimated, but due to the Gaussian process, a well-performing model can be obtained with low-order polynomials. Therefore, a model order of zero is chosen for all models.

Radial basis function network

RBF networks are of the form

$$\hat{y} = \sum_{i=1}^{k} w_i h_i(x) \tag{4.23}$$

with $\hat{y}$ the estimated output, x the input vectors, k the number of basis functions h_i, and w_i the weights. A typical Gaussian basis function is of the form

$$h_i(x) = \exp\left(-\frac{\|x - c_i\|^2}{r_i^2}\right) \tag{4.24}$$

with c_i the centre and r_i the radius of basis functions h_i (Orr, 1996). Other similar basis functions are used as well, like the Cauchy, the multiquadric, and the inverse function. Both weights w_i, and basis function parameters, c_i and r_i, have to be determined. The centres are usually taken to be equal to the input matrix X. Each basis function centre is thus p-dimensional and as many basis functions as initial samples are created. In general, for each dimension, the radii are chosen to be equal to the span of the training set inputs, and are thus the same for each basis function. However, it is preferable to apply a scale factor ($\leq$ 100 %) to this radius to avoid underfitting, as otherwise the RBFs will probably be too wide. A set of scale factors can be provided by the user and the best scale is then selected in the algorithm based on the Bayesian Information Criterion (BIC) score. BIC is very similar to AIC of Eq. 4.13 and is calculated as

$$BIC = n\log(SSE) + n_p\log(n) \tag{4.25}$$

Either forward selection or ridge regression can be performed to select some of the available basis functions (including a bias unit). If all basis functions are selected, RBF is seen as an interpolation technique. Forward selection compares models made up of different subsets of basis functions. Basis functions that best reduce the sum-squared error are added one by one, until the BIC score stops decreasing to avoid models that are too complex. Weight factors are determined based on the sum-squared error as well. Ridge regression selects all available basis functions and augments the sum-squared error with an extra term penalising large weights to avoid overfitting analogous to polynomial regression. Several regularisation factor values have to be provided by the user and the best one is then internally selected based on the BIC scores (Orr, 1999).

Ten scale factors between 10 % and 100 % and 50 regularisation factors logarithmically distributed between 10^{-6} and 10^{6} are chosen in order to automatically determine an optimum. The four basis function types are used to create networks with both forward selection and ridge resression.

Sigmoidal transfer function network

Sigmoidal transfer function networks are standard neural networks (NN). Neural networks consist of a first layer with input neurons, a final layer with output neurons, and any number of hidden layers in between, as illustrated in Fig. 4.15a. The neurons are transfer functions and in this thesis they are sigmoidal in all layers except the final layer, in which they are linear. In particular, tan-sigmoidal functions are selected as illustrated in Fig. 4.15b. A single feed forward neural network with one output is

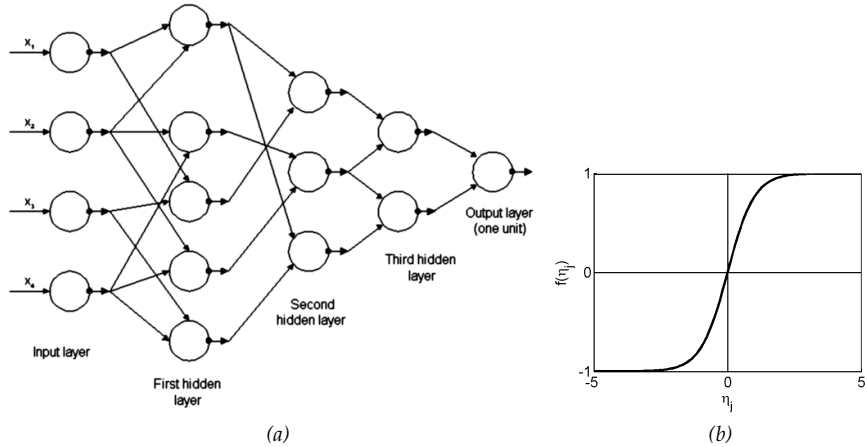

Figure 4.15: Feedforward neural network with three hidden layers. Figure (a) taken from (Galkin and Lowell, 2014) (a) and tan-sigmoid transfer function (b).

constructed with the following equations:

$$\eta_j = \sum_{i=1}^{p} w_{xi} x_i + \beta_{xj} \tag{4.26}$$

$$f(\eta_j) = \frac{2}{1 + \exp(-2\eta_j)} - 1 \tag{4.27}$$

$$\hat{y} = \sum_{j=1}^{m} w_{yj} f(\eta_j) + \beta_{yj} \tag{4.28}$$

Here, a weighted, sum η_j, of the p input parameter values x_i, with input weights w_{xi}, and a bias value β_{xj} (Eq. 4.26) feeds forward to m tan-sigmoidal transfer functions $f(\eta_j)$ (Eq. 4.27). The m outputs of the hidden layer are then linearly combined with a bias β_{yj}, and weights w_{yj}, into the estimated output $\hat{y}$ (Eq. 4.28) (Simpson et al., 2001). When more hidden layers are available, the outputs of the previous hidden layer are considered as inputs and Eq. 4.26 and 4.27 are repeated. The outputs of the final hidden layer are then linearly combined into $\hat{y}$. A cascade forward construction is also considered, in which connections between non-adjacent layers are possible. Biases and weights are trained by least-squares minimisation, which is modified for regularisation similar to Eq. 4.18 to improve generalisation. For that purpose, Bayesian regularisation is applied, which uses an iterative approach to determine weights, biases and the regularisation factor by considering them as random variables (MathWorks, 2014*d*; Foresee and Hagan, 1997; MacKay, 1992). Bayesian regularisation should not be confused with BIC.

Creating a well-performing neural network depends on the choice for the number of layers and neurons in the network (Das et al., 2014). Therefore, one or two hidden layers each with up to 20 neurons and both feed forward and cascade forward constructions are used to build sigmoidal neural networks (MathWorks, 2014*e*).

4.4.3 Meta-modelling strategy

In this section, a meta-modelling strategy independent of the meta-model type is proposed in which the meta-models are both fitted and validated while the number of simulation runs is constrained. Since the sampling strategy used to fit the meta-model might be of importance, this topic is handled first.

Sampling strategy

Several studies have highlighted the importance of selecting a well-performing sampling scheme (see also section 4.2) for training and validation (Hussain et al., 2002; Alam et al., 2004; Johnson et al., 2010). Random sampling, Latin Hypercube schemes, space-filling sampling such as optimised Latin Hypercubes, orthogonal arrays and quasi-Monte Carlo methods, and also classic schemes such as (fractional) factorial, central composite and optimal schemes have been explored for meta-modelling. Simpson et al. (2001) state that a consensus on the best-performing scheme across several problems is only reached for space-filling sampling schemes. Such schemes are thus preferred and will be used in this thesis. More information on space-filling schemes can be found in section 4.2.1.

Fitting and validation strategy

Section 4.4.1 described both fitting and validation theory using training and validation samples. Van Gelder et al. (2013) illustrate that different sample sets might result in different validation indicator values. To avoid getting good or bad values by coincidence, it is thus recommended to train and validate the meta-model for as many samples as possible. This set of indicator values can then be evaluated on minimal, average and maximal values in order to reliably evaluate the created meta-model. Such an approach is proposed by Tian et al. (2014). They used the bootstrap technique in order to obtain reliable validation indicators. Two main problems are however observed: the bootstrap technique is not compatible with LHS sampling (Janssen, 2013) and usually requires numerous iterations.

To balance between time efficiency and reliability however, another meta-modelling strategy is proposed (see Fig. 4.16). A meta-model is first trained on one small sample set according to one of the techniques in section 4.4.2 while seeking the best user-defined settings. Then an additional sample set is created and a *k-fold cross-validation* is performed using the optimal settings to check the reliability of validation indicator values. This implies that of the k available sample sets, one set is used as a validation set, while the other $k-1$ sets are training sets. This is

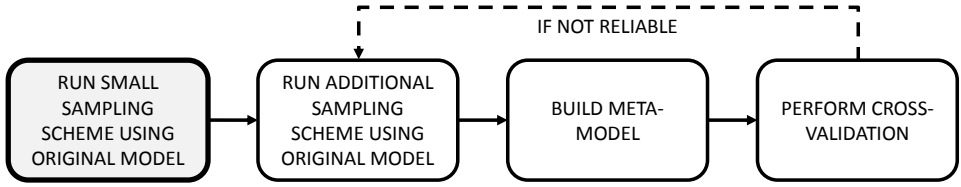

Figure 4.16: Flowchart of meta-modelling strategy.

repeated k times with each of the k sample sets used exactly once as a validation set, resulting in k validation indicator values (Wang and Shan, 2007). Sample sets are systematically added until the minimal, average and maximal values of selected validation indicators converge to the desired validation criteria. The reliability of the meta-model can be judged on the spread of these indicator values.

In this strategy, users can select a meta-modelling technique of their choice. Hence, if the built meta-model remains insufficiently reliable, another meta-modelling technique can be selected to obtain a potentially better reliability of the validation indicators.

4.4.4 Application

The described meta-modelling techniques and strategy are illustrated using the global case study of Chapter 3. When performing probabilistic design (see section 4.1), the calculation time of the dynamic BES model will be a barrier. The construction of meta-models can greatly facilitate this, because of their highly reduced calculation time. Therefore, following application example aims at constructing a reliable meta-model to replace the time-consuming original BES model.

For that purpose, the case study of Chapter 3 is simplified following section 4.2.4. However, no input correlations are taken into account because more independent input parameters will imply more complex models. Including these input correlations can however be easily done as described in section 4.2.3. In this example, we consider the heat demand and TE25 outputs. The heat demand output, as will be seen, will be simple to meta-model, while the TE25 output more challenging.

Following section 4.4.3, a space-filling sampling scheme is chosen to create training and validation samples: in this case a maximin sampling scheme (see section 4.2.1). To allow for several different sample sizes for model training and cross-validation, 25 sets of 20 maximin samples are created and run with the original model, therefore giving 500 samples in total.

Since both reliability and calculation efficiency are crucial in meta-modelling, techniques with good approximation ability using only a few samples are preferable, however, more samples usually increase the goodness of fit. Therefore, training sets with several different sample sizes are used to construct meta-models for heat demand and TE25 with the techniques described in section 4.4.2. The models based on 500 training samples can be considered as the best possible meta-models. In order to make the meta-models physically relevant, the meta-model outputs for heat demand and TE25 values are forced to be strictly positive. As described before, the best settings for each technique and sample size are chosen based on AIC scores, resulting in one meta-model per technique per training sample size.

The goodness of the fit of these meta-models is first validated on 20 unseen samples according to section 4.4.1. This will provide insight into the approximation ability of the techniques and the influence of the sample size in order to mutually compare them. The best settings per technique and per sample size are furthermore used in

the k-fold cross-validation described in section 4.4.3, performed for k sample sets varying between two and ten. This cross-validation allows the examination of the reliability of the meta-modelling techniques.

Setting comparison

As mentioned earlier, several settings have to be defined and selected by the user for each of the meta-modelling techniques. In this case study, only the best meta-model for each technique is retained, based on the AIC model comparison criterion. The lower this value, the better the generalisation ability of the model. Table 4.7 compares the best and worst settings in view of this AIC score for meta-models trained on 100 samples. One can see that the settings have larger influence on AIC scores for PR, RBF and NN than for MARS and KR. MARS and KR are thus more robust.

Note that the best and worst settings in Table 4.7 are only valid for the considered case study, settings and training sample size. Other problems, settings and sample sizes might result in other optimal settings. Therefore, it is needed to always test several settings as proposed in this thesis. Furthermore, a comparison of AIC scores of several techniques is not meaningful since model structures are totally different.

Calculation time

Table 4.6 presents a brief comparison of calculation times. These calculation times are computed by timing the training and running process of multiple samples and settings. These times are averaged to obtain the time indicators of Table 4.6.

First of all, one can notice a huge reduction in calculation time once a meta-model is constructed. All meta-modelling techniques result in very time-efficient models, although the calculation times still differ.

More differences can be found in training times. Training one single output with one collection of model settings on 100 training samples is also very time-efficient. However, variation can be found in these single training times; major differences are due to the number of potential model settings as seen in Table 4.5. While for MARS models only a set of maximal number of basis functions needs to be tested, NN require a comparison of numerous network architectures and layers. Furthermore, following Table 4.7, these NN settings seem to be more dominant in obtaining well-performing models than the maximal number of basis functions.

Note that the time needed to construct the meta-models of computational-expensive models is usually far below the time needed to get the training data, even when numerous settings have to be compared. As the computation time of the original

Table 4.6: Indicative calculation time for one output and one set of model settings.

	PR	**KR**	**MARS**	**RBF**	**NN**
training time 100 samples	2 s	4 s	3 s	2 s	40 s
running time 100 samples	0.2 s	0.08 s	0.03 s	0.02 s	0.1 s
reference running time for 1 simulation in original model: 500 s					

Table 4.7: Best and worst user-defined setting combinations in view of AIC for meta-models trained on 100 samples.

		best setting combination	**AIC**	**worst setting combination**	**AIC**
PR	heat demand	- model order: 3 - regularisation factor: 10^{-6}	-3 512	- model order: 1 - regularisation factor: 10^{6}	459
	TE25	- model order: 3 - regularisation factor: 10^{-6}	-3 467	- model order: 2 - regularisation factor: 10^{6}	460
MARS	heat demand	max. # basis functions: 50	136	max. # basis functions: 20	215
	TE25	max. # basis functions: 40	133	max. # basis functions: 20	246
KR	heat demand	corr. function: Matérn32	-5 739	corr. function: Gaussian	-5 532
	TE25	corr. function: Matérn32	-5 698	corr. function: Gaussian	-5 635
RBF	heat demand	- basis func. type: Gaussian - technique: ridge regression	-5 941	- basis func. type: inverse - technique: forward selection	-3 468
	TE25	- basis func. type: Gaussian - technique: ridge regression	-5 891	- basis func. type: inverse - technique: forward selection	-3 393
NN	heat demand	- architecture: feed forward - number of layers: 2 - number of neurons: 17, 19	-3 070	- architecture: feed forward - number of layers: 2 - number of neurons: 16, 1	461
	TE25	- architecture: feed forward - number of layers: 1 - number of neurons: 9	-2 983	- architecture: feed forward - number of layers: 2 - number of neurons: 1, 16	439

model can be easily reduced by parallel computing, the training time might be important for less expensive models such as the BES model in this example. As stated by Mullur and Messac (2006), a slightly longer calculation time is usually tolerated when this is improving accuracy.

Validation

Fig. 4.17 compares meta-model outputs and original outputs of the validation set for models trained on 20, 200, and 500 samples. It illustrates that adding more training

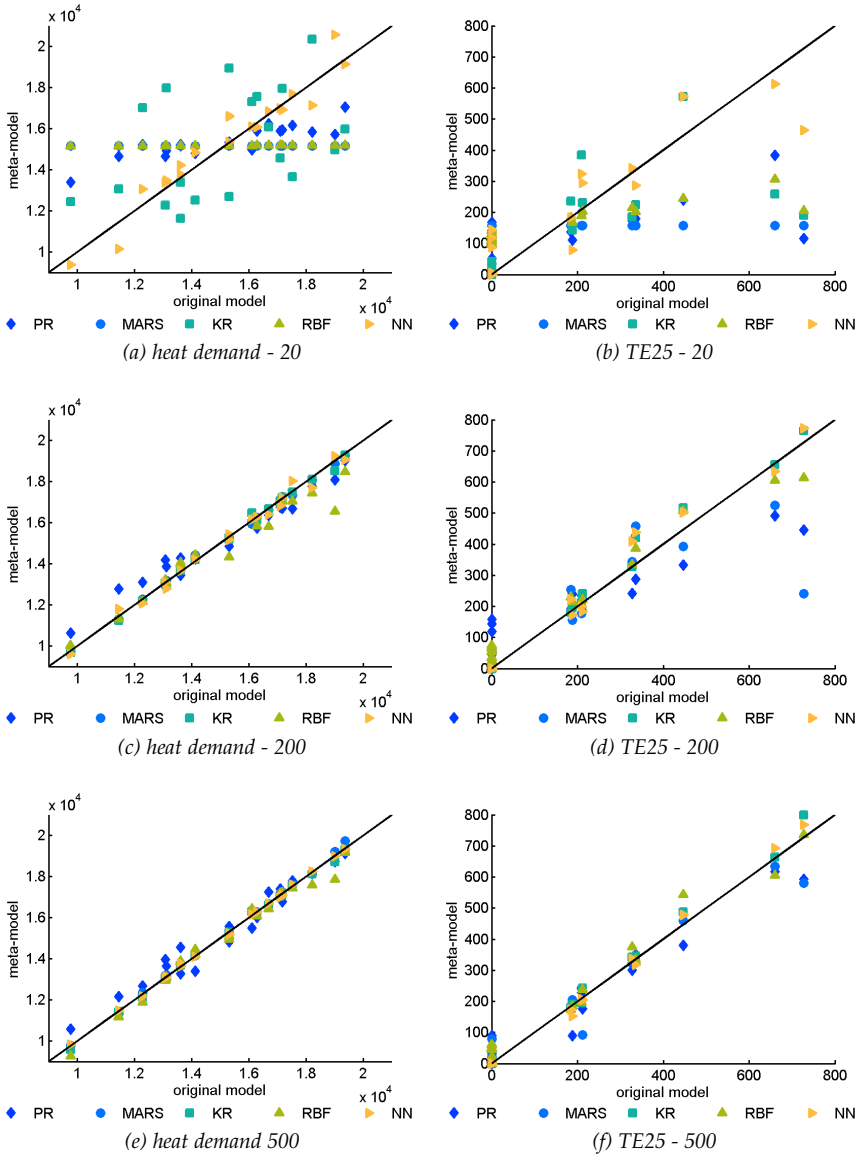

(a) heat demand - 20 *(b) TE25 - 20*

(c) heat demand - 200 *(d) TE25 - 200*

(e) heat demand 500 *(f) TE25 - 500*

Figure 4.17: Comparison of original model output with meta-models trained on 20, 200 and 500 samples.

samples results in better meta-models. Fig. 4.17 also shows that some outputs are more difficult to reproduce with a meta-model than others. For heat demand, KR and NN can already provide well-approximating models with only 20 training samples, while not for TE25. All applied techniques appear to be suitable to create meta-models of heat demand, while KR and NN seems best for TE25.

The reliability of validation indicators as a function of the number of sample sets is illustrated in Fig. 4.18. As described earlier, all sets are used once as a validation set,

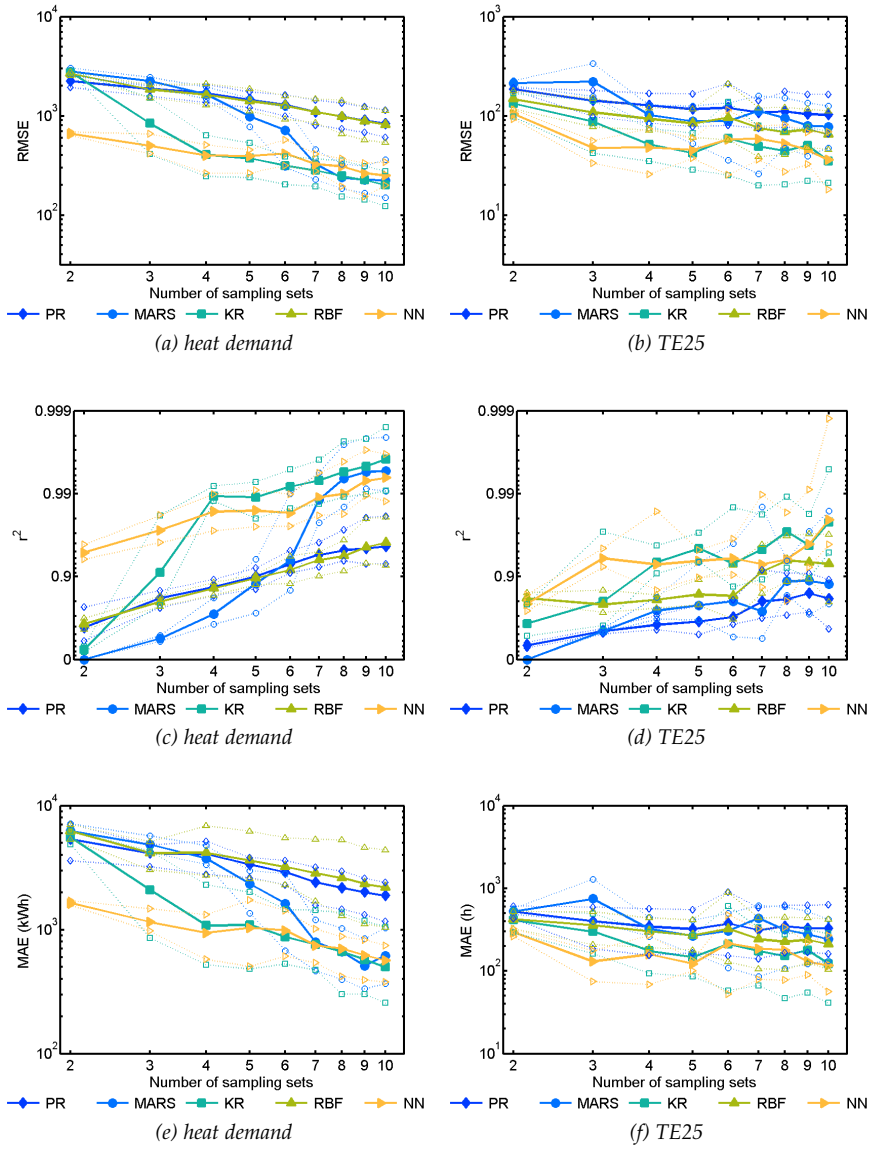

Figure 4.18: Reliability of validation indicators as a function of the number of training samples for heat demand and TE25 output. Mean values (in thick lines) as well as minima and maxima (in dotted lines) are shown for all techniques.

while the remaining sets are used as training sets. Minimum, average, and maximum values of the indicators for a given sample size indicate how sensitive the values are to training and validation samples. The better the mean value is and the closer the minimum and maximum are to each other, the more reliable the constructed model. Although such a cross-validation provides an interval of plausible validation indicator values, validation data sets for which the meta-model performs outside this interval can still be found, especially for the MAE indicator. This is illustrated in Table 4.8 for the meta-models build on ten sample sets in the cross-validation and an additional validation set of 320 samples. Nevertheless, the performance interval supplies an indication of the overall performance. Examining the exact interval is, however, not possible with a limited set of samples.

This being said, in Fig. 4.18 one can again see that adding more training samples generally results in better meta-models and that some outputs are more difficult to model than others. From this perspective, KR and NN are most reliable for heat demand, although when more samples are used, MARS also performs well. For TE25, it seems to be much harder to have very accurate meta-models: only KR and NN seem to match the original model and many more training samples are needed to obtain similar indicator values. Therefore, particular attention needs to be paid to the construction of a meta-model TE25 when a high accuracy is desired.

Table 4.8: Comparison of validation indicator ranges from cross-validation with validation on 320 samples for meta-model based on ten sample sets. Indicators outside the range are indicated in bold.

		heat demand			**TE25**		
		min	max	val	min	max	val
RMSE	PR	607	1140	815	66	165	109
	MARS	149	362	178	48	125	73
	KR	123	277	196	21	69	56
	RBF	538	1136	844	46	112	79
	NN	199	339	280	18	69	41
$\mathbf{r^2}$	PR	0.93	0.98	0.95	0.57	0.89	0.81
	MARS	0.99	1.00	1.00	0.79	0.98	0.89
	KR	0.99	1.00	1.00	0.95	0.99	**0.94**
	RBF	0.93	0.98	0.95	0.80	0.97	0.89
	NN	0.99	1.00	0.99	0.96	1.00	0.97
MAE	PR	1163	2407	2306	161	634	**663**
	MARS	367	1033	508	132	420	**652**
	KR	256	1052	829	41	284	**500**
	RBF	1047	4406	3011	104	424	**508**
	NN	378	747	**1110**	56	271	225

4.4.5 State space model

A completely different approach can be obtained when the original simulation model is dynamic as in the case study of Chapter 3. In that case, the time-variant

model outputs can be meta-modelled instead of the post-processed results, while considering the dynamics of the studied problem. The post-processing is then afterwards done on the dynamic meta-model output. Since some model outputs, such as TE25, are significantly influenced by the system dynamics, it is thought that this approach might perform better than the previous presented 'static' meta-modelling techniques. For that purpose, a state space model is described below. Furthermore, the validation of such meta-models is discussed and the case study of section 4.4.4 is used to compare with the previous techniques.

State space model with subspace method

A state space model (SSM) not only focuses on the time-variant input-output regression, but also on the internal state of the system. This internal state is the 'memory' of the system and causes the dynamical aspect of the model (Madsen, 2008). A linear SSM consists of the following equations:

$$X_t = AX_{t-1} + BU_{t-1} + Ke_t \tag{4.29}$$

$$Y_t = CX_t + DU_t + e_t \tag{4.30}$$

with t the discrete time, $U_t \in \mathbb{R}^{p\times 1}$ the input vector at time t, $Y_t \in \mathbb{R}^{q\times 1}$ the output vector at time t, $X_t \in \mathbb{R}^{m\times 1}$ the state vector at time t, $A \in \mathbb{R}^{m\times m}$ the state transition matrix, $B \in \mathbb{R}^{m\times p}$ the matrix with influence of input on state, $C \in \mathbb{R}^{q\times m}$ the matrix with influence of state on output, $D \in \mathbb{R}^{q\times p}$ the matrix with direct influence of input on output, $K \in \mathbb{R}^{m\times q}$ the disturbance matrix and $e_t \in \mathbb{R}^{q\times 1}$ the disturbance at time t. The state vector X is related to the system dynamics and its size, the model order m, determines the number of time steps influencing the output. If D is considered, the inputs can bypass the system dynamics. The disturbance e_t contains all information that is not explained by the inputs and states. To estimate the matrices A, B, C, D and K based on n samples of time-variant input U and output Y, the subspace identification algorithm N4SID can be used (Van Overschee and De Moor, 1994; Ljung, 1999; MathWorks, 2014*b*). Input U is therefore sampled similar to static inputs (see section 4.4.1), however the time-variance is included as well, as will be illustrated further on. Although several original simulation samples with different dynamic behaviour can be supplied, the resulting meta-model can only contain the averaged dynamics over these considered samples. SSM is thus only sufficient when the system dynamics are not greatly varying over the samples.

Several model orders m can be used to create SSMs. In this thesis, the best model order (1-8) is selected based on the Akaike Information Criterion (AIC), similar to section 4.4.1 Eq. 4.13, however in a slightly revised form:

$$\log(MSR) + \frac{2n_p}{n} \tag{4.31}$$

with MSR the mean of squared residuals instead of the sum of squared residuals (MathWorks, 2014*a*). The focus of the SSMs is set on 'simulation' in order to obtain a stable model with an optimised simulation performance (MathWorks, 2014*b*).

Validation

SSMs can be validated by comparing the post-processed model outputs, equal to the previous meta-modelling techniques as described in section 4.4.1. The meta-modelling strategy of section 4.4.3 can therefore also be applied. Besides this model output validation, first the model dynamics need to be validated. Therefore, a residual analysis is performed on the one-step ahead prediction residuals of validation samples to test whether these residuals can be considered as white noise. White noise residuals have zero mean, are uncorrelated and indicate that all dynamics are included in the model. For that purpose, residuals are (1) plotted as a function of time, (2) tested on autocorrelation and (3) tested in the cumulated periodogram (Madsen, 2008).

Autocorrelation is the correlation of the residuals with a delayed version of these residuals. Autocorrelation thus indicates to what extent the residuals contain repeating patterns. In order to consider the residuals to be white noise, no significant correlations between delayed residuals should be found. When correlations are observed, not all dynamics of the considered system are included in the SSM.

The cumulated periodogram shows the cumulated amount of variation related to a certain frequency of the residuals. These frequencies are i/n_{obs} with $i = 0, 1, ..., n_{obs}/2$ and n_{obs} the number of observations in the residuals. For white noise, the variation is uniformly distributed on all frequencies (Madsen, 2008). Fig. 4.19 illustrates how these cumulated periodograms should be interpreted: Fig. 4.19a shows the residuals of an adequate model since the cumulated periodogram is within the confidence interval of white noise, while Fig. 4.19b shows the residuals of an inadequate model since the residuals still contain low-frequent fluctuations. In the latter figure, the high-frequent dynamics are, however, sufficiently included in the model.

When the residuals are not white noise, the model can be improved, amongst others, by increasing the model order, by adding other significant inputs or by improving the prediction of the noise model (ie. matrix K).

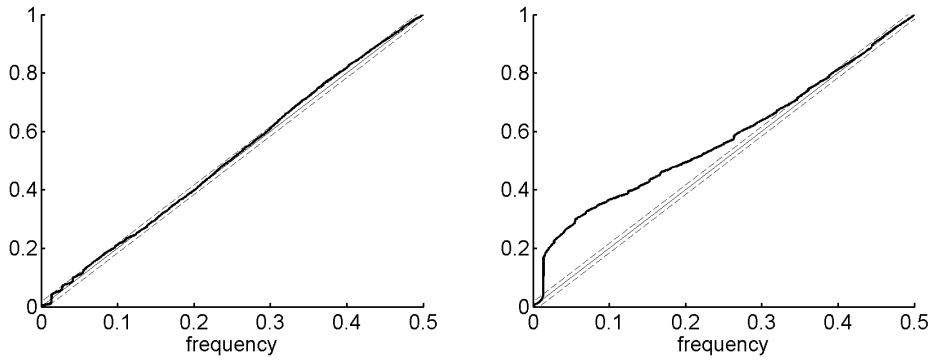

(a) adequate model *(b) inadequate model*

Figure 4.19: Cumulated periodogram of residuals (in thick line) with 90 % confidence intervals (in dotted lines).

Application

The case study of section 4.4.4 is revisited in order to compare the dynamic modelling approach to the previous meta-modelling techniques. Only model output TE25 is considered since this was the most difficult to meta-model, potentially because this is significantly influenced by the system dynamics. TE25 can be obtained by first calculating the time-variant indoor temperature. A dynamic meta-model for the indoor temperature of both day and night zone is thus created.

Because usually only in summer indoor temperatures above 25 °C are reached, the winter period is excluded in the considered data. This reduces the calculation time and facilitates the modelling process since summer and winter period are characterised by different dynamic behaviour due to the fact that the zones are heated in winter. The time step is taken equal to the time step in the original dynamic model, ie. 1200 s. Time-variant output matrix Y, which contains both indoor temperatures for up to six sets of 20 samples, is thus easily obtained from the Monte Carlo simulation of section 4.4.4. A maximum of six sets is considered due to the high computational effort of such SSMs.

To transfer the input matrix of the Monte Carlo simulation to the time-variant input matrix U needed for the SSM construction, several steps are taken. Firstly, although the climatic variables are considered deterministic in this case study, these are added in the dynamic modelling because their influence is significant for the dynamic behaviour of the system. Therefore, the outdoor air temperature, the global horizontal solar radiation and both direct and diffuse solar radiation for the three orientations of the dwelling are selected from the meteorological weather data file. Furthermore, the occupancy profiles, set point temperatures and internal heat gains are for each sample combined into time-variant profiles. Finally, the remaining probabilistic inputs that are considered constant over time in the original model, such as U-values, are for each sample translated into a vector with the same value for every time step. All these inputs then result in time-variant input matrix U with up to six sets of 20 samples.

As described earlier, model orders one till eight are tested for each sample size and the model with the lowest AIC score is selected. The optimal model order in this case study is five. The dynamics of this fifth order SSM trained on 20 samples are checked in Fig. 4.20 for the indoor temperature of the day zone for the first sample in the validation set. The other validation samples result in similar plots. To have an idea of the time-variant model output of the constructed SSM, the predicted output is compared to the original model output in Fig. 4.20a. One can see that the original model output is mimicked to a large extent. Fig. 4.20b shows the one-step ahead prediction residuals of this output. One can see that the residuals have zero mean and no strange patterns are observed. When studying the relative autocorrelations in Fig. 4.20c, no significant autocorrelations are observed for lags greater than zero. Finally, the white noise hypothesis is also tested in Fig. 4.20d. Since the cumulated periodogram of the residuals is located close to the 90 % reliability interval, the residuals are also in this test almost white noise. One can thus conclude that most significant system dynamics, however not all, are included in the SSM.

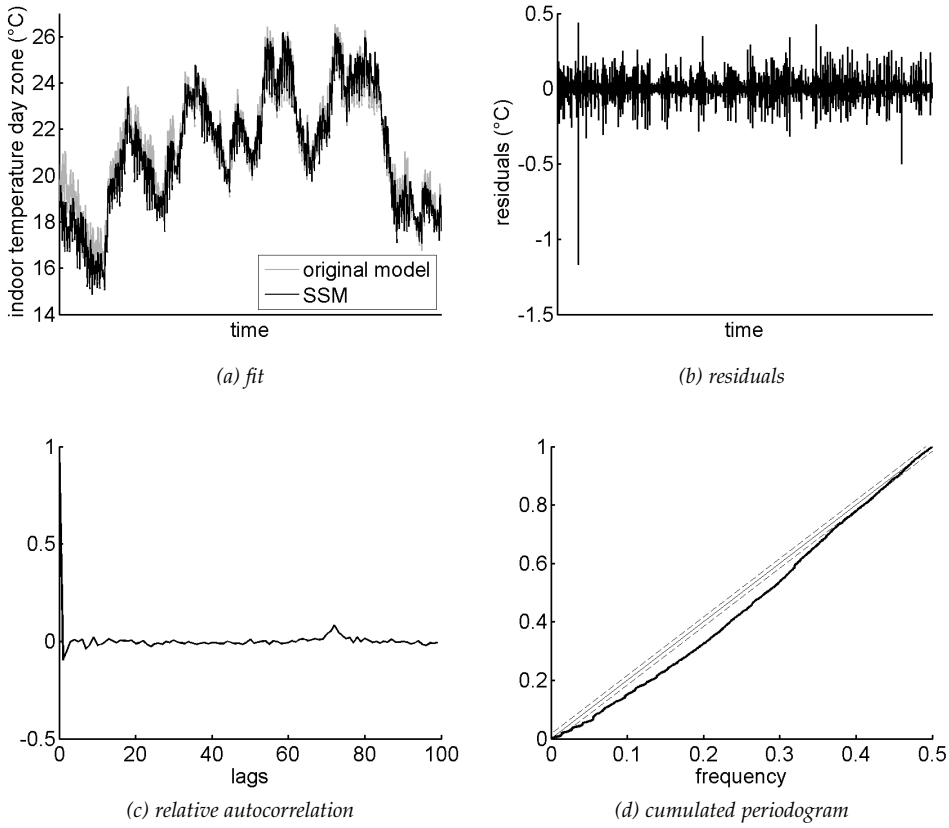

(a) fit

(b) residuals

(c) relative autocorrelation

(d) cumulated periodogram

Figure 4.20: Validation of SSM dynamics for first sample in validation set for SSM trained on 20 samples.

Since the dynamics are sufficiently modelled, the SSM indoor temperature outputs can be used to calculate TE25 for each sample size. These post-processed outputs are then cross-validated as described in section 4.4.3. The results of this cross-validation are shown in Fig. 4.21. One can see that adding more training samples does not necessarily improve the SSM. When comparing these results with MARS and NN, SSM seems to result in better models with far less samples than MARS, although NN is still performing better. When using more samples than six sample sets, both MARS and NN models still improve, as was shown in Fig. 4.18. The lack of such an improvement for SSM can be explained by the fact that, because of the time-variant outputs, much more data is used per sampling set compared to MARS and NN. Hence, the 'average' system dynamics can be captured with a relatively small sample size.

Furthermore, the calculation time of SSM is compared with these of the previous static techniques as presented in Table 4.6. Where MARS only needs some seconds to train 100 samples and NN needs roughly ten times more, SSM is less time efficient and needs about half an hour. Also the running time of SSM is significantly increased, since time-variant outputs need to be calculated first and then these outputs also need some post-processing.

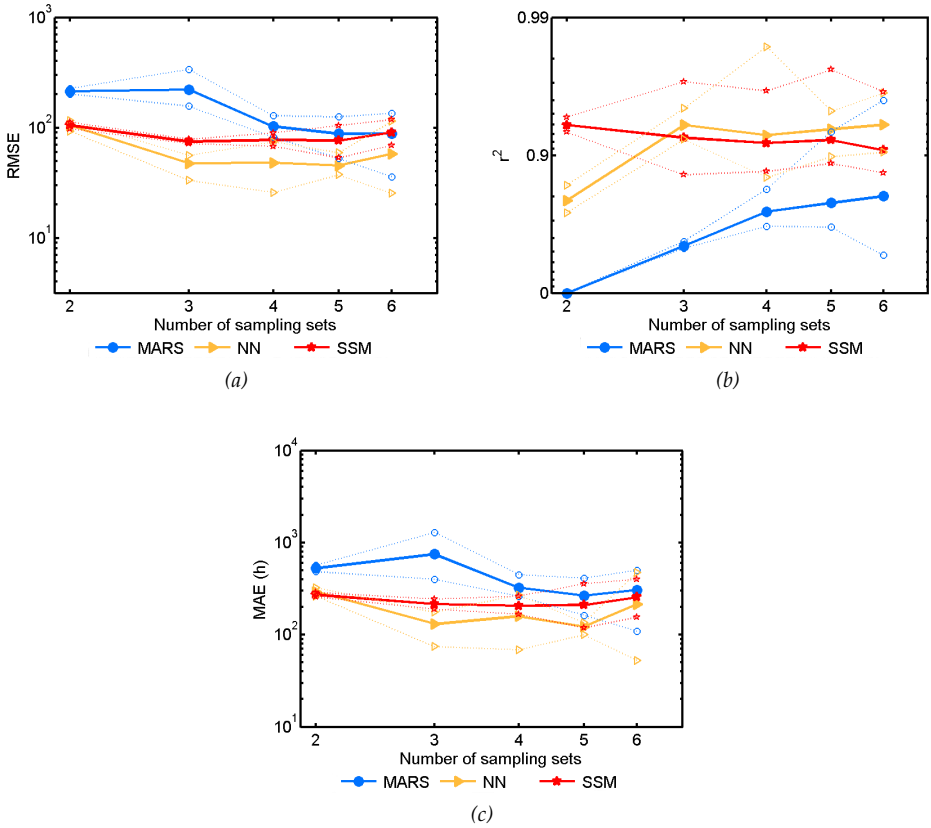

Figure 4.21: Reliability of validation indicators in function of number of training samples for TE25 output. Mean values as well as minimum and maximum are shown for SSM as well as for MARS and NN.

4.4.6 Conclusions on meta-modelling

This section described how a simplified mathematical model can be created based on input/output combinations of a time-consuming model in order to replace this. Usually, the more training samples available, the better the original model is approximated by the meta-model. Unfortunately, it is not always possible to create as many samples as desired due to calculation time. For that reason, it is important to examine how accurate the meta-model has to be. However, this is dependent on the goal of the model: predictive models usually need to be highly accurate. It is important that the accuracy is checked on validation data not used in the training and that the meta-model can only be used within the range of the training data values. It should be mentioned that the accuracy of the meta-model is at least as important as the calculation time: as long as we need less initial samples for the meta-model than we should need for an analysis on the original model, we can expect that time will be saved.

In order to construct a reliable meta-model with as few simulation sets as needed, a meta-modelling strategy was proposed. Because training and validation sets may be

of influence for the validation of the model, cross-validation is preferred. Sample sets are systematically added to construct a meta-model meeting the validation criteria. It is shown that for some meta-models, reliable performance is obtained with a small sample size, while for other models more samples were needed.

Depending on the case study, other techniques can provide better models. The comparison in section 4.4.4, however, confirms the findings in the literature as summarised in section 4.4.2 (Simpson et al., 2001; Jin et al., 2001; Hussain et al., 2002; Jin et al., 2003; Fang et al., 2005; Mullur and Messac, 2006; Chen et al., 2006). The overall best performing meta-modelling techniques for this case study were KR and NN. PR performed worst. Well-performing models could, however, be obtained with all techniques. When dealing with a very time-consuming original model, KR and NN are preferred because less training data would be needed. Of these two, KR has a far lower training time as concluded from Table 4.5 and Table 4.6, however, the models are much harder to interpret. When comparing the meta-modelling techniques in usability, MARS is preferred to KR and NN because of its simplicity and clear relationship between inputs and outputs. Compared to other techniques, fewer settings with less influence have to be chosen by the user (see Table 4.7). MARS can thus be considered as more robust. It should also be noted that preferences are dependent on the selected algorithms. Further development of these algorithms might thus result in other preferred techniques.

Furthermore, SSM was described as a promising alternative approach when the original simulation model is dynamic. In that case, the time-variant model outputs are meta-modelled instead of the post-processed results, while considering the dynamics of the studied problem. For such models, not only the post-processed model outputs have to be validated, but also the dynamics of the model. The latter can be done through a residual analysis of the one-step ahead prediction residuals. The computational cost of such models is, however, much higher than for the simple meta-models and no better performance is obtained. It was shown that even for few training samples, NN performs better and is easier to use. Moreover, modelling the system dynamics in SSM demands far more knowledge on the case study since also deterministic input parameters have to be added and some probabilistic parameters have to be transformed in time-variant parameters. Furthermore, when creating SSM to simulate all possible input parameters, the SSM only contains the average dynamics of the original model outputs. When dealing with input parameters that highly influence these dynamics, such as the thermal mass of the dwelling, well-performing SSMs are even harder to obtain. Therefore, MARS, KR and NN models are preferred for this case study.

4.5 Multi-layered sampling

Several input parameter types can be recognised in probabilistic design and analysis: design parameters (such as the intended air tightness), scenario parameters (such as the future climate) and uncertainty parameters (such as the deviation on the design air tightness). Multi-layered sampling allows to compare such design options for several considered scenarios while accounting for the inherent uncertainties.

Section 4.5.1 first describes these multi-layered sampling schemes and gives an overview of several possibilities to sample the layers. Section 4.5.2 explains how the sampling schemes can be efficiently used while controlling the output convergence. Furthermore, section 4.5.3 illustrates these concepts for a good undertsanding.

4.5.1 Multi-layered sampling scheme

In probabilistic design problems, contributing input parameters can be divided into three categories concerning their conceptual meaning as already introduced in section 4.1. **Design parameters**, such as the intended air tightness, the type of sunscreens or the aimed thermal resistance of walls and roofs, are fully controllable. They are the unknown parameters in the design process, but once a **design option** is selected, the parameter values are known (Sanchez et al., 1996; Dehlendorff et al., 2011; Hopfe and Hensen, 2011). Inherently **uncertain parameters**, such as the impact of user behaviour, are completely uncontrollable by the designer as their values are neither known in the design process nor after, but they can significantly influence the design performance. They are often also referred to as noise or uncontrollable factors (Sanchez et al., 1996; Dehlendorff et al., 2011). Finally, **scenario parameters** are inherently uncertain parameters dealing with potential future scenarios, such as economic or climatic evolutions, for which an explicit evaluation is wanted. The potential of such a scenario evaluation was already suggested by (Hopfe and Hensen, 2011).

These parameter categories cannot be fully employed when sampling all inputs together following section 4.2, as will be illustrated in section 4.5.3. For that purpose, they have to be ascribed to separated layers in a multi-layered Monte Carlo sampling scheme as shown in Fig. 4.22, which will be explained below. Similar to section 4.2.1, this set of input values, input matrix X, is then run in simulation model $f(x)$ to obtain a set of output values, output matrix Y. This matrix is thus layered as well. In this way, the probability distributions (or derived Monte Carlo results) of all design options can be compared for all considered scenarios while accounting for the inherent uncertainties.

In the most simple case, one wants to compare several design options while considering the uncertainties in the design process. The multi-layered sampling scheme of Fig. 4.22 then consists of only two layers: the design options and the uncertainty layer. The u values of the uncertainty layer parameters are combined with all d considered design options, so that every design is subjected to the same uncertainties in matrix $X \in \mathbb{R}^{n \times p}$, with $n = d \times u$ the total number of samples. This way, the design options can be fairly compared as illustrated in (Booth and Choudhary, 2013). In robust design, this approach is referred to as product arrays (Sanchez et al., 1996) or crossed arrays (Dehlendorff et al., 2011).

Several possibilities are available to sample this layered X. The design layer contains all design options that have to be compared in the probabilistic design (Booth and Choudhary, 2013). When multiple design parameters are considered, a full factorial scheme is the simplest and thus default option. In such a scheme, discrete potential values - called levels - are selected for each design parameter - called factors - and

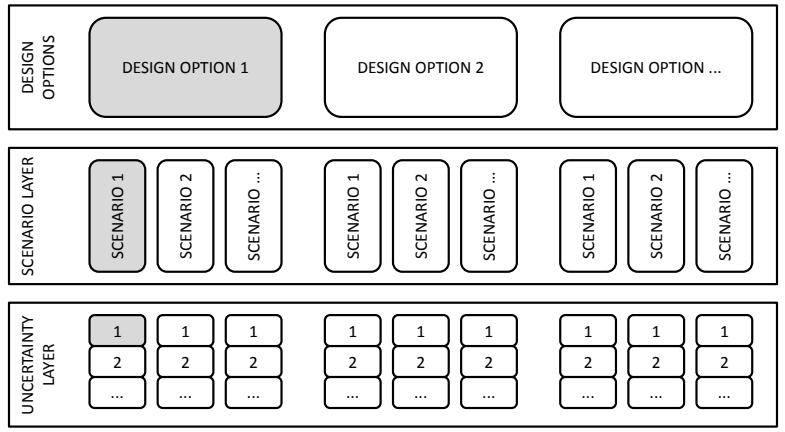

Figure 4.22: Multi-layered sampling scheme with crossed array approach. The first Monte Carlo run is indicated in grey.

all level combinations across all factors are made (Box et al., 1978). More schemes are discussed further on. To create the uncertainty layer values, several sampling techniques such as those described in section 4.2.1 can be used.

If the explicit evaluation of design options for potential scenarios is requested, more layers can be added to the simple two-layered scheme. When one is for example seeking for the design option with the lowest median and lowest spread, regardless of the future economic situation, the energy price evolution would be considered in the scenario layer and not in the uncertainty layer. The latter would be the case if the explicit evaluation was not asked. Again, all d design options are combined with all u uncertainty values and all s scenario values, thus in crossed arrays in matrix $X \in \mathbb{R}^{n \times p}$, such as is done in Fig 4.22 with $n = d \times s \times u$ the total number of samples. The scenario layer can be created with a small sampling scheme or based on potential discrete scenario options. In more advanced cases, multiple scenario layers can be taken into account as well.

Usually, these multi-layered schemes need a large number of runs, ie. $n = d \times s \times u$. If for example only two design options are compared for two scenarios and 50 uncertainty samples are taken into account, already 200 runs are required. When however much more design options are to be compared and more scenario layers are taken into account, even millions of runs might be needed. Since this is unfeasible with most simulation models, meta-modelling, as described in section 4.4, is recommended. Furthermore, a sensitivity analysis as described in section 4.3 can be used to eliminate unimportant parameters and to guide to the considered values of the layers. This can significantly reduce the number of design options and scenario layers, and hence the calculation time.

If after such a sensitivity analysis still numerous design parameters remain, it is possible to study a coarse scheme with few levels or a fractional factorial scheme first, and then to refine based on the corresponding results. Such a fractional factorial scheme considers a two-level full factorial scheme for part of the input parameters and the remaining parameters are determined based on interactions (Box et al., 1978).

Instead of calculating the output distributions for all design options in order to select the most optimal one(s), one can also opt to use an optimisation algorithm which automatically guides to the optimal design option(s). A review of such optimisation algorithms is given in (Machairas et al., 2014). This approach will be illustrated in section 5.4.3.

In the literature, other sampling approaches can be found to deal with design options and uncertainties in robust design (Shoemaker et al., 1991; Sanchez et al., 1996; Dehlendorff et al., 2011). Especially for physical experiments, in which robust design has its origin as seen in section 2.1.4, sampling efficiency is crucial. Instead of creating a meta-model to mimic the input-output relations first and then apply a multi-layered sampling scheme, the controllable and uncontrollable parameters are directly sampled in crossed or combined arrays. The input values are selected very carefully to obtain a limited number of samples containing as much information as possible. Very simple meta-models are then created, including only the interactions available in the limited number of samples. These models are then used to derive mean and variance of the response to select the optimal design. The proposed approach in this section is thus more flexible and more information is obtained to compare for example the output distributions.

4.5.2 Convergence

In order to perform the multi-layered Monte Carlo analysis of Fig. 4.22 in an efficient and reliable way, convergence has to be monitored to be able to decide on the number of samples needed in the layers. Therefore, the approach for the single layer analysis as described in section 4.2.2 is transformed into the multi-layered approach in Fig. 4.23. This approach sequentially adds samples until sufficient accuracy has been reached. To obtain reliable comparisons, all considered Monte Carlo results - be it one or more percentiles, the average or the standard deviation - should converge.

In Fig. 4.23, first a single design and scenario value are selected and the uncertainty layer values are run. The sampling scheme of this layer, which initially contains two sampling sets, is enlarged until the Monte Carlo results based on s sampling sets are sufficiently converged. The results are thus calculated for each of these s sets and according to Eq. 4.2 the expected internal standard deviation is calculated. The results are sufficiently converged when their relative deviations are below a user defined percentage. As concluded in section 4.2, small space-filling schemes are thus also recommended for the sequential addition of samples in the uncertainty layer of the multi-layered approach.

Secondly, the following scenario value is selected and again the uncertainty layer is run and enlarged until convergence. This is analogously done for all other scenario values. Thereafter, the convergence of the scenario layer is investigated and if necessary, more scenario samples can be added. The latter is not needed when discrete, equiprobable scenarios are used in the scenario layer. After all output indicators converge on every layer, one can continue with the next design option.

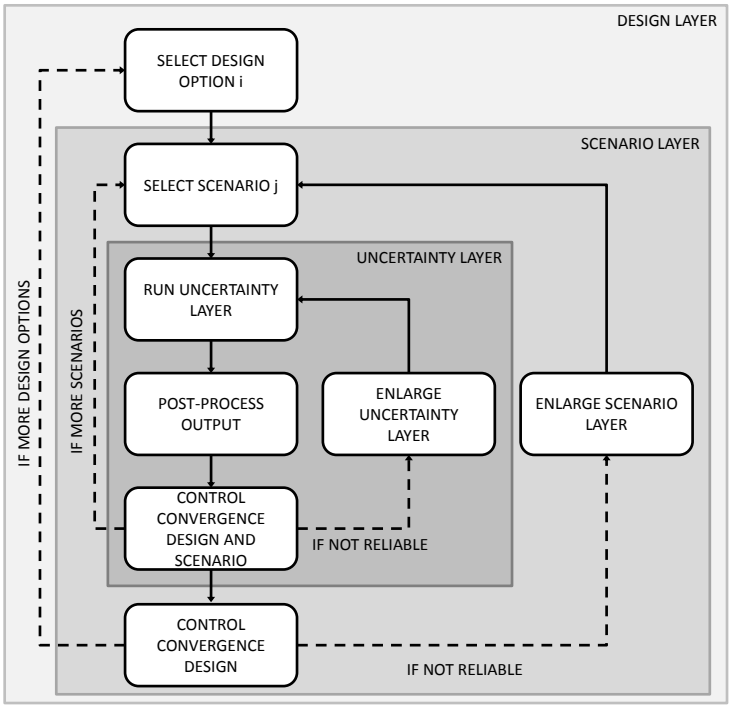

Figure 4.23: Flowchart multi-layered Monte Carlo with convergence control.

The total number of runs n of the multi-layered scheme is thus

$$n = \sum_{i=1}^{d} \sum_{j=1}^{s_i} u_{ij} \tag{4.32}$$

If more scenario layers are taken into account, this Monte Carlo loop can be easily expanded.

When design and scenario options have scenario and uncertainty layers respectively, with different sizes, one should be very careful with calculation of aggregated results for these design options. If for example 40 uncertainty values are needed for a first scenario value and 60 for a second, this second scenario will be more dominant in for example the calculation of the overall percentiles for the current design option. Therefore, weight factors need to be used to equally weigh every branch in the multi-layered scheme.

4.5.3 Application

The multi-layered sampling approach of section 4.5.1 is applied on the global case study of Chapter 3, which is simplified as described in section 4.2.4, in order to compare several design options based on their heat demand distribution. Instead of the original model, the MARS meta-model for heat demand created in section 4.4

on ten sampling sets is used for sampling efficiency purpose. Therefore, input correlations are also in this section not taken into account.

Firstly, it is proven that single layer sampling schemes are not able to fairly compare design options. Then, two design options are compared while focussing on the output convergence of section 4.5.2, followed by the comparison of multiple design options.

Single layer sampling

Fig. 4.24 shows the comparison of the five considered window types based on the 200 single layer maximin samples used to create the MARS model. This Monte Carlo set is for that purpose divided into five subsets with 40 samples each. In Fig. 4.24a the heat demand distribution for these subsets is shown. It seems that the heat demand for the window type with a U-value of 1.31 W/m^2K is significantly higher than for the window type with a U-value of 1.29 W/m^2K, which is quite surprising. This can however be explained when investigating the input distributions in these subsets. Fig. 4.24b shows for example the air change rate of the day zone. Because of the subsampling, the input distributions obtained for each of the window types are not exactly the same. As seen in Table 4.4 on page 56, the air change rate is however significantly influencing the heat demand. A change in input distribution might thus have a significant impact on the output distribution. Hence, this results in an unfair comparison. The strange results of Fig. 4.24a are thus explained and proven to be not reliable.

Sampling both design options and uncertain parameters in a single layer is thus not resulting in reliable design comparisons, since input distributions of the uncertain parameters might be transformed due to the subsampling. Furthermore, the convergence of these subsample outputs is not assured. Multi-layered sampling is therefore required to ensure that each design option is subjected to the same uncertainty layer distributions.

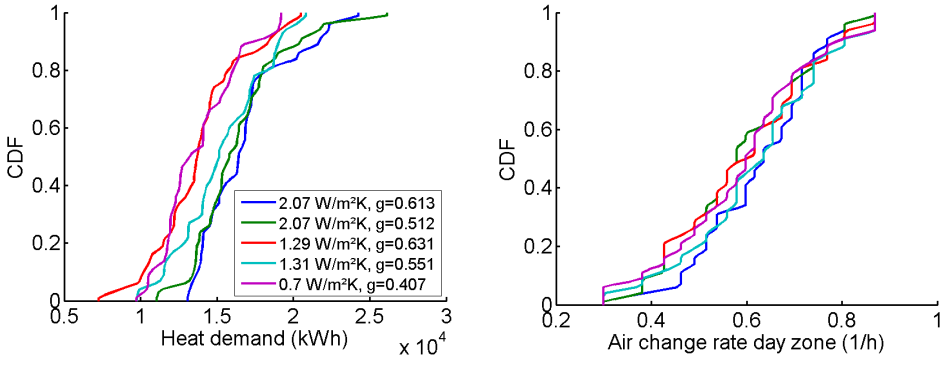

Figure 4.24: Comparison of heat demand output distribution (a) and air change rate input distribution (b) for five window types based on single layer Monte Carlo simulation.

Comparison of two design options

In order to ensure a reliable analysis and to illustrate the benefits of a multi-layered sampling scheme, Fig. 4.25 visually compares the two earlier used window types through such a scheme, and this for three potential scenarios. For this illustration, only the window types are changed and all other design parameters are assumed at an average value. Set temperatures, air change rates and internal heat gains are considered in the uncertainty layer, which contains 100 samples in sets of 20 in order to control the output convergence as will be described further on. The deviation from design values of envelope insulation and air tightness is taken into account in the scenario layer. This means that the heat demand distribution for the two window types can be evaluated for actual U-values and n_{50}-values below (e_{dev}=0.8), on (e_{dev}=1) and above (e_{dev}=1.2) the assumed targets following Eq. 3.6. This might provide some useful information on the sensitivity of the considered designs concerning this deviation. As can be seen in Fig. 4.25, this deviation is only slightly influencing the heat demand, what could have been observed in the sensitivity analysis of Table 4.4 on page 56 as well.

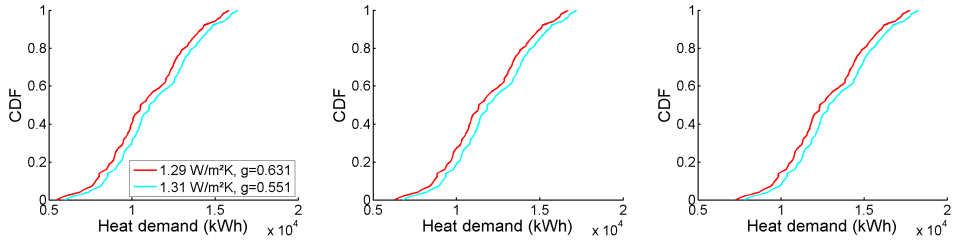

Figure 4.25: Comparison of heat demand output distribution for two window types and three envelope deviation scenarios based on multi-layered Monte Carlo simulation.

In order to ensure that the results are reliable, the output indicators that are compared have to converge. In this case, we are comparing the entire distributions, however one might think of comparing mean values, standard deviations or some of the percentiles. Therefore, Table 4.9 shows the convergence of mean values and 50 % and 75 % percentiles for up to five sets of 20 samples as an illustration, similar to Fig. 4.6 on page 45 for the single layer approach.

For each design option and scenario combination, after four uncertainty layer sets, the relative deviations are less than 2 %, which is considered sufficiently converged. Even after two sets, the relative deviations are already below 5 %. As five sets of 20 samples were calculated for all three scenario values to illustrate this, the cumulative distributions of Fig. 4.25 are created from 100 runs each.

One can actually see that for each design option and scenario combination, a standard Monte Carlo analysis such as in section 4.2 is performed and sampling efficiency and convergence is treated equally. Because of the multi-layered scheme, design options can be reliably compared for several potential scenarios.

Table 4.9: Relative deviation of mean values and 50 % and 75 % percentiles of heat demand for two design options and three envelope deviation scenarios for several number of sample sets. Relative deviations above 2 % are indicated in grey.

	number of sample sets		2	3	4	5
mean	design 1	scenario 1	0.000006	0.000287	0.000658	0.000571
		scenario 2	0.000016	0.000280	0.000612	0.000535
		scenario 3	0.000069	0.000291	0.000567	0.000507
	design 2	scenario 1	0.000013	0.000272	0.000629	0.000544
		scenario 2	0.000012	0.000267	0.000587	0.000512
		scenario 3	0.000069	0.000283	0.000545	0.000488
P50	design 1	scenario 1	0.044145	0.025515	0.018437	0.017024
		scenario 2	0.040928	0.023658	0.017094	0.015789
		scenario 3	0.037457	0.021657	0.015645	0.014464
	design 2	scenario 1	0.042118	0.024348	0.017598	0.016209
		scenario 2	0.039162	0.022642	0.016364	0.015077
		scenario 3	0.035928	0.020778	0.015014	0.013847
P75	design 1	scenario 1	0.019368	0.011215	0.011650	0.012035
		scenario 2	0.018093	0.010465	0.010831	0.011131
		scenario 3	0.016890	0.009752	0.009993	0.010126
	design 2	scenario 1	0.018411	0.010660	0.011107	0.011465
		scenario 2	0.017266	0.009985	0.010360	0.010631
		scenario 3	0.016201	0.009352	0.009592	0.009688

Comparison of all design options

Since Fig. 4.25 showed that the multi-layered sampling approach is very flexible and reliable in comparing design options, the number of design options is significantly enlarged in the current application. Table 4.10 shows the considered design parameters with all target values of interest. The design layer is sampled as a full factorial scheme of these target values, resulting in 2 560 design options. The uncertainty and scenario layers are the same as for the previous example.

In the current application, all design options are run under influence of the scenario and uncertainty layer, while checking for convergence. Here, a relative deviation of 3 % was sought for the 25 %, 50 % and 75 % percentiles, which are thought to be representative for the whole distributions. For that purpose, a maximum of five sets of 20 samples was needed. This multi-layered Monte Carlo analysis resulted in 2 560 cumulative distribution functions of the heat demand for the three considered scenarios as shown in Fig. 4.26. By comparing the output distributions, an optimal design can be selected, which is indicated in grey in Fig. 4.26 and in bold in Table 4.10. Minimising the U-values and n_{50}-values indeed results in a minimal heat demand. By comparing the three output distributions for the optimal design option in Fig. 4.26, one can see that the deviation from design value still has a small influence on the actual heat demand after construction. Moreover, this actual heat demand is even more influenced by the uncertainty layer, which is representing the user behaviour.

Table 4.10: Design parameters and target values. Optimal values are indicated in bold.

PARAMETER	TARGET VALUES
Building fabric	
U-value roof (W/m^{2}K)	0.24 / 0.18 / 0.15 / **0.1**
U-value floor (W/m^{2}K)	0.3 / 0.2 / 0.15 / **0.1**
U-value wall (W/m^{2}K)	0.24 / 0.18 / 0.15 / **0.1**
window type	2.07 W/m^{2}K & g = 0.613 / 2.07 W/m^{2}K & g = 0.512 / 1.29 W/m^{2}K & g = 0.631 / 1.31 W/m^{2}K & g = 0.551 / **0.7 W/m^{2}K & g = 0.407**
infiltration rate at 50 Pa (1/h)	**0.6** / 1 / 3 / 5
Building systems	
sunscreen type	**none** / 30 %

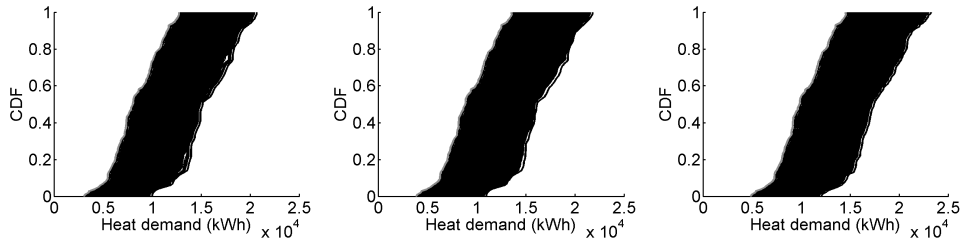

(a) below target *(b) on target* *(c) above target*

Figure 4.26: Comparison of heat demand output distribution for 2 560 design options and three envelope deviation scenarios based on multi-layered Monte Carlo simulation. The optimal design option is indicated in grey.

Limited comparison of design options

The number of simulations needed in the previous example (ie. between 2 560 $\times$ 3 $\times$ 40 and 2 560 $\times$ 3 $\times$ 100) can be significantly reduced by limiting the design layer. Therefore, a coarse scheme for the design options can be created by looking at the sensitivity analysis of Table 4.4 on page 56 and considering only the most dominant input parameters. In this example, the U-values of roof, floor and walls are not dominant for the heat demand. Therefore, the U-values are fixed at 0.15 W/m^{2}K, and only 40 design options are obtained, resulting in a calculation time reduction of almost 99 %. When comparing the optimal design option of this coarse scheme with the overal optimal design of Fig. 4.26 in Fig. 4.27, one can indeed see that the new optimal result is close to the optimum when all input parameters are taken into account, especially compared to the spread in Fig. 4.26. When one is, however, interested in the absolute optimum, a full factorial scheme with many levels need to be considered.

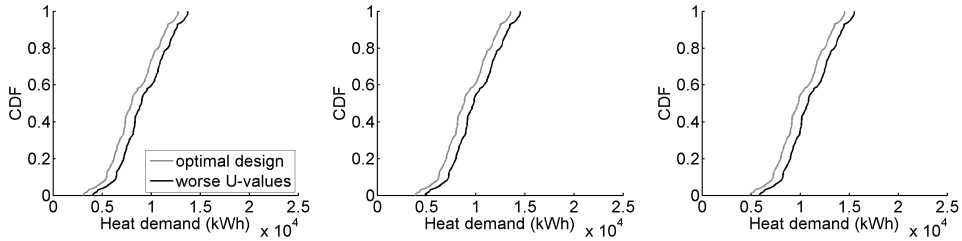

(a) below target *(b) on target* *(c) above target*

Figure 4.27: Comparison of heat demand output distribution for optimal design and design with worse U-values (0.15 W/m^{2}K) and three envelope deviation scenarios based on multi-layered Monte Carlo simulation.

4.5.4 Conclusions on multi-layered sampling

This section described how multi-layered sampling can be used to compare design options for several considered scenarios while accounting for the inherent uncertainties. For that purpose, each parameter category has to be sampled in a separated layer. All values of the design layer are then compared with all values of the scenario layer(s) and with all values of the uncertainty layer in a crossed array scheme. In fact, one thus performs a simple uncertainty analysis for every design and scenario combination.

Several possibilities are available to sample these layer values. A full factorial scheme is the simplest and thus default option for the design layer. The scenario layer can be created with a small sampling scheme or based on potential discrete scenario options. To create the uncertainty layer values, several sampling techniques such as those described in section 4.2 can be used.

Such a multi-layered sampling scheme usually requires numerous runs. Since this is unfeasible with most simulation models, the meta-modelling of section 4.4 can be very useful. Furthermore, the sensitivity analysis of section 4.3 can be used to eliminate unimportant parameters and to guide to the considered values of the layers. This can significantly reduce the number of design options and scenario layers, and hence the calculation time.

In order to perform the multi-layered Monte Carlo analysis in an efficient and reliable way, convergence has to be monitored to be able to decide on the number of samples needed in the layers. The presented approach sequentially adds samples until sufficient accuracy has been reached.

Visually comparing several design options through the multi-layered approach can be very interesting in design processes. However, this approach is even more promising when numerically evaluating the design options. This will be further studied in Chapter 5.

4.6 Conclusions

This chapter described the four fundamentals included in the probabilistic design methodology introduced in section 4.1: uncertainty quantification (section 4.2), sensitivity analysis (section 4.3), meta-modelling (section 4.4) and multi-layered sampling (section 4.5). In order to provide a good understanding of these fundamentals, a concise overview of available techniques was given and applied on the global case study introduced in Chapter 3. The different techniques were compared and discussed and benefits for the probabilistic design methodology described in the next chapter were demonstrated.

Now these fundamentals are extensively described, the probabilistic design methodology of section 4.1 can be handled in more detail in the next chapter.

5

Design methodology

The probabilistic design methodology that was briefly introduced in Chapter 4 to create a framework for the fundamentals explained and illustrated there, is described in more detail in this chapter. These fundamentals are uncertainty quantification, sensitivity analysis, meta-modelling and multi-layered sampling.

The design methodology consists of four main steps: preprocessing (section 5.1), preliminary screening (section 5.2), updating (section 5.3) and the actual probabilistic design (section 5.4), as can be seen in Fig. 5.1. In order to provide a good understanding of the possibilities and advantages of this methodology, it is illustrated on the design of cost effective and cost robust low-energy dwellings (see Chapter 3). Furthermore, section 5.5 provides a second application in order to show that the use of meta-models is reliable in the probabilistic design methodology. This is done because meta-modelling is the most innovative technique used in the methodology. A comprehensive illustration of this design methodology is furthermore given in Chapter 6 in order to provide guidelines for low-energy dwelling design.

5.1 Preprocessing

The first step in the probabilistic design methodology of Fig. 5.1 is the preprocessing step. The output parameters which are needed in the probabilistic design problem, and a suitable model to simulate them are selected. Successive models can be used as well to calculate derived output parameters. Most deterministic models can be included in a Monte Carlo loop by changing the input values, thus stationary or dynamic and both simplified or very complex models can be chosen. In this chapter, a simplified version of the global case study of Chapter 3 is studied with the net present cost as output parameter. As explained in section 3.2.4, a transient BES model is therefore used to calculate the net heat demand, whereafter the net present cost is computed with a subsequent cost calculation tool.

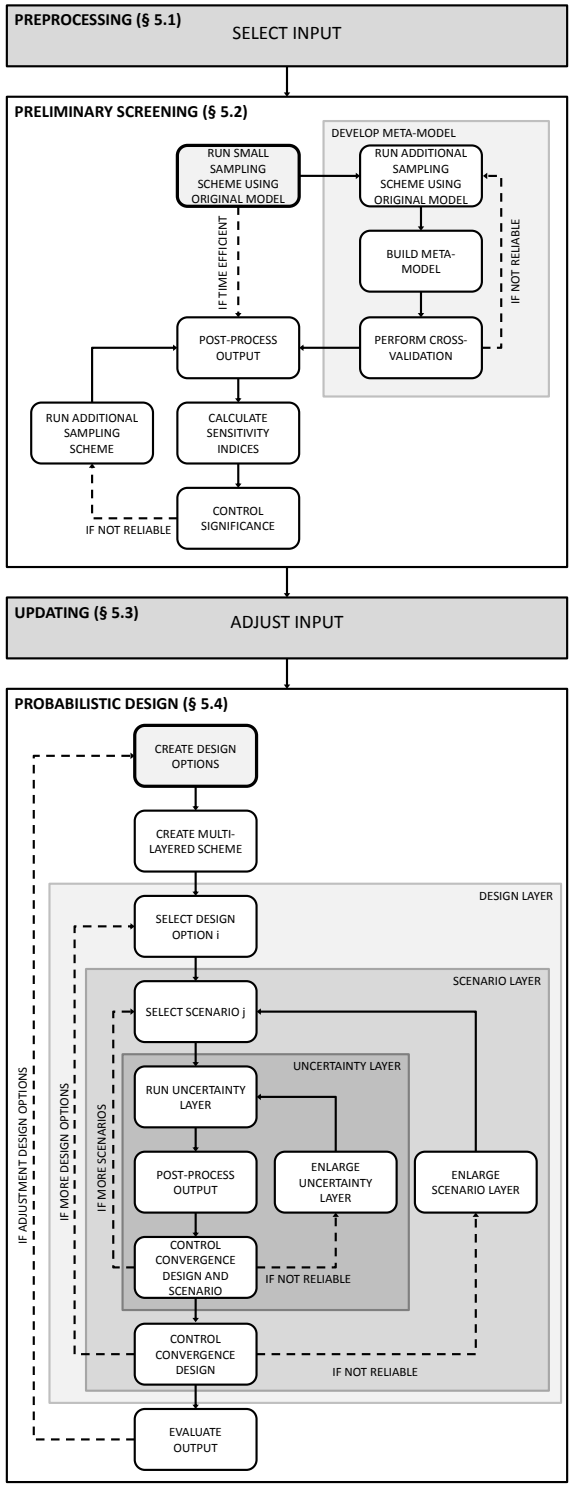

Figure 5.1: Flowchart of probabilistic design methodology. Replica of Fig. 4.1.

After this output selection, the potentially contributing input parameters can be identified through a qualitative approach exploring the problem such as described in (Janssen et al., 2014). Based on expertise or measurement campaigns, one then can determine which parameters are to be considered deterministic and which stochastic. Parameters inherently having a significant uncertainty, such as user behaviour, are obviously stochastic. When it is not sure whether parameter uncertainties will influence the investigated outputs, it is desirable to assume them stochastic, since their impact will be checked anyway in the preliminary screening of section 5.2. The input parameters taken into account in the current illustrative case study are described in section 3.2.3 for the global case study. They are however slightly adapted to accelerate simulations. All stochastic input parameters are relisted in the first column of Table 5.1, according to the parameter categories (design, scenario and uncertainty) described in section 4.5 and already ascribed in section 3.3.

Table 5.1: Stochastic design, uncertainty and scenario parameters.

PARAMETER	**DISTR.***	**META-MODEL**	**SELEC-TION**	**MULTI-LAYERED***
	§5.1	§5.2	§5.3	§5.4
Design				
U-value roof (W/m^{2}K)	Uni(0.1,0.3)	✗	✗	0.2
U-value floor (W/m^{2}K)	Uni(0.1,0.3)	✗	✗	0.2
U-value wall (W/m^{2}K)	Uni(0.1,0.3)	✓	✓	0.1 / 0.15 / 0.18 / 0.24
window type	**	✓	✓	**
inf. rate at 50 Pa (1/h)	Uni(0.44,12.3)	✓	✓	0.6 / 1 / 3 / 5
ventilation system	C / D	✓	✓	C / D 0.7 / D 0.8 / D 0.9
heat recovery eff. (D)	Uni(0.7,0.95)	✓	✓	
sunscreen type	none / 30 %	✓	✓	none / 30 %
Scenario				
nom. energy price evol. (%)	-1.5 / 2.3 / 10		✓	-1.5 / 2.3 / 10
Uncertainty				
dev. from design U-values	Nor(1,0.1)	✗	✗	1
dev. from design inf. rate	Nor(1,0.1)	✗	✗	1
set temp. occ. day z. (°C)	Nor(21,1.35)	✓	✓	Nor(21,1.35)
set temp. abs. day z. (°C)	15 / no reduction	✓	✓	15 / no reduction
set temp. occ. night z. (°C)	Nor(19,2)	✓	✓	Nor(19,2)
air ch. rate day z. (1/h)	Wei(0.6576,4.67)	✓	✓	Wei(0.6576,4.67)
air ch. rate night z. (1/h)	Wei(1.7847,4.67)	✓	✓	Wei(1.7847,4.67)
internal heat gains (W)	Uni(100,500)	✓	✓	Uni(100,500)

* Explanation of the symbols used:
Uni(a,b): uniform distribution between a and b
Nor(μ,σ): normal distribution with mean value μ and standard deviation σ
Wei(λ,k): Weibull distribution with scale factor λ and shape factor k
Discrete uniform distributions are indicated by the sample values
** Window types: 2.07 W/m^{2}K & g = 0.613 / 2.07 W/m^{2}K & g = 0.512 / 1.29 W/m^{2}K & g = 0.631 / 1.31 W/m^{2}K & g = 0.551 / 0.7 W/m^{2}K & g = 0.407

Finally, for all considered input parameters, fixed values and probability distributions for respectively deterministic and stochastic parameters need to be assigned as accurately as possible for the considered problem and its context. For example, data for renovation studies might differ from data for new constructions, and may furthermore depend on location, climate and building tradition. Moreover, some parameters may be variable in time and space. This, as well as the fact that certain parameters may be correlated, can be taken into account. For the current application, the deterministic parameter values can be found in Table 3.2 on page 29. For reasons of simplicity, also following parameters are considered deterministic with their values mentioned between brackets: 'construction type' (massive), 'deviation from design heat recovery efficiency' (1), 'sunscreen control' (automatic 1), 'occupancy profile day zone' (1) and 'occupancy profile night zone' (5). The distributions of the stochastic parameters can be found in the second column of Table 5.1. When comparing this to Table 3.3 on page 30, one can see that for the parameter 'ventilation system' only values 'C' and 'D' are taken into account and for 'sunscreen type' only 'none' and '30 %'. The internal heat gains are simplified by a uniform distribution between 100 and 500 W assigned to 'basis internal heat gains appliances day zone'.

5.2 Preliminary screening

In the preliminary screening, the second block in Fig. 5.1, first all input parameters - irrespective of their place in the design, scenario or uncertainty layer - are sampled together in a small sampling scheme, and the original model is run to investigate the output uncertainty range that can be expected. According to section 4.2, space-filling sampling is preferred as it has faster convergence than random or basic LHS sampling. In order to replace time-inefficient original models, meta-models can be constructed according to section 4.4. If the original model is already time efficient, following meta-modeling steps can be skipped. To balance between time efficiency and reliability, section 4.4.3 proposed a meta-modelling strategy which is also included in Fig. 5.1. At least one extra sample set is needed and more are added until the constructed meta-model is considered sufficiently reliable based on the cross-validation. Remember that the meta-model can only be used in the range of the training data values.

These Monte Carlo sets are then used for a sensitivity analysis to determine the most influencing parameters. First, the outputs of the original model optionally need to be post-processed to obtain the derived output parameters. The sensitivity indices can be calculated in several ways as described in section 4.3. The meta-model can provide some information on the influencing input parameters as well. Since as few samples as needed are preferred in the screening phase, it is essential to monitor convergence of the sensitivity indices. This can be done by studying the p-values as also explained in section 4.3: low p-values, usually smaller than 0.05, indicate significant indices.

Section 4.5 already pointed out the relevance of this preliminary screening. Because the multi-layered sampling used in the probabilistic design step (see section 5.4) usually requires lots of samples, both meta-modelling and sensitivity analysis may significantly reduce calculation time.

For the current case study, a maximin LHS scheme as explained in section 4.2 is chosen. The parameters in Table 5.1 are sampled 20 times and these samples are run in the BES model, resulting in yearly heat demands between 43 kWh/m^2 and 153 kWh/m^2. Column permutations will be used to gradually add sample sets for meta-modelling and sensitivity analysis.

The BES model is replaced by a meta-model for net heat demand simulation. For that purpose, the MARS method as described in section 4.4 is used because of its simplicity and clear relationship between input and output. As validation indicators, the coefficient of determination r^2 and the maximal absolute error MAE are used. Because a good performance of the meta-model is crucial, the predetermined validation criteria are: (1) the average r^2 has to be above 0.95 with a small spread, and (2) the maximal MAE (arbitrarily) has to be smaller than half of 43 kWh/m^2, which was the minimal value in the first screening. Note that one can also opt for a relative error in this case, since higher heat demands may allow for higher errors. The sequential addition of sample sets is shown in Fig. 5.2. In Fig. 5.2a, one can see that six sample sets, thus five column permutations from the original maximin sampling scheme, were needed to meet the validation criteria for r^2. The minimal and maximal r^2 are respectively 0.93 and 0.97. For MAE however, seven sets are needed as can be seen in Fig. 5.2b. The minimal and average MAE are respectively 10 and 13 kWh/m^2. The meta-model based on seven sample sets is thus used to replace the BES model in the further analysis.

These seven sample sets are then used to calculate Spearman's rank correlations between the net present cost and the contributing input parameters, as well as their p-values. Table 5.2 shows the parameters in descending order of influence. As can be

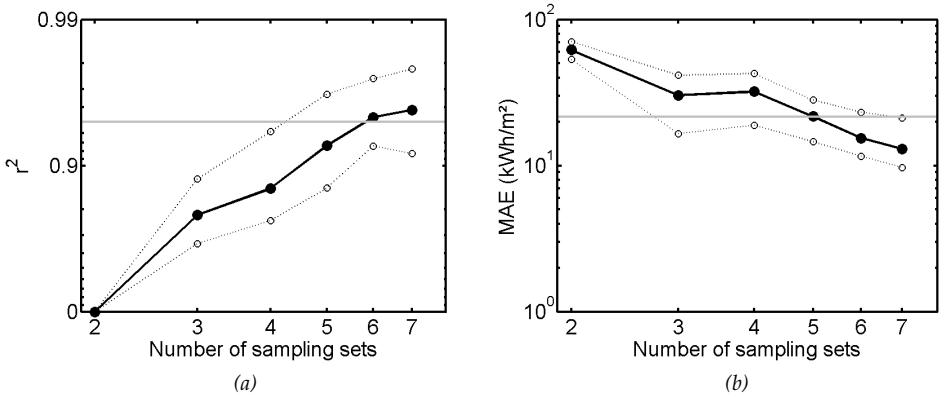

Figure 5.2: Addition of sample sets for MARS model construction until the validation indicators in the cross-validation meet the validation criteria. The validation criteria are marked in grey.

seen, increasing absolute ρ means decreasing p. In this example, only the nominal energy price evolution, the sunscreen type and the infiltration rate significantly influence the net present cost. Since the nominal energy price evolution will be considered as scenario parameter in section 5.4, the sensitivity analysis is repeated for a constant energy price evolution (in this case 2.3 %) in Table 5.3. For that purpose,

Table 5.2: Spearman's ρ and p-values of net present cost in descending order of influence. Insignificant indices are indicated in grey.

PARAMETER	ρ	**p**
nominal energy price evolution	0.74	0.00
sunscreen type	0.43	0.00
infiltration rate at 50 Pa	-0.24	0.00
U-value wall	-0.11	0.19
set temperature occupancy day zone	0.11	0.20
U-value roof	-0.09	0.28
heat recovery efficiency	0.09	0.32
U-value floor	-0.08	0.36
ventilation system	0.08	0.37
set temperature occupancy night zone	-0.07	0.43
deviation from design infiltration rate	-0.05	0.52
internal heat gains	-0.05	0.56
deviation from design U-values	0.05	0.59
air change rate	-0.03	0.77
set temperature absence day zone	-0.02	0.81
window type	-0.02	0.77

Table 5.3: Spearman's ρ and p-values of net present cost without scenario parameter in descending order of influence. Insignificant indices are indicated in grey.

PARAMETER	ρ	**p**
sunscreen type	0.70	0.00
infiltration rate at 50 Pa	-0.28	0.00
U-value wall	-0.19	0.02
set temperature occupancy day zone	0.15	0.08
U-value floor	-0.12	0.17
deviation from design U-values	0.09	0.31
deviation from design infiltration rate	-0.09	0.31
set temperature absence day zone	-0.08	0.32
internal heat gains	-0.08	0.35
heat recovery efficiency	0.08	0.38
ventilation system	0.05	0.53
window type	-0.04	0.65
U-value roof	-0.04	0.67
air change rate	0.03	0.71
set temperature occupancy night zone	-0.03	0.77

the cost calculation post-processing has to be repeated. Again the sunscreen type and infiltration rate, but also the U-value of the wall, significantly influence the net present cost. To get the comprehensive picture, this can be analogously done for the other scenario values.

Because a MARS model takes only the most influencing parameters into account, the created heat demand meta-model, replacing the original BES model, can equally be used as sensitivity tool for the heat demand. The contributing parameters are indicated in the third column of Table 5.1. When calculating ρ as well, these parameters are indeed most influencing for heat demand. As heat demand is only part of the net present cost, important parameters for heat demand might be less important for net present cost. Furthermore, decreasing energy cost due to design options might be associated with increasing investment costs, resulting in a zero contribution. However, for this case study the dominant parameters for net present cost of Table 5.3 also appear in the meta-model.

5.3 Updating

The updating step, the third block in Fig. 5.1, may appear to be a small and unimportant step. This step is however crucial in view of the time efficiency of the design methodology. Section 4.3 showed that including only dominant parameters in an uncertainty analysis provides reliable results. Therefore, based on the sensitivity results, one can judge which parameters need accurate distributions and which parameter variations can be neglected. Omitting input parameters with little influence reduces labour cost to find all distributions, and may improve sampling efficiency of space-filling sampling schemes as also shown in section 4.3. Moreover, this can limit the number of design options in the probabilistic design of section 5.4, significantly improving optimisation efficiency as illustrated in section 4.5.

In the considered case study, the U-values of roof and floor and both deviation parameters are omitted as their variation was apparently not significant for the heat demand, nor for the net present value. Note that the considered U-values indicate already well insulated components. The respective average values are therefore considered in the probabilistic design, as shown in Table 5.1. As the distributions of design, uncertainty and scenario parameters were already based on a measurement campaign, no further adjustments are needed. Based on the sensitivity results, one can expect that design parameters 'sunscreen type', 'infiltration rate' and 'U-value of wall' will dominate the optimal design options.

When a sufficient number of input and output measurements is available, the input distributions of the most influencing parameters can be refined based on Bayesian calibration (Kennedy and O'Hagan, 2001). This can be the case in renovation design of existing buildings as illustrated in (Heo et al., 2012; Booth et al., 2012; Booth and Choudhary, 2013). This Bayesian calibration considers prior distributions of the input parameters based on expertise knowledge. These prior distributions are then updated through matching the model outputs and the monitored outputs, resulting in plausible distributions of the calibrated parameters, the so called

posterior distributions. Unfortunately, the buildings of interest are usually ór not measured to a sufficient extent ór still to be build. Therefore, a Bayesian calibration is often not possible and thus out of the scope of this thesis.

5.4 Probabilistic design

After the problem is screened and all input distributions are known, the actual probabilistic design, which is shown in the fourth block in Fig. 5.1, can be performed based on the meta-model. In order to calculate the output distributions for all considered design options, a multi-layered sampling as described in section 5.4.1 is performed. The resulting output distributions then allow a visual comparison of the considered design options. However, when numerous design options and multiple output parameters are included, this becomes difficult. Therefore, section 5.4.2 describes how these outputs can be numerically evaluated. The effectiveness and robustness indicators are introduced in order to use them to select the most effective and robust design options in view of robust design. Furthermore, section 5.4.3 handles several ways of using these output indicators in the design optimisation.

5.4.1 Multi-layered sampling

Since multi-layered sampling is extensively described in section 4.5, it is only briefly handled here. First the competing design options have to be selected and a sampling scheme for the inherently uncertain parameters and for the scenario parameters has to be created. In order to calculate the output distributions for all considered design options and to allow an explicit evaluation for the considered scenarios, these options are combined in a multi-layered sampling scheme with the scenario and uncertain parameter values. The Monte Carlo loop, which was already seen in Fig. 4.23, is then run and the multi-layered scheme is enlarged until the considered output indicators converge.

Note that in a probabilistic analysis only one design is investigated, thus this is examined as a probabilistic design problem with only one value in the design layer.

In the current application example, every design parameter is sampled with several design values (see Table 5.1 column 4) and these values are combined in a full factorial scheme, leading to 640 considered design options in the design layer. The scenario layer is created based on potential discrete scenario options, such as in Table 5.1. The inherently uncertain parameters are sampled in a maximin LHS scheme (see section 4.2.1) with a size of 20 samples. This scheme can be enlarged by adding new maximin schemes.

When optimising the design for cost effectiveness and robustness as will be described in section 5.4.2, we are interested in the minimum, the median and the 2.5 % and 97.5 % percentiles of the net present cost. In order to obtain convergence for a 1 % deviation level for these output indicators, an uncertainty sampling size of 40 samples is needed. A total of 76 800 runs is thus performed. Because of the time-efficient MARS meta-model of section 5.2, this only takes a few minutes.

This multi-layered sampling results in 640 cumulative distribution functions for net present costs as shown in Fig. 5.3. The vertical shift at 67 % is due to the third considered economic scenario. An energy price evolution of 10 % will highly influence the net present cost as indicated in Table 5.2. It should be mentioned that weighted percentiles should be used to calculate these distributions if the uncertainty layer samples are not the same for every design and scenario combination, as already explained in section 4.5.2. In Fig. 5.4, the cumulative distributions are splitted out for the three considered scenarios. A visual comparison of the design options, overall or over the scenarios, is possible in Fig. 5.3 and 5.4, however, this is not very efficient in selecting the most optimal one.

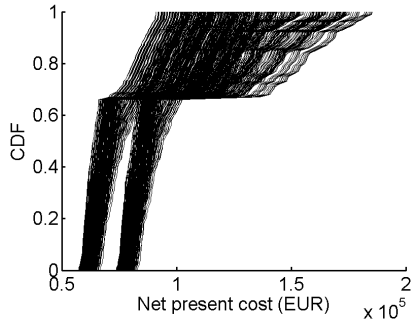

Figure 5.3: Comparison of net present cost output distribution for 640 design options.

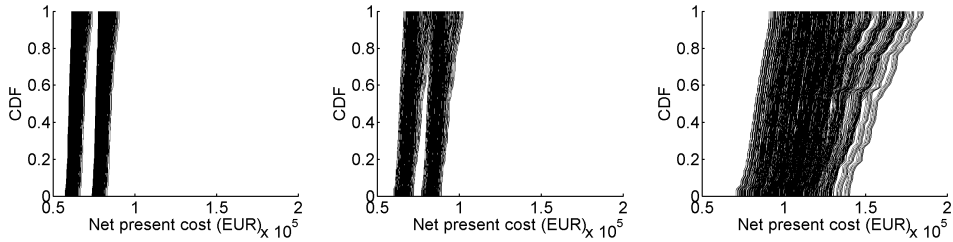

(a) -1.5 % *(b) 2.3 %* *(c) 10 %*

Figure 5.4: Comparison of net present cost output distribution for 640 design options and three energy price scenarios.

5.4.2 Output indicators

Since a visual comparison of cumulative distributions such as in Fig. 5.3 and 5.4 is not always feasible, especially not for numerous design options and multiple performances, these output distributions need to be evaluated numerically through output indicators. Output indicators can be used in multi-objective optimisation in order to select the most favourable design option, which will be introduced here and handled in more detail in section 5.4.3.

Depending on the problem, several output indicators can be used for that purpose. One can consider, for example, minimum, maximum, average or median values. In risk analysis, one might opt for the percentage that a certain value is exceeded. For

the robust design approach used in the current example, the use of the effectiveness ε and robustness R_P indicators is proposed. These indicators are thus first explained and illustrated. Then, it is shown that the use of these indicators is very flexible.

Effectiveness and robustness indicators

In robust design, mean performance is optimised while spread is minimised, resulting in a design that can resist the influence of uncontrollable factors as good as possible without eliminating these factors (Sanchez et al., 1996; Zang et al., 2005). For that purpose, **effectiveness** ε and **robustness** R_P indicators are proposed in this thesis as intuitive robust design output indicators. In here, performance variation, and thus robustness, is evaluated through percentile differences as has been done in literature (Rathod et al., 2013). This is thought to be a better approach than using standard deviations since percentiles can account for the tails of the distribution and are thus more flexible (Du et al., 2004). Moreover, the indicators are made relative to the performance and spread for the full set of design options, thus the probability distribution before a design option is chosen. This provides intuitive measures to evaluate how good the selected design option is in relation to the set of all potential options. For a design option x_i, which is a set of design parameter values, ε and R_P are formulated as

$$\varepsilon(x_i) = 1 - \frac{y_{50}(x_i) - y_{\min}}{y_{50} - y_{\min}} \tag{5.1}$$

$$R_P(x_i) = 1 - \frac{y_{50+P/2}(x_i) - y_{50-P/2}(x_i)}{y_{50+P/2} - y_{50-P/2}} \tag{5.2}$$

with y_q the q^{th} percentile under full uncertainty, $y_q(x_i)$ the q^{th} percentile after selecting design option x_i and P the user specified percentage of included sample points, as illustrated in Fig. 5.5. y_{min} corresponds to the minimal calculated value which is not an outlier, whereby an outlier is defined as a sample point smaller than $y_{25} - 1.5(y_{75} - y_{25})$. In this definition the performance indicator y is defined in such a way that it is greater or equal to zero and to be minimised.

In these equations, effectiveness thus describes how the deviation between median performance and realistic optimal performance (y_{min}) for a design option improves compared to the deviation under full uncertainty. The robustness is analogously determined as the improvement the performance spread of a design option makes in proportion to the performance spread under full uncertainty. According to this definition a measure with an effectiveness and robustness of one is the best possible, while negative values are to be avoided. Note that these indicators are depending on the considered scenarios and the set of potential design options.

For a proper understanding, Fig. 5.6 illustrates the usage of these effectiveness and robustness definitions by linking them to a visual selection based on the probabilistic distributions. When three design options are considered, the effectiveness ε will be improved when the grey option is selected instead of the other two. The robustness R_p will moreover be improved when the dotted black design option is chosen.

In the current application, P is taken equal to 95 % in order to include most of the potential net present costs for each design option. Since we are interested in the

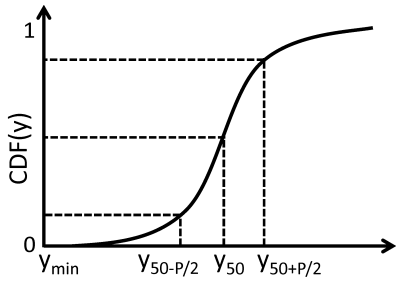

(a) CDF of output parameter value y under full uncertainty of design and uncertain parameters and considered scenarios.

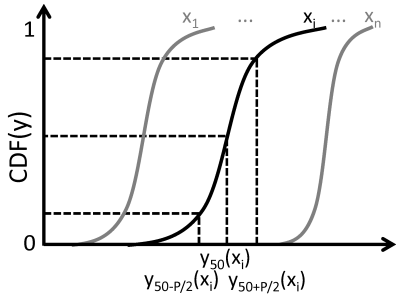

(b) CDF of output parameter value y for design options x_i under uncertainty of uncertain parameters and considered scenarios.

Figure 5.5: Cumulative distribution functions (CDF) of output parameter value y under full uncertainty and after selection of design options x_i.

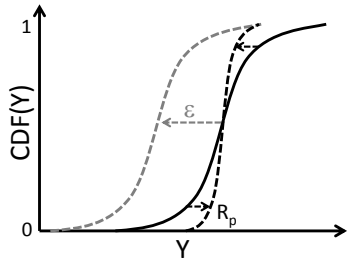

Figure 5.6: Cumulative distribution function of output performance Y of three design options. An effectiveness improvement is indicated in grey, while a robustness improvement in black.

most effective and robust design option x_i for this net present cost NPC, Eq. 5.1 and Eq. 5.2 become

$$\varepsilon(x_i) = 1 - \frac{NPC_{50}(x_i) - NPC_{\min}}{NPC_{50} - NPC_{\min}} \tag{5.3}$$

$$R_{95}(x_i) = 1 - \frac{NPC_{97.5}(x_i) - NPC_{2.5}(x_i)}{NPC_{97.5} - NPC_{2.5}} \tag{5.4}$$

Since a full factorial scheme is applied for the design options, all percentiles are known and ε and R_{95} can thus be easily calculated for all design options.

Fig. 5.7a shows this R_{95} as a function of ε for all 640 design options, subjected to both uncertainty and scenario parameters. Based on these two indicators, the Pareto optimal design options can be calculated. Pareto optimality indicates in multi-objective optimisation those design options for which there is no other design option with a better performance for one objective without a worse for at least one other. The set of Pareto optimal design options is called the Pareto frontier (Machairas et al., 2014; Nguyen et al., 2014). The Pareto frontier in this example includes the lower infiltration rates, a balanced ventilation system, the lower U-values for walls and windows and no sunscreens. These optimal designs are also indicated in Fig. 5.8 to illustrate that these are indeed the preferred options when visually comparing the output distributions.

Because of the economic scenario layer in the multi-layered sampling scheme, an explicit check of these overall optimal designs for potential economical scenarios is desired. This is shown in Fig. 5.7b. ε and R_{95} are therefore calculated per design and scenario option:

$$\varepsilon(x_i, s) = 1 - \frac{NPC_{50}(x_i, s) - NPC_{\min}}{NPC_{50} - NPC_{\min}} \tag{5.5}$$

$$R_{95}(x_i, s) = 1 - \frac{NPC_{97.5}(x_i, s) - NPC_{2.5}(x_i, s)}{NPC_{97.5} - NPC_{2.5}} \tag{5.6}$$

with $NPC_P(x_i, s)$ the percentiles after design options x_i and scenario s are selected. One can see that the selected optimal designs are not really optimal in all scenarios, but close to optimal, indicating that they are reliable in this case study. One can see that the variability of the net present cost is reduced while selecting the scenario values and thus that the R_{95} indicators are increased, because the energy price evolution is highly influencing the net present cost. The difference in robustness between the design options is therefore also reduced. This can be seen in Fig. 5.4 compared to Fig. 5.3 as well. When looking at ε of the design options, one can see that this can be highly influenced by the future scenario as well. Selecting one of the overall Pareto front solutions is in this case advised. Especially when a sharp increase of the energy price will occur in future, the selection of a well-performing design option seems to be important.

The effectiveness and robustness indicators for the different scenarios (Eq. 5.5 and 5.6) can also be calculated as

$$\varepsilon(x_i, s) = 1 - \frac{NPC_{50}(x_i, s) - NPC_{\min}(s)}{NPC_{50}(s) - NPC_{\min}(s)} \tag{5.7}$$

$$R_P(x_i, s) = 1 - \frac{NPC_{97.5}(x_i, s) - NPC_{2.5}(x_i, s)}{NPC_{97.5}(s) - NPC_{2.5}(s)} \tag{5.8}$$

In here, the indicators are defined for each scenario separately, thus without considering the other potential scenarios in the overall distributions. By doing so, the indicators can only be studied for the considered scenario as shown in Fig. 5.9. A comparison of the values between the scenarios is therefore not meaningful. Eq. 5.5 and 5.6 are in that case preferred.

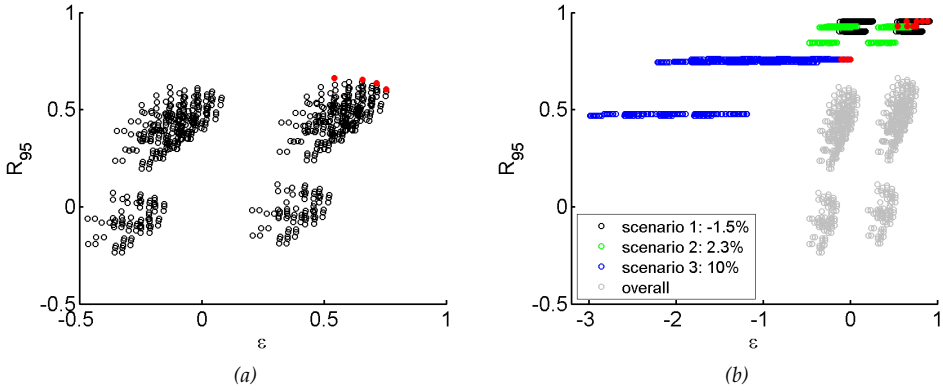

Figure 5.7: (a) R_{95} of net present cost in function of ε for all design options. Pareto frontier is indicated in red. (b) R_{95} and ε for three scenarios. Overall R_{95} and ε of (a) are indicated in grey. Overall optimal designs of (a) are indicated in red.

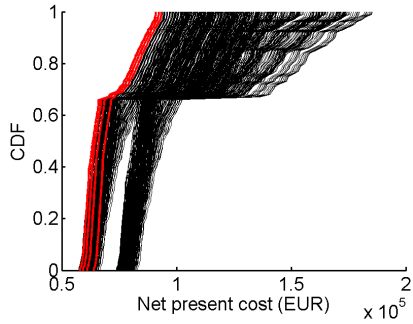

Figure 5.8: Comparison of net present cost output distribution for 640 design options of Fig. 5.3. Optimal designs of Fig. 5.7a are indicated in red.

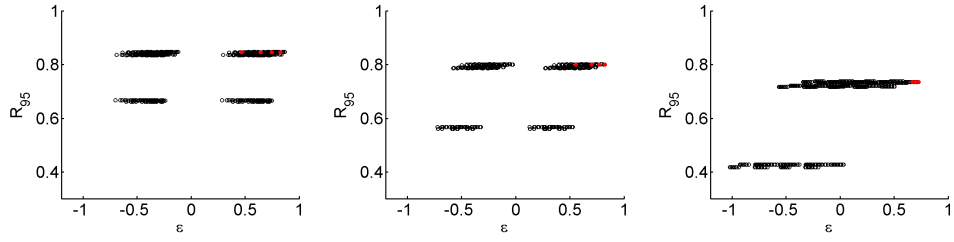

Figure 5.9: ε and R_{95} of net present cost calculated separately for three design options for 640 design options. Optimal design options of Fig. 5.7 are indicated in red.

In the above application, we compared all potential design options and selected the best performing ones based on Pareto optimality. Section 5.4.3 will illustrate other possibilities to select optimal design options. First, alternative formulations for the effectiveness and robustness equations are given.

Flexibility of effectiveness and robustness indicators

Eq. 5.3 - 5.8 showed already three possibilities of using the effectiveness and robustness indicators, applied to the illustrative example in which the aim is to minimise the net present cost. The general effectiveness and robustness equations Eq. 5.1 and 5.2 can however also been used for other purposes of which three are described here. A combination of all given equations is of course possible as well.

1 Performance y to be maximised Instead of an optimisation for which the performance is to be minimised (Eq. 5.1), a maximisation problem can be considered as well. One can for example not minimise the net present cost, but maximise the energy savings related to a specific design option. In that case, ε has to be calculated with

$$\varepsilon(x_i) = 1 - \frac{y_{\max} - y_{50}(x_i)}{y_{\max} - y_{50}} \tag{5.9}$$

with $y_{\max}$ the maximal calculated value which is not an outlier, whereby an outlier is defined as a sample point smaller than $y_{75} + 1.5(y_{75} - y_{25})$. The robustness indicator is not changed for this purpose.

2 Performance y to be optimised with a specific target value When the goal is not to minimise or maximise the performance as such, but to obtain a performance as close as possible to a considered target, ε has to be calculated with

$$\varepsilon(x_i) = 1 - \frac{|y_{50}(x_i) - y^*|}{|y_{50} - y^*|} \tag{5.10}$$

with y^* the target value. The smallest or largest feasible value of Eq. 5.1 or Eq. 5.9 ($y_{\min}$ or $y_{\max}$) is thus replaced by the target value y^*. This can be the case when a certain budget has to be spent over a specific lifespan. It should be remarked that if y_{50} is equal to target value y^*, ε cannot be calculated. This means that, on average, the target value is already reached when no decisions on the design options have been made. In that case, a very small value can be chosen for the denominator. R_P is also in this case calculated with 5.2.

3 Performance y to be minimised for a certain subset of design options When the effectiveness and robustness indicators have to be calculated after a subset of all potential design options is selected, one can use

$$\varepsilon(x_i \in X_d^*) = 1 - \frac{y_{50}(x_i \in X_d^*) - y_{\min}(X_d^*)}{y_{50}(X_d^*) - y_{\min}(X_d^*)} \tag{5.11}$$

$$R_P(x_i \in X_d^*) = 1 - \frac{y_{50+P/2}(x_i \in X_d^*) - y_{50-P/2}(x_i \in X_d^*)}{y_{50+P/2}(X_d^*) - y_{50-P/2}(X_d^*)} \tag{5.12}$$

with $X_d^* \subseteq X_d$, whereby X_d is the set of all potential design options and X_d^* the

considered subset. This subset can be needed, for example, when first all adverse design options are omitted. This can be the case when multiple performances are considered and one or more of the performances are used to eliminate design options because of, for example, potential discomfort.

5.4.3 Optimisation procedures

In the previous section, Pareto optimal design options were selected based on a comparison of the cost effectiveness and robustness of all potential design options. In this section, several alternative optimisation procedures are compared.

Pareto optimality versus weighted sum method

As illustrated in Fig. 5.7, a set of optimal design options can be selected based on Pareto optimality. Effectiveness is therefore traded off against robustness as explained in section 5.4.2. One of the Pareto optimal design options can then be chosen based on user preferences. In the current example in Fig. 5.7, the Pareto frontier contains four design options. When comparing these options, one might select the most effective one since its robustness it only slightly lower than that of the most robust one, however, its effectiveness is significantly larger.

An alternative approach is the weighted sum method (Machairas et al., 2014; Nguyen et al., 2014), in which the objective function

$$\varepsilon + wR_P \tag{5.13}$$

has to be maximised. In here, w is the user-defined weight factor which explicitly trades off effectiveness against robustness. Inspired by (Janssen et al., 2014), this objective function can be considered

- risk-neutral ($w = 0$) when only the effectiveness of the design options is taken into account,
- risk-averse ($w > 0$) when both a high effectiveness and robustness is desired, or
- risk-taking ($w < 0$) when a low robustness combined with a high effectiveness is sought because a higher probability of poor performances is accepted in order to increase the average performance.

w is thus chosen dependent on how important an actual performance close to the target performance is, or in other words, to what extent a spread around the target performance is accepted. In robust design, risk-averse objective functions are considered. When $0 < w < 1$, effectiveness is more dominant, while when $w > 1$, robustness is more dominant.

For the current example, w is varied between zero and four in steps of 0.1, resulting in the optimal ε and R_{95} of Fig. 5.10. One can see that three optimal design options are found. These options were also obtained in the Pareto frontier of Fig. 5.7a. When

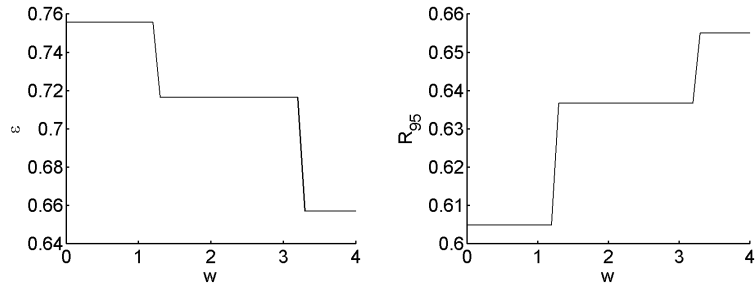

Figure 5.10: Risk-averse optimisation of ε and R_{95} for w between zero and four.

robustness is gaining importance in the decision-making, better design values for the air infiltration and window types are obtained.

In this example, ε and R_{95} for only the net present cost were traded off in the multi-objective optimisation. More performances can of course be included as well. This will be illustrated in Chapter 6.

Design layer versus search algorithm

In section 5.4.2, the output indicators are computed for all design options of the design layer created in section 5.4.1. This allows to compare all potential design options and to decide on good and bad choices for the design values. This approach moreover guarantees that the global optimum is found.

Alternatively, the optimal design options can be selected based on an optimisation algorithm (Machairas et al., 2014) as already mentioned in section 4.5.1. A genetic algorithm, for example, is based on natural selection and evolution (Michalewicz et al., 1996) and is sometimes used in building performance optimisation (Verbeeck and Hens, 2007; Gossard et al., 2013; Malatji et al., 2013; Nguyen et al., 2014). In such an algorithm, a first guess is made for the optimal design and the design parameter values of a set of potential options (the population) evolve towards the optimum based on the calculated output indicators in some iterations (the generations). There is however no guarantee that the found optimum is a global optimum and not a local, since the global optimum can be overlooked. Based on all calculated generations of populations, a study of good and bad choices for the design values is possible as well, however, not as detailed as when considering all potential options.

When such an optimisation algorithm is used instead of the full design layer for selecting design options based on the effectiveness and robustness calculations of section 5.4.2, some minor changes are required. Since the full set of design options is not calculated, in each generation only the percentiles of the design options of the current population are known for computing Eq. 5.1 and 5.2. The overall percentiles in the denominator are thus to be calculated in advance. In the most simple case, no scenario-dependent percentiles such as in Eq. 5.7 and 5.8 have to be created and the design parameter boundaries are not adapted in the design process. Then, the preliminary screening (see section 5.2) can provide the overall percentiles.

When, however, the design parameter boundaries are changed, an updated single-layered scheme of section 5.2 can be created. In case that overall percentiles for specific scenarios need to be calculated, a design layer scheme which is preferably space-filling sampled is used and combined with the already created scenario and uncertainty layers. This small design layer is then also enlarged until convergence is reached for the used percentiles.

For the current example, a genetic algorithm is applied as follows. Because the design parameter boundaries are adapted in the multi-layered scheme as can be seen in Table 5.1, the single-layered design of section 5.2 cannot be used to calculate the overall parameters. Therefore, an adapted single-layered sampling scheme is generated because no explicit evaluation for scenarios is wanted. Again, a maximin scheme with 20 samples is chosen, which is enlarged until internal standard deviations below 5 % are reached for the minimum and the 2.5 %, 50 % and 97.5 % percentiles because they are needed in the denominators of Eq. 5.1 and 5.2. Since a meta-model was constructed in section 5.2, this can be used to accelerate the calculations. Then, a genetic algorithm with objectives ε and R_{95} is run with the *Global Optimization Toolbox* of Matlab (MathWorks, 2014*c*). A population size of 100 in each generation is chosen. For the non-discrete parameters, such as the U-value and n_{50}-value, a uniform distribution is handled. For each design option in the population, the uncertainty and scenario layers are run and enlarged as explained in section 5.4.1. Thereafter, ε and R_{95} are calculated for these design options and the design values are changed in order to improve these indicators. The resulting Pareto frontier is presented in Fig. 5.11. When comparing this frontier to the Pareto frontier obtained when studying the full set of design options (see Fig. 5.7a), no major differences are found. Because the denominator percentiles can slightly differ between the two approaches, the ε and R_{95} values are not exactly the same for same design options. In this example, the R_{95} values are for example slightly smaller in the genetic algorithm approach. Because for U- and n_{50}-values a continuous distribution instead of levels is considered, slightly better ε's are found. These options can be obtained as well by refining the levels after the optimal options of Fig. 5.7a are studied.

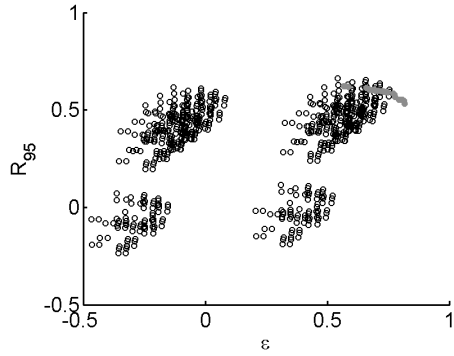

Figure 5.11: ε and R_{95} indicators of net present cost for all 640 design options of Fig. 5.7a with the indication of the Pareto frontier obtained from the genetic algorithm.

One of the advantages of this genetic algorithm approach is that continuous ranges of design values can be taken into account, while for the design layer approach only some levels are studied. However, when the levels are chosen relatively close to each other, the optimal values are very similar. Although in the genetic algorithm approach not all design options are evaluated, the uncertainty and scenario layers are still to be considered. Therefore, a meta-model is still needed in many case studies. Because of this meta-model, the calculation time for evaluating all potential design options is not too high compared to the genetic algorithm calculations since multiple generations with a certain population need to be evaluated as well. More efficient in further reducing calculation time is the use of limited design layers as explained in section 4.5.1.

Exclusion or penalising of design options

In more advanced applications, it is conceivable that not all output parameters are handled in the same way. If, for example, negative ε and R_{95} have to be explicitly excluded, one can exclude corresponding design options from the full set and find the optimum of the remaining options as also shown in Eq. 5.11 and 5.12. Another example is the exclusion of designs resulting in undesirable outcomes such as discomfort by overheating as will be illustrated in section 5.5. Alternatively to excluding the options, large weight factors can be chosen to minimise these undesired performances in the weighted sum method.

5.5 Reliability of meta-modelling in probabilistic design

Since uncertainty and sensitivity analyses are already quite common in the building physics field, the main success of the presented probabilistic design approach is attributed to the use of meta-models in order to significantly improve the calculation time. Without these meta-models, the methodology would not be feasible for most building physical calculation models. However, because of the simplicity of the meta-models - some aspects of the original model are inherently neglected - the reliability of the results might be affected. A study of this aspect is thus essential for the validity of the probabilistic design methodology. The principles of sections 5.1 - 5.4 are therefore in this section applied on a slightly more advanced case study, which is explained in section 5.5.1, in order to illustrate that the use of meta-models is reliable in the design methodology. Optimisation is therefore performed on both the original model and several meta-models, differing in sample size. The results are shown in section 5.5.2.

5.5.1 Case study

The case study used in this section is a simplified version of the global case study of Chapter 3. Several low-energy design options are compared to select the most cost effective and robust option, with a comfortable indoor climate as auxiliary constraint. Therefore, both net present costs and maximal temperatures are considered. As

explained in section 3.2.4, a transient BES model is used to calculate the indoor temperatures and heat demand. This BES model will be replaced by a meta-model.

5.5.2 Results

The results of the probabilistic design will be described according to the four steps in the methodology as presented in Fig. 5.1.

Preprocessing

The model and model outputs were selected as described in section 5.5.1. The considered input parameters are presented in Table 5.4 with their input distributions. In order to make probabilistic design with the original model feasible, calculation time is reduced by selecting only a limited set of design parameters. Due to the simplifications, following parameters are considered deterministic with their values mentioned between brackets: 'construction type' (massive), 'U-value roof' (0.2), 'U-value floor' (0.2), 'sunscreen control' (automatic 1), 'occupancy profile day zone' (1) and 'occupancy profile night zone' (5). When comparing this table to Table 3.3 on page 30, one can see that a limited number of values is taken into account for 'ventilation system', 'window type' and 'sunscreen type'. The internal heat gains

Table 5.4: Stochastic design, uncertainty and scenario parameters.

PARAMETER	DISTRIBUTION*	MULTI-LAYERED*
Design		
U-value wall (W/m^2K)	Uni(0.05,0.3)	0.1 / 0.15 / 0.2 / 0.25
window type	1.29 W/m^2K & g = 0.631 / 1.31 W/m^2K & g = 0.551 / 0.7 W/m^2K & g = 0.407	1.29 W/m^2K & g = 0.631 / 1.31 W/m^2K & g = 0.551 / 0.7 W/m^2K & g = 0.407
infiltration rate at 50 Pa (1/h)	Uni(0.5,1.5)	0.6 / 1 / 1.4
ventilation system	C / D 0.7 / D 0.8 / D 0.9	C / D 0.7 / D 0.8 / D 0.9
sunscreen type	none / 30 %	none / 30 %
Scenario		
nom. energy price evol. (%)	-1.5 / 2.3 / 10	-1.5 / 2.3 / 10
Uncertainty		
dev. from design U-values	Nor(1,0.1)	Nor(1,0.1)
dev. from design inf. rate	Nor(1,0.1)	Nor(1,0.1)
dev. from design heat rec. eff.	Nor(1,0.1)	Nor(1,0.1)
set temp. occ. day zone (°C)	Nor(21,1.35)	Nor(21,1.35)
set temp. absence day (°C)	15 / no reduction	15 / no reduction
set temp. occ. night zone (°C)	Nor(19,2)	Nor(19,2)
air ch. rate day zone (1/h)	Wei(0.6576,4.67)	Wei(0.6576,4.67)
air ch. rate night zone (1/h)	Wei(1.7847,4.67)	Wei(1.7847,4.67)
internal heat gains (W)	Uni(100,500)	Uni(100,500)

* Explanation of the symbols used:
Uni(a,b): uniform distribution between a and b
Nor(μ,σ): normal distribution with mean value μ and standard deviation σ
Wei(λ,k): Weibull distribution with scale factor λ and shape factor k
Discrete uniform distributions are indicated by the sample values

are simplified by a uniform distribution between 100 and 500 W assigned to 'basis internal heat gains appliances day zone'.

Preliminary screening and updating

In order to build the meta-models, all parameters are sampled together and both a sample size of 100 and 20 with up to ten sets of these sample sizes are created and run in the BES model. For that purpose, a maximin LHS scheme as presented in section 4.2.1 is used for sampling and the MARS method as presented in section 4.4.2 for meta-modelling.

Fig. 5.12 shows the cross-validation of created meta-models for heat demand and Fig. 5.13 for maximal temperature. One can see that the model reliability increases with the total number of samples. Out of all presented models, four are selected to study the resulting reliability:

- reference meta-model: this is considered as the reference model as it is based on 10 sets of 100 runs and is the most reliable out of the available models,

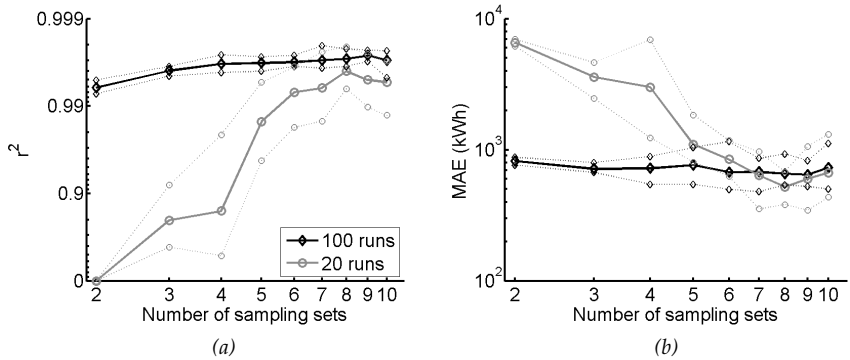

Figure 5.12: Minimal, average and maximal r^2 and MAE cross-validation indicators of the heat demand meta-model for different number of sets and samples.

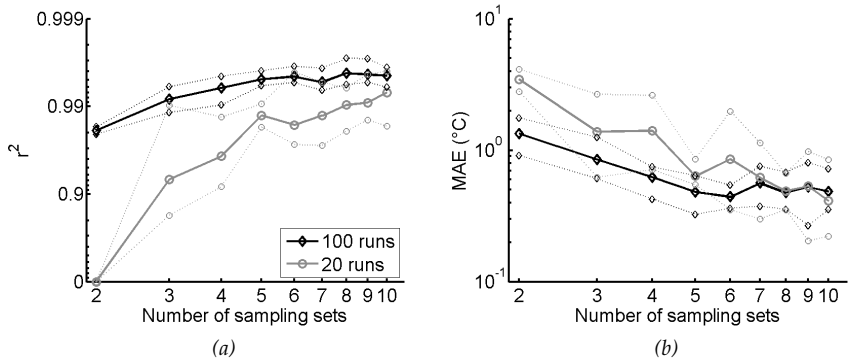

Figure 5.13: Minimal, average and maximal r^2 and MAE cross-validation indicators of the maximal temperature meta-model for different number of sets and samples.

- meta-model 1: this model is built and validated on two sets of 100 runs and is considered as sufficiently reliable,
- meta-model 2: this model is built and validated on 10 sets of 20 runs, thus containing as many samples as meta-model 1, and the indicators are clearly converged, and
- meta-model 3: this model is built and validated on five sets of 20 runs and is the model containing the minimal number of samples to create a reliable meta-model according to Fig. 5.12 and 5.13.

Because already a limited number of input parameters was selected in Table 5.4, the sensitivity analysis and input updating were not performed for this example. The results would be similar to section 5.2 and 5.3.

Probabilistic design

In order to optimise the net present cost effectiveness and robustness, first a multi-layered sampling scheme is created. The input parameter distributions of design, scenario and uncertainty layer are listed in Table 5.4. In order to make probabilistic design with the original model feasible, calculation time is reduced by selecting only a limited set of design parameters in the preprocessing step and also a limited set of design values in this probabilistic design step. All relevant combinations of the considered design values result in 216 design options. As we are interested in the net present costs, the energy price evolution is of major interest. By considering this as a scenario parameter, we are able to study the optimal results for each potential evolution. Three discrete values are considered. 100 uncertainty values are sampled in sets of 20 with a maximin LHS scheme. In order to be able to compare all output values of the four models, the same uncertainty layer size is considered for all design and scenario combinations. This results in a total of 64 800 simulations. This multi-layered sampling scheme is thus run and the convergence of the 100 uncertainty samples is checked. The relative internal standard deviation of all outputs used is for all models and all design and scenario combinations below 2 % after these five sets. When comparing the model outputs in Fig. 5.14, one can see that the original model outputs are mimicked very well by both meta-models. No significant differences between the reference meta-model and meta-model 3 are found.

As mentioned before, the effectiveness and robustness of the net present cost has to be maximised, while avoiding the risk on overheating. For that purpose, ε and R_{95} indicators are calculated with Eq. 5.1 and 5.2 and those designs where the indoor temperature may rise above 28 °C (which is taken as the limit in section 3.2.4) are excluded for all considered models. Because of this exclusion, ε and R_{95} could also be calculated with Eq. 5.11 and 5.12. The resulting Pareto frontier of the original model is shown in Fig. 5.15 and Table 5.5.

When comparing net present cost effectiveness and robustness between BES model reference meta-model and meta-model 3, slightly deviating values are found, as shown in Fig. 5.16. Although these deviations become slightly larger when fewer samples are used to build the meta-model, very similar Pareto frontiers are obtained, as presented in Table 5.6. Only one option (i.e. 135) appears in a meta-model frontier

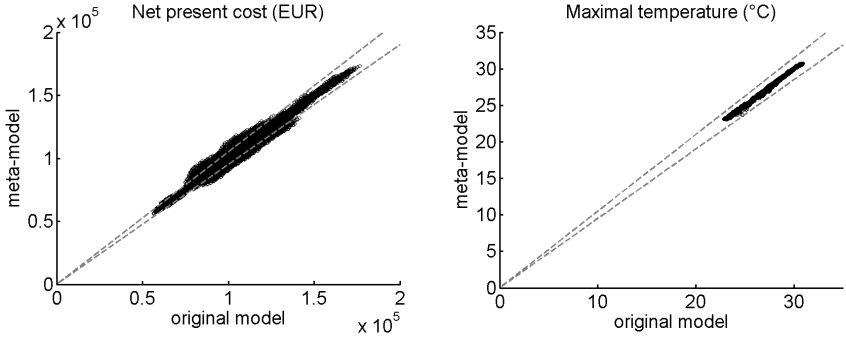

(a) net present cost - reference *(b) maximal temperature - reference*

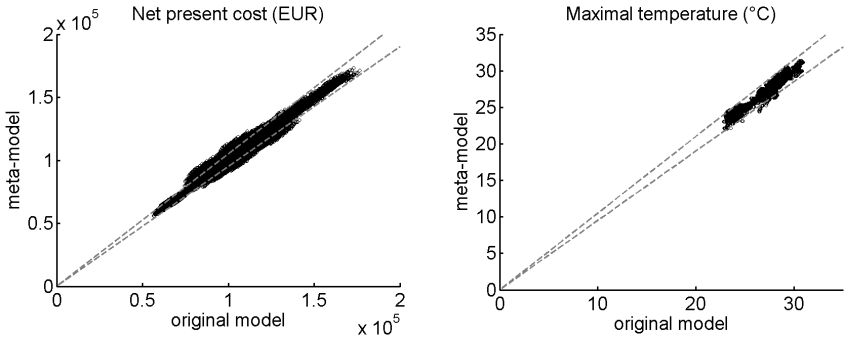

(c) net present cost - meta-model 3 *(d) maximal temperature - meta-model 3*

Figure 5.14: Comparison of 64 800 simulation outputs of original model, reference meta-model and meta-model 3. Deviations of 5 % are indicated by the grey lines.

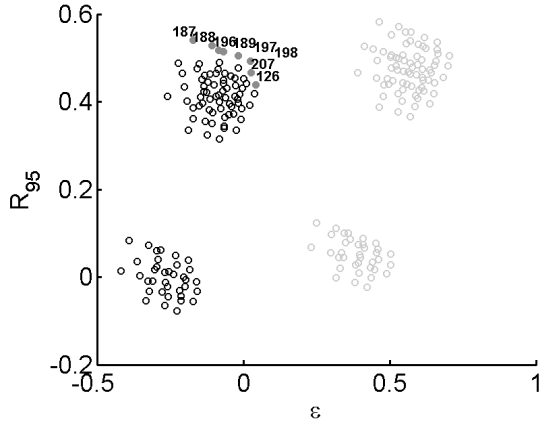

Figure 5.15: R_{95} and ε of net present cost for all 216 design options for dynamic BES model. The design options with an overheating risk are indicated in grey. The Pareto frontier is indicated in full grey with their design option numbers.

Table 5.5: Pareto frontier of dynamic BES model.

N°	U-VALUE	WINDOW	n_{50}	VENTILATION	SUNSCREEN
126	0.15 W/m^{2}K	1.29 W/m^{2}K	1.4 /h	D 0.8	30 %
187	0.10 W/m^{2}K	0.7 W/m^{2}K	0.6 /h	D 0.8	30 %
188	0.10 W/m^{2}K	0.7 W/m^{2}K	1 /h	D 0.8	30 %
189	0.10 W/m^{2}K	0.7 W/m^{2}K	1.4 /h	D 0.8	30 %
196	0.15 W/m^{2}K	0.7 W/m^{2}K	0.6 /h	D 0.8	30 %
197	0.15 W/m^{2}K	0.7 W/m^{2}K	1 /h	D 0.8	30 %
198	0.15 W/m^{2}K	0.7 W/m^{2}K	1.4 /h	D 0.8	30 %
207	0.20 W/m^{2}K	0.7 W/m^{2}K	1.4 /h	D 0.8	30 %

Table 5.6: Comparison of ε and R_{95} indicators of Pareto frontier. Grey values are not in the considered Pareto frontier.

	BES MODEL		REFERENCE META-MODEL		META-MODEL 1		META-MODEL 2		META-MODEL 3	
N°	ε	R_{95}	ε	R_{95}	ε	R_{95}	ε	R_{95}	ε	R_{95}
126	0.043	0.438	0.051	0.463	0.056	0.457	0.058	0.475	0.060	0.486
135	0.038	0.418	0.049	0.445	0.057	0.436	0.056	0.451	0.059	0.464
187	-0.171	0.540	-0.179	0.545	-0.176	0.535	-0.175	0.553	-0.177	0.556
188	-0.108	0.528	-0.113	0.536	-0.110	0.525	-0.112	0.540	-0.108	0.550
189	-0.067	0.515	-0.070	0.525	-0.067	0.515	-0.064	0.534	-0.065	0.540
196	-0.084	0.517	-0.089	0.521	-0.087	0.513	-0.084	0.532	-0.091	0.533
197	-0.018	0.505	-0.022	0.511	-0.021	0.503	-0.022	0.518	-0.022	0.526
198	0.025	0.493	0.020	0.501	0.022	0.492	0.027	0.512	0.021	0.517
207	0.025	0.467	0.018	0.483	0.023	0.471	0.025	0.489	0.021	0.494

that was not in the original Pareto frontier. This design option is, however, very similar to option 126, as only the U-value changes (0.2 W/m^{2}K). On the other hand, options 196 and 207 do not appear in the meta-model Pareto frontier, but they are almost equal to the other options as seen in Table 5.5, and are still close to the Pareto frontier of the meta-models. Note that the optimal values of Table 5.6 are very small due to the fact that the most effective solutions result in overheating risks. If Eq. 5.11 and 5.12 would have been used, these values would be much larger. The same would be true when 'no sunscreen' was not considered as potential design value since sunscreens '30 %' are crucial for indoor comfort, but more expensive.

Similar observations remain when comparing Pareto frontiers per scenario. Those results are, however, not explicitly presented here. When comparing Pareto frontiers from meta-models built on fewer samples than meta-model 3, larger deviations are found. Moreover, design options with an overheating potential might be selected as this risk is unreliably detected. Fig. 5.12 and 5.13 show that these meta-models are indeed less reliable as they have low r^2-values and large maximal errors.

This example shows that meta-models constructed based on the strategy presented in section 4.4.3 can be used to reliably replace time-consuming models in the probabilistic design method. Small schemes are preferred as it is seen that meta-models built on those schemes perform as well as the others, however, less samples are needed.

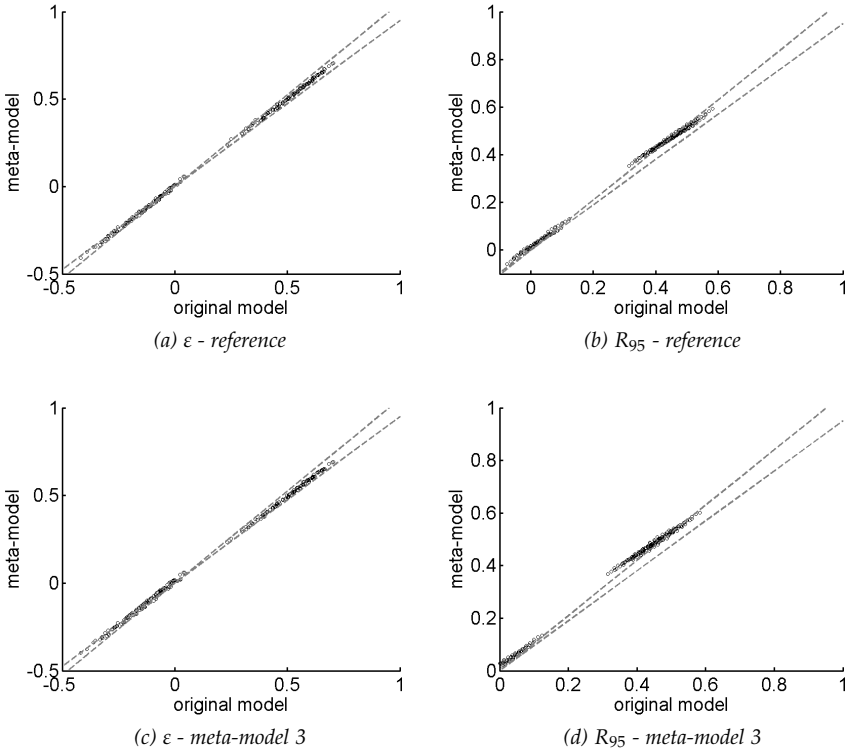

(a) ε - reference *(b) R_{95} - reference*

(c) ε - meta-model 3 *(d) R_{95} - meta-model 3*

Figure 5.16: Comparison of ε and R_{95} indicators for original model, reference meta-model and meta-model 3. Deviations of 5 % are indicated by the grey lines.

5.6 Conclusions

This chapter described and illustrated the probabilistic design methodology as introduced in Chapter 4 in more detail. It relies on the four probabilistic procedures that are extensively explained and illustrated in Chapter 4: uncertainty quantification, sensitivity analysis, meta-modelling and multi-layered sampling. The design methodology consists of four main steps as illustrated in Fig. 5.1: preprocessing (section 5.1), preliminary screening (section 5.2), updating (section 5.3) and the actual probabilistic design (section 5.4).

In the preprocessing step, a simulation model and input and output parameters are selected. All input parameters are assigned fixed values or probability distributions as accurate as known for the considered problem. Each parameter can be variable in time and space as well and correlations can be taken into account.

The preliminary screening provides a meta-model to replace the potentially time-inefficient original model (see section 4.4). Then, the input parameters samples are used to calculate sensitivity indices (see section 4.3). Both sampling efficiency and output convergence are therefore considered.

These sensitivity indices are used to update the input parameters. Based on the ranking, one can judge which parameters need accurate distributions and which can be neglected to improve design and sampling efficiency.

To subject all design options to the same uncertainties and moreover to check the validity of optimisation results for potential scenarios, a multi-layered sampling scheme (see section 4.5) is created in the actual probabilistic design step. This scheme contains the design options, the scenarios and the inherently uncertain parameters. All values of this scheme are combined across the layers and run in a Monte-Carlo loop while controlling output convergence as described in section 5.4.1. To facilitate numerical evaluation and optimisation of the output distributions in robust design, effectiveness and robustness indicators were described in section 5.4.2. Effectiveness is defined as the ability of the design option to optimise the performance, while robustness is defined as the ability to stabilise this performance for the entire range of input uncertainties. A selection of variants of the two basis formulas Eq. 5.1 and 5.2 are presented in Eq. 5.5 - 5.12. Section 5.4.3 furthermore described several possibilities to select design options with optimised output indicators. Pareto optimality was compared with the weighted sum method and the evaluation of a full set of design options with a genetic search algorithm.

Section 5.5 showed that meta-models constructed based on the strategy presented in section 4.4.3 can be used to reliably replace time-consuming models in the probabilistic design method. Small schemes are preferred as it is seen that meta-models built on those schemes perform as well as the others, however, less samples are needed.

This design methodology thus outlined the steps needed to be taken in both reliable probabilistic analysis and design, making many applications in research, industry and government feasible. The methodology will be illustrated on a complex case study in Chapter 6 in order to provide guidelines for low-energy dwelling design.

6

Design guidelines for low-energy dwellings

Based on the robust design methodology described in Chapter 5, the case study of Chapter 3 can be handled. This will demonstrate the benefits of this methodology and furthermore illustrate its applicability.

In section 6.1 of this Chapter, the dwelling geometry of Fig. 3.1 on page 23 is chosen and its performances - WTE25, net energy demand, net present cost and initial investment cost - are optimised by selecting the most effective and robust low-energy design options. Furthermore, the design options are selected with consideration of potential users and energy prices in order to ensure that they will perform well, regardless of which of these scenarios will happen.

Afterwards, sections 6.2 and 6.3 describe the results for a small terraced and a large detached dwelling, respectively. The results of these three geometries are compared and generalised in section 6.4 in order to provide some guidelines for designing comfortable and affordable low-energy dwellings.

6.1 Robust design of medium semi-detached dwelling

In this section, the semi-detached dwelling described in Chapter 3 is used to study the most effective and robust low-energy measures concerning thermal comfort, energy and costs, given the considered input distributions of Chapter 3. Building physical decisions such as the choice of insulation thickness and ventilation system are being made without changing the architecture of the dwelling. In order to deduce illustrative guidelines for the design of this specific dwelling, the robust design methodology of Chapter 5 is applied.

6.1.1 Preprocessing

All contributing input and output parameters as well as the building model and the cost calculation tool are described in Chapter 3: the dwelling geometry in section 3.1, the building model in section 3.2.1, the cost calculation tool in section 3.2.2, the input parameters in section 3.2.3 and the considered building performances in section 3.2.4.

Amongst the probabilistic input parameters in Table 3.3 on page 30, one can find parameters regarding the building itself, user preferences and energy price evolutions. The building performances considered in this case study are WTE25, the net energy demand for heating, the net present cost and the initial investment cost.

In order to study the most effective and robust design options regardless the occupants and the future, three user type scenarios and three future economic scenarios are considered, as shown in Table 6.1. The first user has a full-time job and is energy-conscious, the second is working half-time and the third is retired, mostly at home and desires a higher indoor temperature. In order to vary in internal heat gains, a variation in these is coupled to the user types as well. Note that, due to this user type selection, the 'wasting' user would be even more wasting if his internal heat gains would be lower. These user types thus only indicate a range of potential users and other types are possible as well. The three economic scenarios are described by the energy price evolution and refer to a small drop, a price evolution equal to inflation and a sharp increase.

Table 6.1: Considered user type and nominal energy price evolution scenarios.

	SCENARIO 1	**SCENARIO 2**	**SCENARIO 3**
User type	**conscious**	**average**	**wasting**
set temp. occ. day zone (°C)	18	21	24
set temp. abs. day zone (°C)	15	21	24
set temp. occ. night zone (°C)	15	19	23
summer int. gains appl. (W)	140	565	990
winter int. gains appl. (W)	170	740	1 290
spring and autumn int. (W)	150	645	1 140
	SCENARIO 1	**SCENARIO 2**	**SCENARIO 3**
Future economy	**decrease**	**average**	**increase**
nominal energy price evolution	-1.5 %	2.3 %	10 %

6.1.2 Preliminary screening and updating

All parameters in Table 3.3 are sampled according to their distributions in a set of 30 samples with the maximin LHS algorithm (see section 4.2.1). In accordance to section 4.2.2, the columns of these 30 input samples are then permutated to create multiple sets of 30 samples. As many sets as needed in the further study are run in the original model and the additional cost calculation tool to compute all output parameters indicated in section 6.1.1.

Model validation

In addition to these performances, Fig. 6.1 first compares the average indoor temperatures with the measurement data described in section 2.1.1, because this provides an indication of the reliability of the building model and the considered input parameter distributions. In order to obtain reliable cumulative distributions, the 5, 25, 50, 75 and 95 % percentiles of the simulated temperatures are checked following section 4.2.2, as well as the mean value and standard deviation. Seven sample sets, thus 210 samples, are needed for a relative internal error lower than 1 %. Hence, seven sets are used to create Fig. 6.1. Fig. 6.1a and 6.1b show a good agreement with the measured data of a sample of 74 representative Flemish dwellings (see section 2.1.1). This is logical as the set temperatures are chosen based on these measurements. Fig. 6.1c and 6.1d, however, show that the simulated summer temperatures are significantly lower than the measured values. This can be explained by the fact that the simulated dwellings have a higher probability for sunscreens and an additional summer ventilation is implemented (see section 3.2.1). When these improvements concerning thermal comfort are omitted, the simulation would result in higher summer temperatures, as can be seen in Fig. 6.1 as well. Because of the large windows in the south facade for the day zone, the indoor temperatures would in that case even be higher. This proves that the addition of sunscreens and summer ventilation has a positive effect on the summer comfort.

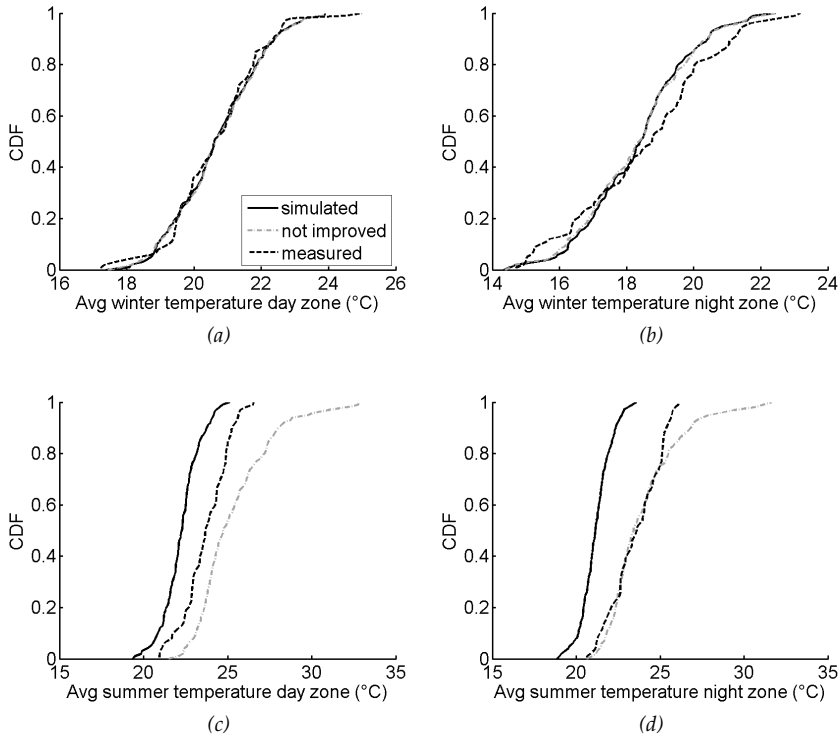

Figure 6.1: Average winter and summer temperatures of both day and night zone for simulated dwelling (see Fig. 3.1) and 74 measured Flemish dwellings (see section 2.1.1).

Output variability

To have an idea of the performance spread, the output parameters are studied for these seven sample sets as well. The net energy demand varies between 1 337 and 18 987 kWh, WTE25 between 0 and 6 791 h, the net present cost between 55 317 and 170 910 EUR and the initial investment cost between 50 869 and 95 472 EUR. Note that this is only an indication and both higher and lower values can still be observed. These large spreads, however, indicate that the considered input parameters are highly influencing these performances and it will be crucial to select the design options carefully. Which parameters are most influencing will be studied further on.

Note that the initial investment cost and net present cost only include the energy-related costs. To have an idea of the basis investment of the calculated investment costs and net present costs, we have a look at average prices of new dwellings in Flanders. The total investment cost of a dwelling of 140 m^2 at about 1 300 EUR/m^2 is 182 000 EUR, VAT and architect costs included, but without land (Livios, 2014). This dwelling cost is related to simple energy-related investments, which are estimated at about 51 000 EUR of this total investment cost in the cost calculation tool. The additional investment cost is thus about 131 000 EUR for a fully finished dwelling. Since the surcharge for the energy-related measures varies between about 51 000 and 95 000 EUR, the total investment cost of this specific dwelling geometry varies between about 182 000 and 226 000 EUR. Maintenance and additional energy costs, such as electricity and domestic hot water, are however still not included for comparison with calculated net present cost.

Meta-model construction

In order to enable the comparison of multiple design options in the robust design method, a meta-model is constructed for heat demand and WTE25, which are the BES model outputs. As concluded in section 4.4.4, NN and KR seem to be the best techniques to model output parameters that are more difficult to meta-model, such as WTE25. Because of the inefficient calculation time of NN in order to obtain a suitable network architecture, KR is used in this application.

At first, a KR model is built according to section 4.4.3 for each of the BES model outputs based on the seven sample sets that were needed for convergence of the average temperatures. More sample sets are added in this meta-model construction until the obtained models are sufficiently reliable. In this case study, we are interested in the coefficient of determination r^2 and maximal absolute error MAE of the meta-models, which have to be as high and as low as possible, respectively. This addition and cross-validation is presented in Fig. 6.2. In order to obtain minimal r^2 values above 0.75, average above 0.90 and maximal above 0.95 for each of the outputs, at least 20 sample sets (600 samples) are needed. Both r^2 and MAE are converged and adding more samples is not significantly improving the models. The MAEs for 20 sample sets are between 1 086 and 7 637 kWh and 714 and 3 813 h for heat demand and WTE25 respectively. Although the reliability of these models is not as good as the reliability obtained in the previous simplified case studies, a test in which the input parameter values of a validation set are individually changed showed that the outputs of the meta-models change the way they should. Hence, the meta-models

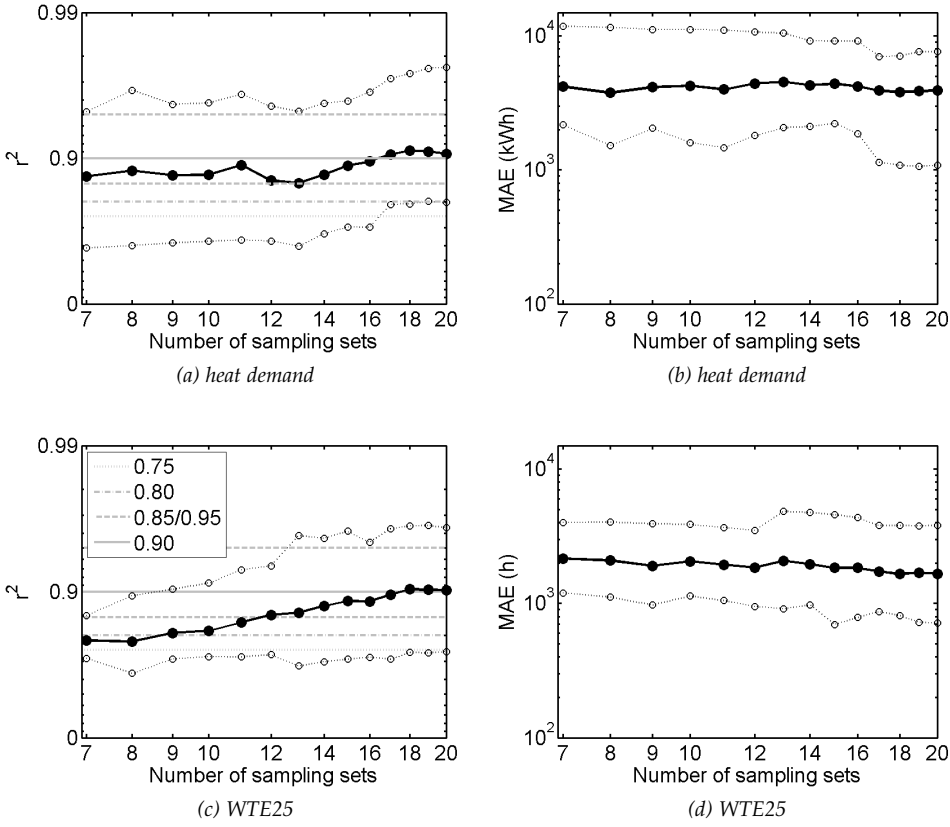

(a) heat demand *(b) heat demand*

(c) WTE25 *(d) WTE25*

Figure 6.2: Addition of sample sets for KR model construction until the validation indicator r^2 (coefficient of determination) in the cross-validation meets the validation criteria. Minimal and maximal indicator values are presented by dotted lines, while the average indicator values by the black dots. The validation criteria are marked in grey. The figures on the right also present the improvement of the MAE (maximal absolute error).

are considered to be sufficiently reliable. Previous examples were much easier to mimic because of the lack of differentiation in capacity (massive versus timberframed construction) and in sunscreen control, which are the only changes. It is thought that the performance of the meta-models can be improved by creating a meta-model for massive and timberframed constructions and for both control possibilities separately. However, this would also require a different sample set, similar to the multi-layered sampling principle explained in section 4.5.

Sensitivity analysis

In order to limit the number of input parameters and facilitate the selection of design options in section 6.1.3, a sensitivity analysis is performed on the 600 available samples. The calculated Spearman's ρ-values are presented in Table 6.2 accompanied with their p-values to indicate the significance (see section 4.3). As one can see, different input parameters are dominant for different performances. The infiltration rate, ventilation system and heat recovery efficiency influence the

Table 6.2: Spearman's ρ and p-values for net energy demand (NED), WTE25, net present cost (NPC) and initial investment cost (IIC). Insignificant indices are indicated in grey.

PARAMETER	NED		WTE25		NPC		IIC	
	ρ	p	ρ	p	ρ	p	ρ	p
construction type	0.00	0.96	0.32	0.00	0.40	0.00	0.86	0.00
U-value roof	0.09	0.03	0.04	0.32	0.02	0.68	-0.01	0.74
U-value floor	0.06	0.18	-0.07	0.10	-0.02	0.63	-0.13	0.00
U-value wall	0.18	0.00	-0.05	0.24	0.05	0.23	-0.15	0.00
window type U-value	0.26	0.00	-0.03	0.52	0.02	0.62	-0.05	0.24
window type g-value	0.07	0.09	0.11	0.01	0.02	0.57	-0.03	0.45
infiltration rate at 50 Pa	0.49	0.00	-0.10	0.01	0.11	0.01	-0.15	0.00
dev. from design U-values	0.08	0.06	-0.03	0.55	0.04	0.32	0.01	0.81
dev. from design infiltration rate	0.10	0.02	0.00	0.98	0.05	0.29	0.03	0.52
ventilation system	-0.44	0.00	0.06	0.18	0.03	0.54	0.09	0.03
heat recovery efficiency	-0.40	0.00	0.00	0.91	0.01	0.73	0.11	0.01
dev. from design heat rec. efficiency	0.02	0.72	-0.03	0.54	0.00	0.94	-0.03	0.56
sunscreen type	0.08	0.06	-0.66	0.00	0.33	0.00	0.28	0.00
sunscreen control	-0.07	0.11	0.19	0.00	0.01	0.74	-0.01	0.85
occupancy profile day zone	-0.01	0.74	0.03	0.53	0.02	0.71	0.01	0.79
occupancy profile night zone	0.04	0.34	0.01	0.82	0.05	0.23	0.02	0.71
set temp. occupancy day zone	0.27	0.00	0.11	0.01	0.12	0.01	0.01	0.76
set temp. absence day zone	0.15	0.00	0.05	0.25	0.08	0.08	-0.02	0.69
set temp. occupancy night zone	0.14	0.00	0.02	0.62	0.06	0.13	0.02	0.66
air change rate	0.20	0.00	-0.10	0.02	0.10	0.02	0.03	0.43
internal gains persons	-0.07	0.10	0.00	0.94	0.00	0.91	-0.02	0.61
basis internal gains appl. day zone	-0.06	0.15	0.05	0.23	0.02	0.58	0.05	0.24
internal gains appliances day zone	-0.22	0.00	0.30	0.00	-0.02	0.56	0.03	0.52
nominal energy price evolution	0.03	0.51	0.03	0.52	0.73	0.00	0.04	0.40

net energy demand the most, followed by the set temperatures, the U-values of windows, walls and roof, the internal heat gains by appliances, the air change rate and the deviation from design infiltration rate. In contradiction, WTE25 is mostly dominated by the sunscreen type, the construction type and the internal heat gains by appliances, followed by the sunscreen control, the g-value of the windows, the set point temperature occupancy day zone, the infiltration rate and the air change rate. The net present cost is mainly influenced by the nominal energy price evolution, but also by the construction type and the sunscreen type, followed by the set point temperature occupancy day zone, infiltration rate and air change rate. Finally, the initial investment cost is only determined by building fabric and systems, of which the construction and sunscreen type are the most significant.

Scatter plots are created as well to visually verify the calculated sensitivities. As an example, Fig. 6.3 shows the scatter plots of the net energy demand as a function of the infiltration rate and the U-value of the walls. One can see that the infiltration rate is indeed more dominant than U-values below 0.3 W/m^{2}K for a reduction in net energy demand.

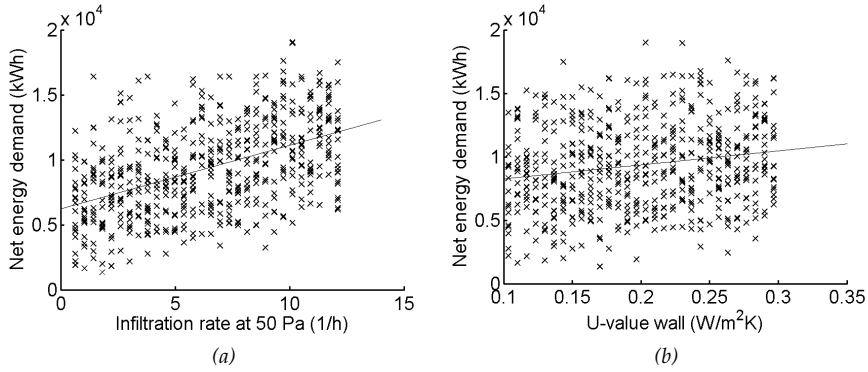

Figure 6.3: Scatter plots of infiltration rate and U-value. The first can be seen as a dominant input parameter for net energy demand, while the second is clearly less dominant.

Since the user type and future economy are influencing the net energy demand and net present cost, and as they will be studied as scenario layer in section 6.1.3, the sensitivity analysis is repeated with fixed values for these input parameters (see Table 6.1). The meta-models are used to replace the BES-model to calculate the new samples. Table 6.3 shows that when users are less energy-conscious, the same dominant parameters are found as when users are conscious, however, the ventilation system becomes a more dominant parameter. This can be explained by the fact that a higher set temperature significantly increases the ventilation losses. In addition, Table 6.4 shows that when energy prices sharply increase in future, U-values, infiltration rate and ventilation system becomes more dominant for the net present cost. One can see that for these energy-saving measures, the sign of the indices changes over the price evolutions. This is due to the fact that the initial investment cost of these measures is traded off against the energy cost. The higher the energy price evolution is, the more dominant this energy cost is in this trade-off.

Table 6.3: Spearman's ρ and p-values for net energy demand and the three user types of Table 6.1. Insignificant indices are indicated in grey.

PARAMETER	user 1		user 2		user 3	
	ρ	p	ρ	p	ρ	p
construction type	0.00	1.00	0.01	0.83	0.02	0.59
U-value roof	0.13	0.00	0.11	0.01	0.10	0.02
U-value floor	0.09	0.03	0.07	0.09	0.05	0.24
U-value wall	0.14	0.00	0.13	0.00	0.11	0.01
window type U-value	0.26	0.00	0.26	0.00	0.24	0.00
window type g-value	0.05	0.22	0.09	0.03	0.11	0.01
infiltration rate at 50 Pa	0.60	0.00	0.56	0.00	0.49	0.00
dev. from design U-values	0.07	0.07	0.09	0.03	0.09	0.03
dev. from design inf. rate	0.13	0.00	0.13	0.00	0.11	0.01
ventilation system	-0.42	0.00	-0.53	0.00	-0.68	0.00
heat recovery efficiency	-0.38	0.00	-0.52	0.00	-0.64	0.00
dev. from design heat rec. eff.	0.04	0.36	0.03	0.45	0.06	0.15
sunscreen type	0.07	0.08	0.05	0.22	0.04	0.31
sunscreen control	-0.05	0.20	-0.05	0.20	-0.04	0.31
occupancy profile day zone	0.00	0.98	-0.02	0.67	-0.02	0.61
occupancy profile night zone	-0.04	0.33	-0.01	0.78	0.00	0.99
air change rate	0.23	0.00	0.21	0.00	0.17	0.00
internal gains persons	-0.07	0.07	-0.07	0.07	-0.06	0.12
basis internal gains appl. day zone	-0.04	0.31	-0.05	0.26	-0.04	0.30

Table 6.4: Spearman's ρ and p-values for net present cost, average user and the three price evolutions of Table 6.1. Insignificant indices are indicated in grey.

PARAMETER	price 1		price 2		price 3	
	ρ	p	ρ	p	ρ	p
construction type	0.68	0.00	0.68	0.00	0.47	0.00
U-value roof	-0.03	0.41	-0.01	0.78	0.08	0.06
U-value floor	-0.04	0.38	-0.02	0.63	0.05	0.20
U-value wall	-0.08	0.06	-0.04	0.29	0.07	0.07
window type U-value	0.07	0.09	0.11	0.01	0.24	0.00
window type g-value	-0.02	0.69	0.00	0.90	0.05	0.19
infiltration rate at 50 Pa	0.03	0.53	0.11	0.01	0.43	0.00
dev. from design U-values	0.00	0.93	0.01	0.78	0.07	0.10
dev. from design infiltration rate	0.04	0.30	0.06	0.16	0.12	0.00
ventilation system	0.10	0.02	0.02	0.70	-0.26	0.00
heat recovery efficiency	0.05	0.24	-0.03	0.51	-0.29	0.00
dev. from design heat rec. efficiency	-0.06	0.13	-0.06	0.16	-0.03	0.47
sunscreen type	0.52	0.00	0.52	0.00	0.39	0.00
sunscreen control	-0.08	0.06	-0.08	0.06	-0.08	0.05
occupancy profile day zone	-0.04	0.34	-0.04	0.29	-0.04	0.37
occupancy profile night zone	0.02	0.69	0.01	0.76	-0.01	0.72
air change rate	0.07	0.11	0.09	0.02	0.19	0.00
internal gains persons	-0.03	0.51	-0.04	0.33	-0.08	0.04
basis internal gains appl. day zone	0.03	0.49	0.02	0.58	0.00	0.97

Note that in both tables, all indices are relative to the others for the same scenario. This means that if some parameters are more dominant due to the considered scenario, other parameters will be relatively less dominant.

Updating

Following the results of the sensitivity analysis in Table 6.2, the input parameters that are not significantly influencing any of the considered performances are eliminated. Therefore, in the robust design of section 6.1.3, 'deviation from design U-values' (1), 'deviation from design heat recovery efficiency' (1), 'occupancy profile day zone' (3), 'occupancy profile night zone' (6), 'internal gains persons' (105 W) and 'basis internal gains appliances day zone' (100 W) are set at their average value, which is indicated between brackets. The sensitivity results will be used as well to select the studied design options.

6.1.3 Robust design

Based on the meta-models constructed in section 6.1.2 and the calculated sensitivity indices, the actual robust design can be performed. The most effective and robust design options for the current case study concerning the net energy demand, WTE25, the net present cost and the initial investment cost will be selected.

Layer values

The first step in the robust design is to select the values for each of the layers. For this case study, two layers - a user type layer and an economic future layer - and their values were already selected in Table 6.1. The design layer is created based on the above described sensitivity results and is presented in Table 6.5. Since, for example, the infiltration rate is dominant for all considered performances and the sign of its influence differs over these performances, multiple values over a considerable range are selected. In contrast, the U-values appeared to be not that important for each of

Table 6.5: Design layer parameters and values.

PARAMETER	VALUES
construction type	massive / timberframe
U-value roof (W/m^2K)	0.15 / 0.25
U-value floor (W/m^2K)	0.15 / 0.25
U-value wall (W/m^2K)	0.15 / 0.25
window type	1.29 W/m^2K & g = 0.631 / 1.31 W/m^2K & g = 0.551 / 0.7 W/m^2K & g = 0.407
infiltration rate at 50 Pa (1/h)	0.6 / 1 / 3 / 5
ventilation system	A / A+ / C / C+ / D 0.7 / D 0.8 / D+ 0.7 / D+ 0.8
sunscreen type	none / 10 % / 10 % south 30 % / 30 % south
sunscreen control	manual / automatic 1

the performances and hence, only two 'average' values are selected. Better window types, however, influence both the net energy demand and WTE25 in a positive way, without significantly increasing the related costs. Therefore, the worst performing windows are not considered anymore. The remaining parameters - the inherently uncertain parameters - are ór taken constant when insignificant, as explained earlier, ór ascribed the distributions of Table 3.3.

Multi-layered sampling

All design parameter values are combined in a full factorial scheme, resulting in 13 824 design options, and the inherently uncertain parameters are 'maximin' sampled in a small set of 20 samples. Each design option is combined with each value of the two scenario layers and with the uncertainty sample set according to Fig. 4.22 on page 81. These combinations are run in the meta-models and postprocessed to obtain the considered performances. Note that, since the initial investment cost is only determined by the design options, this performance is deterministic. The convergence of the other performances is checked following section 4.5.2, while sequentially adding extra uncertainty sample sets. To obtain a relative internal standard deviation below 5 % for all performances, between 80 and 200 uncertainty samples are needed. In total, this robust design requires 2 000 360 meta-model runs, which corresponds to about two hours of simulation time.

Because WTE25 is significantly influenced by the design options and the magnitude of these performances thus changes over these options, the internal standard deviation is not divided by the mean value of each design option to make this relative for the convergence control, but by the overall mean value obtained from the 600 initial samples in section 6.1.2.

Output evaluation

Due to the focus on robust design in this case study, the effectiveness ϵ and the robustness R_{95} are calculated for each design option, for each of the scenario combinations and for each of the performances analogously to Eq. 5.7 and 5.8. Since the initial investment cost is deterministic, only an effectiveness can be calculated for this performance.

In order to study the different design options and their corresponding performances, Fig. 6.4, 6.5, 6.6 and 6.7 show the effectiveness and robustness of all performances for the second user and second energy price evolution. Each dot in the figures corresponds with one of the 13 824 considered design options. The different design parameter values are indicated in order to compare them. In all these plots, the most effective and robust solutions can be found in the upper right corner.

Fig. 6.4 compares the design parameter values for the net energy demand. One can see that four clouds of solutions appear. These are caused by the different ventilation systems. Systems A, A+ and C form the lower cloud, of which the systems A+ are slightly more robust. The second cloud is formed by the C+ systems and the third and fourth by the D and D+ systems with a heat recovery efficiency of 80 and 70 % respectively. The more the system is designed to reduce the ventilation losses,

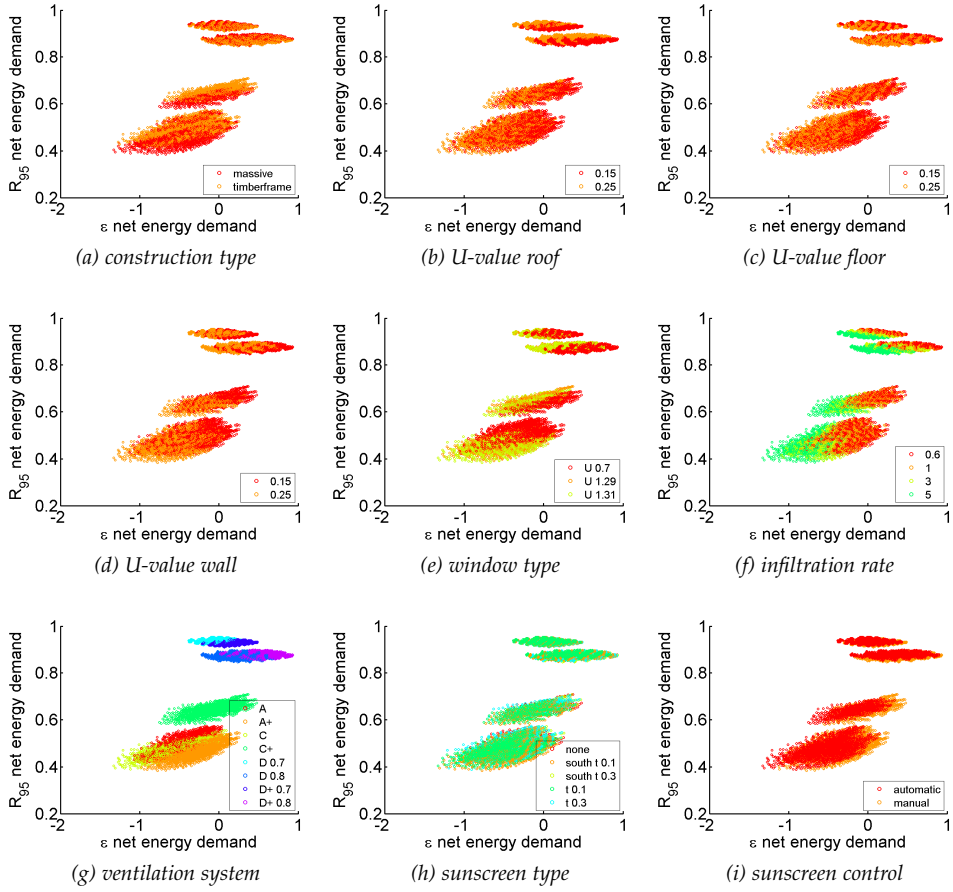

(a) construction type *(b) U-value roof* *(c) U-value floor*

(d) U-value wall *(e) window type* *(f) infiltration rate*

(g) ventilation system *(h) sunscreen type* *(i) sunscreen control*

Figure 6.4: Net energy demand effectiveness and robustness for all design options. The different design parameter values are marked in the subplots.

the more robust and effective the ventilation system is concerning its net energy demand. The choice of ventilation system thus seems to be most dominant in order to obtain effective and robust net energy demands. Types D(+) appear to be the best solution, of which the system D+ with a heat recovery efficiency of 80 % is the most effective and the system D with an efficiency of 70 % the most robust. In a second phase, also the choice of the window type and the infiltration rate affect the net energy demand significantly, although not so much that separated clouds are formed. The window with a U-value of 0.7 W/m^2K and an n_{50}-value of 0.6 /h are the most effective, while the robustness of all options is similar. Very similar results can be found for the energy-conscious and energy-wasting user. Remark that these results are in correspondence with the sensitivity indices calculated before.

Fig. 6.5 compares the design parameter values for WTE25. In here, two main clouds can be distinguished: one cloud with low robustnesses and negative effectivenesses and the other one with higher robustnesses and overall higher effectivenesses. This separation is caused by the choice of sunscreen type. Only the application of sunscreens can cause a positive effectiveness. This is due to the fact that sunscreens

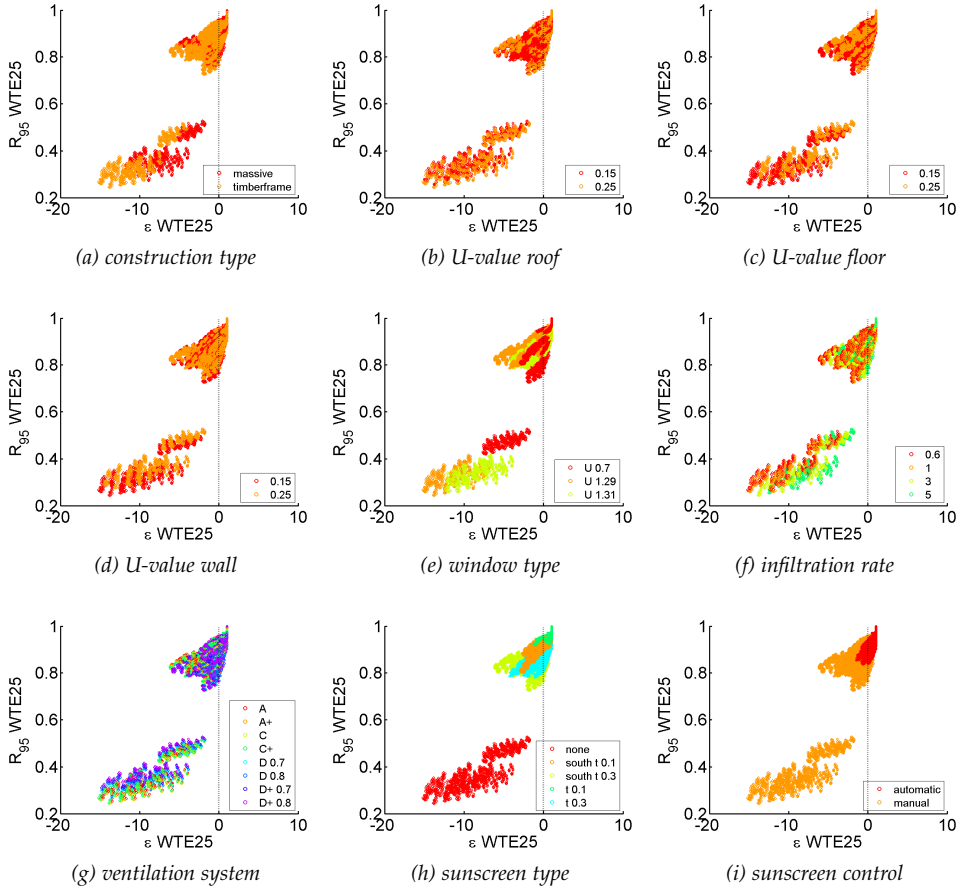

(a) construction type *(b) U-value roof* *(c) U-value floor*

(d) U-value wall *(e) window type* *(f) infiltration rate*

(g) ventilation system *(h) sunscreen type* *(i) sunscreen control*

Figure 6.5: WTE25 effectiveness and robustness for all design options. The different design parameter values are marked in the subplots.

are very effective in reducing WTE25, similar to the sensitivity results presented before. Moreover, the better the sunscreens are, the more robust the design option is concerning WTE25. The large range of effectiveness values indicates that the choice of the design parameter values is crucial for comfortable indoor climates. In a second phase, the sunscreen control (no sunscreens are also indicated with manual control), and the construction and window type, are most dominant. The most effective solutions are characterised by the presence of sunscreens (preferable 10 % transmission) with automatic control, a massive construction and windows with low g-value (U-value 0.7 W/m^{2}K). These most effective solutions are also the most robust solutions. The results for the other user scenarios are very similar.

The net present cost is studied in Fig. 6.6. In here, three columns and four rows of clouds can be found. The different columns are formed by the differences in construction type and sunscreen type. The effectiveness of the net present cost is thus mostly influenced by the construction type, sunscreen type and related sunscreen control (no sunscreens are also indicated with manual control): a massive construction with no sunscreen (or manually controlled) is the most cost effective,

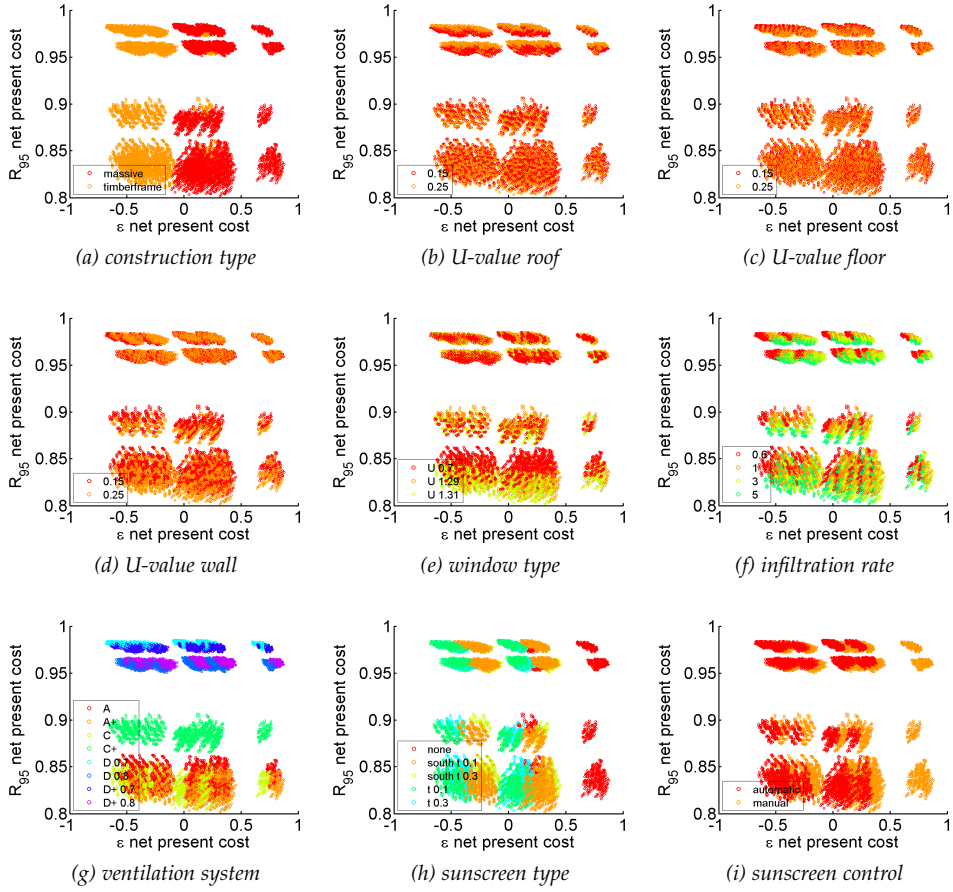

(a) construction type *(b) U-value roof* *(c) U-value floor*

(d) U-value wall *(e) window type* *(f) infiltration rate*

(g) ventilation system *(h) sunscreen type* *(i) sunscreen control*

Figure 6.6: Net present cost effectiveness and robustness for all design options. The different design parameter values are marked in the subplots.

because of its lower initial investment cost as will be seen in Fig. 6.7. The ventilation system and infiltration rate also slightly influence this effectiveness. A ventilation system D+ with a heat recovery efficiency of 80 % and an infiltration rate of 3 /h are most effective solutions. The four rows, however, are formed by the ventilation system type, similar to what was seen in Fig. 6.4. The robustness is thus mostly influenced by the ventilation system and also slightly by the infiltration rate and U-value of the roof: a ventilation system D with efficiency of 70 %, an infiltration rate of 0.6 or 1 /h and U-value of 0.25 W/m^{2}K are the most robust solutions concerning this net present cost. For the other user and energy price scenarios, very similar results are found. However, the more energy-wasting the user is and the sharper the energy price increase, the more the robustness is influenced by the ventilation system and the infiltration rate. This is explained by the fact that the energy cost in that case becomes more dominant in the net present cost.

The initial investment cost is presented in Fig. 6.7. Since this is a deterministic performance, only the effectiveness can be calculated. Hence, this effectiveness is plotted against the net present cost effectiveness. The same clouds as formed by the

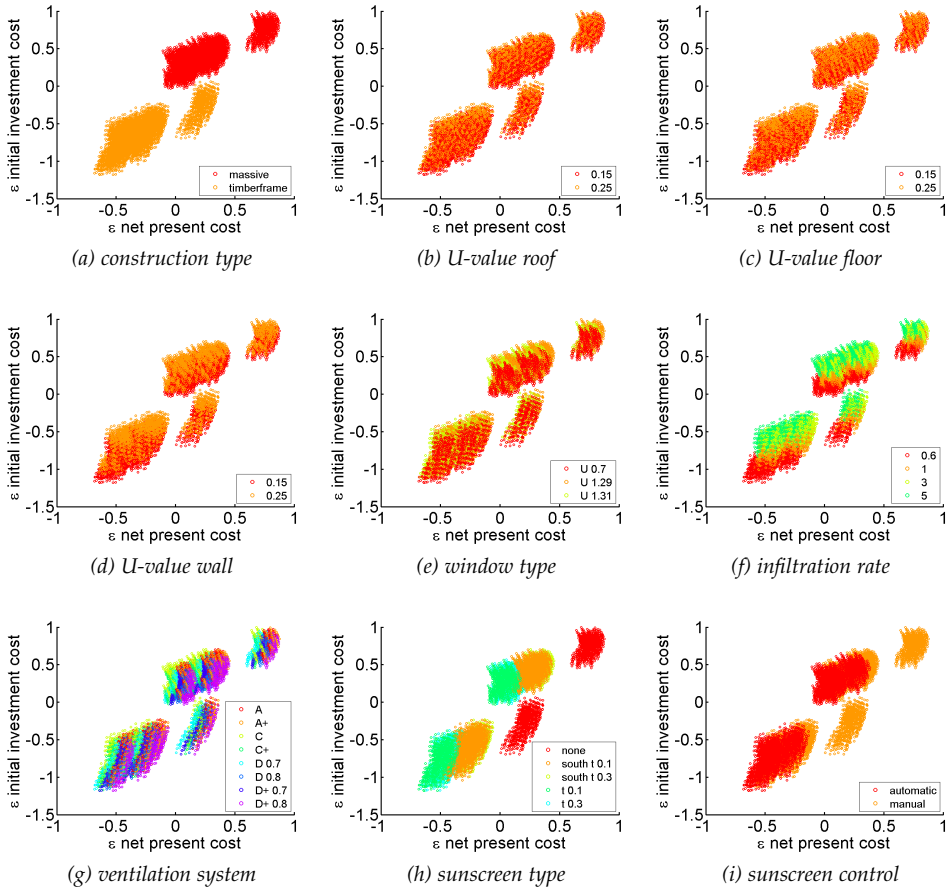

(a) construction type *(b) U-value roof* *(c) U-value floor*

(d) U-value wall *(e) window type* *(f) infiltration rate*

(g) ventilation system *(h) sunscreen type* *(i) sunscreen control*

Figure 6.7: Initial investment cost effectiveness as a function of net present cost effectiveness for all design options. The different design parameter values are marked in the subplots.

latter effectiveness are formed by the initial investment cost effectiveness. This initial investment cost effectiveness is dominated by the construction type, the sunscreen type and control, and the infiltration rate. When the initial investment cost is crucial in the decision-making, a massive construction, no sunscreens or sunscreens on the south facade with automatic control, and an n_{50}-value of 5 /h will be preferred.

Scenario-independent robust design options

When only considering one of the presented performances, the robust design is quite easy, since one only has to look at the upper-right corner of the figures. However, when multiple of these performances have to be traded off in the decision-making, a visual selection will not be sufficient anymore. Moreover, when it is desired that the selected design options will perform well for each of the potential user types and in each of the considered future scenarios, even more complexity is added to the decision-making. In order to guide this, Pareto frontiers based on several performance priorities are calculated. First, the optimisation is performed from the perspective of the user of the dwelling, followed by the governmental perspective.

To conclude this section, both perspectives are combined and overall optimal design options are derived. This will provide guidelines for the design of the current dwelling geometry.

1. User perspective Users are typically mostly interested in the combination of low initial investment costs and low energy costs. The net present cost is thus studied first. Since this cost is highly variable and also dominated by the potential future economic scenarios and the user type, the overall most robust design options concerning this cost are sought. That way, the presented optimal design options can be generalised for all potential economic scenarios and user types. As users want a comfortable indoor climate as well and some of them might be interested in a low energy demand, both WTE25 and the net energy demand are used to select options from the Pareto frontier.

Fig. 6.8 presents the net present cost robustness compared to the net present cost effectiveness for the extreme scenario combinations of Table 6.1. All other user type and scenario combinations are included in the calculations, but not presented here. Each dot corresponds to one of the 13 824 design options. The more effective options are the ones with a low initial investment cost, while the more robust options have a low energy cost. Of all these design options, the individual Pareto frontier is calculated and indicated in hollow red dots on Fig. 6.8. By comparing this figure and Fig. 6.6, the Pareto optimal solutions can be studied. Depending on the user type and economic scenario, other Pareto optimal solutions are found. The energy price evolution is highly influencing the net present cost, as the scenario value has a high impact on the robustness and effectiveness. Therefore, more energy saving measures, such as a low infiltration rate and lower U-values are more optimal for high cost increases. A massive construction and ventilation system D or D+ are common in all Pareto fronts. Only for users of type 'conscious' and 'average' and energy price evolutions of -1.5 % or 2.3 %, a system A or A+ can be optimal. These options are less robust, but most effective.

Since the users are sometimes also interested in a low net energy demand of their dwelling, Fig. 6.8 indicates the net energy demand effectiveness in a grayscale, with in white the least effective and in black the most effective net energy demands. Fig. 6.4 already showed that the robustness and effectiveness of this net energy demand are highly correlated. The grayscale is thus also an indication of the net energy demand robustness. One can see that the more robust options concerning the net present cost are the options with the lower net energy demand. This is explained by the lower energy cost of them.

Because indoor comfort is even more important for the users, the Pareto optimal solutions are compared on their WTE25 effectiveness and robustness. When only considering those Pareto optimal solutions with a WTE25 effectiveness that is strictly positive and a robustness above 80 %, the full red dots in Fig. 6.8 indicate a selection of the most optimal design solutions. These correspond to solutions with sunscreens and automatic control. Fig. 6.9 compares these design options by means of the WTE25 distributions. The user type seems to influence the overheating the most, because of the difference in internal heat gains. Although the application of

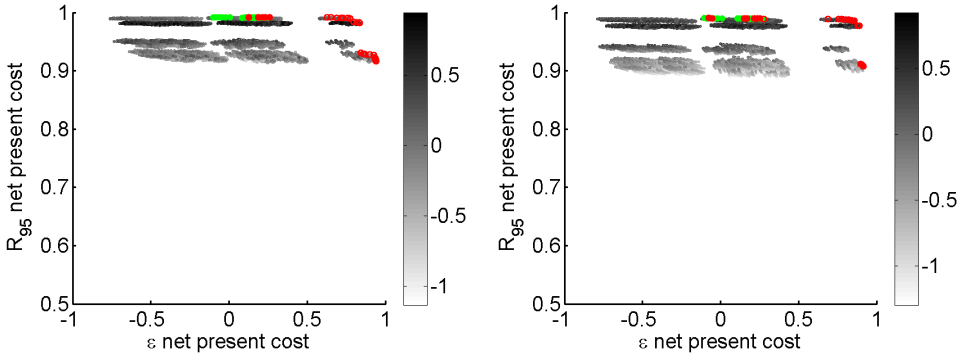

(a) user 1 - economic scenario 1 (b) user 3 - economic scenario 1

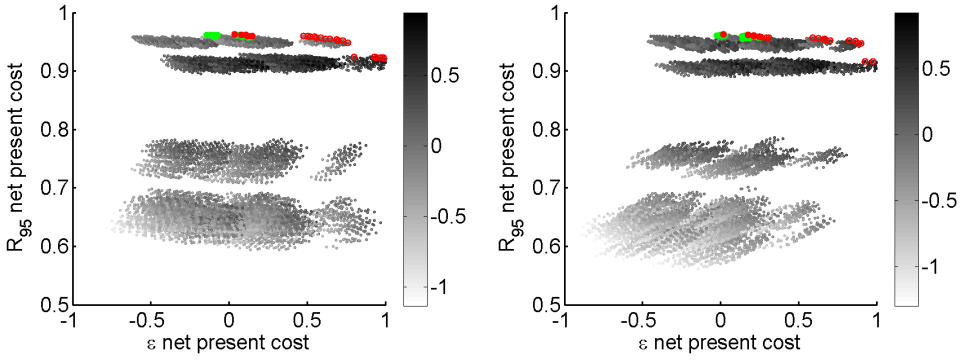

(c) user 1 - economic scenario 3 (d) user 3 - economic scenario 3

Figure 6.8: Net present cost R_{95} as a function of net present cost ε for the extreme user type and economic scenario combinations. Each dot corresponds to one of the 13 824 design options. The grayscale refers to the net energy demand ε. The individual Pareto frontier is indicated in red, while the overall Pareto frontier in green.

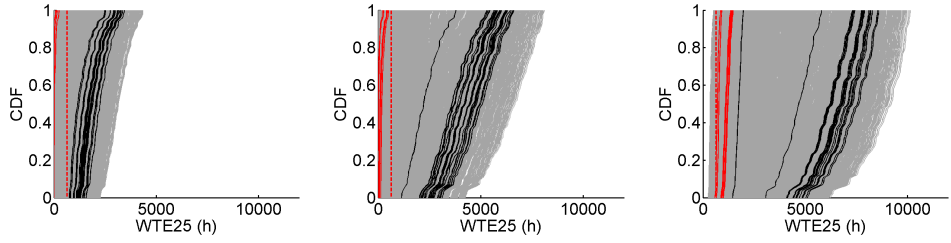

(a) user 1 - economic sc. 2 (b) user 2 - economic sc. 2 (c) user 3 - economic sc. 2

Figure 6.9: Comparison of WTE25 distribution of all design options in grey, Pareto optimal solutions in black and final selection in red for the average economic scenario and the three user types. The preferred performance criteria of WTE25 below 650 h is indicated by the dotted red line.

sunscreens is not the most cost effective, it seems that it is essential for a comfortable indoor climate. The Pareto optimal solutions (in black and red) do not guarantee this comfort. However, of these solutions, the final selection (in red) is the most preferred. It can be seen in Fig. 6.9 that a comfortable indoor climate is less easy to obtain for the 'wasting' user due to its higher internal heat gains and more expensive (and thus less cost optimal) sunscreen need to be provided.

In order to generalise the results for the range of potential users and energy price scenarios, it is better to apply scenario-independent measures. Therefore, the overall Pareto frontier of effective and robust design options concerning net present cost is calculated. The optimisation criteria therefore used are all effectivenesses ε and robustnesses R_{95} of the nine considered scenario combinations. In this 18-dimensional Pareto frontier, all design options with an overheating risk (negative WTE25 ε and WTE25 R_{95} below 0.8) in one of the scenarios are excluded from the final selection to study only the better solutions. The obtained 18-dimensional final selection is indicated in green in Fig. 6.8. To reduce the net present cost and its spread - regardless of the scenario values and with paying attention to reduce the risk on overheating - the most important design values are a massive construction, lower infiltration rates, a ventilation system D and sunscreens. Because the sunscreens and control are the least cost effective and their choice is highly influenced by the user behaviour, one can opt to only install them once needed. Because the overall Pareto frontier selection is quite independent of the inherently uncertain parameters, the net present cost of these design options can be reliably predicted with a small range. This final selection is thus most interesting for all potential user types.

2. Governmental perspective Due to the Kyoto Protocol, the governmental focus is on low net energy demands. Since the application of air conditioning is not energy-efficient at all, it is better to prevent overheating in the design stage. Therefore, in this section, a trade-off between net energy demand and WTE25 is made. Since not only high performances but also a low spread is preferred, both effectiveness and robustness are considered. Similar to the previous section, both the individual and the overall Pareto frontiers are studied.

Fig. 6.10 shows the net energy demand robustness as a function of the net energy demand effectiveness for all 13 824 design options and the three user scenarios. Note that the economic scenario has no influence on both the net energy demand and WTE25. The grayscale indicates the WTE25 effectiveness. Fig. 6.5 already illustrated that the WTE25 effectiveness is highly correlated with the WTE25 robustness. The grayscale thus also refers to the WTE25 robustness. One can see that a comfortable indoor climate can be obtained almost regardless of the optimal net energy demand.

The individual four-dimensional Pareto frontiers (red dots in Fig. 6.10) can be studied by a comparison of Fig. 6.10b and Fig. 6.4. Depending on the user type, only slightly different Pareto optimal solutions are found. Most effective and robust solutions have a ventilation system D or D+. Systems A+ and C+ appear in the Pareto frontiers as well (A+ not for user 3), however, they are less effective and less robust. In order to reduce the risk on overheating, all Pareto optimal solutions are

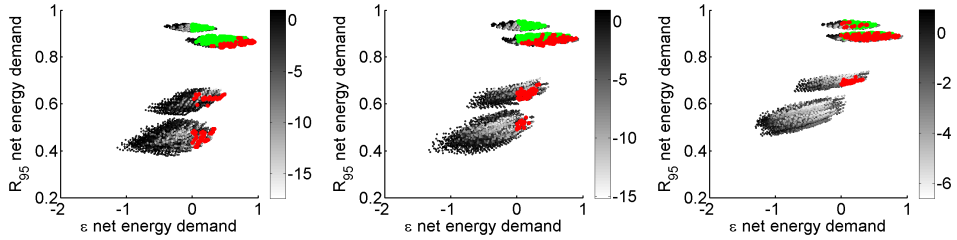

Figure 6.10: Net energy demand R_{95} as a function of net energy demand ε for all user type scenarios. Each dot corresponds to one of the 13 824 design options. The grayscale refers to the WTE25 ε. The individual Pareto frontier is indicated in red, while the overall Pareto frontier in green.

equipped with sunscreens. When more internal heat gains are produced, such as by user 3, the least effective sunscreens ('30 % south') are not optimal anymore.

The overall 12-dimensional Pareto frontier is indicated in green in Fig. 6.10. To calculate this frontier, first all design options with a negative effectiveness concerning the net energy demand or WTE25 and a robustness lower than 0.7 in at least one of the scenarios were penalised, as we are interested in the overall most optimal design options. This penalisation means that the actual effectiveness and robustness values are replaced by a very low value (i.e. -100) to avoid them to appear in the Pareto frontier. In order to obtain these robust and effective solutions, a ventilation system D or D+ has to be chosen. In order to limit the WTE25, these solutions are mostly massive constructions and all have improved sunscreens with automatic control. These options guarantee a low energy demand and a good indoor comfort for all potential user types in the dwelling.

The previous study illustrates that focussing on passive standards for the insulation level (U-values below 0.15 W/m^{2}K) is not effective. U-values of 0.15 W/m^{2}K don't significantly improve the net energy demand. Therefore, it is more interesting to focus on user behaviour and ventilation losses.

3. Overall perspective Since the designed dwelling is preferably optimal in both the user and governmental perspective, the overall Pareto frontier is calculated. This optimisation includes the effectiveness and robustness for WTE25, the net energy demand and the net present cost for all nine scenario combinations. Because such a large-dimensional Pareto frontier typically includes multiple optimal values, the search space is reduced by penalising all design options with an effectiveness for one of the performances below 0.2 or a robustness below 0.8 in at least one of the considered scenarios. For WTE25, this criterium is chosen even more severe to assure comfortable indoor climates: effectivenesses below 0.3 are penalised. This means that the robustness of the solutions is considered as very important in this case study and that the overall performance of the optimal solutions has to be above average.

The resulting Pareto optimal solutions are presented in Table 6.6 and can be interpreted based on the previous described results. In order to improve WTE25,

Table 6.6: Optimal design parameter values for case study dwelling when simultaneously considering effectiveness and robustness of WTE25, net energy demand and net present cost.

PARAMETER	VALUES
construction type	massive
U-value roof (W/m^2K)	0.15 / 0.25
U-value floor (W/m^2K)	0.15 / 0.25
U-value wall (W/m^2K)	0.15 / 0.25
window type	1.29 W/m^2K & g = 0.631 / 1.31 W/m^2K & g = 0.551 / 0.7 W/m^2K & g = 0.407
infiltration rate at 50 Pa (1/h)	1 / 3 / 5
ventilation system	D 0.8 / D+ 0.8
sunscreen type	10 % south
sunscreen control	automatic 1

sunscreens are preferred. To improve the net energy demand in relation to the net present cost, the most important design measure is the application of a balanced ventilation system. The improvement of U-values, the window type and the infiltration rate seems to be less crucial once already considerably good values are applied. A massive construction is selected because of its lower initial investment cost, hence its lower net present cost.

This overall Pareto frontier is indicated in red in Fig. 6.11. One can see that, because of the trade-off between six performance indicators, the optimal solutions have a high effectiveness and robustness for the net energy demand. However, by selecting other design options, this energy demand can be still improved. The same is true for the net present cost, of which the effectiveness is indicated by the grayscale. Fig. 6.12 presents the WTE25 distributions for all design options and for the three user types. When opting for the Pareto optimal design options (in red), the indoor comfort will be guaranteed compared to the non-optimal solutions. Only for the third user type - with high internal heat gains - WTE25 will probably exceed the preferred limit of 650 h, however, most other design options are even less preferable. When having a look at the initial investment cost effectiveness of the Pareto optimal solutions, these options also perform above average. This is due to the fact that by optimising the net present cost, the initial investment cost is also optimised.

6.2 Robust design of small terraced dwelling

In this section, the most effective and robust low-energy measures concerning thermal comfort, energy and costs are studied for the small terraced dwelling described in section 6.2.1, similar to the medium semi-detached dwelling in section 6.1. Guidelines for this specific dwelling design will thus be provided, given the considered input distributions of Chapter 3. In section 6.4, the results will be compared with the results obtained for the semi-detached dwelling, to see whether some conclusions can be generalised for other dwelling geometries.

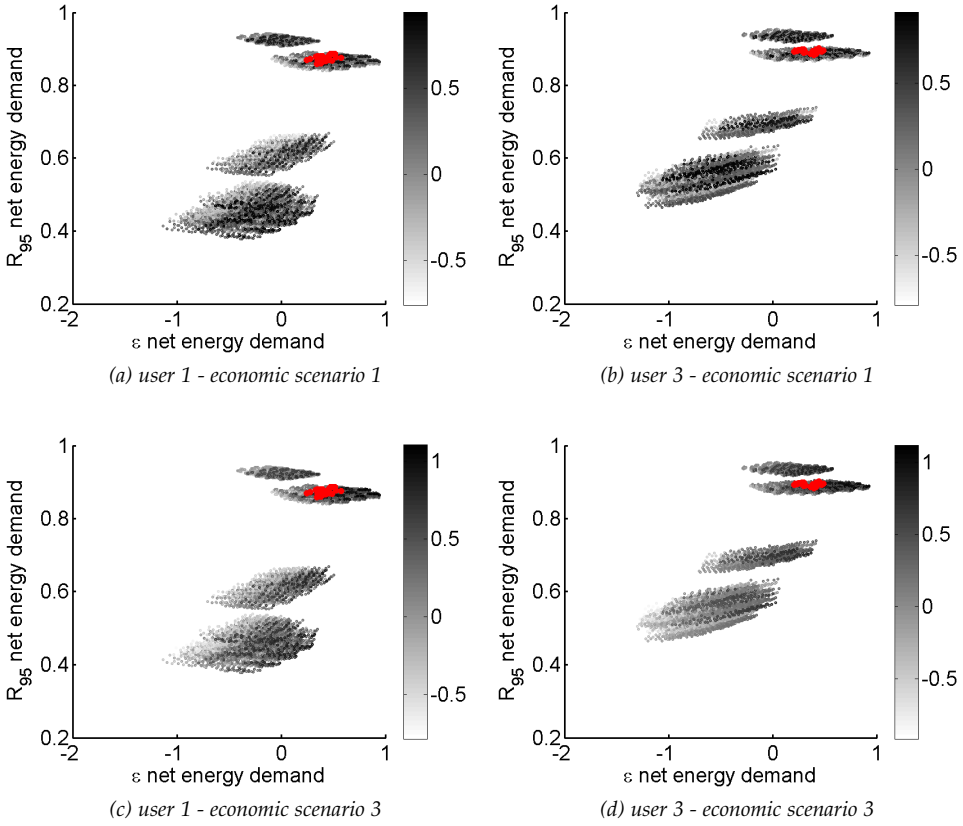

(a) user 1 - economic scenario 1

(b) user 3 - economic scenario 1

(c) user 1 - economic scenario 3

(d) user 3 - economic scenario 3

Figure 6.11: Net energy demand R_{95} as a function of net energy demand ε for the extreme user type and economic scenario combinations. Each dot corresponds to one of the 13 824 design options. The grayscale refers to the net present cost ε. The overall Pareto frontier is indicated in red.

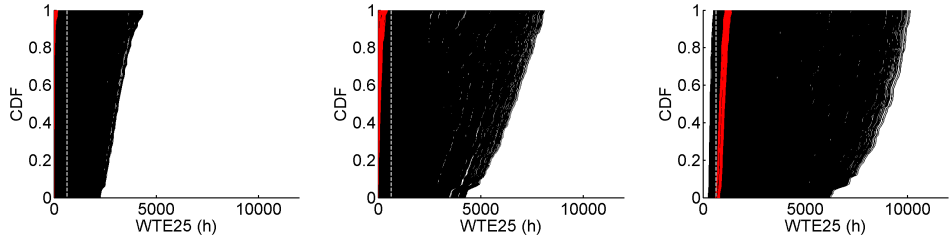

(a) user 1 - economic sc. 2

(b) user 2 - economic sc. 2

(c) user 3 - economic sc. 2

Figure 6.12: Comparison of WTE25 distribution of all design options in black and overall Pareto optimal solutions in red. The preferred performance criteria of WTE25 below 650 h is indicated by the dotted gray line.

6.2.1 Dwelling geometry

The second geometry studied in this thesis was also included as one of the representative geometry types in the *IWT TETRA BEP2020* project (Staepels et al., 2013*a*) and is built in a social housing neighbourhood. This small terraced dwelling is presented in Fig. 6.13 and 6.14. In the latter figure, the day zone is marked in yellow and the night zone in blue. More characteristics are found in Table 6.7.

6.2.2 Preprocessing

The preprocessing for this dwelling geometry is performed almost identical to the case study geometry of Chapter 3. Since the air change rate distributions are determined by the design rates, which are geometry-dependent, the new air change rate distributions are $Wei(1.0816, 4.670)$ and $Wei(0.6814, 4.670)$ for the day and night zone respectively.

6.2.3 Preliminary screening and updating

The preliminary screening, which is performed similar to section 6.1.2, results in a meta-model for the heat demand and WTE25 and in the sensitivity indices. Since the performance of the meta-models is similar to those for the previous case study, this is not described here.

The Spearman's ρ-values are presented in Table 6.8. When comparing these to the sensitivity indices of the first dwelling in Table 6.2, one can see some similarities. For this dwelling, the ventilation system with heat recovery efficiency and the infiltration rate influence the net energy demand the most, followed by the (basis) internal heat gains by appliances, the air change rate, the set temperatures and the U-values of windows, walls and roof. WTE25 is mostly dominated by the internal heat gains by appliances, the sunscreen type and the construction type, followed by the set point temperature during occupancy of the day zone, the basis internal heat gains, the U-value of the floor, the occupancy profile of the day zone, the sunscreen control, the air change rate and the ventilation type. The influencing parameters for the net present cost are identical to the first case study. The initial investment cost is mostly determined by the construction and sunscreen type, followed by the U-value of the wall and the ventilation system.

Based on this sensitivity analysis, least influencing parameters are eliminated when performing the robust design. Therefore, in the next section, 'deviation from design U-values' (1), 'deviation from design infiltration rate' (1), 'deviation from design heat recovery efficiency' (1), 'occupancy profile night zone' (6) and 'internal gains persons' (105 W) are set at their average value, which is indicated between brackets.

6.2.4 Robust design

Based on the constructed meta-models and the sensitivity results, the robust design can be performed.

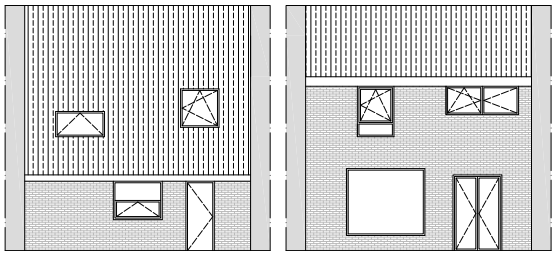

(a) north (b) south

Figure 6.13: Facades of small terraced dwelling.

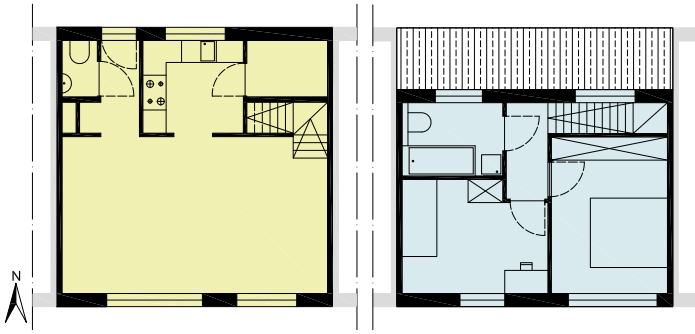

(a) ground floor (b) storey

Figure 6.14: Architectural plans of small terraced dwelling with day zone indicated in yellow and night zone in blue. North orientation is on the top of the figure.

*Table 6.7: Small terraced dwelling characteristics. All areas and volumes are calculated based on outer dimensions similar to EPBD, except for the area marked with *.*

Volume day zone	186 m^3
Volume night zone	153 m^3
Area roof	55 m^2
Area wall	86 m^2
Area floor	52 m^2
Area windows	18 m^2
Area party wall	22 m^2
Width	7.02 m
Depth	7.23 m
Height	7.55 m
Liveable floor area*	87 m^2
Compactness	1.72 m
Percentage glazing/floor	19 %

Table 6.8: Spearman's ρ and p-values for net energy demand (NED), WTE25, net present cost (NPC) and initial investment cost (IIC). Insignificant indices are indicated in grey.

PARAMETER	NED		WTE25		NPC		IIC	
	ρ	p	ρ	p	ρ	p	ρ	p
construction type	-0.02	0.63	0.33	0.00	0.20	0.00	0.65	0.00
U-value roof	0.08	0.05	0.06	0.16	0.01	0.88	-0.10	0.02
U-value floor	0.04	0.30	-0.13	0.00	-0.02	0.67	-0.16	0.00
U-value wall	0.12	0.00	-0.03	0.46	0.04	0.33	-0.24	0.00
window type U-value	0.15	0.00	-0.01	0.82	-0.03	0.45	-0.15	0.00
window type g-value	0.06	0.18	0.05	0.28	-0.01	0.74	-0.10	0.02
infiltration rate at 50 Pa	0.37	0.00	-0.06	0.13	0.12	0.00	-0.14	0.00
dev. from design U-values	0.07	0.08	-0.01	0.83	0.04	0.35	0.01	0.79
dev. from design infiltration rate	0.06	0.14	0.03	0.42	0.04	0.39	0.01	0.89
ventilation system	-0.57	0.00	0.09	0.03	0.03	0.44	0.21	0.00
heat recovery efficiency	-0.51	0.00	0.05	0.28	0.00	0.99	0.18	0.00
dev. from design heat rec. efficiency	0.03	0.49	-0.03	0.43	0.01	0.84	0.00	0.97
sunscreen type	0.07	0.12	-0.44	0.00	0.42	0.00	0.43	0.00
sunscreen control	-0.09	0.03	0.12	0.00	0.03	0.48	-0.02	0.67
occupancy profile day zone	-0.06	0.19	0.13	0.00	0.00	0.96	0.02	0.67
occupancy profile night zone	0.03	0.53	0.03	0.53	0.05	0.20	-0.02	0.58
set temp. occupancy day zone	0.20	0.00	0.15	0.00	0.09	0.03	-0.01	0.90
set temp. absence day zone	0.13	0.00	0.07	0.12	0.06	0.13	-0.05	0.24
set temp. occupancy night zone	0.19	0.00	0.01	0.76	0.07	0.09	0.03	0.55
air change rate	0.22	0.00	-0.09	0.03	0.10	0.02	0.01	0.75
internal gains persons	-0.07	0.09	0.05	0.26	0.00	0.95	-0.01	0.73
basis internal gains appl. day zone	-0.09	0.03	0.14	0.00	0.03	0.49	0.05	0.21
internal gains appliances day zone	-0.26	0.00	0.60	0.00	-0.07	0.10	0.01	0.74
nominal energy price evolution	0.01	0.73	0.04	0.36	0.70	0.00	0.00	0.98

Layer values

The scenario layers of the first case study dwelling in Table 6.1 are revisited. Since also the occupancy profile for the day zone (1 - 3 - 4) and the basis internal heat gains (20 W - 100 W - 180 W) are significant for the current dwelling geometry, the values between brackets are added to the three user types. The design layer is created based on the sensitivity results, leading to the same design layer as for the previous geometry. The remaining parameters are sampled in the uncertainty layer.

Output evaluation

The multi-layered sampling, similarly performed as in section 6.1.3, results in an effectiveness and robustness value for each performance indicator and for each design option and scenario combination. In Fig. 6.15, 6.16, 6.17 and 6.18, these indicators are presented for the second user and second energy price evolution.

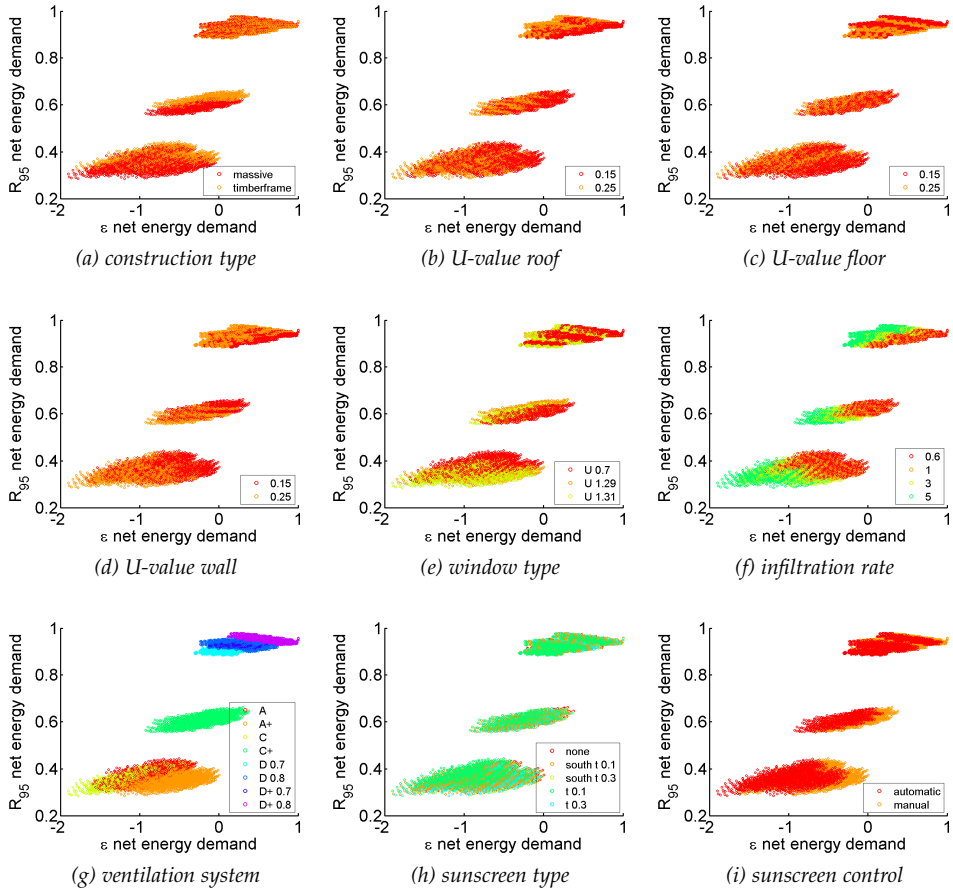

(a) construction type *(b) U-value roof* *(c) U-value floor*

(d) U-value wall *(e) window type* *(f) infiltration rate*

(g) ventilation system *(h) sunscreen type* *(i) sunscreen control*

Figure 6.15: Net energy demand effectiveness and robustness for all design options. The different design parameter values are marked in the subplots.

Fig. 6.15 compares the design parameter values for the net energy demand. One can see that three clouds of solutions appear. These are caused by the different ventilation systems, which is similar to the first dwelling. The choice of ventilation system thus seems to be most dominant in order to obtain effective and robust net energy demands. Types D(+) appear to be the best solution, of which the system D+ with a heat recovery efficiency of 80 % is the most effective and robust. In a second phase, also the infiltration rate influences the net energy demand significantly. An n_{50}-value of 0.6 /h is the most effective. Very similar results can be found for the other user types.

Fig. 6.16 compares the design parameter values for WTE25. Both effectiveness and robustness are more or less equally dominated by the U-value of the wall, the window type, the infiltration rate, the ventilation system and the sunscreen type and control. The most effective and robust solutions are characterised by U-values of 0.25 W/m^{2}K, windows with a U-value 1.31 W/m^{2}K, n_{50}-values of 5 /h, ventilation systems A(+) or C(+) and the presence of sunscreens with 10 % transmission and automatic control. The results for the other user scenarios are similar.

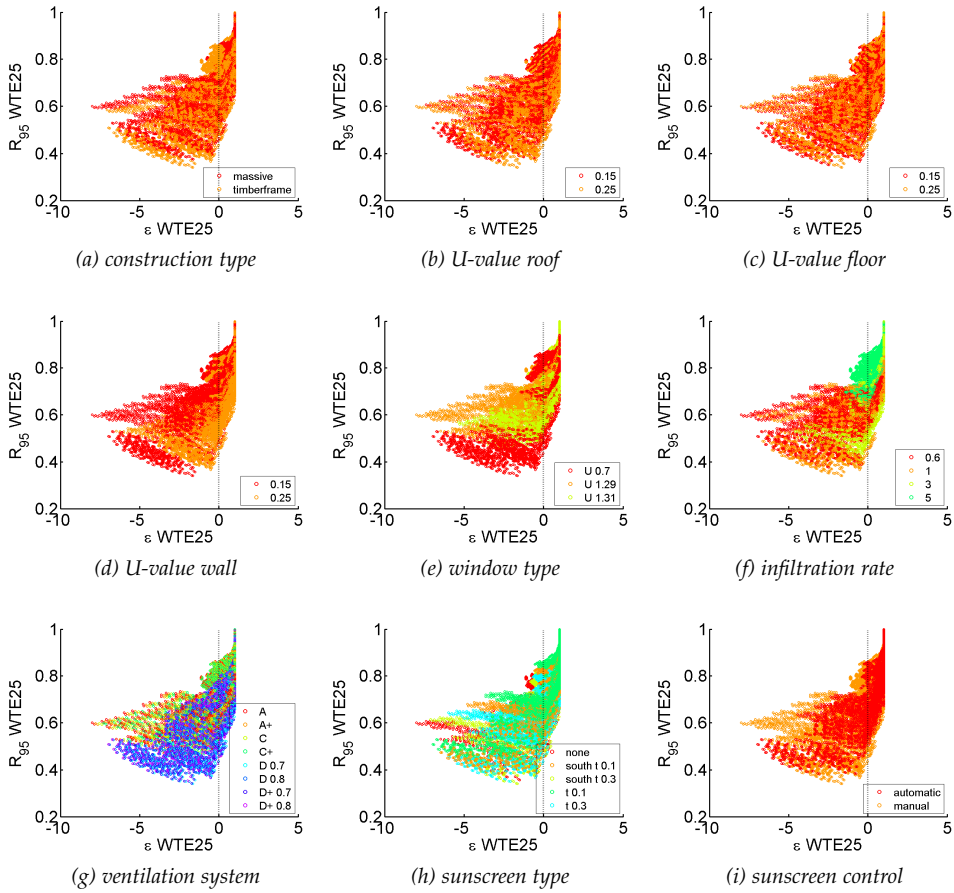

(a) construction type *(b) U-value roof* *(c) U-value floor*

(d) U-value wall *(e) window type* *(f) infiltration rate*

(g) ventilation system *(h) sunscreen type* *(i) sunscreen control*

Figure 6.16: WTE25 effectiveness and robustness for all design options. The different design parameter values are marked in the subplots.

The net present cost is studied in Fig. 6.17. Four columns and three rows of clouds can be found, comparable to the first dwelling. The effectiveness of the net present cost is thus mostly influenced by the construction type, sunscreen type and related sunscreen control (no sunscreens are also indicated with manual control). The U-value of the wall, window type, ventilation system and infiltration rate also slightly influence this effectiveness. U-values of the wall of 0.25 W/m^{2}K, windows with a U-value of 1.29 W/m^{2}K, an infiltration rate of 5 /h and a ventilation system D+ with a heat recovery efficiency of 80 % are most effective solutions. The robustness is mostly influenced by the ventilation system and also slightly by the infiltration rate: a ventilation system D+ with efficiency of 80 % and an infiltration rate of 5 /h are the most robust solutions concerning this net present cost. For the other user and energy price scenarios, very similar results are found.

The initial investment cost is presented in Fig. 6.18. Similar results as for the first dwelling are found.

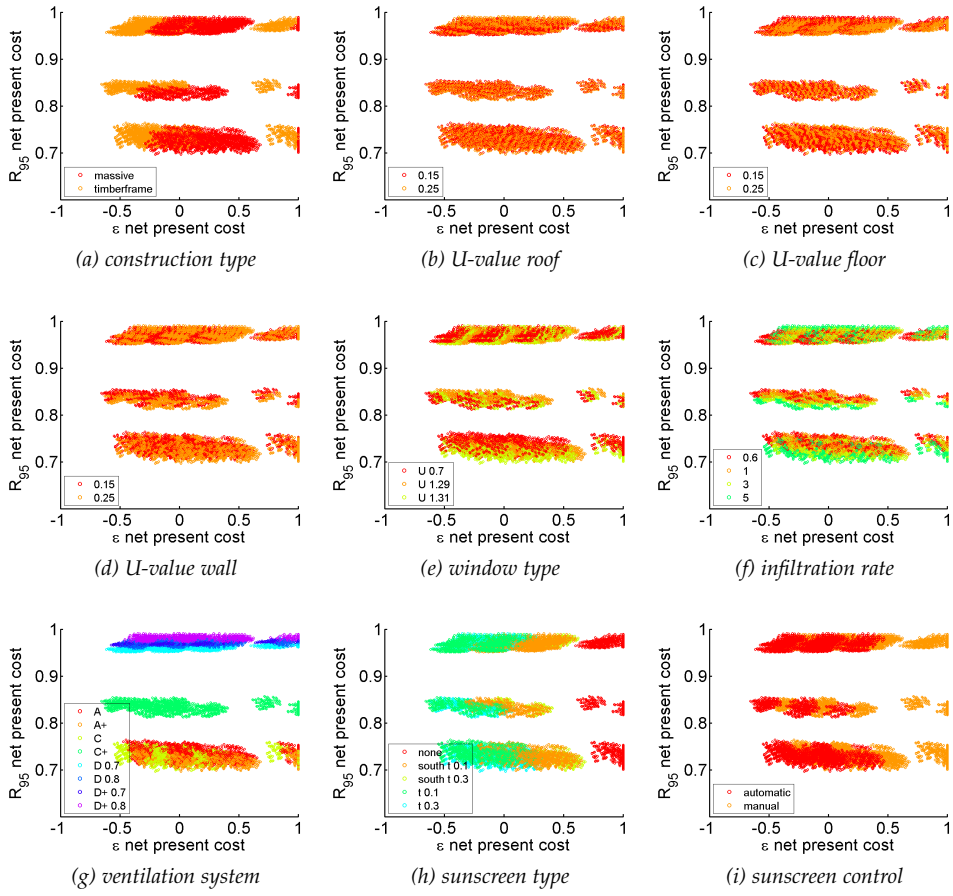

(a) construction type (b) U-value roof (c) U-value floor

(d) U-value wall (e) window type (f) infiltration rate

(g) ventilation system (h) sunscreen type (i) sunscreen control

Figure 6.17: Net present cost effectiveness and robustness for all design options. The different design parameter values are marked in the subplots.

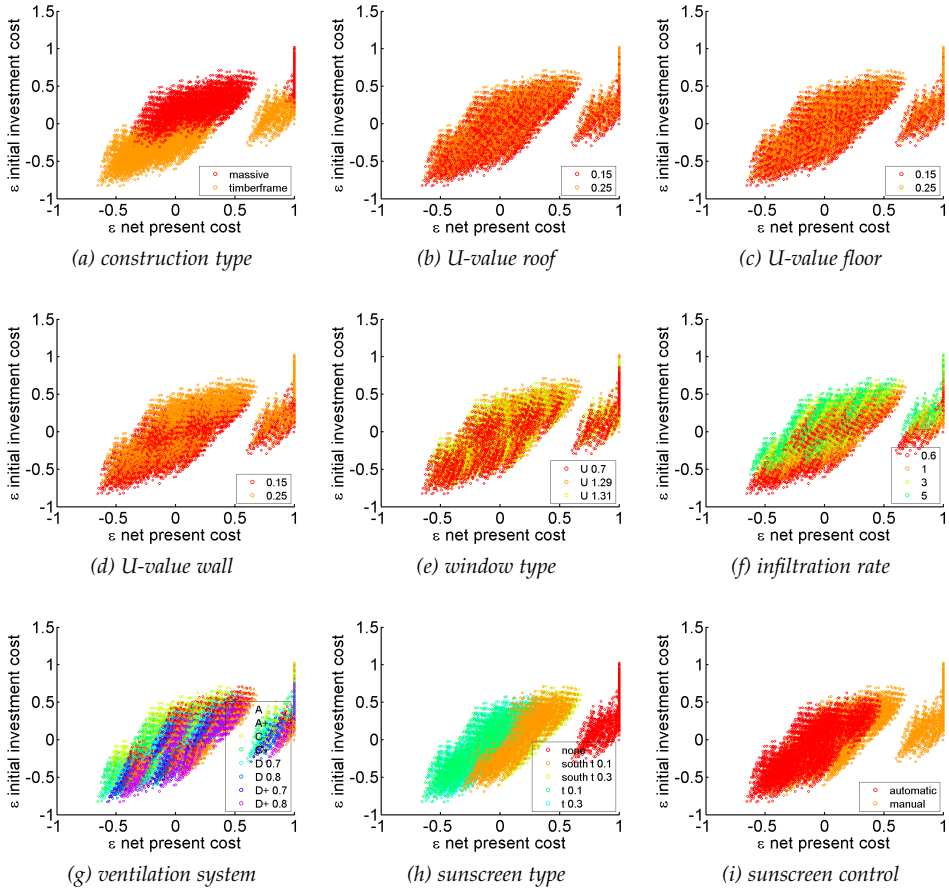

(a) construction type *(b) U-value roof* *(c) U-value floor*

(d) U-value wall *(e) window type* *(f) infiltration rate*

(g) ventilation system *(h) sunscreen type* *(i) sunscreen control*

Figure 6.18: Initial investment cost effectiveness as a function of net present cost effectiveness for all design options. The different design parameter values are marked in the subplots.

Scenario-independent robust design options

The overall optimal solutions regarding WTE25, net energy demand and net present cost for all potential user types and future economic scenarios are sought, analogously to the previous dwelling. Therefore, the overall Pareto frontier is calculated after the search space is reduced by penalising all design options with an effectiveness for one of the performances below 0.1 or a robustness below 0.8 in at least one of the considered scenarios. For WTE25, this criterium is chosen even more severe to assure comfortable indoor climates: effectivenesses below 0.2 are penalised.

The resulting Pareto optimal solutions are presented in Table 6.9 and can be interpreted based on the previous described results and the first dwelling geometry. In order to improve WTE25, sunscreens are preferred. To improve the net energy demand in relation to the net present cost, the most important design measures are the application of a ventilation system D+, a window type with U-value 1.29 W/m^{2}K and an infiltration rate of 5 /h.

Table 6.9: Optimal design parameter values for small terraced dwelling when simultaneously considering effectiveness and robustness of WTE25, net energy demand and net present cost.

PARAMETER	VALUES
construction type	massive
U-value roof (W/m^{2}K)	0.15 /0.25
U-value floor (W/m^{2}K)	0.15 /0.25
U-value wall (W/m^{2}K)	0.25
window type	1.29 W/m^{2}K & g = 0.631
infiltration rate at 50 Pa (1/h)	5
ventilation system	D+ 0.8
sunscreen type	10 % / 10 % south
sunscreen control	manual / automatic 1

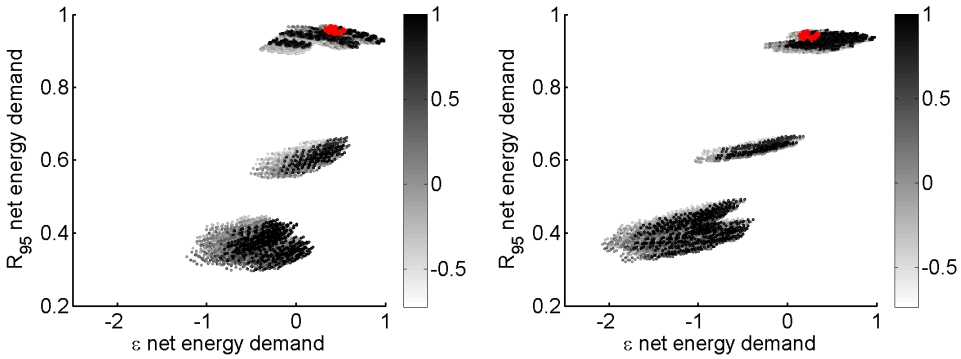

(a) user 1 - economic scenario 1

(b) user 3 - economic scenario 1

(c) user 1 - economic scenario 3

(d) user 3 - economic scenario 3

Figure 6.19: Net energy demand R_{95} as a function of net energy demand ε for the extreme user type and economic scenario combinations. Each dot corresponds to one of the 13 824 design options. The grayscale refers to the net present cost ε. The overall Pareto frontier is indicated in red.

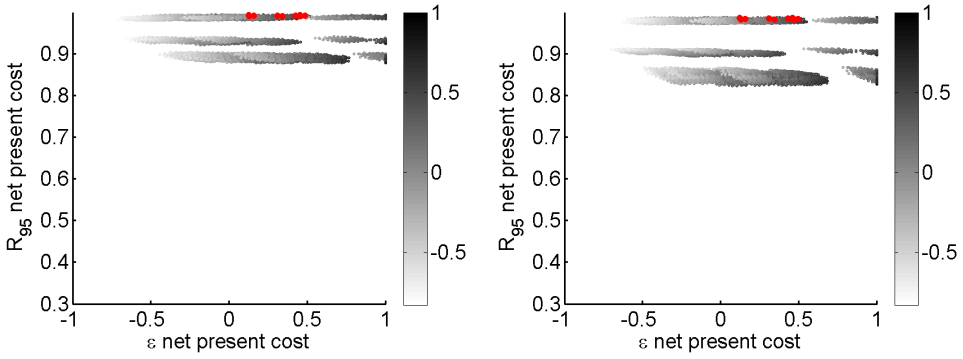

(a) user 1 - economic scenario 1

(b) user 3 - economic scenario 1

(c) user 1 - economic scenario 3

(d) user 3 - economic scenario 3

Figure 6.20: Net present cost R_{95} as a function of net present cost ε for all user type and economic scenario combinations. Each dot corresponds to one of the 13 824 design options. The grayscale refers to the initial investment cost ε. The overall Pareto frontier is indicated in red.

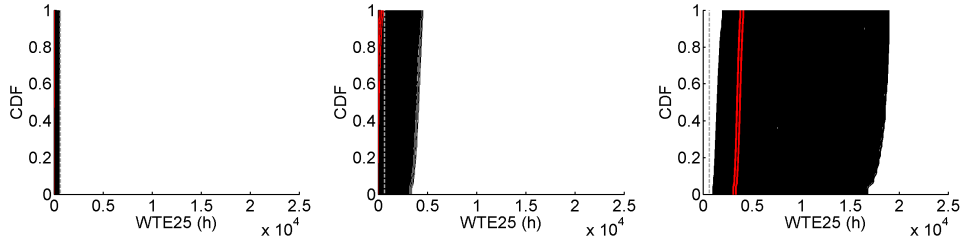

(a) user 1 - economic sc. 2

(b) user 2 - economic sc. 2

(c) user 3 - economic sc. 2

Figure 6.21: Comparison of WTE25 distribution of all design options in black and overall Pareto optimal solutions in red. The preferred performance criteria of WTE25 below 650 h is indicated by the dotted gray line.

This overall Pareto frontier is indicated in red in Fig. 6.19 and 6.20. The grayscale in Fig. 6.19 shows that more effective and robust energy demands results in effective net present costs, especially for energy-wasting users and sharp energy price increases. The grayscale in Fig. 6.20 moreover indicates that design options with a high effectiveness for the net present cost also have a high effectiveness for the initial investment cost. Fig. 6.21 presents the WTE25 distributions for all design options and for the three user types. When opting for the Pareto optimal design options, the indoor comfort will be guaranteed compared to the non-optimal solutions. Only for the third user type - with high internal heat gains - WTE25 will probably exceed the preferred limit of 650 h, however, most other design options are even less preferable. These results are similar to what was found for the first dwelling.

6.3 Robust design of large detached dwelling

In this section, the most effective and robust low-energy measures concerning thermal comfort, energy and costs are studied for the large detached dwelling described in section 6.3.1, similar to the medium semi-detached dwelling in section 6.1 and the small terraced dwelling in section 6.2. Guidelines for this specific dwelling design will thus be provided, given the considered input distributions of Chapter 3. The comparison of the results in section 6.4 will allow to generalise the results to other dwelling geometries and to draw up general guidelines.

6.3.1 Dwelling geometry

The third representative geometry, that was also included in the *IWT TETRA BEP2020* project, is the large detached dwelling of Fig. 6.22. The architectural plans are presented in Fig. 6.23. In these, the day zone is marked in yellow and the night zone in blue. One can see that part of the basement belongs to the day zone, the other part is a ventilated crawl space. The largest windows have overhangs for sun shading and the day zone has a double-height zone which is marked in grey. More characteristics can be found in Table 6.10.

6.3.2 Preprocessing

The preprocessing for this dwelling geometry is performed almost identical to the two other geometries as described in Chapter 3. Since the air change rate distributions are determined by the design rates, which is geometry-dependent, the new air change rate distributions are $Wei(0.2488, 4.670)$ and $Wei(0.7680, 4.670)$ for the day and night zone respectively.

6.3.3 Preliminary screening and updating

The preliminary screening, which is performed similar to section 6.1.2, results in a meta-model for the heat demand and WTE25 and in the sensitivity indices. Since

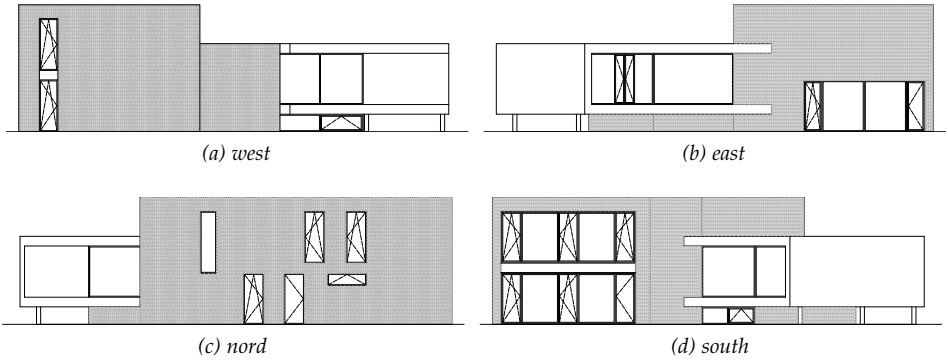

(a) west *(b) east*

(c) nord *(d) south*

Figure 6.22: Facades of large detached dwelling.

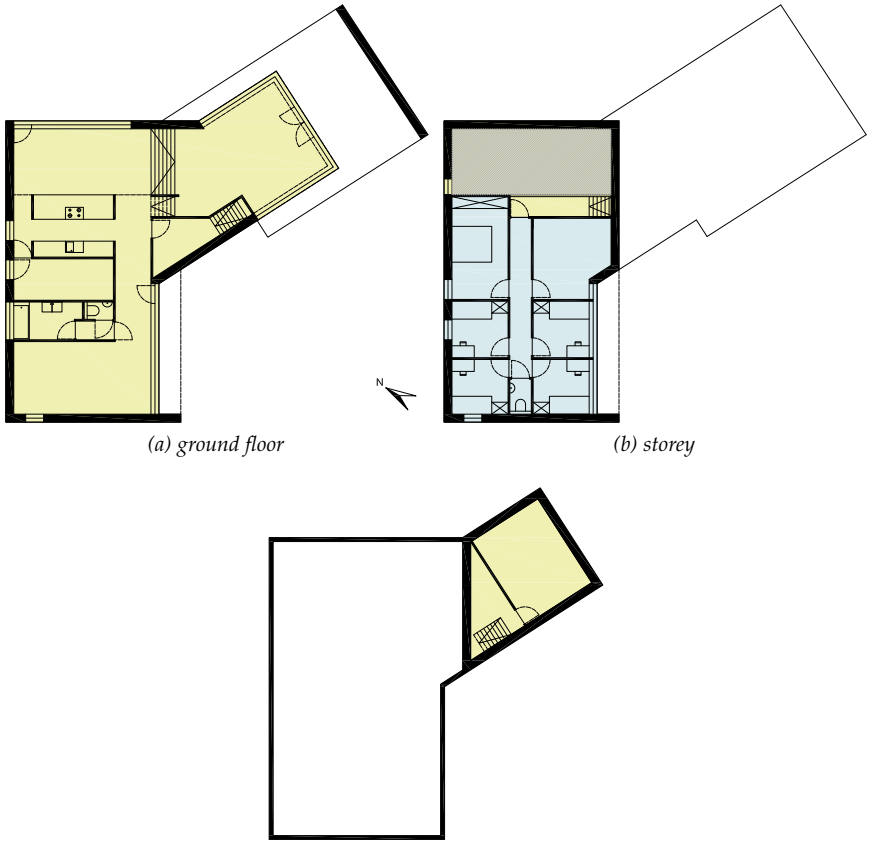

(a) ground floor *(b) storey*

(c) basement

Figure 6.23: Architectural plans of large detached dwelling with day zone indicated in yellow and night zone in blue. North orientation is on the left of the figure.

*Table 6.10: Large detached dwelling characteristics. All areas and volumes are calculated based on outer dimensions similar to EPBD, except for the area marked with *.*

Volume day zone	796 m^3
Volume night zone	270 m^3
Volume basement	190 m^3
Area roof	164 m^2
Area wall	258 m^2
Area floor	164 m^2
Area windows	150 m^2
Width	18 m
Depth	21 m
Height	6.7 m
Double-height zone*	27 m^2
Liveable floor area*	260 m^2
Compactness	1.44 m
Percentage glazing/floor	31 %

the performance of the meta-models is also similar to those of the first case study, this is not described here.

The Spearman's ρ-values are presented in Table 6.11. These results are similar to the other studied dwellings in Table 6.2 and 6.8. The infiltration rate, the U-value of the windows, the ventilation system with heat recovery efficiency and the set temperature for occupancy in the day zone influence the net energy demand the most, followed by the U-value of the walls and roofs, the other set temperatures, the deviation on the design infiltration rate and design U-values, the air change rate and the internal heat gains by appliances. WTE25 is mostly dominated by the sunscreen type, followed by the construction type, the sunscreen control, the window type, the internal heat gains by appliances, the infiltration rate and the U-value of the walls. The net present cost is mainly influenced by the nominal energy price evolution, but also by the sunscreen and construction type, followed by the infiltration rate. At last, the initial investment cost is only determined by building fabric and systems, of which the construction type is the most significant, followed by the sunscreen type, the U-value of the floor and the ventilation system.

The input parameters that are not significantly influencing one or more of the considered performances are eliminated in the robust design. Therefore, in the next section, 'deviation from design heat recovery efficiency' (1), 'occupancy profile day zone' (3), 'occupancy profile night zone' (6), 'internal gains persons' (105 W) and 'basis internal gains appliances day zone' (100 W) are set at their average value, which is indicated between brackets.

Table 6.11: Spearman's ρ and p-values for net energy demand (NED), WTE25, net present cost (NPC) and initial investment cost (IIC). Insignificant indices are indicated in grey.

PARAMETER	NED		WTE25		NPC		IIC	
	ρ	p	ρ	p	ρ	p	ρ	p
construction type	-0.02	0.72	0.28	0.00	0.40	0.00	0.87	0.00
U-value roof	0.11	0.01	0.07	0.12	.02	0.63	-0.02	0.57
U-value floor	0.02	0.69	-0.05	0.25	-0.04	0.40	-0.12	0.01
U-value wall	0.20	0.00	-0.11	0.01	0.07	0.09	-0.05	0.28
window type U-value	0.35	0.00	-0.02	0.71	0.02	0.60	-0.08	0.06
window type g-value	0.10	0.01	0.14	0.00	0.02	0.66	-0.02	0.66
infiltration rate at 50 Pa	0.58	0.00	-0.12	0.00	0.13	0.00	-0.05	0.23
dev. from design U-values	0.11	0.01	-0.06	0.13	0.03	0.52	0.00	0.98
dev. from design infiltration rate	0.14	0.00	-0.01	0.88	0.05	0.27	0.00	1.00
ventilation system	-0.32	0.00	0.02	0.69	0.06	0.19	0.08	0.05
heat recovery efficiency	-0.28	0.00	-0.01	0.79	0.05	0.21	0.08	0.05
dev. from design heat rec. efficiency	0.06	0.15	-0.05	0.22	0.02	0.58	0.01	0.79
sunscreen type	0.06	0.13	-0.70	0.00	0.44	0.00	0.33	0.00
sunscreen control	-0.10	0.02	0.15	0.00	0.04	0.35	0.02	0.68
occupancy profile day zone	-0.02	0.70	-0.02	0.66	0.04	0.38	0.03	0.54
occupancy profile night zone	0.05	0.26	-0.01	0.73	0.04	0.34	0.00	0.99
set temp. occupancy day zone	0.29	0.00	0.06	0.16	0.06	0.13	-0.04	0.36
set temp. absence day zone	0.18	0.00	0.02	0.62	0.02	0.61	-0.05	0.29
set temp. occupancy night zone	0.12	0.01	0.01	0.80	0.04	0.40	0.01	0.81
air change rate	0.13	0.00	-0.05	0.21	0.07	0.09	0.04	0.39
internal gains persons	-0.02	0.60	-0.06	0.16	0.00	0.98	-0.04	0.36
basis internal gains appl. day zone	-0.05	0.25	-0.03	0.55	0.05	0.28	0.07	0.09
internal gains appliances day zone	-0.12	0.01	0.14	0.00	0.02	0.70	0.01	0.85
nominal energy price evolution	0.03	0.52	-0.01	0.90	0.66	0.00	0.05	0.22

6.3.4 Robust design

Based on the constructed meta-models and the sensitivity results, the robust design can be performed. The obtained layer values are identical to the first dwelling geometry, excluding the adapted air change rate distribution.

Output evaluation

The multi-layered sampling, similarly performed as in section 6.1.3, results in an effectiveness and robustness value for each performance and for each design option and scenario combination. In Fig. 6.24, 6.25, 6.26 and 6.27, these indicators are presented for the second user and second energy price evolution.

Fig. 6.24 compares the design parameter values for the net energy demand. Also for this geometry, the choice of ventilation system seems to be most dominant in order to obtain effective and robust net energy demands. Types D(+) appear to be the best solution, of which the system D(+) with a heat recovery efficiency of 80 % is the

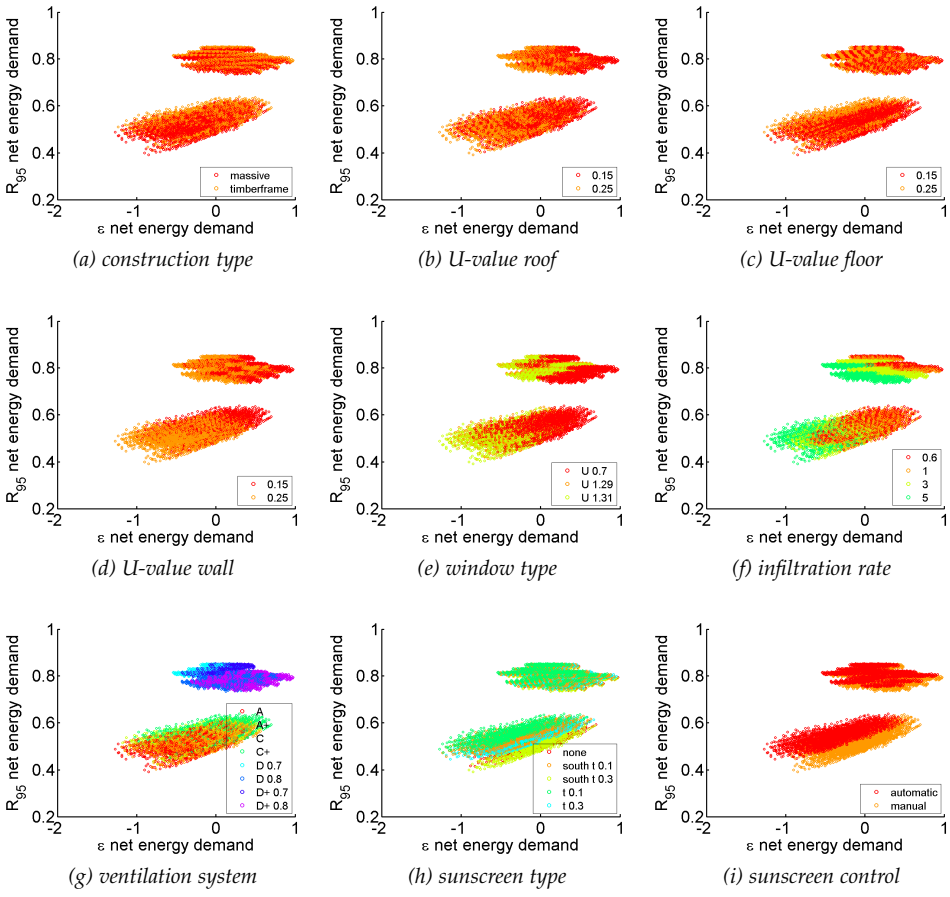

(a) construction type *(b) U-value roof* *(c) U-value floor*

(d) U-value wall *(e) window type* *(f) infiltration rate*

(g) ventilation system *(h) sunscreen type* *(i) sunscreen control*

Figure 6.24: Net energy demand effectiveness and robustness for all design options. The different design parameter values are marked in the subplots.

most effective, while system D(+) with an efficiency of 70 % is the most robust. In a second phase, also the U-value of the walls, the window type and the infiltration rate influence the net energy demand significantly. A U-value of 0.15 W/m^{2}K, a window type with a U-value of 0.7 W/m^{2}K and an n_{50}-value of 0.6 or 1 /h are the most effective. Very similar results can be found for the other user types.

Fig. 6.25 compares the design parameter values for WTE25. One can see that two clouds are formed due to the differences in sunscreen type, similar to the other geometries. Also the window type and sunscreen control seem essential in order to obtain robust and effective solutions. The most effective and robust solutions are characterised by windows with a U-value 0.7 W/m^{2}K and the presence of sunscreen with 10 % transmission and automatic control. The results for the other user scenarios are similar.

The net present cost is studied in Fig. 6.26. These results are similar to the other dwellings as well. The different columns are formed by the differences in construction type and sunscreen type. A massive construction with no sunscreen (or manually

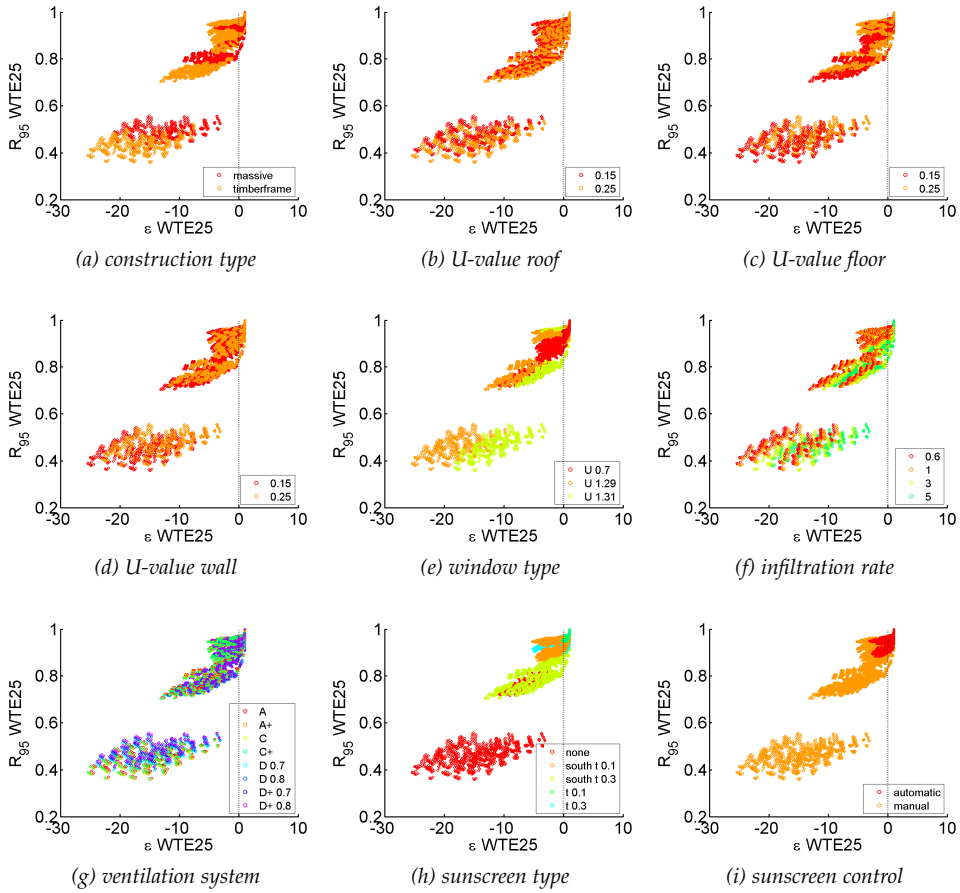

(a) construction type *(b) U-value roof* *(c) U-value floor*

(d) U-value wall *(e) window type* *(f) infiltration rate*

(g) ventilation system *(h) sunscreen type* *(i) sunscreen control*

Figure 6.25: WTE25 effectiveness and robustness for all design options. The different design parameter values are marked in the subplots.

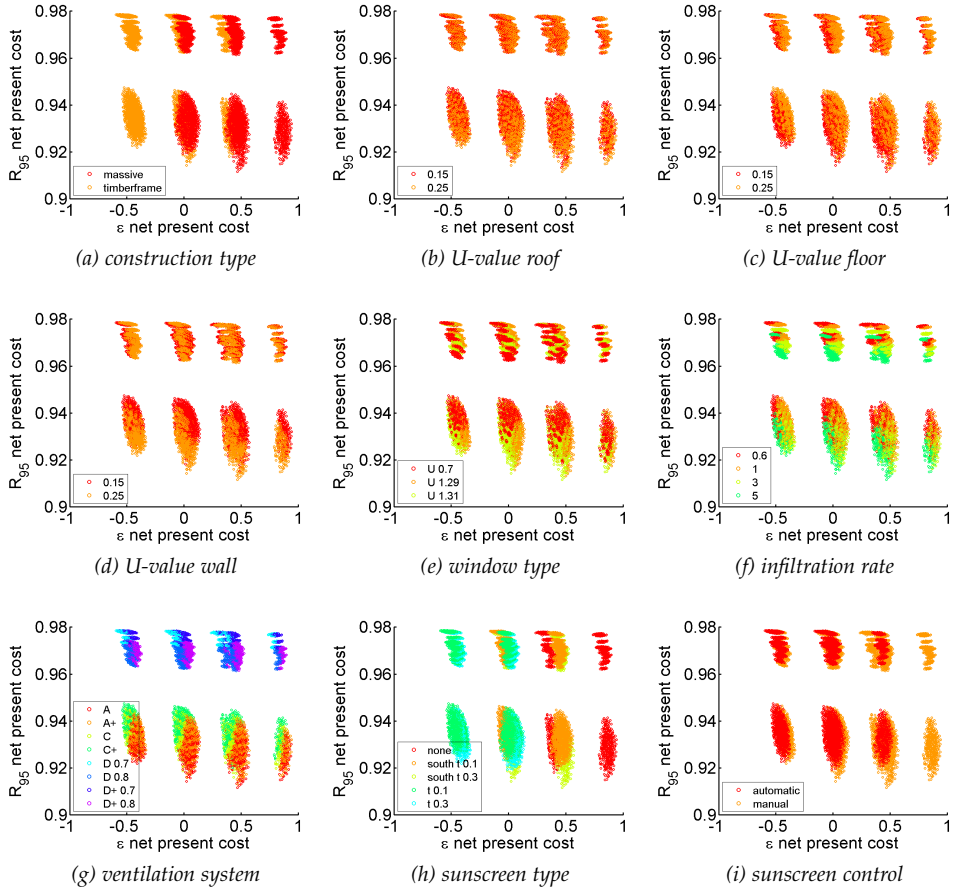

(a) construction type *(b) U-value roof* *(c) U-value floor*

(d) U-value wall *(e) window type* *(f) infiltration rate*

(g) ventilation system *(h) sunscreen type* *(i) sunscreen control*

Figure 6.26: Net present cost effectiveness and robustness for all design options. The different design parameter values are marked in the subplots.

controlled) is the most cost effective, because of its lower initial investment cost as will be seen in Fig. 6.27. The ventilation system also slightly influences this effectiveness. A ventilation system A, A+ or D+ with a heat recovery efficiency of 80 % are most effective solutions. The two rows, however, are formed by the ventilation type. The robustness is thus mostly influenced by the ventilation system and also slightly by the U-value of the walls, the window type and the infiltration rate: a ventilation system D with efficiency of 70 %, U-values of 0.15 W/m^{2}K, a window with U-value of 0.7 W/m^{2}K and an infiltration rate of 0.6 /h are the most robust solutions concerning this net present cost. For the other user and energy price scenarios, very similar results are found. However, the more energy is used and the more expensive the energy price is, the more effective an n_{50}-value of 0.6 /h and a window type with a U-value of 0.7 W/m^{2}K are.

The initial investment cost is presented in Fig. 6.27 with similar results to the other geometries. The initial investment cost effectiveness is dominated by the construction type and the sunscreen type, as already indicated by the net present cost. Also the U-values, the window type and the infiltration rate slightly influence this initial

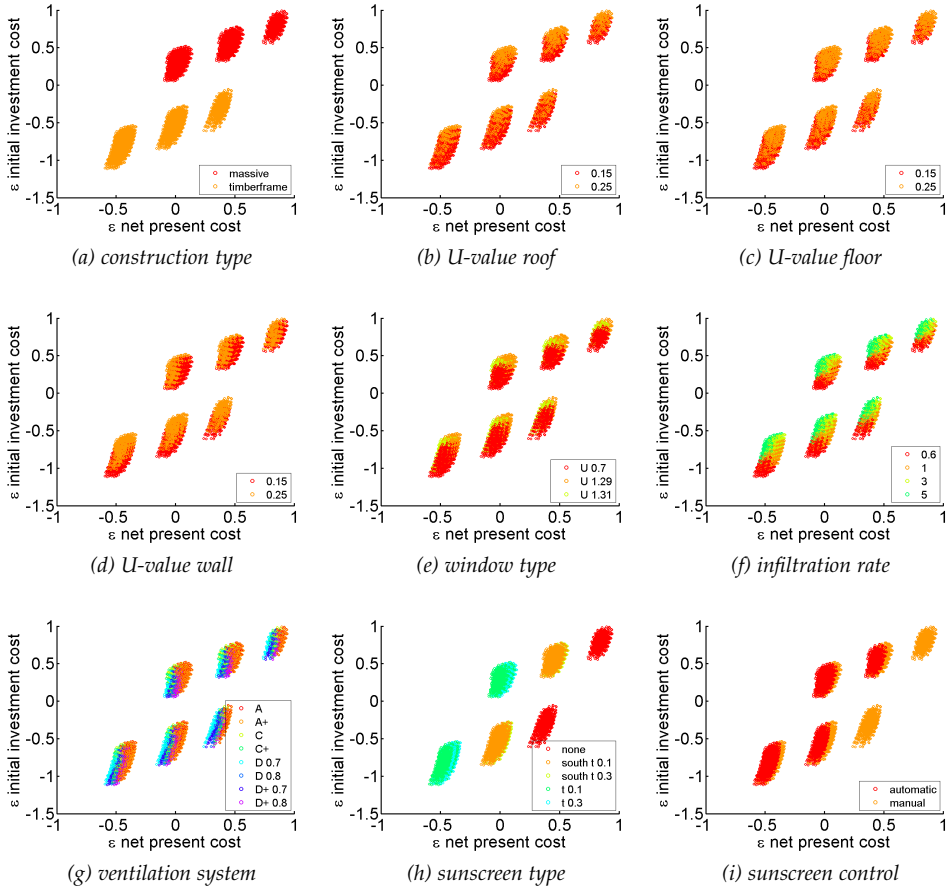

(a) construction type *(b) U-value roof* *(c) U-value floor*

(d) U-value wall *(e) window type* *(f) infiltration rate*

(g) ventilation system *(h) sunscreen type* *(i) sunscreen control*

Figure 6.27: Initial investment cost effectiveness as a function of net present cost effectiveness for all design options. The different design parameter values are marked in the subplots.

investment cost. They seem, however, more or less to be compensated by the energy costs in the net present cost. When the initial investment cost is crucial in the decision-making, a massive construction, no sunscreens, U-values of 0.25 W/m^{2}K, a window type with U-value of 1.29 W/m^{2}K and an n_{50}-value of 5 /h will be preferred.

Scenario-independent robust design options

Similar to the previous case studies, the overall optimal solutions regarding WTE25, net energy demand and net present cost for all potential user types and future economic scenarios are sought. Therefore, the overall Pareto frontier is calculated with an arbitrarily reduced search space. All design options with an effectiveness for one of the performances below 0.2 or a robustness below 0.8 in at least one of the considered scenarios are penalised.

Table 6.12: Optimal design parameter values for the large detached dwelling when simultaneously considering effectiveness and robustness of WTE25, net energy demand and net present cost.

PARAMETER	VALUES
construction type	massive
U-value roof (W/m^2K)	0.15 /0.25
U-value floor (W/m^2K)	0.15 /0.25
U-value wall (W/m^2K)	0.15 / 0.25
window type	1.31 W/m^2K & g = 0.551 / 0.7 W/m^2K & g = 0.407
infiltration rate at 50 Pa (1/h)	0.6 / 1
ventilation system	D 0.8 / D+ 0.8
sunscreen type	10 % south
sunscreen control	automatic 1

The resulting Pareto optimal solutions are presented in Table 6.12 and can be interpreted based on the previous described results. This table is highly comparable to Table 6.6 and 6.9.

This overall Pareto frontier is indicated in red in Fig. 6.28. Fig. 6.29 presents the WTE25 distributions for all design options and for the three user types. The net present cost is shown in Fig. 6.30. Design options with a high effectiveness for the net present cost also have a high effectiveness for the initial investment cost as indicated by the grayscale. The grayscale in Fig. 6.28 also shows that more effective energy demands result in effective net present costs.

6.4 Guidelines and conclusions

Sections 6.1, 6.2 and 6.3 described the robust design for a medium semi-detached, a small detached and a large detached dwelling respectively as an illustration of the developed methodology. By comparing the results of these different dwellings, general observations can be made and guidelines for also other geometries can be developed. It need to be emphasised that the results are dependent of the considered input distributions.

6.4.1 Comparison of robust design of three dwelling geometries

A comparison of the sensitivity results of Table 6.2 on page 122, Table 6.8 on page 139 and Table 6.11 on page 149 learns that the same input parameters are dominant, although, small differences in the ranking are found. With regard to the net energy demand, overall most dominant parameters are the infiltration rate, the ventilation system and the set temperatures. The influence of the infiltration rate increases with the compactness of the considered dwellings. The larger the window, wall and roof areas, the more dominant the respective U-values become. Furthermore, the larger the volume, the more important are the set temperatures and the less important are

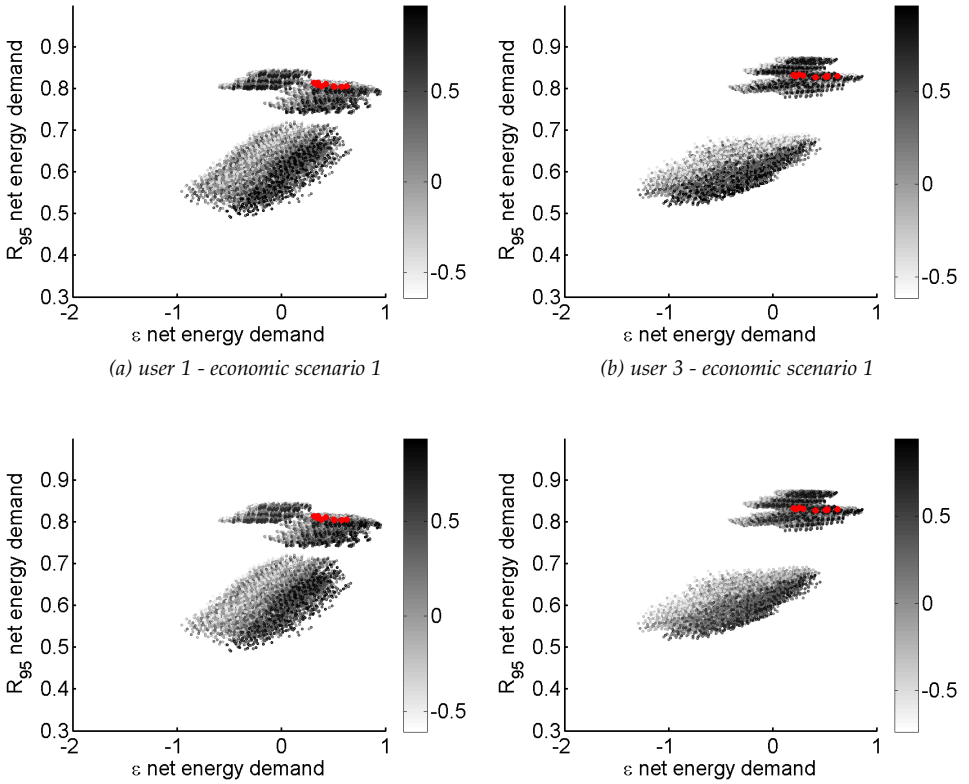

(a) user 1 - economic scenario 1

(b) user 3 - economic scenario 1

(c) user 1 - economic scenario 3

(d) user 3 - economic scenario 3

Figure 6.28: Net energy demand R_{95} as a function of net energy demand ε for the extreme user type and economic scenario combinations. Each dot corresponds to one of the 13 824 design options. The grayscale refers to the net present cost ε. The overall Pareto frontier is indicated in red.

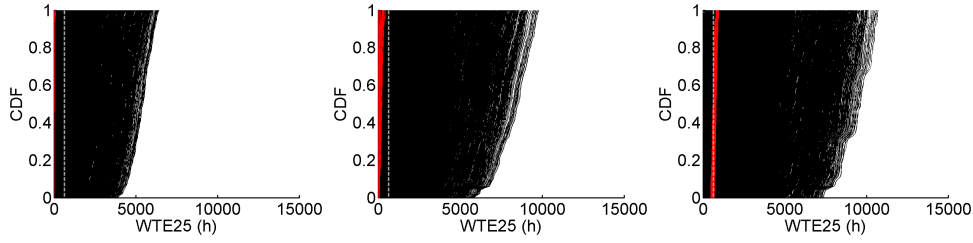

(a) user 1 - economic sc. 2

(b) user 2 - economic sc. 2

(c) user 3 - economic sc. 2

Figure 6.29: Comparison of WTE25 distribution of all design options in black and overall Pareto optimal solutions in red. The preferred performance criteria of WTE25 below 650 h is indicated by the dotted gray line.

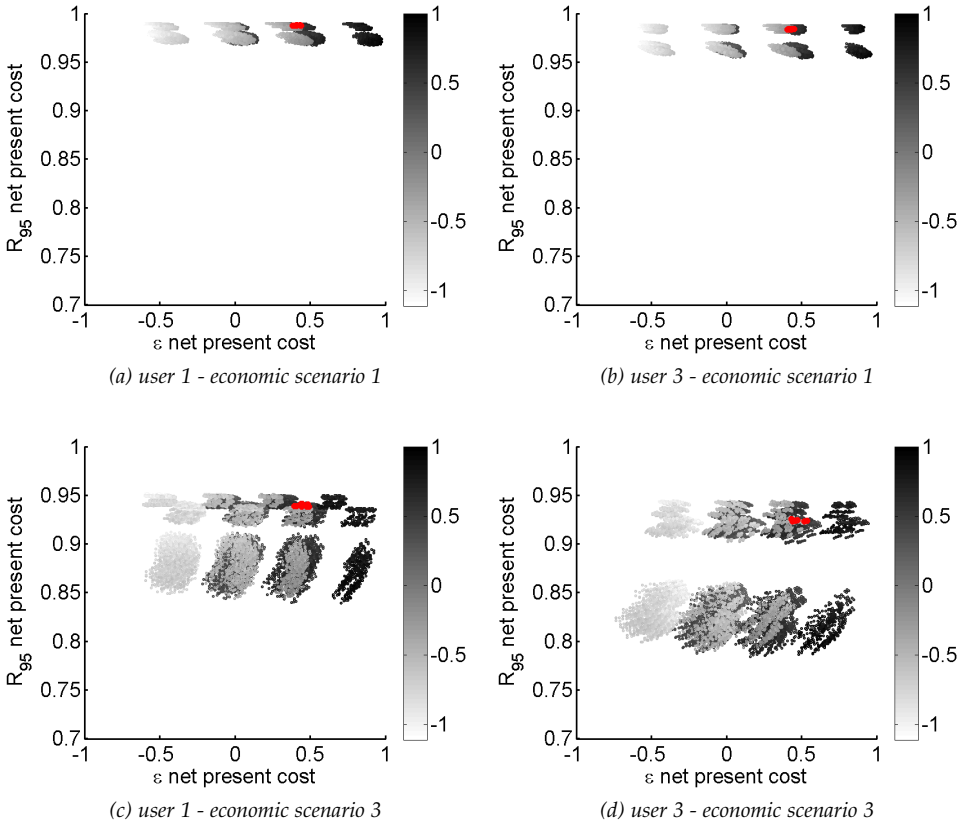

(a) user 1 - economic scenario 1

(b) user 3 - economic scenario 1

(c) user 1 - economic scenario 3

(d) user 3 - economic scenario 3

Figure 6.30: Net present cost R_{95} as a function of net present cost ε for the extreme user type and economic scenario combinations. Each dot corresponds to one of the 13 824 design options. The grayscale refers to the initial investment cost ε. The overall Pareto frontier is indicated in red.

the internal heat gains. The internal heat gains are also more important for the small dwelling in view of WTE25, which is overall mostly dominated by the sunscreen type. In order to guarantee the thermal comfort in the small dwelling, also the set temperatures and the air change rate are crucial. Furthermore, the larger the windows are, the more important is the window type. For the net present cost, the sensitivity results are very similar for the three considered dwellings. The energy price evolution is for all three geometries most important. The initial investment costs are mostly influenced by the construction and sunscreen type. The remaining significant parameters are strongly dependent of the considered geometry.

The probability distributions for the net energy demand and WTE25 are also interesting to compare. Fig. 6.31 and 6.32 show these for all considered 13 824 design options for the average user type. First of all, one can see a significant difference in the net energy demand of the three dwelling geometries, in addition to the variability of the net energy demand due to air change rates and deviations from design rates. It is not surprising that the large dwelling has a much larger net energy demand than the small dwelling. Moreover, the robustness of the design

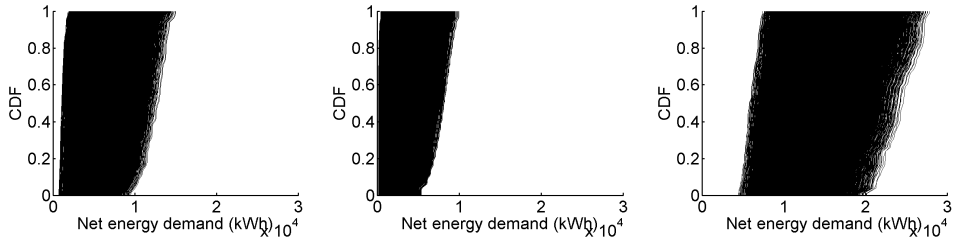

(a) medium semi-detached *(b) small terraced* *(c) large detached*

Figure 6.31: Comparison of net energy demand distribution of all design options for the three considered dwellings for the average user.

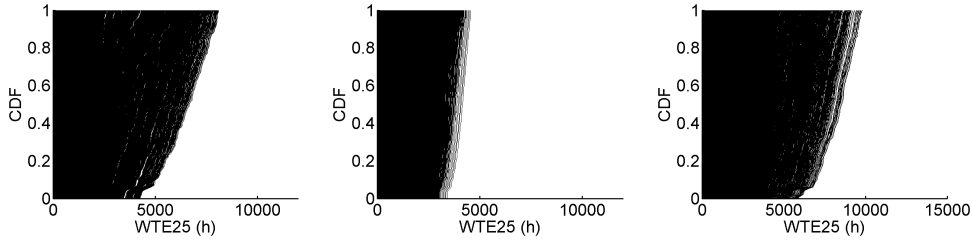

(a) medium semi-detached *(b) small terraced* *(c) large detached*

Figure 6.32: Comparison of WTE25 distribution of all design options for the three considered dwellings for the average user.

solutions of the small dwelling is much higher. WTE25 seems to be lower for the smallest dwelling, although this is more sensitive for overheating due to internal heat gains. The larger window areas of the other two dwelling result in a higher probability for overheating, especially when no sunscreens are applied. When the same results would be compared for the third user type with more internal heat gains, the probability for overheating is larger for the small dwelling.

Finally, also the robust design options of Table 6.6 on page 135, Table 6.9 on page 144 and Table 6.12 on page 154 are compared. Because of the lower initial cost and thus higher net present cost, a massive construction is preferred for all geometries. In order to limit the net energy demand, a ventilation system D or D+ with heat recovery efficiency of 80 % is optimal. Once such a ventilation system is applied, U-values of about 0.2 W/m^2K are sufficient. Only for larger window areas, the window U-value is best reduced. The n_{50}-value needs to be lower for smaller compactnesses. Furthermore, in order to obtain a comfortable indoor climate, sunscreens need to be provided. Since the latter are dependent on the user behaviour and less cost effective, one can opt to only install them once needed.

6.4.2 Guidelines for robust low-energy dwellings

Although the three considered geometries are sufficiently different, the same conclusions are found. Therefore, illustrative guidelines based on these results

Table 6.13: Optimal design parameter values concerning WTE25, net energy demand and net present cost.

PARAMETER	VALUES
construction type	massive
U-value roof (W/m^2K)	0.15 /0.25
U-value floor (W/m^2K)	0.15 /0.25
U-value wall (W/m^2K)	0.15 / 0.25
window type	1.29 W/m^2K & g = 0.631 / 1.31 W/m^2K & g = 0.551 / 0.7 W/m^2K & g = 0.407
infiltration rate at 50 Pa (1/h)	1 / 3
ventilation system	D 0.8 / D+ 0.8
sunscreen type	10 % south / 10 %
sunscreen control	manual / automatic 1

can be drawn up. In order to obtain low-energy dwellings that are comfortable and affordable in a robust way and regardless of the occupants and the future energy price evolutions, the design measures of Table 6.13 are preferred.

Most attention needs to be paid on the ventilation system and air tightness. For low-energy dwellings, the ventilation losses are more important than the conductive heat losses. The U-values of walls, roofs and floor have an optimal value around 0.2 W/m^2K. The windows are preferably equipped with improved glazing, and when the window area increases, also the U-values becomes more dominant. The lower the net energy demand is, also the lower is the net present cost and the higher its robustness. Depending on the volume of the dwelling, the presence of overhangs for sun shading and the user behaviour in the dwelling, the use of more or less sunscreens is recommended. Sunscreens can be installed afterwards once needed as well.

The performances of such an optimised dwelling can still significantly vary due to the set temperatures, the air change rate and the internal heat gains, as was seen in the sensitivity analyses. The set temperature, for example, is even more dominant for the net energy demand than the U-values. Lowering this set temperature is thus crucial for a low net energy demand and thus also a low energy cost. Raising the awareness of the occupants is thus as important as the improvement of the design options. The use of energy-efficient appliances (with lower internal heat gains) has a positive effect on the thermal summer comfort, especially for small dwellings. Furthermore, the increase of the air change rate in summer can effectively reduce WTE25.

As was seen in Fig. 6.31, not only the selection of design options from Table 6.13 has a positive effect on the net energy demand and the net present cost. These performances can also be improved by the selection of the dwelling geometry itself. Smaller dwellings with overhangs for sun shading are more effective and robust.

7

Conclusions and future research

As described in Chapter 1 and Chapter 2, the overall aim of this thesis was twofold. An overall applicable probabilistic design methodology had to be developed and to be illustrated on the design of affordable and comfortable low-energy dwellings. The conclusions concerning these objectives are summarised in section 7.1 and 7.2, respectively. The future perspectives for follow-up research will be described in section 7.3.

7.1 Probabilistic design methodology

Building performance problems are commonly solved in a deterministic way. The neglection of the inherent variability of involved parameters may, however, lead to inconclusive analyses and non-optimal designs. Hence, a **probabilistic methodology** is preferred as already extensively developed in other research fields. Because building performance problems, amongst many other problems, are often characterised by transient and non-linear behaviour and multiple contributing parameters have to be taken into account, the methods used in other fields cannot be translated in a straightforward way. And although lots of research have already been done on uncertainty and sensitivity analysis in building performance, much of this research has focused on specific and delimited issues without providing an overall applicable methodology. The development of the methodology in this thesis to quantify performance spread and to use that in design, while taking uncertainties into account in an efficient and reliable way, is thus a major step forward.

Furthermore, since **robust design** implies quality improvement and assurance, the demand for robust design solutions has increased over the last decade. The development and promotion of effective and robust building envelopes and service solutions is an important step to avoid large deviations between design and actual performances, and thus to reduce the influence of uncertain conditions. However, until now, the building performance applications only dealt with a limited approach to robustness. Therefore, these robust design principles are incorporated in the

probabilistic design methodology in a very intuitive way. Hence, this robust design tool is one of the greatest achievements of the proposed methodology.

Since it is not possible to predict parameters such as the future climate, energy price evolutions and user behaviour, and they might be important in the assessment of probabilistic or robust design problems, an explicit evaluation for such **scenarios** might be wanted and therefore enabled in the methodology as well. That way, design options that are (almost) optimal in all future situations can be selected to overcome potentially bad future performances. Such design options are called scenario-independent.

This probabilistic design methodology was described in Chapter 5 and relies on the four probabilistic procedures that are explained in Chapter 4. Uncertainty quantification is used to propagate the uncertainties of the input to the uncertainties of the output. Sensitivity analysis moreover identifies those input parameters that are most dominant in this transformation. Furthermore, multi-layered sampling is proposed to reliably compare several design options, optionally for certain future scenarios. The main success of this methodology is ascribed to the use of **meta-models** in order to significantly improve the calculation time. Without these meta-models, the methodology would not be feasible for most building performance models.

7.2 Robust low-energy dwellings

In the frame of the Kyoto Protocol and the 20-20-20 targets, as described in Chapter 1, several governments agreed on limiting their greenhouse gas emissions and increasing the energy efficiency. As a consequence, governments aim at reducing the net energy demand of new buildings as much as possible. However, it is not clear how to design a dwelling that will perform as targeted. Large performance gaps are undesirable, both from the point of view of the building owner and/or occupant in particular as well as society in general. Building owners and/or occupants need confidence in the return on their investments in, for example, energy efficiency and indoor climate, while governments want to ensure that their subsidy programs have the desired impact to meet the described targets. In order to provide illustrative guidelines for affordable and comfortable low-energy dwellings with robust performances, three different dwelling geometries were studied in Chapter 6. In order to optimise their performances, building physical decisions such as the choice of insulation thickness and ventilation system were made without changing the architecture of the dwellings. Because this application is simplified, only general observations can be made.

Although the three considered geometries are sufficiently different, the same conclusions were found. Therefore, guidelines based on these results could be drawn up. In order to obtain low-energy dwellings that are comfortable and affordable in a robust way and regardless of the occupants and the future energy price evolutions, the design measures of Table 7.1 are preferred. Most attention needs to be paid on the ventilation system and air tightness. For low-energy dwellings, the ventilation

Table 7.1: Optimal design parameter values concerning WTE25, net energy demand and net present cost. Replica of Table 6.13.

PARAMETER	VALUES
construction type	massive
U-value roof (W/m^2K)	0.15 /0.25
U-value floor (W/m^2K)	0.15 /0.25
U-value wall (W/m^2K)	0.15 / 0.25
window type	1.29 W/m^2K & g = 0.631 / 1.31 W/m^2K & g = 0.551 / 0.7 W/m^2K & g = 0.407
infiltration rate at 50 Pa (1/h)	1 / 3
ventilation system	D 0.8 / D+ 0.8
sunscreen type	10 % south / 10 %
sunscreen control	manual / automatic 1

losses were found to be more important than the conductive heat losses. The U-values of walls, roofs and floor have an optimal value around 0.2 W/m^2K. The windows are preferably equipped with improved glazing, and when the window area increases, also the U-values become more important in the optimal design. The lower the net energy demand is, also the lower is the net present cost and the higher its robustness. Depending on the volume of the dwelling, the presence of overhangs for sun shading and the user behaviour in the dwelling, the use of more or less sunscreens is recommended. Sunscreens can be installed afterwards once needed as well.

The performances of such an optimised dwelling can still significantly vary due to the set temperatures, the air change rate and the internal heat gains. The set temperature, for example, is even more dominant for the net energy demand than the U-values. Lowering this set temperature is thus crucial for a low net energy demand and thus also a low energy cost. Hence, raising the awareness of the occupants is found to be as important as the improvement of the design options. The use of energy-efficient appliances (with lower internal heat gains) has a positive effect on the thermal summer comfort, especially for small dwellings. Furthermore, the increase of the air change rate in summer can effectively reduce WTE25.

Finally, not only the selection of design options has a positive effect on the net energy demand and the net present cost. These performances can also be improved by the selection of the dwelling geometry itself. Overall, the obtained optimal designs are more effective and robust for smaller dwellings.

7.3 Perspectives for future research

Since both sampling efficiency and meta-modelling are essential techniques for the developed design methodology and this thesis provided only a first major step, the methodology would benefit from further research on those topics. Especially for computationally expensive building models, e.g. when applying computational fluid

dynamics, the sampling efficiency is crucial for the applicability of the methodology. The meta-modelling approach presented in this thesis, however, may require a considerable number of simulations, which are not feasible within the usual time constraints for such studies. Therefore, more research on sampling schemes and meta-modelling techniques for the construction of such meta-models is suggested.

Furthermore, based on the (robust) design methodology more and also more extensive case studies could be elaborated. The case study of Chapter 6 could be extended with the consideration of a variety of heating systems, climatic conditions and investment cost uncertainties, since these were assumed deterministic in the current analysis. Other interesting studies, that can be performed with the developed methodology, is to determine which (retrofit) measures the government needs to subsidise in order to meet the energy efficiency targets. Similar studies can be performed for the development of a new neighbourhood commissioned by a social housing company or project developer, or for the retrofitting of a housing neighbourhood or office building commissioned by an ESCO. In those studies, it might be interesting to also include geometric design parameters such as the volume, the orientation and the glass ratio. Because the availability of statistical data is important for such case studies as well and this is unfortunately lacking, more efforts need to be done in that direction first. Since the case study illustrated that user behaviour is very influential in building performance problems, more research on user profiles and their probability distributions would be beneficial as well.

Bibliography

Abuku, M., Janssen, H. and Roels, S. (2009), 'Impact of wind-driven rain on historic brick wall buildings in a moderately cold and humid climate: Numerical analyses of mould growth risk, indoor climate and energy consumption', *Energy and Buildings* **41**(1), 101–110.

Alam, F. M., McNaught, K. R. and Ringrose, T. J. (2004), 'A comparison of experimental designs in the development of a neural network simulation metamodel', *Simulation Modelling Practice and Theory* **12**(7-8), 559–578.

Apel, H., Thieken, A. H., Merz, B. and Blöschl, G. (2006), 'A Probabilistic Modelling System for Assessing Flood Risks', *Natural Hazards* **38**, 79–100.

Baetens, R., De Coninck, R., Van Roy, J., Verbruggen, B., Driesen, J., Helsen, L. and Saelens, D. (2012), 'Assessing electrical bottlenecks at feeder level for residential net zero-energy buildings by integrated system simulation', *Applied Energy* **96**, 74–83.

Beyer, H.-G. and Sendhoff, B. (2007), 'Robust optimization - A comprehensive survey', *Computer Methods in Applied Mechanics and Engineering* **196**(33-34), 3190–3218.

Booth, A. and Choudhary, R. (2013), 'Decision making under uncertainty in the retrofit analysis of the UK housing stock: Implications for the Green Deal', *Energy and Buildings* **64**, 292–308.

Booth, A., Choudhary, R. and Spiegelhalter, D. (2012), 'Handling Uncertainty in Housing Stock Models', *Building and Environment* **48**, 35–47.

Bordass, W. and Leaman, A. (1997), 'Future buildings and their services', *Building Research & Information* **25**(4), 190–195.

Box, G. E. P., Hunter, W. G. and Hunter, J. (1978), *Statistics for experimenters*, John Wiley & Sons, Chichester.

Bozzano, M., Cimatti, A., Katoen, J.-P., Katsaros, P., Mokos, K., Nguyen, V. Y., Noll, T., Postma, B. and Roveri, M. (2014), 'Spacecraft early design validation using formal methods', *Reliability Engineering & System Safety* **132**, 20–35.

Bratley, P. and Fox, B. (1988), 'ALGORITHM 659: implementing Sobol's quasirandom sequence generator', *ACM Transactions on Mathematical Software* **14**, 88–100.

Breesch, H. and Janssens, A. (2010), 'Performance evaluation of passive cooling in office buildings based on uncertainty and sensitivity analysis', *Solar Energy* **84**(8), 1453–1467.

Brohus, H., Frier, C., Heiselberg, P. and Haghighat, F. (2012), 'Quantification of uncertainty in predicting building energy consumption: A stochastic approach', *Energy and Buildings* **55**, 127–140.

Brohus, H., Heiselberg, P., Hesselholt, A. and Rasmussen, H. (2009), Application of partial safety factors in building energy performance assessment, *in* 'Building Simulation 2009', Glasgow, Schotland, July 27-30, pp. 1014–1021.

Bucher, C. G. (1988), 'Adaptive sampling- an iterative fast Monte Carlo procedure', *Structural safety* **5**, 119–126.

Burhenne, S. (2013), Monte Carlo Based Uncertainty and Sensitivity Analysis for Building Performance Simulation, PhD thesis, Karlsruher Instituts für Technologie. Andreas Wagner and Gregor Henze (supervisors).

Burhenne, S., Jacob, D. and Henze, G. P. (2011), Sampling based on Sobol' sequences for Monte Carlo techniques applied to building simulations, *in* 'Building Simulation 2011', Sydney, Australia, November 14-16, pp. 1816–1823.

Catalina, T., Iordache, V. and Caracaleanu, B. (2013), 'Multiple regression model for fast prediction of the heating energy demand', *Energy and Buildings* **57**, 302–312.

Cellura, M., Di Gangi, A., Longo, S. and Orioli, A. (2013), 'An Italian input-output model for the assessment of energy and environmental benefits arising from retrofit actions of buildings', *Energy and Buildings* **62**, 97–106.

Chen, V. C., Tsui, K.-L., Barton, R. R. and Meckesheimer, M. (2006), 'A review on design, modeling and applications of computer experiments', *IIE Transactions* **38**(4), 273–291.

Chlela, F., Husaunndee, A., Inard, C. and Riederer, P. (2009), 'A new methodology for the design of low energy buildings', *Energy and Buildings* **41**(9), 982–990.

Cools, R., Kuo, F. Y. and Nuyens, D. (2006), 'Constructing Embedded Lattice Rules for Multivariate Integration', *SIAM Journal on Scientific Computing* **28**(6), 2162–2188.

Corrado, V. and Mechri, H. E. (2009), 'Uncertainty and Sensitivity Analysis for Building Energy Rating', *Journal of Building Physics* **33**(2), 125–156.

Couckuyt, I., Forrester, A., Gorissen, D., De Turck, F. and Dhaene, T. (2012), 'Blind Kriging: Implementation and performance analysis', *Advances in Engineering Software* **49**(3), 1–13.

Das, P., Shrubsole, C., Jones, B., Hamilton, I., Chalabi, Z., Davies, M., Mavrogianni, A. and Taylor, J. (2014), 'Using probabilistic sampling-based sensitivity analyses for indoor air quality modelling', *Building and Environment* **78**, 171–182.

de Meester, T., Marique, A.-F., De Herde, A. and Reiter, S. (2013), 'Impacts of occupant behaviours on residential heating consumption for detached houses in a temperate climate in the northern part of Europe', *Energy and Buildings* **57**, 313–323.

de Wilde, P. (2014), 'The gap between predicted and measured energy performance of buildings: A framework for investigation', *Automation in Construction* **41**, 40–49.

de Wit, M. S. (1997), 'Identification of the important parameters in thermal building simulation models', *Journal of Statistical Computation and Simulation* **57**, 305–320.

de Wit, M. S. and Augenbroe, G. (2002), 'Analysis of uncertainty in building design evaluations and its implications', *Energy and Buildings* **34**(9), 951–958.

Debusschere, B. J., Najm, H. N., Pébay, P. P., Knio, O. M., Ghanem, R. G. and Le Maître, O. P. (2004), 'Numercical challenges in the use of polynomial chaos representations for stochastic processes', *SIAM Journal on Scientific Computing* **26**, 698–719.

Dehlendorff, C., Kulahci, M. and Andersen, K. K. (2011), 'Designing simulation experiments with controllable and uncontrollable factors for applications in healthcare', *Journal of the Royal Statistical Society, Applied Statistics* **60**(1), 31–49.

Domínguez-Muñoz, F., Anderson, B., Cejudo-López, J. M. and Carrillo-Andrés, A. (2010), 'Uncertainty in the thermal conductivity of insulation materials', *Energy and Buildings* **42**, 2159–2168.

Domínguez-Muñoz, F., Cejudo-López, J. M. and Carrillo-Andrés, A. (2010), 'Uncertainty in peak cooling load calculations', *Energy and Buildings* **42**(7), 1010–1018.

Du, X. and Chen, W. (2000), 'Towards a Better Understanding of Modeling Feasibility Robustness in Engineering', *Journal of Mechanical Design* **122**, 385–394.

Du, X., Sudjianto, A. and Chen, W. (2004), 'An Integrated Framework for Optimization Under Uncertainty Using Inverse Reliability Strategy', *Journal of Mechanical Design* **126**, 562–570.

EED (2012), Directive 2012/27/EU of the European Parliament and of the Council of 25 October 2012 on energy efficiency, amending Directives 2009/125/EC and 2010/30/EU and repealing Directives 2004/8/EC and 2006/32/EC, Technical report.

Eisenhower, B., O'Neill, Z., Fonoberov, V. A. and Mezić, I. (2012), 'Uncertainty and Sensitivity Decomposition of Building Energy Models', *Journal of Building Performance Simulation* **5**(3), 171–184.

Eisenhower, B., O'Neill, Z., Narayanan, S., Fonoberov, V. A. and Mezić, I. (2012), 'A methodology for meta-model based optimization in building energy models', *Energy and Buildings* **47**, 292–301.

EN ISO 13370 (2004), Thermal performance of buildings - Heat transfer via the ground calculation methods, Technical report.

EN ISO 13790 (2007), Energy performance of buildings - Calculation of energy use for space heating and cooling, Technical report.

EN ISO 15251 (2007), Indoor environmental input parameters for design and assessment of energy performance of buildings addressing indoor air quality, thermal environment, lighting and acoustics, Technical report.

EN ISO 15459 (2007), Energy performance of buildings - Economic evaluation procedure for energy systems in buildings, Technical report.

EPBD (2002), Directive 2002/91/EC of the European Parliament and of the Council of 16 December 2002 on the energy performance of buildings, Technical report.

EPBD (2010), Directive 2010/31/EU of the European Parliament and of the Council of 19 May 2010 on the energy performance of buildings, Technical report.

European Commission (2007), 'Limiting Global Climate Change to 2 degrees Celsius - The way ahead for 2020 and beyond'.

Fabi, V., Buso, T., Andersen, R. K., Corgnati, S. P. and Olesen, B. W. (2013), Robustness of building design with respect to energy related occupant behaviour, *in* 'Building Simulation 2013', Chambéry, France, August 25-28.

Fang, H., Rais-Rohani, M., Liu, Z. and Horstemeyer, M. (2005), 'A comparative study of metamodeling methods for multiobjective crashworthiness optimization', *Computers & Structures* **83**(25-26), 2121–2136.

Fang, K.-T., Ma, C.-X. and Winker, P. (2002), 'Centered L2-discrepancy of random sampling and latin hypercube design, and construction of uniform designs', *Mathematics of Computation* **71**(237), 275–296.

Ferreira, P. M., Ruano, A. E., Silva, S. and Conceic, E. Z. E. (2012), 'Neural networks based predictive control for thermal comfort and energy savings in public buildings', *Energy and Buildings* **55**, 238–251.

Foresee, F. D. and Hagan, M. T. (1997), Gauss-Newton approximation to Bayesian regularization, *in* 'Proceedings of the 1997 International Joint Conference on Neural Networks', pp. 1930–1935.

Friedman, J. H. (1991), 'Multivariate adaptive regression splines', *The Annals of Statistics* **19**(1), 1–141.

Galkin, I. and Lowell, U. (2014), 'Polynomial Neural Networks'. Last consulted on 2014-04-27.
URL: *http://ulcar.uml.edu/ iag/CS/Polynomial-NN.html*

Garcia Sanchez, D., Lacarrière, B., Musy, M. and Bourges, B. (2014), 'Application of sensitivity analysis in building energy simulations: Combining first- and second-order elementary effects methods', *Energy and Buildings* **68**, 741–750.

Gatzert, N. and Wesker, H. (2014), 'Mortality Risk and Its Effect on Shortfall and Risk Management in Life Insurance', *Journal of Risk and Insurance* **81**(1), 57–90.

Ghanem, R. and Spanos, P. (1991), *Stochastic Finite Elements: A Spectral Approach*, Springer Verlag.

Giles, M. (2013), Monte Carlo Methods for Uncertainty Quantification, lecture, KU Leuven Summer School on Uncertainty Quantification, May 30-31, Leuven, Belgium.
URL: *http://people.maths.ox.ac.uk/ gilesm/*

Gossard, D., Lartigue, B. and Thellier, F. (2013), 'Multi-objective optimization of a building envelope for thermal performance using Genetic Algorithms and Artificial Neural Network', *Energy and Buildings* **67**, 253–260.

Guerra-Santin, O. and Itard, L. (2010), 'Occupants' behaviour: determinants and effects on residential heating consumption', *Building Research & Information* **38**(3), 318–338.

Guerra-Santin, O., Tweed, C., Jenkins, H. and Jiang, S. (2013), 'Monitoring the performance of low energy dwellings: Two UK case studies', *Energy and Buildings* **64**, 32–40.

Haarhoff, J. and Mathews, E. (2006), 'A Monte Carlo method for thermal building simulation', *Energy and Buildings* **38**(12), 1395–1399.

Haas, R., Auer, H. and Biermayr, P. (1998), 'The impact of consumer behavior on residential energy demand for space heating', *Energy and Buildings* **27**(2), 195–205.

Halton, J. H. and Smith, G. B. (1964), 'Algorithm 247: Radical-inverse quasi-random point sequence', *Communications of the ACM* **7**(12), 701–702.

Hamby, D. M. (1994), 'A review of techniques for parameter sensitivity analysis of environmental models', *Environmental Monitoring and Assessment* **32**(2), 135–154.

Hamby, D. M. (1995), 'A comparison of sensitivity analysis techniques', *Health Physics* **68**(2), 195–204.

Hammersley, J. M. (1960), 'Monte Carlo methods for solving multivariable problems', *Annals of the New York Academy of Sciences* **86**, 844–874.

Helton, J. C. and Davis, F. J. (2002), 'Illustration of sampling-based methods for uncertainty and sensitivity analysis.', *Risk analysis: an official publication of the Society for Risk Analysis* **22**(3), 591–622.

Helton, J. and Davis, F. (2003), 'Latin hypercube sampling and the propagation of uncertainty in analyses of complex systems', *Reliability Engineering & System Safety* **81**, 23–69.

Helton, J., Davis, F. and Johnson, J. (2005), 'A comparison of uncertainty and sensitivity analysis results obtained with random and Latin hypercube sampling', *Reliability Engineering & System Safety* **89**(3), 305–330.

Hens, H., Verbeeck, G. and Verdonck, B. (2001), 'Impact of energy efficiency measures on the CO_2 emissions in the residential sector, a large scale analysis', *Energy and Buildings* **33**, 275–281.

Heo, Y., Choudhary, R. and Augenbroe, G. (2012), 'Calibration of building energy models for retrofit analysis under uncertainty', *Energy and Buildings* **47**, 550–560.

Hijar-Rivera, H. and Garcia-Castellanos, V. (2009), 'Efficient computer-generated alternatives to Taguchi's crossed arrays for robust parameter design', *Journal of Quality in Maintenance Engineering* **15**(4), 371–382.

Hoes, P., Hensen, J., Loomans, M., de Vries, B. and Bourgeois, D. (2009), 'User behavior in whole building simulation', *Energy and Buildings* **41**(3), 295–302.

Hoes, P., Trcka, M., Hensen, J. L. M. and Hoekstra Bonnema, B. (2011), Optimizing building designs using a robustness indicator with respect to user behavior, *in* 'Building Simulation 2011', Sydney, Australia, November 14-16, pp. 1710–1717.

Hokoi, S. and Matsumoto, M. (1988), 'An analysis of stochastic properties of the heating load in an intermittently air-conditioned building', *Energy and Buildings* **11**, 259–266.

Hong, H. S. and Hickernell, F. J. (2003), 'Algorithm 823: Implementing Scrambled Digital Sequences', *ACM Transactions on Mathematical Software* **29**(2), 95–109.

Hopfe, C. J. (2009), Uncertainty and sensitivity analysis in building performance simulation for decision support and design optimization, PhD thesis, Technische Universiteit Eindhoven. Jan Hensen and Michael Emmerich (supervisors).

Hopfe, C. J., Augenbroe, G. and Hensen, J. L. (2013), 'Multi-Criteria Decision Making Under Uncertainty In Building Performance Assessment', *Building and Environment* **69**, 81–90.

Hopfe, C. J., Emmerich, M. T. M., Marijt, R. and Hensen, J. (2012), Robust multi-criteria design optimisation in building design, *in* 'First Building Simulation and Optimization Conference', Loughborough, UK, September 10-11, pp. 19–26.

Hopfe, C. J. and Hensen, J. L. (2011), 'Uncertainty analysis in building performance simulation for design support', *Energy and Buildings* **43**(10), 2798–2805.

Hussain, M. F., Barton, R. R. and Joshi, S. B. (2002), 'Metamodeling: Radial basis functions, versus polynomials', *European Journal of Operational Research* **138**(1), 142–154.

Husslage, B., Rennen, G., van Dam, E. R. and den Hertog, D. (2008), Space-filling Latin hypercube designs for computer experiments.

Hygh, J. S., DeCarolis, J. F., Hill, D. B. and Ranjithan, S. R. (2012), 'Multivariate regression as an energy assessment tool in early building design', *Building and Environment* **57**, 165–175.

IEA (2008), 'Worldwide Trends in Energy Use and Efficiency'. International Energy Agency.

Janssen, H. (2013), 'Monte-Carlo based uncertainty analysis: Sampling efficiency and sampling convergence', *Reliability Engineering & System Safety* **109**, 123–132.

Janssen, H., Roels, S., Van Gelder, L. and Das, P. (2014), 'IEA EBC Annex 55, Subtask 2, Probabilistic tools'.

Jekabsons, G. (2011), 'ARESLab: Adaptive Regression Splines toolbox for Matlab/Octave'.
URL: *http://www.cs.rtu.lv/jekabsons/regression.html*

Jiang, Y. and Hong, T. (1993), 'Stochastic analysis of building thermal processes', *Building and Environment* **28**(4), 509–518.

Jin, R., Chen, W. and Simpson, T. W. (2001), 'Comparative studies of metamodelling techniques under multiple modelling criteria', *Structural and Multidisciplinary Optimisation* **23**, 1–13.

Jin, R., Chen, W. and Sudjianto, A. (2005), 'An efficient algorithm for constructing optimal design of computer experiments', *Journal of Statistical Planning and Inference* **134**(1), 268–287.

Jin, R., Du, X. and Chen, W. (2003), 'The use of metamodeling techniques for optimization under uncertainty', *Structural and Multidisciplinary Optimization* **25**, 99–116.

Jin, Y. and Sendhoff, B. (2003), Trade-off between Performance and Robustness: An Evolutionary Multiobjective Approach, *in* 'Evolutionary multi-criterion optimization', pp. 237–251.

Johnson, M., Moore, L. and Ylvisaker, D. (1990), 'Minimax and maximin distance designs', *Journal of Statistical Planning and Inference* **26**(2), 131–148.

Johnson, R. T., Montgomery, D. C., Jones, B. and Parker, P. A. (2010), 'Comparing computer experiments for fitting high-order polynomial metamodels', *Journal of Quality Technology* **42**(1), 86–102.

Kalagnanam, J. R. and Diwekar, U. M. (1997), 'An Efficient Sampling Technique for Off-Line Quality Control', *Technometrics* **39**(3), 308–319.

Kennedy, M. C. and O'Hagan, A. (2001), 'Bayesian calibration of computer models', *Journal of the Royal Statistical Society* **63**(3), 425–464.

Kim, Y.-J., Ahn, K.-U. and Park, C.-S. (2014), 'Decision Making of HVAC System using Bayesian Markov Chain Monte Carlo method', *Energy and Buildings* (2014).

Kiureghian, A. D. and Ditlevsen, O. (2009), 'Aleatory or epistemic? Does it matter?', *Structural Safety* **31**(2), 105–112.

Kleijnen, J. P. and Sargent, R. G. (2000), 'A methodology for fitting and validating metamodels in simulation', *European Journal Of Operational Research* **120**, 14–29.

Koehler, J. R. and Owen, A. B. (1996), Computer Experiments, *in* 'Handbook of Statistics 13', Elsevier Science B.V, chapter 9, pp. 1–43.

Lee, P., Lam, P., Yik, F. and Chan, E. (2013), 'Probabilistic risk assessment of the energy saving shortfall in energy performance contracting projects: A case study', *Energy and Buildings* **66**, 353–363.

Lemaire, M. (2009), *Structural reliability*, Wiley.

Leyten, J. L. and Kurvers, S. R. (2006), 'Robustness of buildings and HVAC systems as a hypothetical construct explaining differences in building related health and comfort symptoms and complaint rates', *Energy and Buildings* **38**(6), 701–707.

Livios (2014), 'Hoeveel kost een nieuwbouw?'. Last consulted on 2014-03-31.
URL: *http://www.livios.be/nl/bouwfasen/bouwen-verbouwen-of-kopen/bouwen/budget/hoeveel-kost-een-nieuwbouw/*

Ljung, L. (1999), *System Identification: Theory for the user*, second edn, Upper Saddle River, NJ, Prentice-Hal PTR.

Lomas, K. J. and Eppel, H. (1992), 'Sensitivity analysis techniques for building thermal simulation programs', *Energy and Buildings* **19**, 21–44.

Macdonald, I. A. (2002), Quantifying the Effects of Uncertainty in Building Simulation, PhD thesis, Department of Mechanical Engineering, University of Strathclyde. Joe Clarke (supervisor).

Macdonald, I. A. (2009), Comparison of sampling techniques on the performance of Monte-Carlo based sensitivity analysis, *in* 'Building simulation 2009', Glasgow, Scotland, July 27-30, pp. 992–999.

Macdonald, I. A. and Strachan, P. (2001), 'Practical application of uncertainty analysis', *Energy and Buildings* **33**(3), 219–227.

Machairas, V., Tsangrassoulis, A. and Axarli, K. (2014), 'Algorithms for optimization of building design: A review', *Renewable and Sustainable Energy Reviews* **31**, 101–112.

MacKay, D. J. C. (1992), 'Bayesian Interpolation', *Neural Computation* **4**(3), 415–447.

Madsen, H. (2008), *Time Series Analysis*, Taylor & Francis Group, LLC.

Mahdavi, A. (2009), 'Patterns and Implications of User Control Actions in Buildings', *Indoor and Built Environment* **18**(5), 440–446.

Mahdavi, A. and Gurtekin, B. (2004), 'Generating the design-performance space via simulation and machine learning', *Journal of Architectural and Planning research* **21**(4), 350–362.

Malatji, E. M., Zhang, J. and Xia, X. (2013), 'A Multiple Objective Optimisation Model for Building Energy Efficiency Investment Decision', *Energy and Buildings* (61), 81–87.

Marquardt, D. W. and Snee, R. D. (1975), 'Ridge Regression in Practice', *The American Statistician* **29**(1), 3–20.

Marquès, M., Pignatel, J., Saignes, P., D'Auria, F., Burgazzi, L., Müller, C., Bolado-Lavin, R., Kirchsteiger, C., La Lumia, V. and Ivanov, I. (2005), 'Methodology for the reliability evaluation of a passive system and its integration into a Probabilistic Safety Assessment', *Nuclear Engineering and Design* **235**(24), 2612–2631.

Matheron, G. (1963), 'Principles of geostatistics', *Economic Geology* **58**, 1246–1266.

MathWorks (2014*a*), 'Akaike Information Criterion for estimated model'. Last consulted on 2014-07-14.
URL: *http://www.mathworks.nl/help/ident/ref/aic.html*

MathWorks (2014*b*), 'Estimate state-space model using a subspace method'. Last consulted on 2014-04-29.
URL: *http://www.mathworks.nl/help/ident/ref/n4sid.html*

MathWorks (2014*c*), 'Global Optimization Toolbox'. Last consulted on 2014-07-29.
URL: *http://www.mathworks.nl/help/gads/index.html*

MathWorks (2014*d*), 'Improve neural network generalization and avoid overfitting'. Last consulted on 2014-04-28.
URL: *http://www.mathworks.nl/help/nnet/ug/improve-neural-network-generalization-and-avoid-overfitting.html*

MathWorks (2014*e*), 'Neural network toolbox'. Last consulted on 2014-04-29.
URL: *http://www.mathworks.nl/products/neural-network/*

MathWorks (2014*f*), 'Ridge regression'. Last consulted on 2014-04-29.
URL: *http://www.mathworks.nl/help/stats/ridge.html*

Mcguire, R. K. (2001), 'Deterministic vs. probabilistic earthquake hazards and risks', *Soil Dynamics and Earthquake Engineering* **21**, 377–384.

McKay, M., Beckman, R. J. and Conover, W. J. (1979), 'A Comparison of Three Methods for Selecting Values for Input Variables in the Analysis of Output from a Computer Code', *Technometrics* **21**, 239–245.

Melchers, R. E. (1987), *Structural reliability: analysis and prediction*, Ellis Horwood, Chichester.

Metropolis, N. and Ulam, S. (1949), 'The Monte Carlo Method', *Journal of the American Statistical Association* **44**(247), 335–341.

Michalewicz, Z., Dasgupta, D., Le Riche, R. G. and Schoenauer, M. (1996), 'Evolutionary algorithms for constrained engineering problems', *Computers & Industrial Engineering* **30**(4), 851–870.

Morris, M. D. and Mitchell, T. J. (1995), 'Exploratory designs for computational experiments', *Journal of Statistical Planning and Inference* **43**(3), 381–402.

Mullur, A. A. and Messac, A. (2006), 'Metamodeling using extended radial basis functions: a comparative approach', *Engineering with Computers* **21**(3), 203–217.

Nair, V. N., Abraham, B., Mackay, J., Nelder, J. A., Box, G., Phadke, M. S., Kacker, R. N., Sacks, J., Welch, W. J., Lorenzen, T. J., Shoemaker, A. C., Tsui, K. L., Lucas, J. M., Taguchi, S., Myers, R. H., Vining, G. G. and Wu, C. F. J. (1992), 'Taguchi's Parameter Design: A Panel Discussion', *Technometrics* **34**(2), 127–161.

NBN D 50-001 (1991), Ventilatievoorzieningen in woongebouwen, Technical report.

Nguyen, A.-T., Reiter, S. and Rigo, P. (2014), 'A review on simulation-based optimization methods applied to building performance analysis', *Applied Energy* **113**, 1043–1058.

Niederreiter, H. (1987), 'Point Sets and Sequences with Small Discrepancy', *Monatshefte für Mathematik* **104**(4), 273–337.

Niederreiter, H. (1988), 'Low-Discrepancy and Low-Dispersion Sequences', *Journal of Number Theory* **30**, 51–70.

Niederreiter, H. (1992), *Random Number Generation and Quasi-Monte Carlo*, Society for Industrial and Applied Mathematics.

O'Brien, W. (2013), Occupant-proof buildings: can we design buildings that are robust against occupant behaviour?, *in* 'Building Simulation 2013', Chambéry, France, August 25-28.

Orr, M. J. L. (1996), 'Introduction to Radial Basis Function Networks'.

Orr, M. J. L. (1999), 'Matlab functions for Radial Basis Function Networks'.
URL: *http://www.anc.ed.ac.uk/rbf/rbf.html*

Park, J.-S. (1994), 'Optimal Latin-hypercube designs for computer experiments', *Journal of Statistical Planning and Inference* **39**, 95–111.

Parys, W. (2013), Cost Optimization of Cellular Office Buildings Based on Building Energy Simulation, PhD thesis, KU Leuven. Hugo Hens and Dirk Saelens (supervisors).

Peeters, L., Dear, R. D., Hensen, J. and D'haeseleer, W. (2009), 'Thermal comfort in residential buildings: Comfort values and scales for building energy simulation', *Applied Energy* **86**(5), 772–780.

Pettersen, T. D. (1994), 'Variation of energy consumption in dwellings due to climate, building and inhabitants', *Energy and Buildings* **21**(3), 209–218.

Phadke, M. S. (1989), *Quality engineering using robust design*, P T R Prentice-Hall.

Pietrzyk, K. (2000), Probabilistic modelling of air infiltration and heat loss in low-rise buildings, PhD thesis, School of Architecture, Chalmers University of Technology, Sweden. Kamal Handa, Carl-Eric Hagentoft, Holger Rootzén and Karl-Gunnar Olsson (supervisors).

Pietrzyk, K. and Hagentoft, C.-E. (2008*a*), 'Probabilistic analysis of air infiltration in low-rise buildings', *Building and Environment* **43**, 537–549.

Pietrzyk, K. and Hagentoft, C.-E. (2008*b*), 'Reliability analysis in building physics design', *Building and Environment* **43**, 558–568.

Prada, A., Cappelletti, F., Baggio, P. and Gasparella, A. (2014), 'On the effect of material uncertainties in envelope heat transfer simulations', *Energy and Buildings* **71**, 53–60.

Prozanto, L. and Müller, W. G. (2012), 'Design of computer experiments: space filling and beyond', *Statistics and Computing* **22**, 681–701.

Rathod, V., Yadav, O. P., Rathore, A. and Jain, R. (2013), 'Optimizing reliability-based robust design model using multi-objective genetic algorithm', *Computers & Industrial Engineering* **66**(2), 301–310.

Rysanek, A. and Choudhary, R. (2013), 'Optimum building energy retrofits under technical and economic uncertainty', *Energy and Buildings* **57**, 324–337.

Sacks, J., Welch, W. J., Mitchell, T. J. and Wynn, H. P. (1989), 'Design and Analysis of Computer Experiments', *Statistical Science* **4**(4), 409–423.

Sadovsky, Z., Koronthalyova, O., Matiasovsky, P. and Mikulova, K. (2014), 'Probabilistic modelling of mould growth in buildings', *Journal of Building Physics* **37**, 348–366.

Saltelli, A., Ratto, M., Andres, T., Campolongo, F., Cariboni, J., Gatelli, D., Saisana, M. and Tarantola, S. (2008), *Global sensitivity analysis. The primer*, John Wiley & Sons, Chichester.

Sanchez, S. M., Sanchez, P. J., Ramberg, J. S. and Moeeni, F. (1996), 'Effective engineering design through simulation', *International Transactions in Operational Research* **3**(2), 169–185.

Scheuer, E. M. and Stoller, D. S. (1962), 'On the Generation of Normal Random Vectors', *Technometrics* **4**(2), 278–281.

Seem, J. E. (1987), Modeling of Heat Transfer in Buildings, PhD thesis, University of Wisconsin-Madison. Sanford Klein, William Beckman, and John Mitchell (supervisors).

Shahraki, A. F. and Noorossana, R. (2014), 'Reliability-based robust design optimization: A general methodology using genetic algorithm', *Computers & Industrial Engineering* **74**, 199–207.

Shoemaker, A. C., Tsui, K.-L., Wu and Jeff, C. (1991), 'Economical Experimentation Methods for Robust Design', *Technometrics* **33**(4), 415–427.

Simpson, T. W., Peplinski, J. D., Koch, P. N. and Allen, J. K. (2001), 'Metamodels for computer-based engineering design: survey and recommendations', *Engineering with Computers* **17**, 129–150.

Sobol', I. (1967), 'On the distribution of points in a cube and the approximate evaluation of integrals', *USSR Computational Mathematics and Mathematical Physics* **7**(4), 86–112.

Sonderegger, R. C. (1977), 'Movers and Stayers: The Resident's Contribution to Variation across Houses in Energy Consumption for Space Heating', *Energy and Buildings* **1**, 313–324.

Staepels, L., Verbeeck, G., Roels, S., Van Gelder, L. and Bauwens, G. (2013*a*), BEP2020: betrouwbare energieprestaties van woningen - Naar een robuuste en gebruikersonafhankelijke performantie, Technical Report IWT TETRA 110189. **URL:** *bep2020.pxl.be*

Staepels, L., Verbeeck, G., Roels, S., Van Gelder, L. and Bauwens, G. (2013*b*), Do Ventilation Systems Accomplish the Necessary Indoor Air Quality in Low Energy Houses?, *in* '11th REHVA World Congress and 8th International Conference on IAQVEC', Prague, Czech Republic, June 16-19.

Staepels, L., Verbeeck, G., Roels, S., Van Gelder, L. and Bauwens, G. (2013*c*), Evaluation of Indoor Climate in Low Energy Houses, *in* 'Symposium on Simulation for Architecture and Urban Design', San Diego, USA, April 7-10.

Staum, J. (2009), 'Better simulation metamodeling: The why, what, and how of stochastic kriging', *Proceedings of the 2009 Winter Simulation Conference (WSC)* pp. 119–133.

Stein, M. (1987), 'Large Sample Properties of Simulations Using Latin Hypercube Sampling', *Technometrics* **29**(2), 143–151.

Sudret, B. (2007), 'Uncertainty propagation and sensitivity analysis in mechanical models - Contributions to structural reliability and stochastic spectral methods'.

Sulaiman, H. and Olsina, F. (2014), 'Comfort reliability evaluation of building designs by stochastic hygrothermal simulation', *Renewable and Sustainable Energy Reviews* **40**, 171–184.

Tavner, P. J., Xiang, J. and Spinato, F. (2007), 'Reliability Analysis for Wind Turbines', *Wind Energy* **10**, 1–18.

Taylor, J., Davies, M., Mavrogianni, A., Chalabi, Z., Biddulph, P., Oikonomou, E., Das, P. and Jones, B. (2014), 'The relative importance of input weather data for indoor overheating risk assessment in dwellings', *Building and Environment* **76**, 81–91.

Tian, W. and de Wilde, P. (2011), 'Uncertainty and sensitivity analysis of building performance using probabilistic climate projections: A UK case study', *Automation in Construction* **20**(8), 1096–1109.

Tian, W., Song, J., Li, Z. and de Wilde, P. (2014), 'Bootstrap techniques for sensitivity analysis and model selection in building thermal performance analysis', *Applied Energy* **135**, 320–328.

Tsui, K.-L. (1996), 'A critical look at Taguchi's modelling approach for robust design', *Journal of Applied Statistics* **23**, 81–96.

UNFCCC (2008), 'Kyoto protocol reference manual'. United Nations Framework Convention on Climate Change.

van der Linden, K., Boerstra, A. C., Raue, A. K. and Kurvers, S. R. (2002), 'Thermal indoor climate building performance characterized by human comfort response', *Energy and Buildings* **34**(7), 737–744.

Van Gelder, L., Janssen, H. and Roels, S. (2013), Metamodelling in robust low-energy dwelling design, *in* A. Mahdavi and B. Martens, eds, '2nd Central European Symposium on Building Physics', Vienna, Austria, September 9-11, pp. 93–99.

Van Overschee, P. and De Moor, B. (1994), 'N4SID: Subspace Algorithms for the Stochastic Systems', *Automatica* **30**(I), 75–93.

Van Raaij, W. F. and Verhallen, T. M. (1983), 'A Behavioural Model of Residential Energy Use', *Journal of Economic Psychology* **3**, 39–63.

Vanmarcke, E. (1983), *Random Fields: Analysis and Synthesis*, The MIT Press.

Verbeeck, G. (2007), Optimisation of extremely low energy residential buildings, PhD thesis, KU Leuven. Hugo Hens (supervisor).

Verbeeck, G. and Hens, H. (2005), 'Energy savings in retrofitted dwellings: economically viable?', *Energy and Buildings* **37**, 747–754.

Verbeeck, G. and Hens, H. (2007), 'Life Cycle Optimization of Extremely Low Energy Dwellings', *Journal of Building Physics* **31**(2), 143–177.

Wang, G. G. and Shan, S. (2007), 'Review of Metamodeling Techniques in Support of Engineering Design Optimization', *Journal of Mechanical Design* **129**(4), 370.

Wu, L., Park, J. and Choi, J. (2009), Probabilistic Reliability Evaluation of Power Systems Including Wind Turbine Generators Using a Simplified Multi-State Model: A Case Study, *in* 'IEEE Power & Energy Society General Meeting', IEEE, Calgary, Canada, July 26-30, pp. 1–6.

Zang, C., Friswell, M. and Mottershead, J. (2005), 'A review of robust optimal design and its application in dynamics', *Computers & Structures* **83**(4-5), 315–326.

Curriculum vitae

Liesje VAN GELDER

Verschansingstraat 39/1

2000 Antwerpen

BELGIUM

0032 474 90 57 15

liesje.vangelder@gmail.com

°Diest (BE), February 4, 1987

Belgian nationality

Education

2011-2014	Doctoral program Arenberg doctoral school, KU Leuven, Leuven, Belgium
2005-2010	Master of engineering science: architecture KU Leuven, Leuven, Belgium (distinction) Thesis: *Possibilities of thermal capacity of massive compared to timberframed constructions for low-energy dwellings (in Dutch)*
1999-2005	Latin - mathematics Voorzienigheid, Diest, Belgium

Professional positions

2010-2014	PhD student at Building Physics Section Department of Civil Engineering, KU Leuven, Belgium

Research activities

2010-2014	Preparation of a PhD entitled 'A probabilistic design methodology for building performance optimisation'.
2014-...	IWT VIS Renofase 'Roadmap for a qualitative energetic retrofit' (in Dutch)
2011-2013	IWT TETRA BEP2020 'Reliable energy performances of dwellings - Towards a robust and user independent performance' (in Dutch)
2010-2014	IEA EBC Annex 55 RAP-RETRO 'Reliability of Energy Efficient Building Retrofitting - Probability Assessment of Performance and Cost'

List of publications

Articles in international journals

- Vereecken, E., Roels, S., Janssen, H., Van Gelder, L. Interior insulation for wall retrofitting - a probabilistic analysis of energy savings and hygrothermal risks. *Energy and Buildings. Submitted.*
- Van Gelder, L., Das, P., Janssen, H., Roels, S. Comparative study of metamodelling techniques in building energy simulation: guidelines for practitioners. *Simulation Modelling Practice and Theory, 49,* 245-257.
- Van Gelder, L., Janssen, H., Roels, S. (2014). Probabilistic design and analysis of building performances: methodology and application example. *Energy and Buildings, 79,* 202-211.

Articles in international conference proceedings

- Van Gelder, L., Janssen, H., Roels, S. (2014). Economically effective and robust low-energy dwellings. In Malki-Epsthein, L. (Ed.), Spataru, C. (Ed.), Marjanovic-Halburd, L. (Ed.), Mumovic, D. (Ed.), *Proceedings of the 2014 Building Simulation and Optimization Conference.* Londen, UK, June 23-24.
- Van Gelder, L., Janssen, H., Roels, S. (2014). Reliability of meta-modelling in robust low-energy dwelling design. *Proceedings of 10th Nordic Symposium on Building Physics.* Lund, Sweden, June 15-19.
- Roels, S., Van Gelder, L., Janssen, H. (2014). Including uncertainty in building energy performance calculation methods. *Quality of Methods for Measuring Ventilation and Air Infiltration in Buildings. AIVC International Workshop.* Brussels, Belgium, March 18-19.
- Van Gelder, L., Janssen, H., Roels, S. (2013). Metamodelling in robust low-energy dwelling design. In Mahdavi, A. (Ed.), Martens, B. (Ed.), *2nd Central European Symposium on Building Physics. Central European Symposium on Building Physics.* Vienna, Austria, September 9-11.

- Staepels, L., Verbeeck, G., Roels, S., Van Gelder, L., Bauwens, G. (2013). Evaluation of Indoor Climate in Low Energy Houses. *Symposium on Simulation for Architecture and Urban Design.* San Diego, USA, April 7-10.
- Staepels, L., Verbeeck, G., Roels, S., Van Gelder, L., Bauwens, G. (2013). Energy performance labels for dwellings versus real energy consumption. *Building Simulation 2013.* Chambéry, France, August 25-28.
- Van Gelder, L., Janssen, H., Roels, S., Verbeeck, G., Staepels, L. (2013). Effective and robust measures for energy efficient dwellings: probabilistic determination. *Building Simulation 2013.* Chambéry, France, August 26-28.
- Staepels, L., Verbeeck, G., Roels, S., Van Gelder, L., Bauwens, G. (2013). Do Ventilation Systems Accomplish the Necessary Indoor Air Quality in Low Energy Houses?. *CLIMA 2013.* Prague, Czech Republic, June 16-19.
- Van Gelder, L., Janssen, H., Roels, S. (2012). Retrofitting cavity walls - probabilistic study of energy savings and moisture risks. *Proceedings of the 5th International Building Physics Conference.* Kyoto, Japan, May 28-31.

Research reports

- Staepels, L., Verbeeck, G., Bauwens, G., Deconinck, A., Roels, S., Van Gelder, L. (2013). *BEP2020: betrouwbare energieprestaties van woningen. Naar een robuuste en gebruikersonafhankelijke performantie.* (in Dutch)
- Janssen, H., Roels, S., Van Gelder, L. and Das, P. (2014). *IEA EBC Annex 55, Subtask 2, Probabilistic tools.*

Articles in national journals

- Van Gelder, L. (2014). Invloedrijke parameters voor energieverbruik en zomercomfort van energiezuinige woningen. *Dimension, 31,* 16-19.
- Van Gelder, L., Roels, S., Verbeeck, G., Staepels, L. (2014). Naar robuuste en gebruikersonafhankelijke energiezuinige woningen. *Bouwfysica, 1,* 6-9.

FACULTY OF ENGINEERING SCIENCE
DEPARTMENT OF CIVIL ENGINEERING
BUILDING PHYSICS SECTION
Kasteelpark Arenberg 40 box 2447
B-3001 Heverlee
http://bwk.kuleuven.be/bwf